LinCom

FINAL REPORT

SHUTTLE/TDRSS COMMUNICATIONS SYSTEM PERFORMANCE ANALYSIS

(NASA-CR-160467) SHUTTLE/TDRSS COMMUNICATIONS SYSTEM PERFORMANCE ANALYSIS Final Report, 20 Apr. 1979 - 24 Jan. 1980 (LinCom Corp., Pasadena, Calif.) 126 p HC A07/MF A01 CSCL 17B G3/32

N80-17328

Unclas 47125

PREPARED FOR

NASA LYNDON B. JOHNSON SPACE CENTER
HOUSTON, TX 77058

TECHNICAL MONITORS: W. TEASDALE
S. NOVOSAD

CONTRACT NAS 9-15799

PREPARED BY

W. R. BRAUN
T. M. McKENZIE
W. C. LINDSEY

LINCOM CORPORATION
P.O. BOX 2793D
PASADENA, CA 91105

JANUARY 24, 1980

TR-0180-1179

LinCom

TABLE OF CONTENTS

		PAGE
1.	INTRODUCTION	1
	1.1 General	1
	1.1.1 Final Report Contents	2
	1.2 Summary and Recommendations	3
	1.2.1 Shuttle S-band Return Link Performance Study	3
	1.2.2 Shuttle Ku-Band Return Link Performance Study	5
	1.2.3 Shuttle/TDRSS Ground Station Synchronization Performance	5
	1.2.4 RFI Effects on Shuttle/TDRSS Links	5
	1.2.5 ESTL Hardware RFI Testing	9
2.	LinCsim PREDICTIONS OF SHUTTLE/TDRSS RETURN LINK BER PERFORMANCE	10
	2.1 Introduction	10
	2.2 Performance Prediction for Shuttle S-Band Return Link	10
	2.3 Performance Prediction for Shuttle Ku-Band Return Link, Mode 1	40
	REFERENCES	101
3.	LinCsim MODELING OF CARRIER AND TIMING RECOVERY	102
	3.1 Introduction	102
	3.2 Generalized Link Description	102
	3.3 Carrier Tracking with Costas Loop	106
	3.3.1 Introduction	106
	3.3.2 Further Characterization of Link	106
	3.3.3 Costas Loop Operation	107

TABLE OF CONTENTS (Cont'd)

		PAGE
3.3.4	Statistics of $\bar{x}_1$ and $\bar{x}_2$	110
3.3.5	Expression for δ	110
3.4	Carrier Tracking with Two-Channel Costas Loop	113
3.4.1	Introduction	113
3.4.2	Further Characterization of Link	113
3.4.3	Operation of Two-Channel Costas Loop	115
3.4.4	Properties of $\bar{x}_1$ and $\bar{x}_2$	115
3.4.5	S-Curve $S(\varepsilon\rho)$	117
3.4.6	Psd N_0' of Equivalent Noise	119
3.5	Symbol Tracking with Digital Data-Transition Tracking Loop	119
3.5.1	Introduction	119
3.5.2	Tracking NRZ Symbols	121
3.5.3	Tracking Biphase Symbols	123
REFERENCES		124
4.	RFI EFFECTS ON SHUTTLE/TDRSS LINK	125
4.1	Introduction	125
4.2	RFI Environment	125
4.3	TDRSS RFI Hardware Changes	126
4.4	LinCsim Modeling of RFI Effects on Bit Error Rate	133
4.4.1	Introduction	133
4.4.2	Description of Model	138
4.4.2.1	RFI Model	138
4.4.2.2	Channel Model	141
4.4.3	Conditional Error Probability	143

TABLE OF CONTENTS (Cont'd)

		PAGE
4.4.4	Bit Error Probability	145
4.4.4.1	Low Data Rate Case	146
4.4.4.2	High Data Rate Case	147
4.4.5	Evaluation of Moments	148
4.5	LinCsim Modeling of RFI Effects on Synchronization Loops	151
4.5.1	Introduction	151
4.5.2	RFI Effect on Ground-Station Input Signal	152
4.5.3	RFI Effect on Carrier Tracking	152
4.5.3.1	General Description of RFI in the Loop	152
4.5.3.2	S'(0) and N_0' During No RFI or WGN RFI	154
4.5.3.3	S'(0) and N_0' During CW RFI	154
4.5.4	RFI Effect on Symbol Tracking	157
4.5.4.1	General Description of RFI in the Loop	157
4.5.4.2	S'(0) and N_0' During No RFI or WGN RFI	158
4.5.4.3	S'(0) and N_0' During CW RFI	158
4.6	Preliminary LinCsim Performance Predictions	159
4.6.1	Introduction	159
4.6.2	Predicted BER Performance	159
4.6.3	Predicted Synchronization Performance	169
APPENDIX		197
REFERENCES		199
5.	PROPOSED ESTL RFI TESTING	200
5.1	Introduction	200

TABLE OF CONTENTS (Cont'd)

		PAGE
5.2	Desirable Features for RFI Simulator	200
5.3	Proposed ESTL RFI Simulator	201
6.	MISCELLANEOUS ANALYSES AND RECOMMENDATIONS	205
6.1	Introduction	205
6.2	Waveguide Effects on PSK Signals	205
6.2.1	Introduction	205
6.2.2	Linear Distortion of a Waveguide	205
6.2.3	Interpretation of KSC Measurements	210
6.3	S-Band Low Power Mode	210
6.3.1	Introduction	210
6.3.2	TDRSS Services and Functional Requirements	213
6.3.3	Shuttle Equipment Options	213
6.3.3.1	Low Power PM Mode	213
6.3.3.2	FM Equipment	213
6.3.4	Recommendations	215
6.4	Effect of Spacelab Data Transition Density on Clock Recovery and BER	215
6.4.1	Introduction	215
6.4.2	Characterization of Spacelab Data Transition Density	216
6.4.3	Analysis	216
6.5	Spacelab Risetime and Jitter Specifications	217
6.5.1	Introduction	217
6.5.2	Analysis	217
REFERENCES		220

1. INTRODUCTION

1.1 General

This document presents the final report on the Shuttle/TDRSS Communications System Performance Analysis performed for NASA Johnson Space Center under Contract NAS 9-15799 directed by William Teasdale and Sid Novosad. It represents a portion of the work accomplished during the period April 20, 1979 through January 24, 1980.

The general objectives of the overall contract are the following:

(1) To modify and refine the existing Shuttle/TDRSS link simulation programs to model the post-RFI TDRS hardware and to provide the ability to evaluate the link performance degradation due to RFI effects. This analysis had to include the S-band synchronization vulnerability to the TDRSS RFI environment.

(2) To use the refined link models to determine, evaluate and assess expected link performance that will result from not meeting each TDRSS user constraint; individually, and in various combinations. The effects and system performance implications of the latest user constraint values had to be evaluated. The refined results of this task were to be used by JSC as a technical base for negotiating interface parameters between Shuttle and TDRSS.

(3) To continue the review of ESTL Task 501 TDRSS system configuration (using flight equivalent TDRSS hardware) and recommend changes an/or modifications as required. LinCom continued its support of ESTL Task 501 TDRSS system performance prediction capability by providing math modeling and computer models necessary to provide valid system level performance predictions for forward and return link certification testing.

(4) To identify test requirements to evaluate user-constraints for the refined TDRSS model and update Shuttle Ku-band and S-band system characteristics.

In what follows an overall description of the contractual effort and a brief summary of the results is given. This is followed by backup material which includes simulation data and analyses from which our summary results and recommendations have been drawn.

1.1.1 Final Report Contents

This report addresses and documents LinCom's findings on the task statements detailed in the Statement of Work. All task statements pertain to the performance prediction of Shuttle forward and return links through the Tracking and Data Relay Satellite System (TDRSS).

Chapter 2 presents user constraint sensitivity data for Shuttle/TDRSS S-band and Ku-band return links. These simulation results are based on refined TDRS model and up-to-date user constraint values. They apply to links without RFI problems. The current system parameter values are also listed.

Chapter 3 contains a comprehensive performance analysis for the Shuttle/TDRSS ground station carrier and timing recovery circuits. It contains performance data for the current system parameters and link budget for both Ku-band links and S-band links. The effects of RFI are not considered in this analysis.

Chapter 4 discusses the effects of RFI on link performance. The RFI environment is described in detail and the RFI-related hardware changes in the TDRS and TDRSS ground station are indicated. The analytical models used to characterize the bit error rate and synchronization performance are described. Preliminary results for

the BER and synchronization vulnerability to RFI are also included.

In Chapter 5 the problem of simulating the RFI effects with ESTL's flight equivalent TDRSS hardware is addressed. The RFI pulse characteristics which might have to be considered in the design of an RFI test generator are discussed and a simple implementation based on unclassified RFI characteristics is presented.

Chapter 6 comprises a number of small studies performed under this contract in response to specific requests by JSC.

1.2 Summary and Recommendations

1.2.1 Shuttle S-band Return Link Performance Study

The performance degradation of the Shuttle/TDRSS return link due to Shuttle signal imperfections has been evaluated for the expected Shuttle distortion values based on current link budgets and TDRS/ground station hardware data. The results show a loss relative to ideal BPSK of 1.65 dB at the nominal bit error probability of 10^{-4}. The TDRS and ground station contribute .9 dB to this loss and the Shuttle the remaining .75 dB. This is illustrated in Fig. 1.1.

The single biggest contributor to the Shuttle degradation is the phase noise which is specified as 10° rms in the frequency interval 0 to 270 Hz. We recommend to separate the phase noise into components lying inside and outside the carrier tracking loop bandwidth, respectively, since these components affect the bit error rate performance differently. Such a refinement of the specification could greatly improve the accuracy of the predicted performance results. Since our present prediction is based on worst-case assumptions the overall degradation would be reduced.

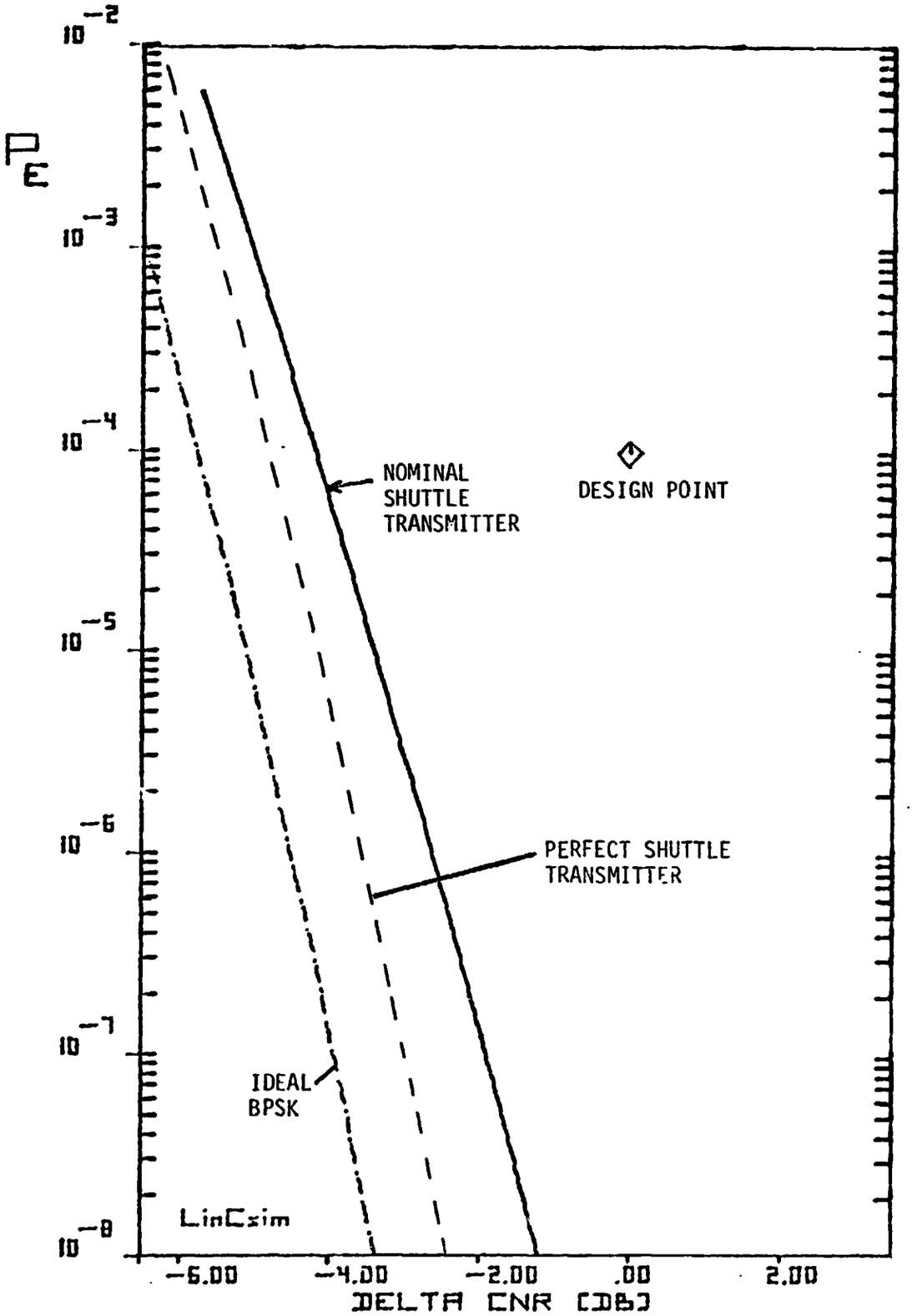

Fig. 1.1. Performance of Shuttle S-Band Return Link.

79 0061

1.2.2 Shuttle Ku-Band Return Link Performance Summary

In the user constraint sensitivity analysis for the Ku-band return link, Mode 1, it was found that the total degradation in link performance due to the TDRS, the ground station and the user constraints set at their nominal values results in a signal-to-noise ratio loss of 3.9 dB for channel 1, 4.6 dB for channel 2 and 2.3 dB for channel 3. (These values do not include the effects of hardware imperfections.) The portion attributable to the TDRS and ground station is 1.9 dB, 2 dB, and 1.2 dB for channels 1, 2, and 3, respectively, while 2 dB, 2.6 dB, and 1.1 dB, respectively, result from the user constraints set to their nominal values.

1.2.3 Shuttle/TDRSS Ground Station Synchronization Performance

The carrier and timing recovery performance was analyzed for the Shuttle/TDRSS S- and Ku-band return link subcarrier extraction was studied. The carrier and clock jitter values for typical link budgets and stable oscillators are summarized in Tables 1-1 and 1-2. From these data it may be concluded that the effects of band limiting, nonlinear amplification and thermal noise on the synchronization performance will not greatly affect the overall link performance.

1.2.4 RFI Effects on Shuttle/TDRSS Links

The effects of RFI both on the bit error rate and the synchronization performance of the Shuttle/TDRSS S-band return link was evaluated.

For the TDRS West (which sees a less severe RFI environment than the TDRS East) and the S-band frequency, 2217.5 MHz the BER was found to be degraded by .2 dB for 4 degrees off-pointing, by .6 dB for 1.5 degrees off-pointing and by almost 6 dB when the Shuttle is directly over the RFI zone. This is illustrated in Fig. 1.2.

Table 1-1. Carrier and Subcarrier Recovery Performance.

Link	Data Rate	E_b/N_0	R.M.S. Jitter (deg)
Ku-Band (Carrier)	10 Mb/s	4 dB	.8
Ku-Band (Subcarrier)	192 kb/s Bi-ϕ	15 dB	1.3
S-Band, Mode 1	96 kb/s	4 dB	2.2

Table 1-2. Timing Recovery Performance.

Channel	Data Rate	E_b/N_0	RMS Jitter (Symbol Fraction)
Ku-Band Channel 1	192 kb/s	10 dB	.056%
K-Band Channel 2	600 kb/s	11 dB	.15%
Ku-Band Channel 2	10 Mb/s	4 dB	2.2%
S-Band	96 kb/s	4 dB	.68%

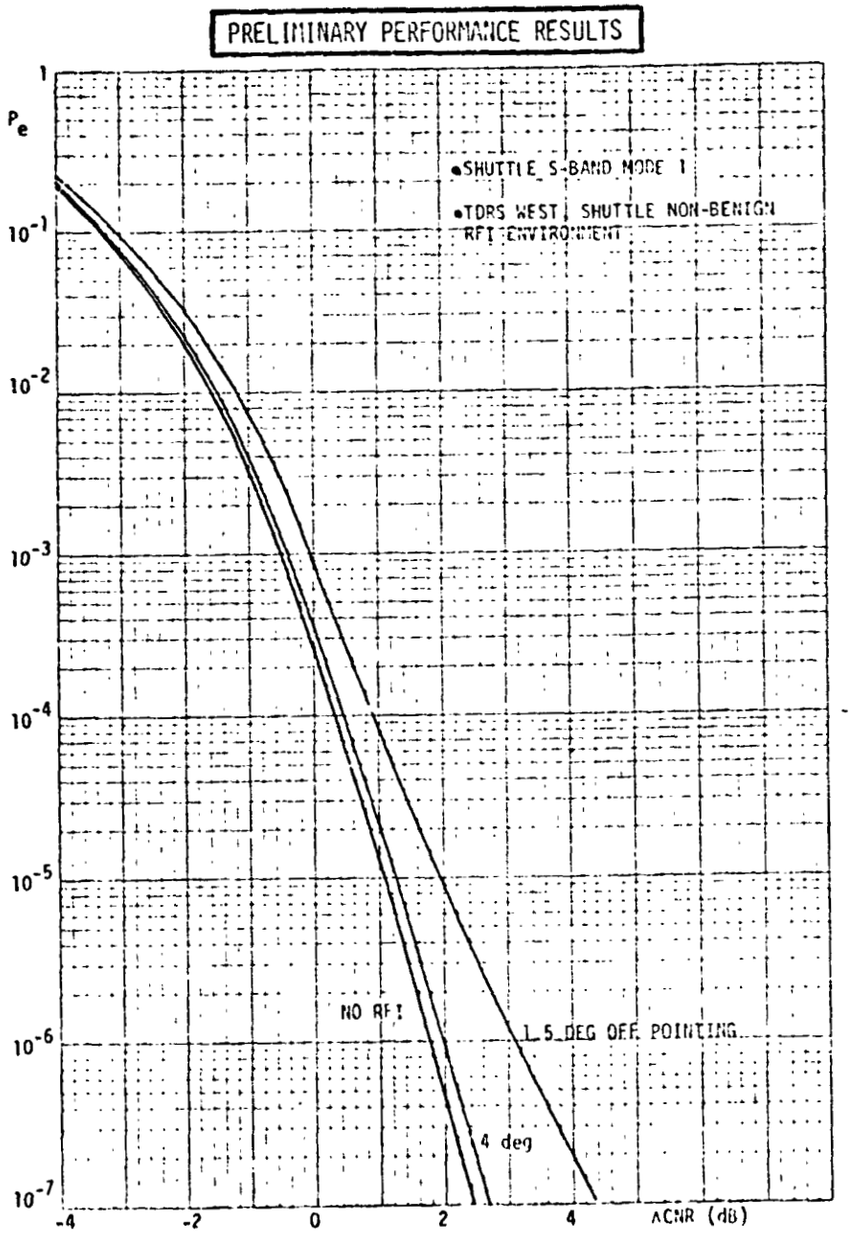

Figure 1.2. RFI Effects on Shuttle S-Band Return Link.

1.2.5 ESTL Hardware RFI Testing

The question of designing an RFI test generator for use in conjution with the ESTL TDRSS flight equivalent nardware is addressed and a simple test generator implementation is proposed. This design is based on unclassified data bases describing the RFI statistics. It is recommended to review the more detailed classified data base prior to the final hardware design to insure that all pertinent RFI pulse characteristics are properly modeled.

2. LinCsim PREDICTIONS OF SHUTTLE/TDRSS RETURN LINK BER PERFORMANCE

2.1 Introduction

The Shuttle return link communications hardware does not meet all the specifications set forth in the User Constraint Table of the TDRSS Users' Guide [1]. Since the TDRSS performance predictions are based on these interface parameter values they may not be applicable to the Shuttle links. In this chapter the performance sensitivity to these user constraint values is documented. The design point is based on the latest hardware data and user constraint values available. All data apply for a non-RFI environment.

Section 2.2 presents sensitivity data for the Shuttle/TDRSS S-band return link, Mode 2. Since this is the high rate mode it is more susceptible to most of the distortion effects and the resulting sensitivities are therefore an upper bound on the degradations in the low-rate mode. Section 2.3 presents the results for all three channels of the Ku-band return link, Mode 1.

2.2 Performance Prediction for Shuttle S-band Return Link

This section presents the sensitivity of the Shuttle S-band return link BER performance to variations of tne user constraint values based on current link budgets, nominal user constraint value estimates and TDRS/ground station hardware data.

The link characteristics assumed are summarized in Table 2.1. The nominal values of the user constraints are listed in Table 2.2. They agree with the expected Shuttle values obtained from JSC. The link budget is reproduced in Table 2.3. It is based on the budgets contained in Ref. 2 with some updates obtained from Dr Kwei Tu. Table 2.4 lists the user constraints whose effect on performance was studied.

Table 2.1. Shuttle S-band Return Link Characteristics Used for LinCsim

Data Rate	192 Kbps
Data Format	BPSK, Biphase, Unspread
Coding	Rate 1/3 Convolutional Code
Carrier	Noncoherent with Forward Link
Design Error Rate	10^{-4}

Table 2.2. Nominal User Constraint Values Used for LinCsim

Data Bit Jitter (3σ)	.6%
Modulator Phase Imbalance	11°
Modulator Gain Imbalance	.1 dB
Data Asymmetry	3.8%
Phase Nonlinearity	3°
Gain Flatness	.4 dB peak
Gain Slope	.1 dB/MHz
AM/PM	14°/dB
3 dB Bandwidth	100 MHz
Phase Noise	
1 Hz - 10 Hz	0°
10 Hz - 100 Hz	1°
100 Hz - 1 kHz	10°
1 kHz - 6 MHz	1°

Table 2.3. Shuttle S-Band Return Link Power Budget.

Shuttle-to-TDRS Link	
Shuttle EiRP	16.7 dBW
Space Loss	192.1 dB
Polarization Loss	.5 dB
TDRS G/T	9.55 dB/°K
TDRS-to-Ground Link	
TDRS TWT max Output Power	13.4 dBW
TWT Output Backoff	2 dB
SSA Power Allocation	-10 dB
TDRS Hardware Losses	2.46 dB
TDRS Antenna Gain	45.9 dB
Pointing Loss	.65 dB
Space Loss	207.7 dB
Polarization Loss	.1 dB
Atmospheric Loss	.8 dB
Ground Station G/T	40.3 dB/°K

Table 2.4. Parameters studied.

Modulator Gain Imbalance

Modulator Phase Imbalance

Data Asymmetry

Data Bit Jitter

Data Static Timing Offset

XTR AM/AM

XTR AM/PM

Static Phase Error

XTR Gain Slope

XTR Gain Flatness

XTR Phase Nonlinearity

Phase Noise R.M.S.

The results are shown in two different forms. The BER curves show the bit error probability as a function of Shuttle-to-TDRS link carrier-to-noise ratio (CNR) variation around the nominal link budget of Table 2.3. The horizontal distance between the bit error rate curve and the design point shown represents the margin in carrier-to-noise ratio which can be allocated to the various subsystems for hardware degradations. The sensitivity curves show the increase in the Shuttle-to-TDRSS CNR needed to offset the performance degradation (relative to the nominal performance) due to the variation of a single parameter at the design error rate of 10^{-4}.

The error rate curve in Fig. 2.1 represents the BER performance of a Shuttle transponder transmitting a perfect signal (i.e., all user constraints are set to zero). The CNR loss shown (.9 dB) can be attributed to the TDRS and the ground station. This BER curve is reproduced on all other BER plots and labeled "Perfect User." The horizontal distance between this curve and one of the other BER curves represents the CNR loss due to the combined effect of all the user constraints. For the nominal conditions this loss amounts to .75 dB.

Fig. 2.20 shows that by far the biggest contribution of degradation comes from the phase noise which is specified as 10° rms in the 0 to 270 Hz frequency range. As a worst-case assumption this noise power was concentrated in the 100-270 Hz range (i.e. outside the tracking loop bandwidth). A more accurate performance prediction could be made if the noise power inside and outside the tracking loop bandwidth were known separately.

Tables 2.5 and 2.6 contain a complete list of all nominal system parameters used in LinCsim, including those pertaining to the TDRS and TDRSS ground station.

Table2.5. Complete List of Simulation Parameters.

PARAMETER	PRESENT VALUE	WHERE OBTAINED	DATE OBTAINED	OLD VALUE	SOURCE OLD VALUE
DATA RATE - I				192 Kbps	S-805-1
DATA RATE - Q				0	S-805-1
POWER SPLIT				1: 0	S-805-1
MODULATOR PHASE IMBALANCE (BPSK)				±3°	S-805-1
REL. PHASE BETWEEN I&Q CHANNELS				NA	S-805-1
DATA ASYMMETRY				±3%	S-805-1
PN ASYMMETRY				NA	S-805-1
DATA SKEW				NA	S-805-1
PN SKEW				NA	S-805-1
MODULATOR GAIN IMBALANCE				±0.25 dB	S-805-1
XTR GAIN FLATNESS				±0.3 dB	S-805-1
XTR GAIN SLOPE				±0.1dB/MHz	S-805-1
XTR PHASE NON-LINEARITY				±3°	S-805-1
XT FILTER BW				1.2 MHz	S-805-1
XT FILTER ORDER				4	LinCom estimate
XT FILTER RIPPLE				0.1 dB	LinCom estimate
XTR AM/AM				1 dB/dB	LinCom estimate
XTR AM/PM				12°/dB	LinCom estimate
TDRS TWT MAX AM/PM				10° /dB	LinCom estimate
TDRS TWT AM/AM				0 dB/dB	LinCom estimate
TDRS TWT AM/PM				6°/dB	LinCom estimate
TDRS FRONT END FILTER BW				10 MHz	LinCom estimate
ORDER				4	LinCom estimate
RIPPLE				0.1	LinCom estimate
TDRS TRANSMIT FILTER BW				621 MHz	LinCom estimate
ORDER				2	LinCom estimate
RIPPLE				0.2	LinCom estimate
PN TIMING OFFSET				1%	LinCom estimate
PN TIMING JITTER				1° peak	S-805-1
DATA TIMINGOFFSET				1%	LinCom estimate
DATA TIMINGJITTER				1% peak	S-805-1

Table 2.6. Complete List of Simulation Parameters.

PARAMETER	PRESENT VALUE	WHERE OBTAINED	DATE OBTAINED	OLD VALUE	SOURCE OLD VALUE
	LINK BUDGET				
XTR EIRP: UNCODED DATA				--	--
XTR EIRP: CODED DATA				19.2 dBW	SS Circuit Margin,3/77
SPACE LOSS				-192.1	SS Circuit Margin,3/77
POLARIZATION LOSS				0.5 dB	SS Circuit Margin,3/77
ATMOSPHERIC LOSS				0 dB	SS Circuit Margin,3/77
TDRS G/T	9.55(nomina)	TPM	3/78	8.3 dB/°K	SS Circuit Margin,3/77
TDRS TWT MAX OUTPUT POWER	13.4 dB	TPM	3/78	12.5 dBW	WU Proposal,7/76
TDRS TWT OUTPUT BACKOFF	2.0 dB	TPM	3/78	2.0 dBW	WU Proposal, 7/76
POWER ALLOCATION	-10.0 dB	TPM	3/78	-9.9 dBW	WU Proposal, 7/76
CHANNEL POWER	1.4 dB	TPM	3/78	0.6 dBW	WU Proposal,7/76
TDRS HARDWARE LOSS	2.46 dB	TPM	3/78	1.7 dB	WU Proposal, 7/76
TDRS ANTENNA GAIN	45.90 dB	TPM	3/78	41.3 dB	WU Proposal, 7/76
POINTING LOSS	0.65 dB	TPM	3/78	0.7 dB	WU Proposal, 7/76
SPACE LOSS				207.7 dB	WU Proposal, 7/76
POLARIZATION LOSS				0.1 dB	WU Proposal, 7/76
ATMOSPHERIC LOSS				0.8 dB	WU Proposal, 7/76
RX ANTENNA G/T				40.3 dB	WU Proposal, 7/76
	PHASE NOISE BUDGET				
XT OSC,COHERENT TURNAROUND					
1 to 10 Hz				1° rms	S-805-1
10 Hz to 1 kHz				1° rms	S-805-1
1 kHz to 6 MHz				1° rms	S-805-1
XT OSC NONCOHERENT TURNAROUND					
1 to 10 Hz				2° rms	S-805-1
10 to 100 Hz				1° rms	S-805-1
100 Hz to 1 kHz				1° rms	S-805-1
1 kHz to 6 MHz				1° rms	S-805-1
TDRS OSCILLATORS	3.2°rms	TPM	3/78	3°	S-805-1
RX OSCILLATORS				1°	S-805-1
RX CARRIER TRACKING LOOP					
STATIC PHASE ERROR				3°	LinCom Estimate
BANDWIDTH				40 Hz	TPM, 8/77
DAMPING				2	LinCom Estimate
SQUARING LOSS				2 dB	LinCom Estimate

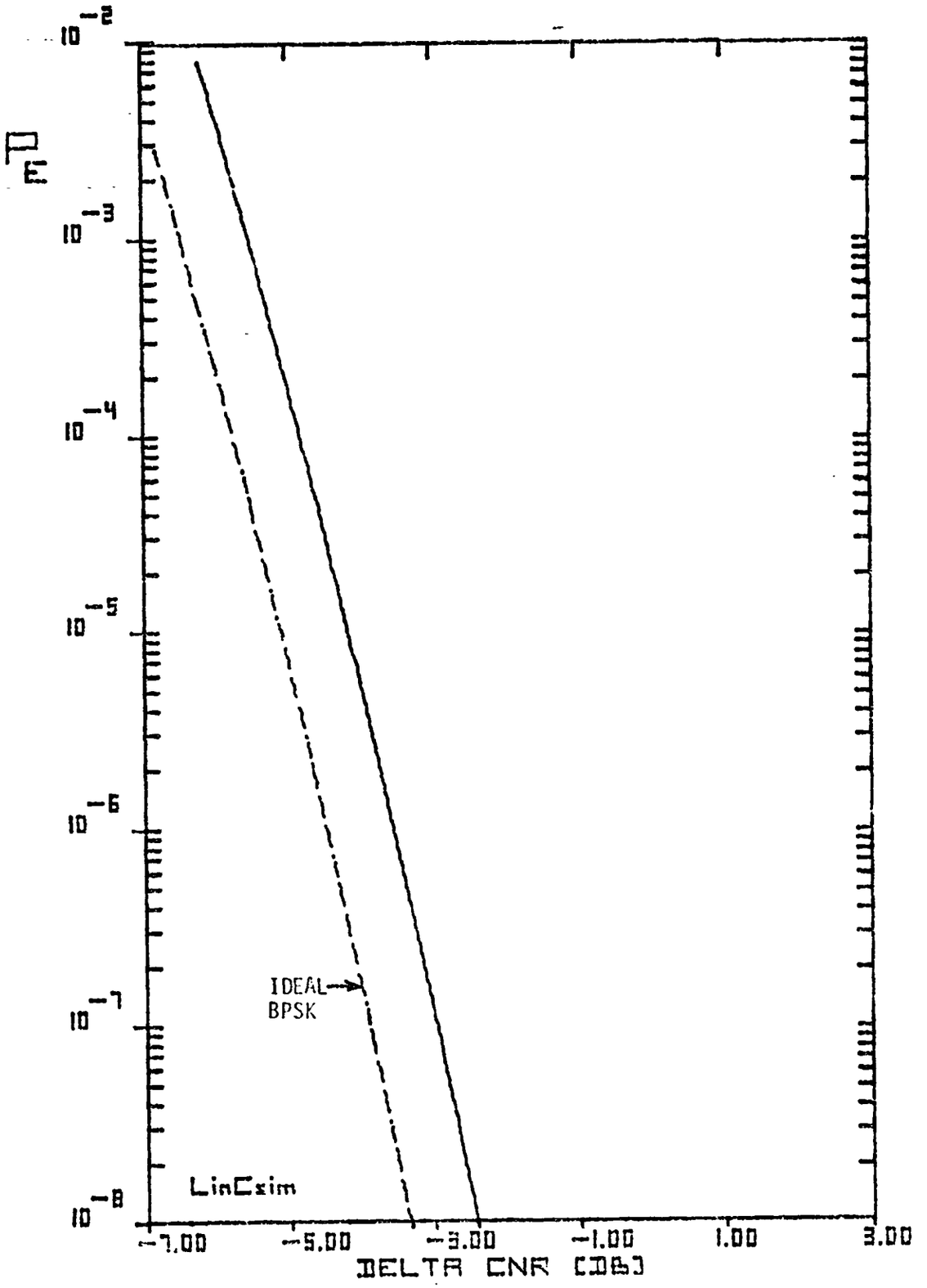

Figure 2.1.BER Plot for Perfect Shuttle Transmitter.

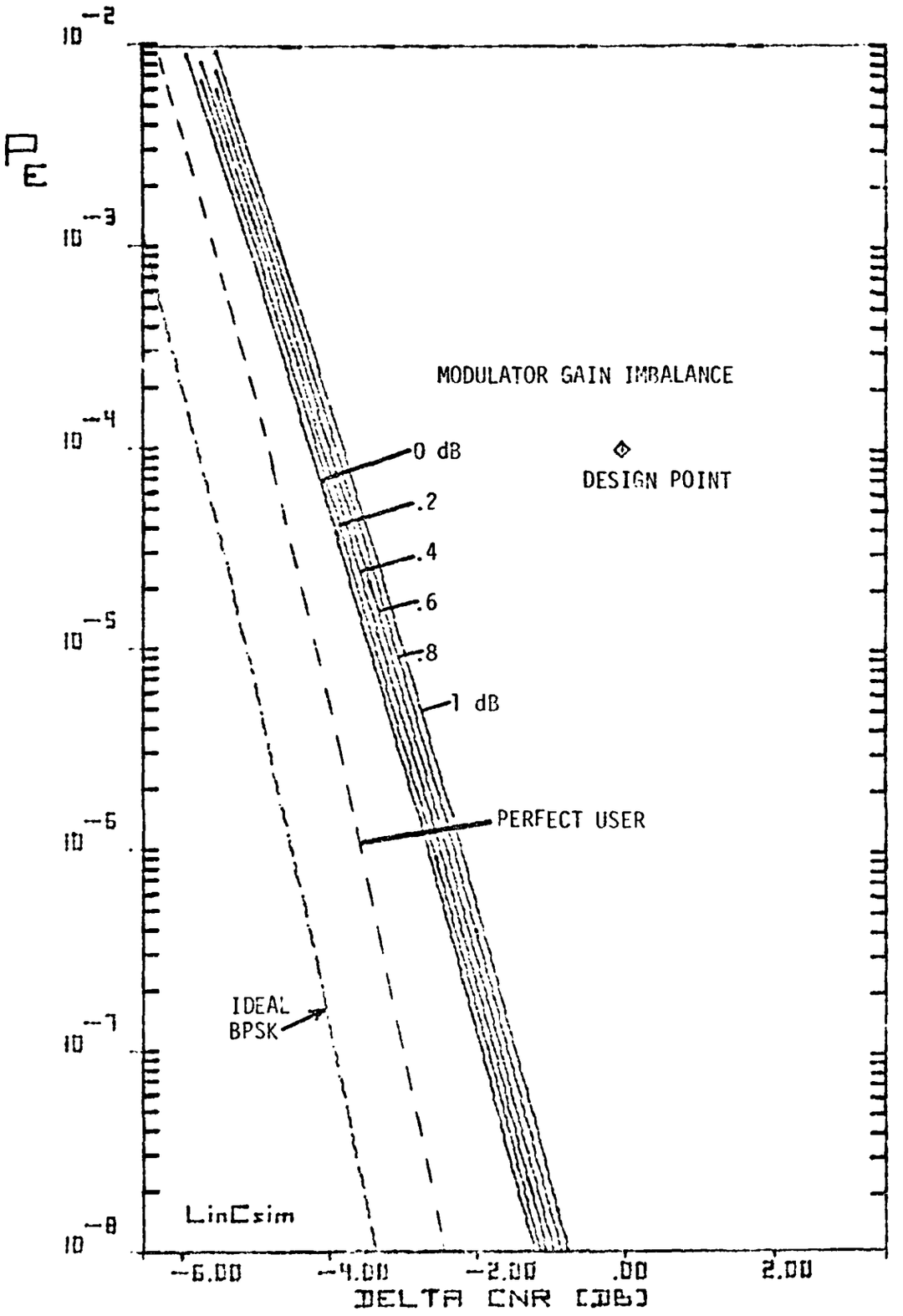

Figure 2.2. BER Plot for Gain Imbalance.

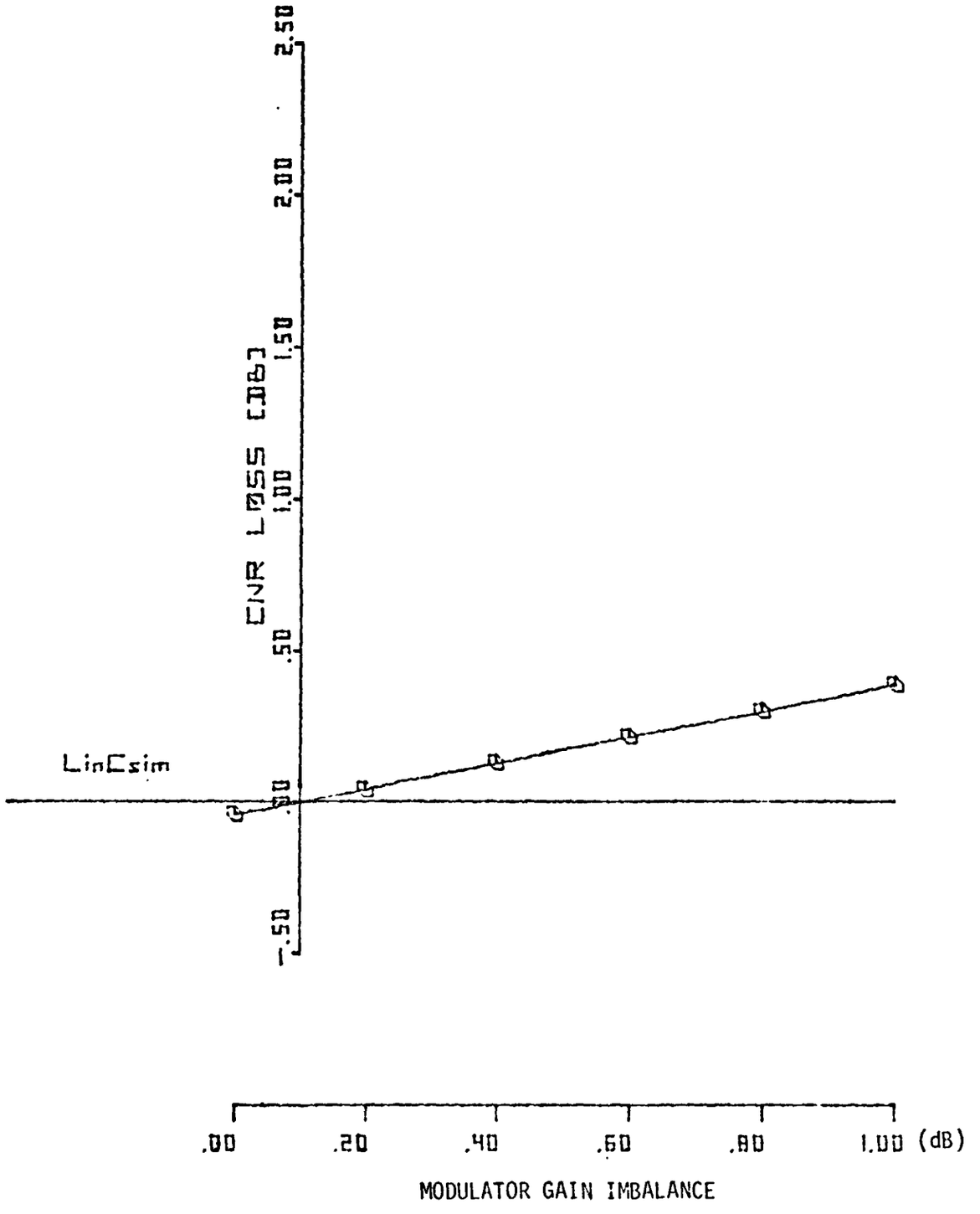

Figure 2.3. Sensitivity Curve.

79 0051

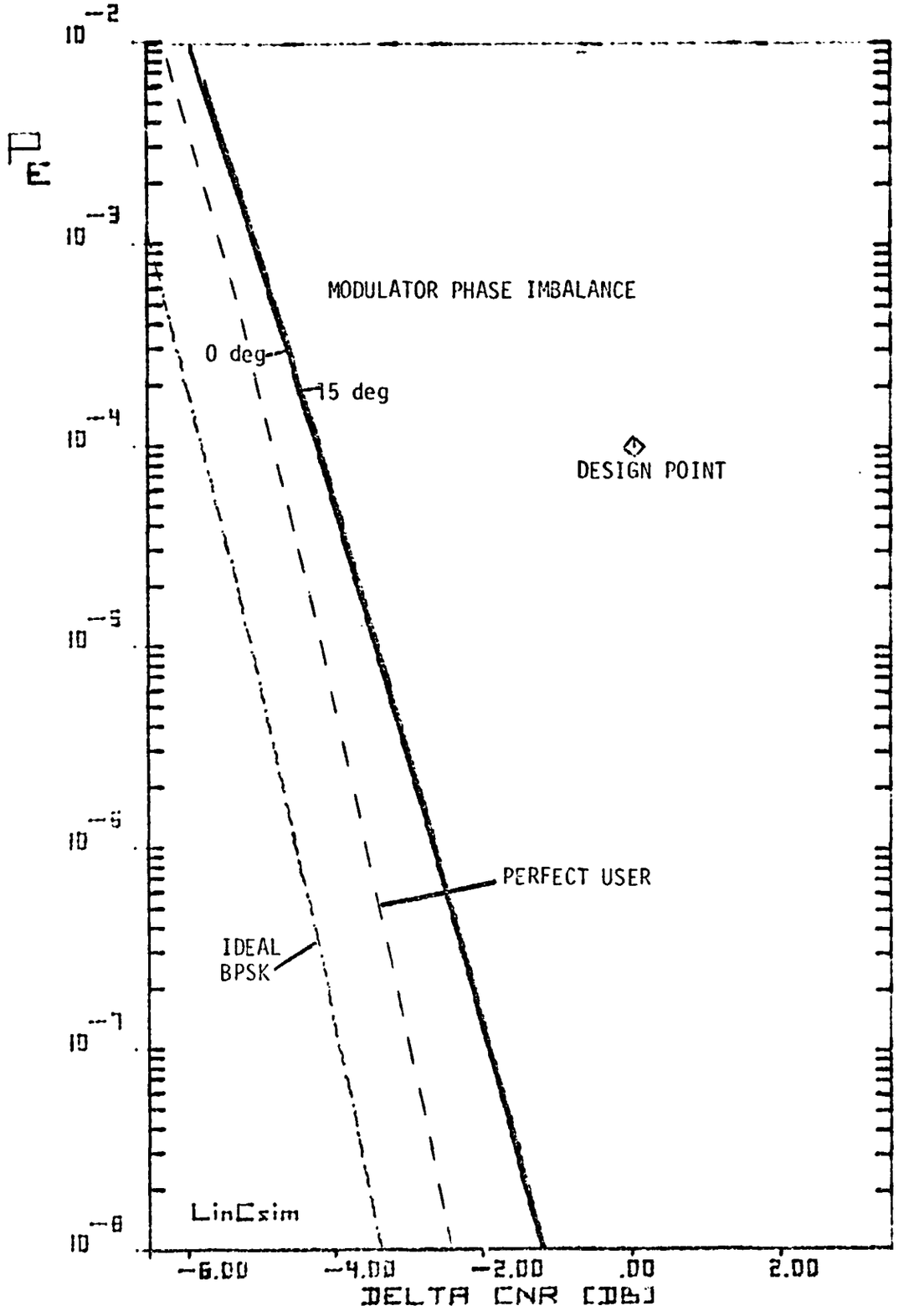

Figure 2.4.BER Plot for Phase Imbalance.

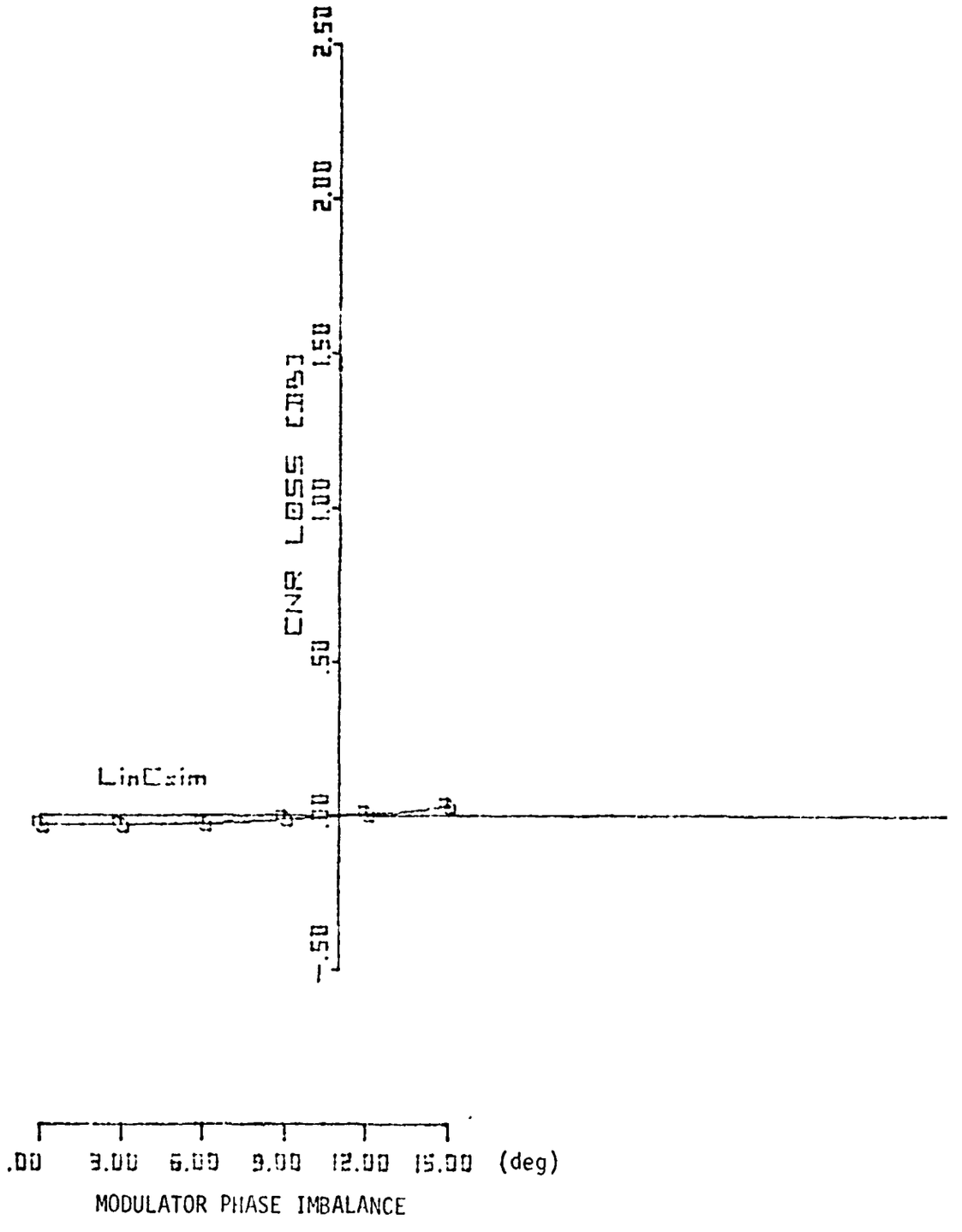

Figure 2.5 Sensitivity Curve.

79 0853

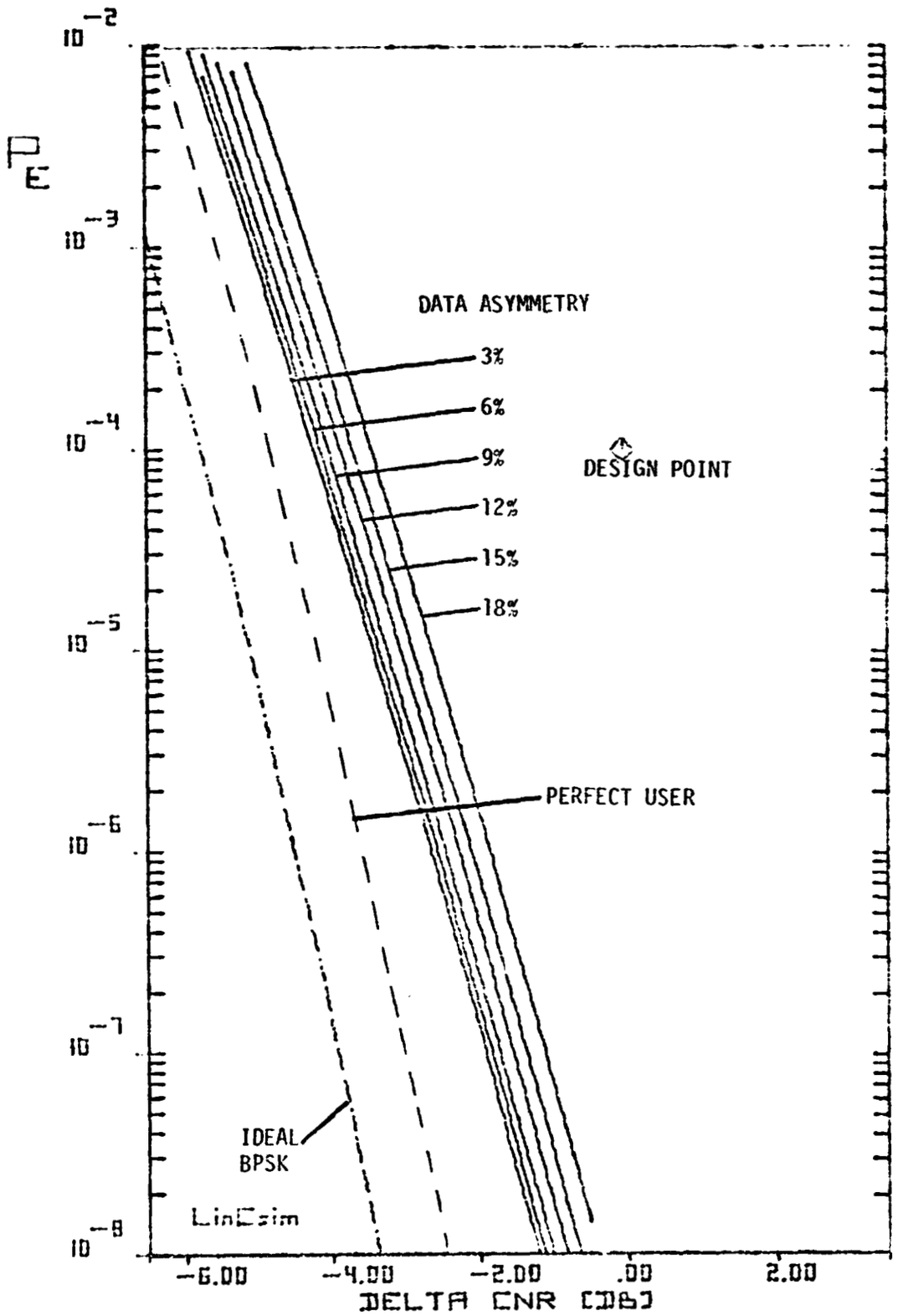

Figure 2.6. BER Plot for Data Asymmetry.

79 0054

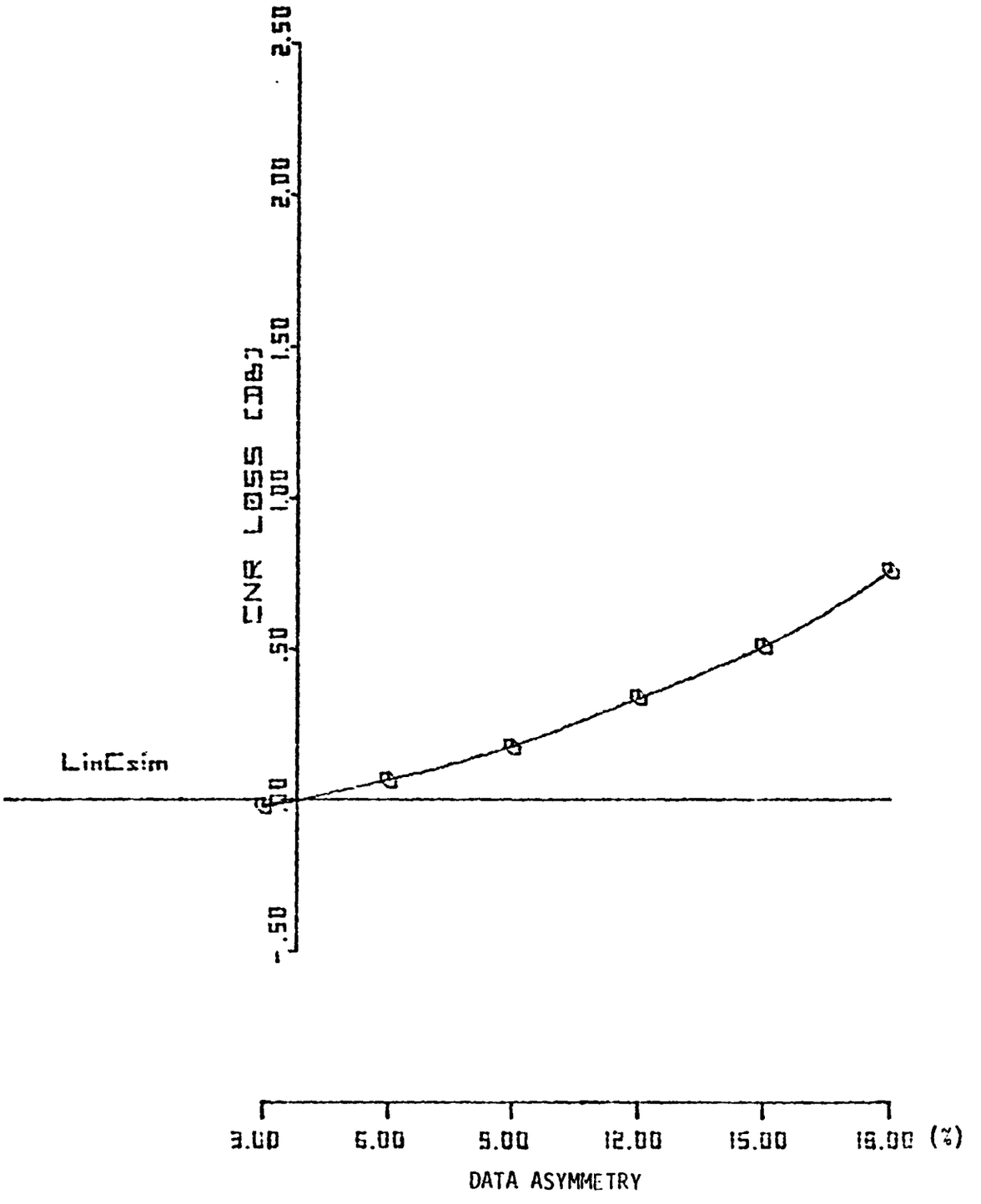

Figure 2.7. Sensitivity Curve.

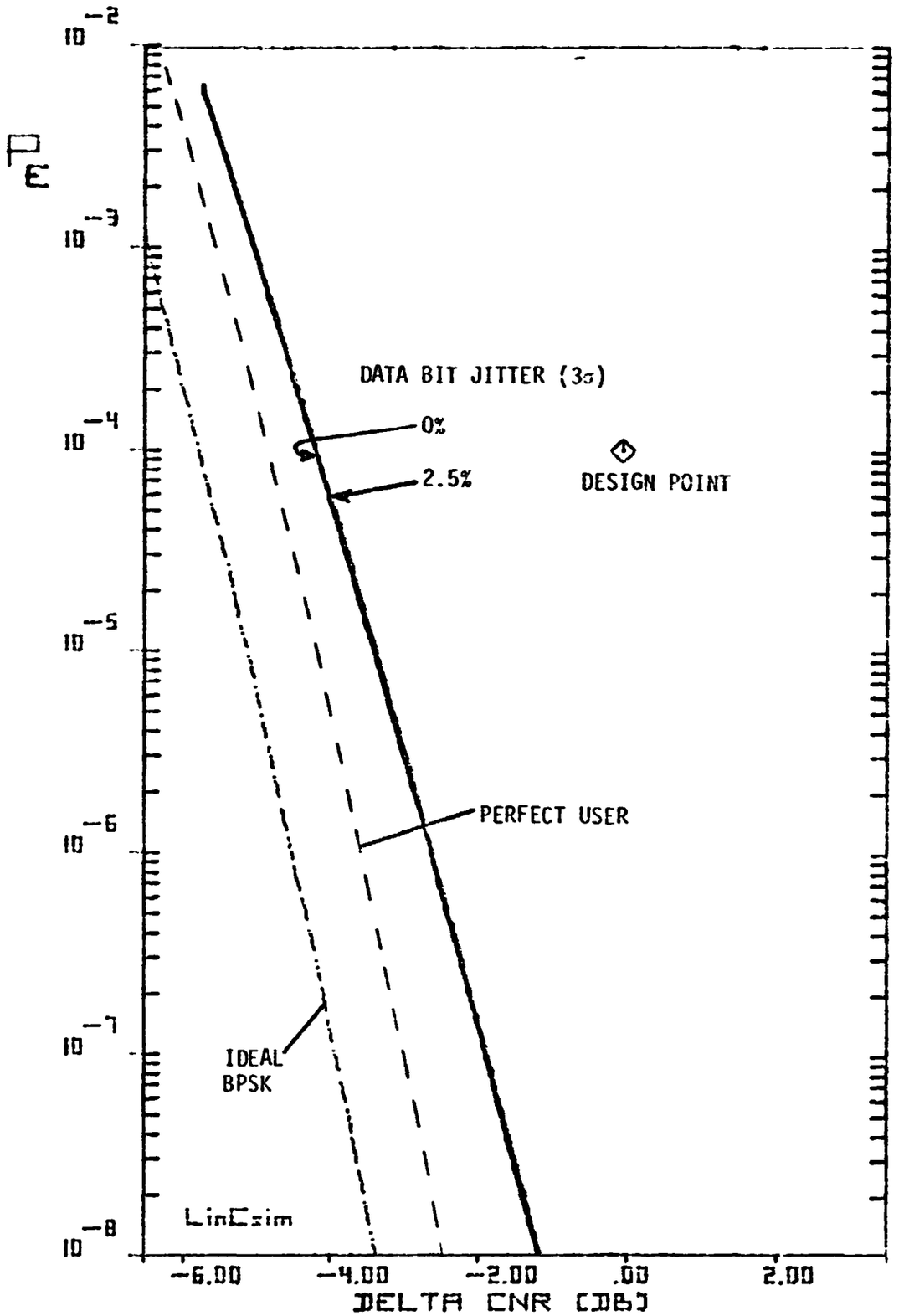

Figure 2.8. BER Plot for Bit Jitter.

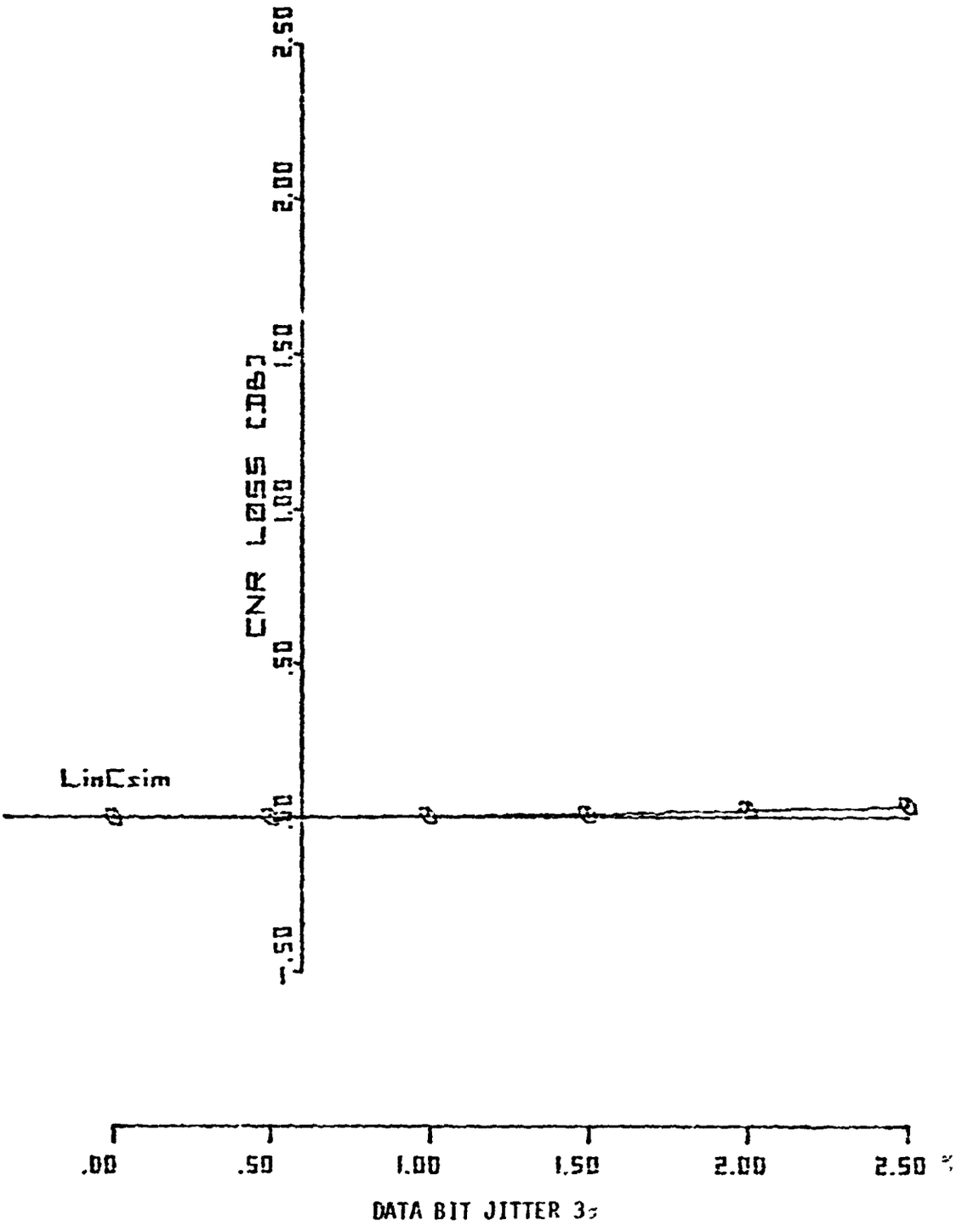

Figure 2.9 .Sensitivity Curve.

79 0857

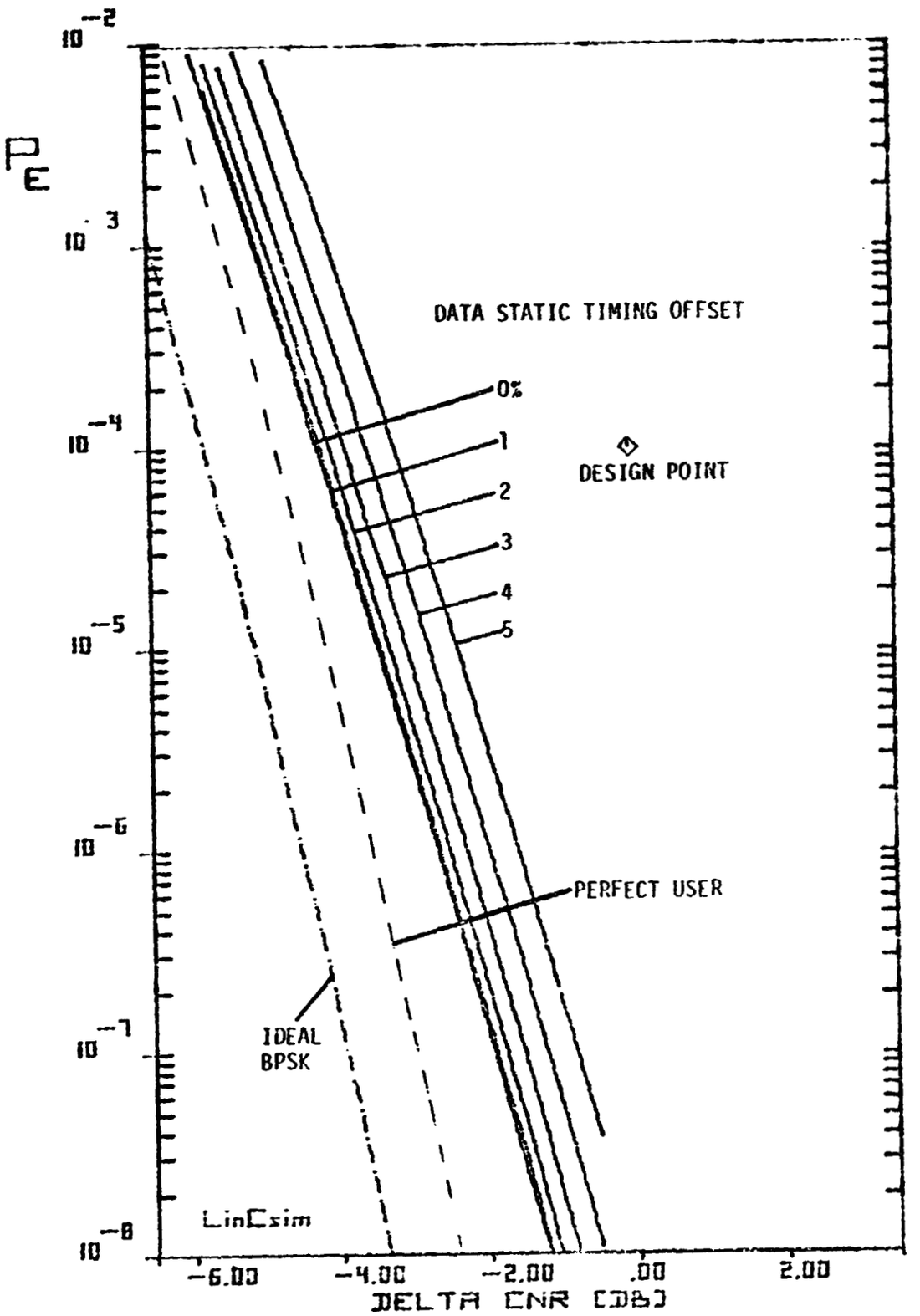

Figure 2.10 BER Plot for Timing Offset.

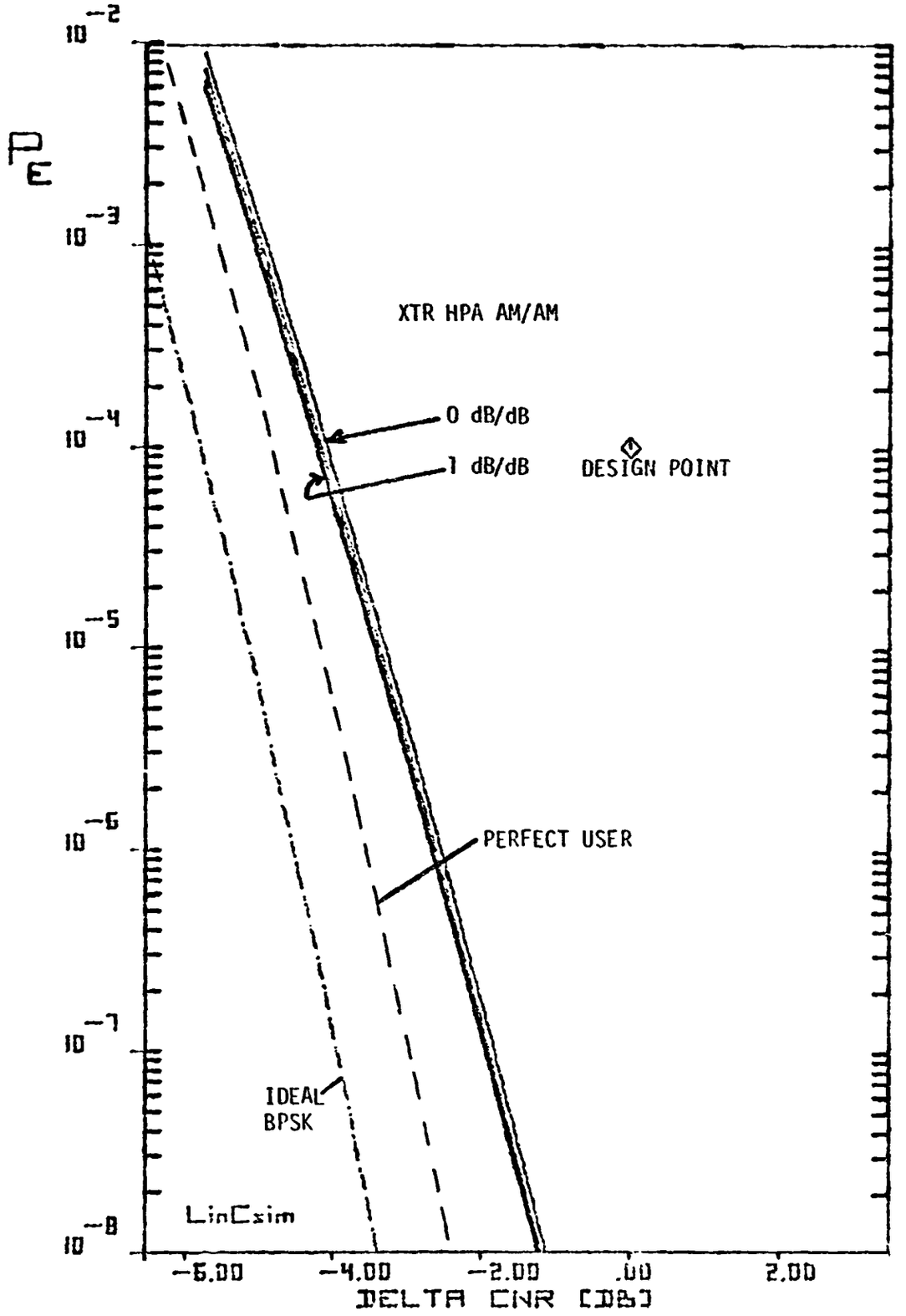

Figure 2.11.BER Plot for AM/AM.

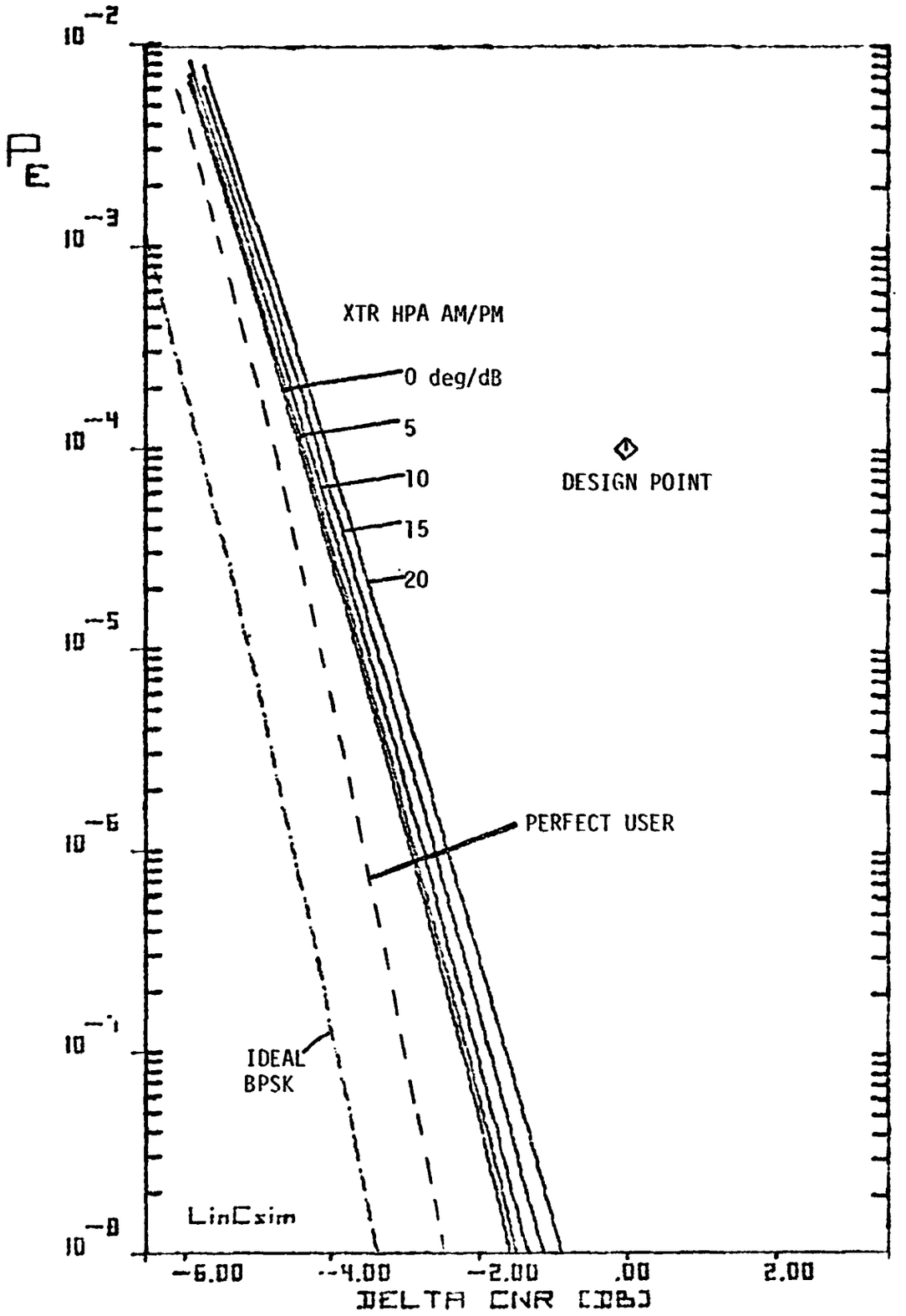

Figure 2.12. BER Plot for AM/PM

79 0030

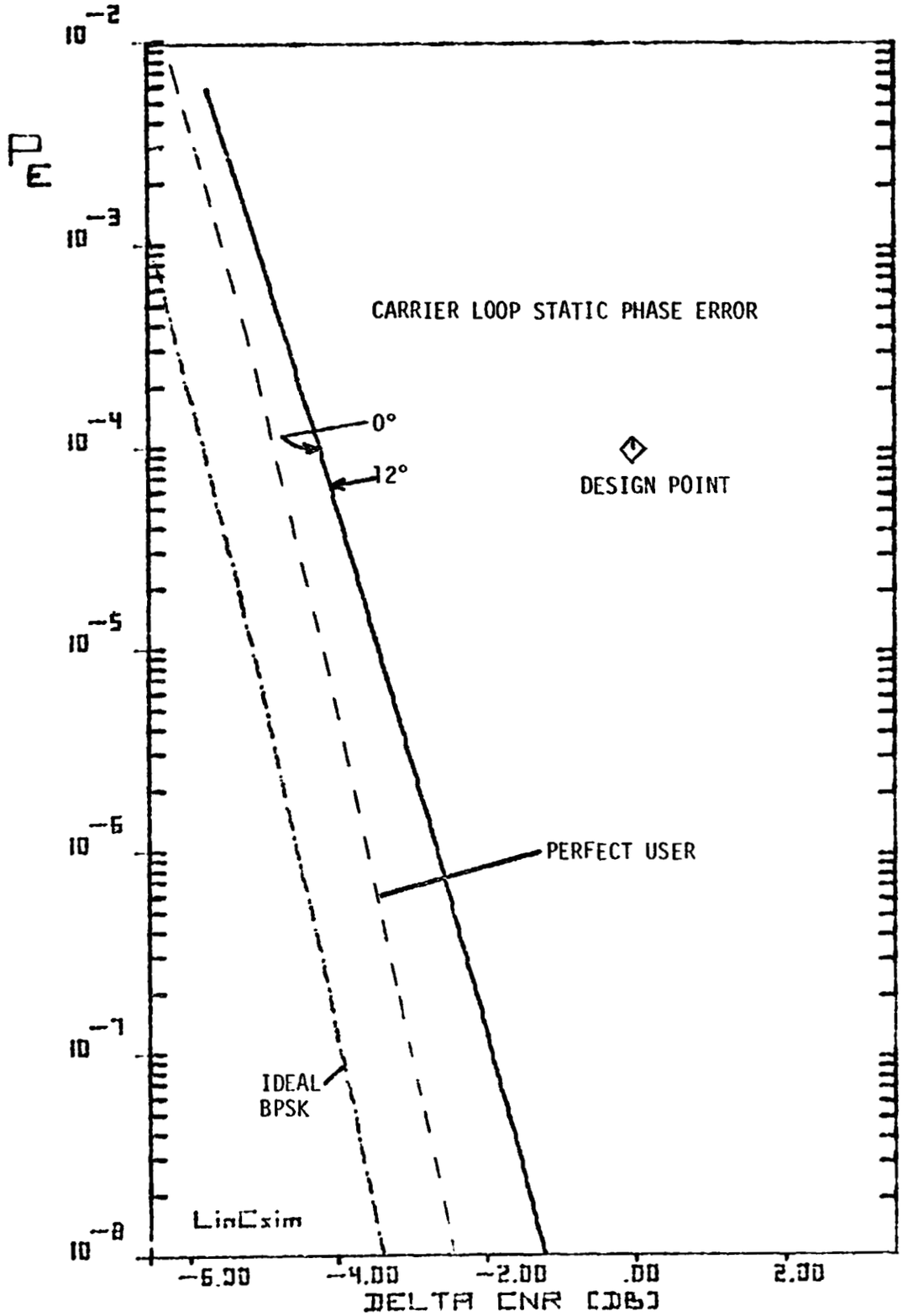

Figure 2.13.BER Plot for Static Phase Error.

79 0061

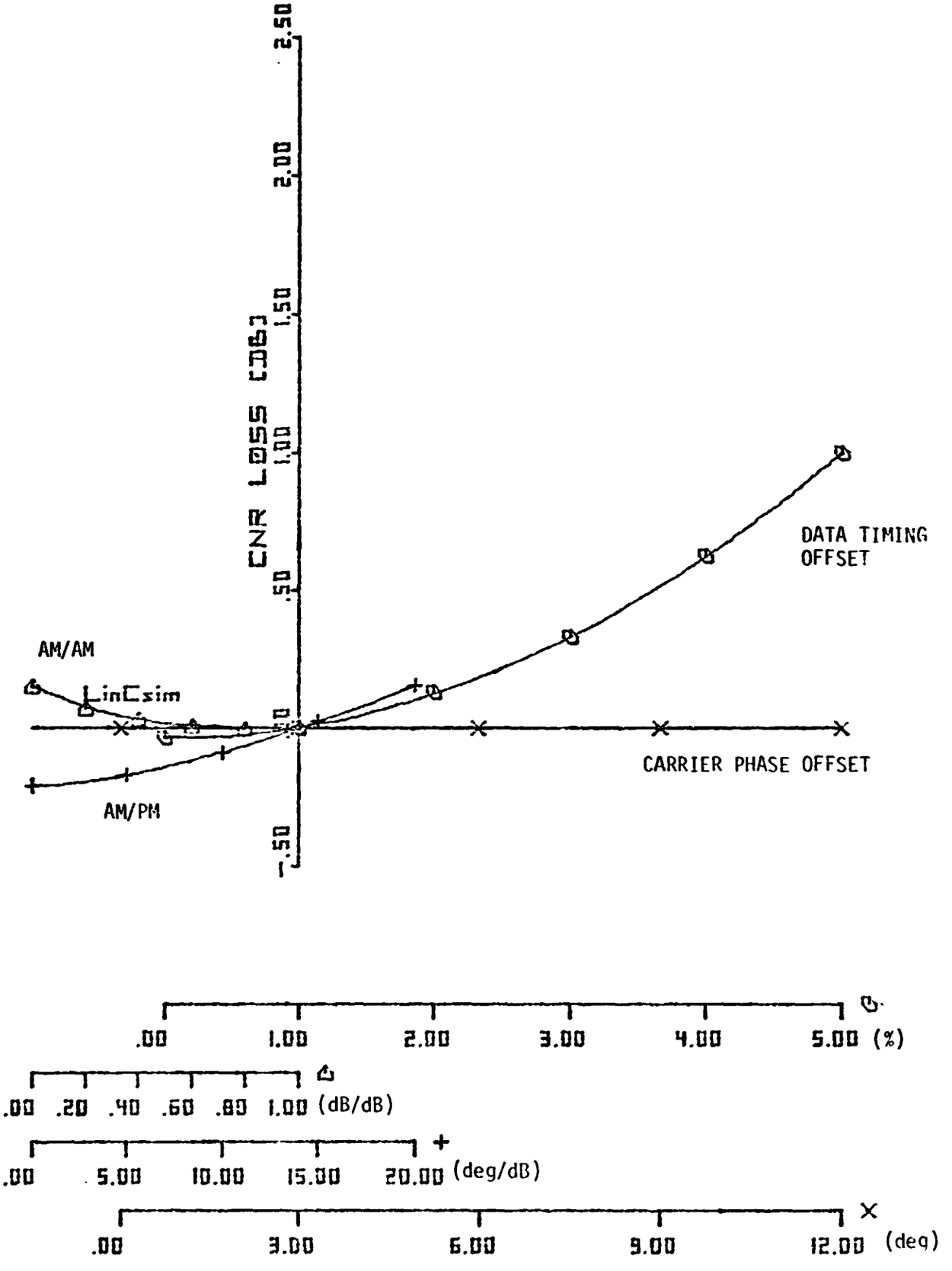

Figure 2.14. Sensitivity Curves.

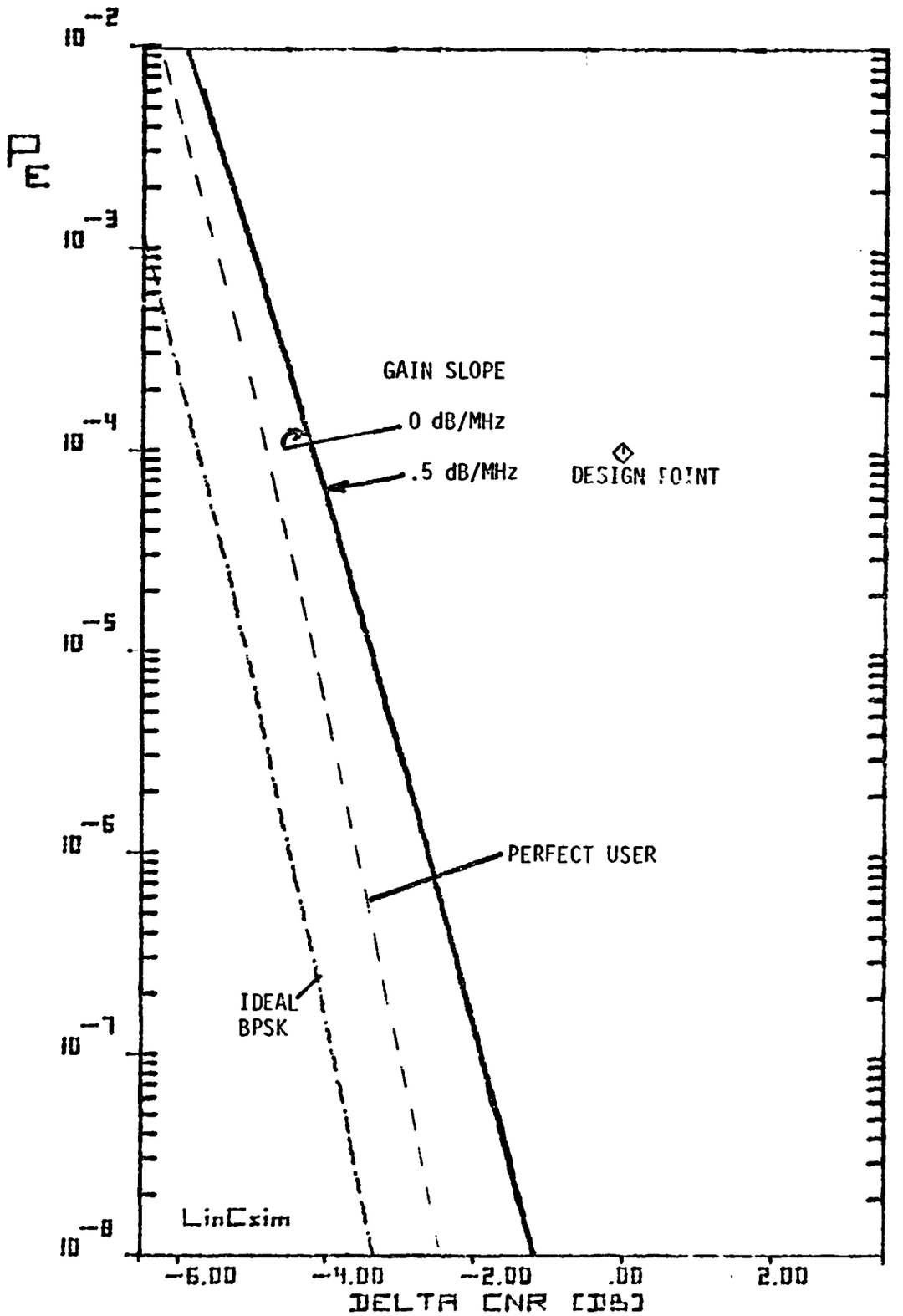

Figure 2.15. BER Plot for Gain Slope.

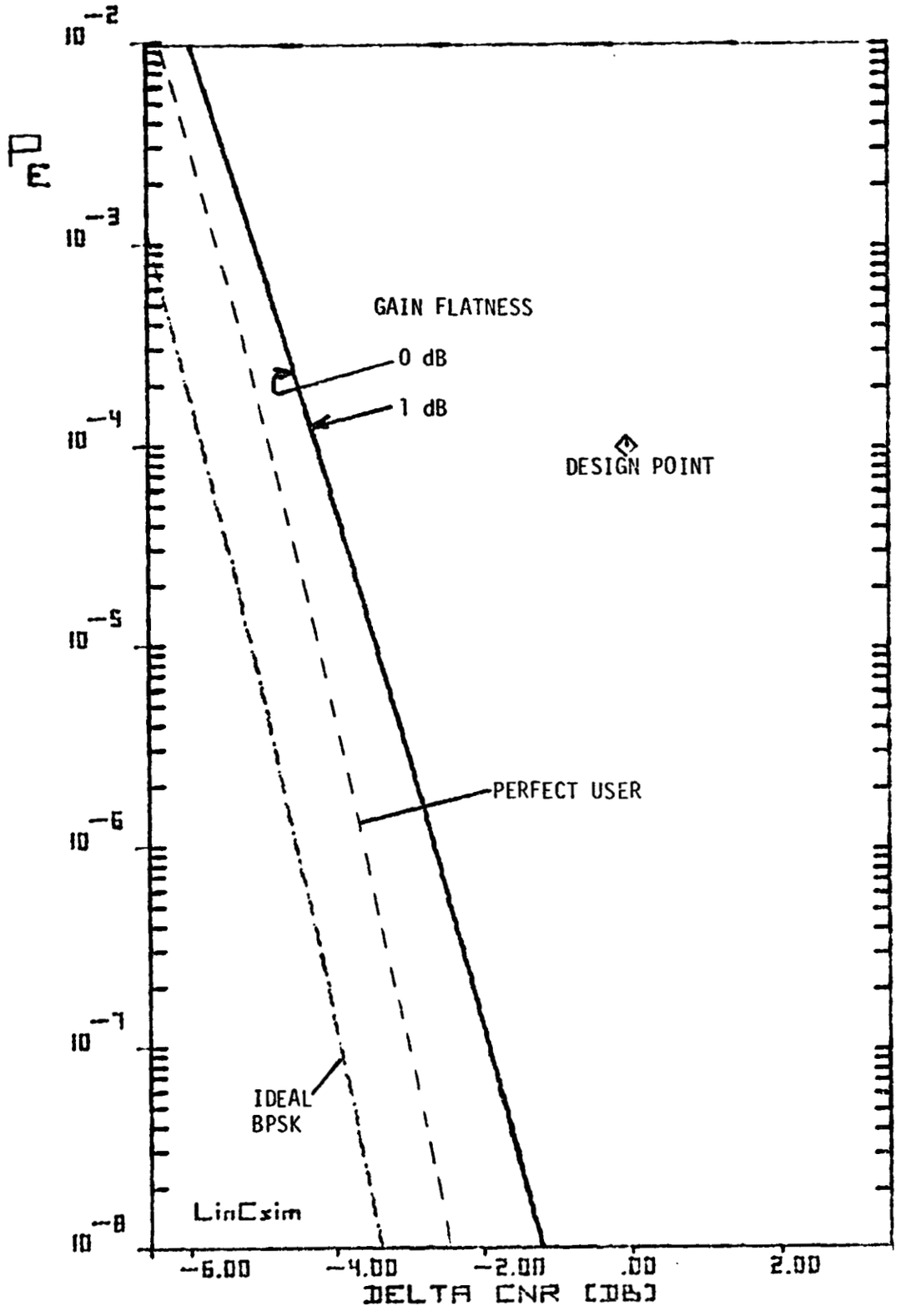

Figure 2.16.BER Plot for Gain Flatness.

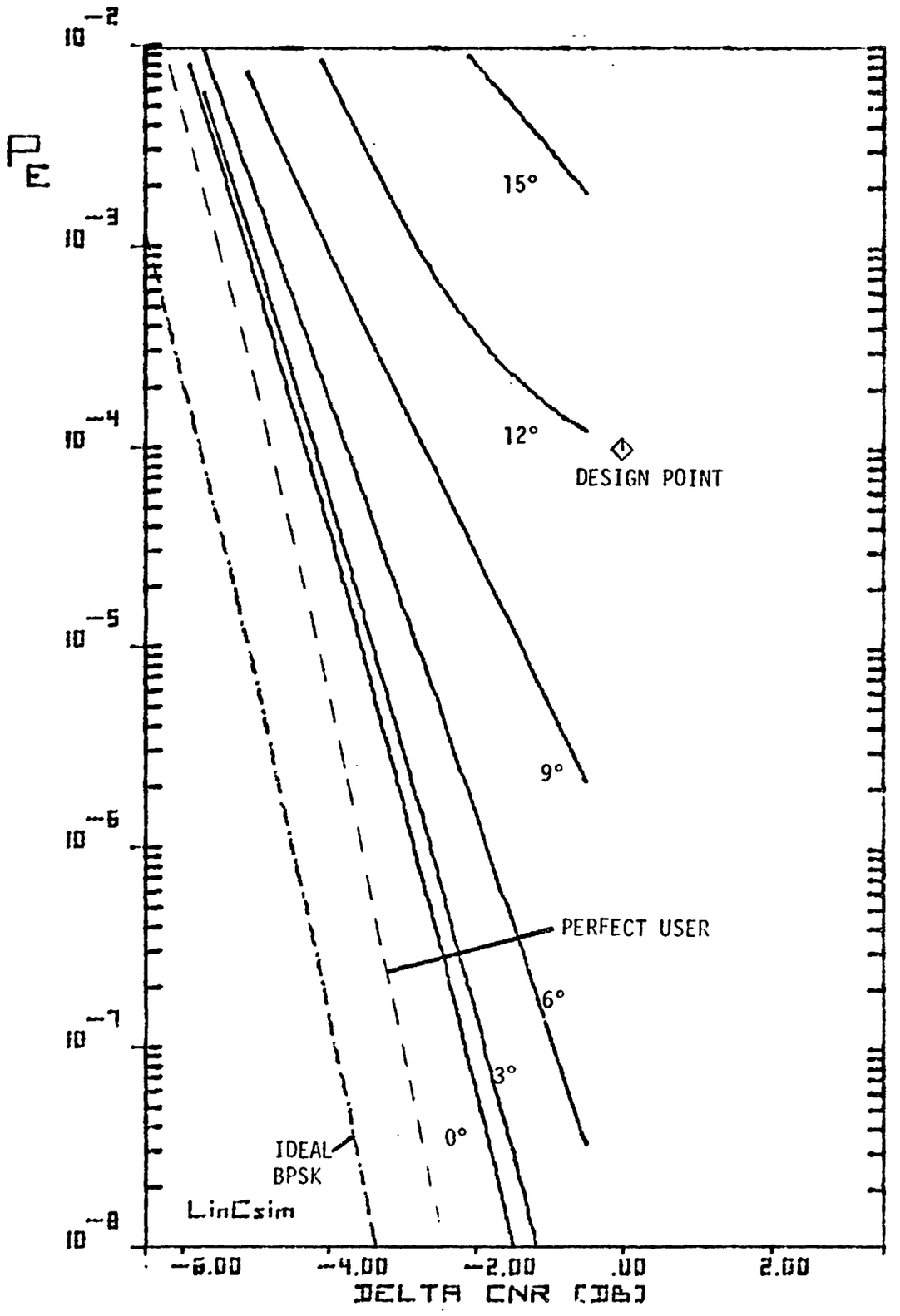

Figure 2.17.BER Plot for Phase Nonlinearity.

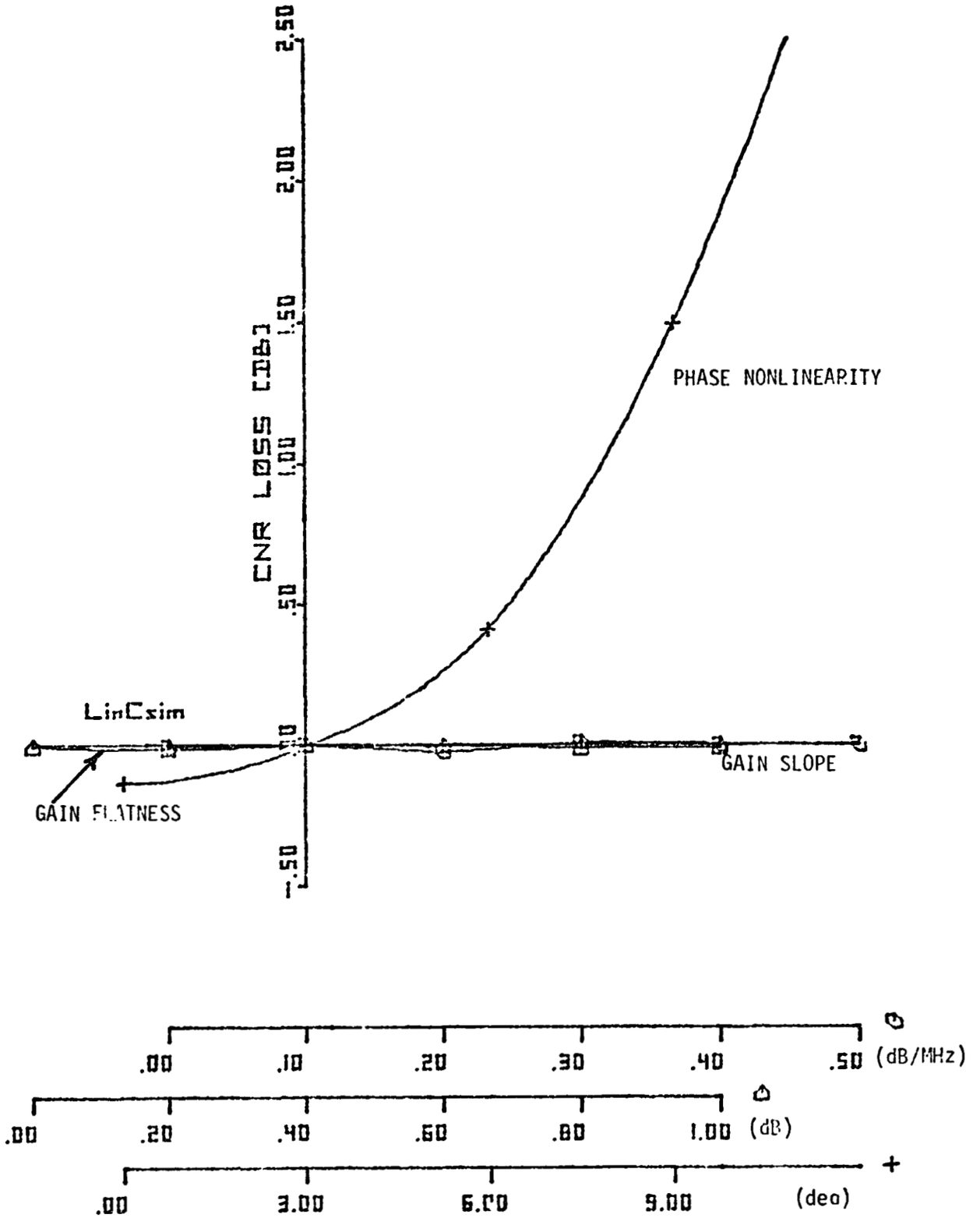

Figure 2.18. Sensitivity Curves.

79 0066

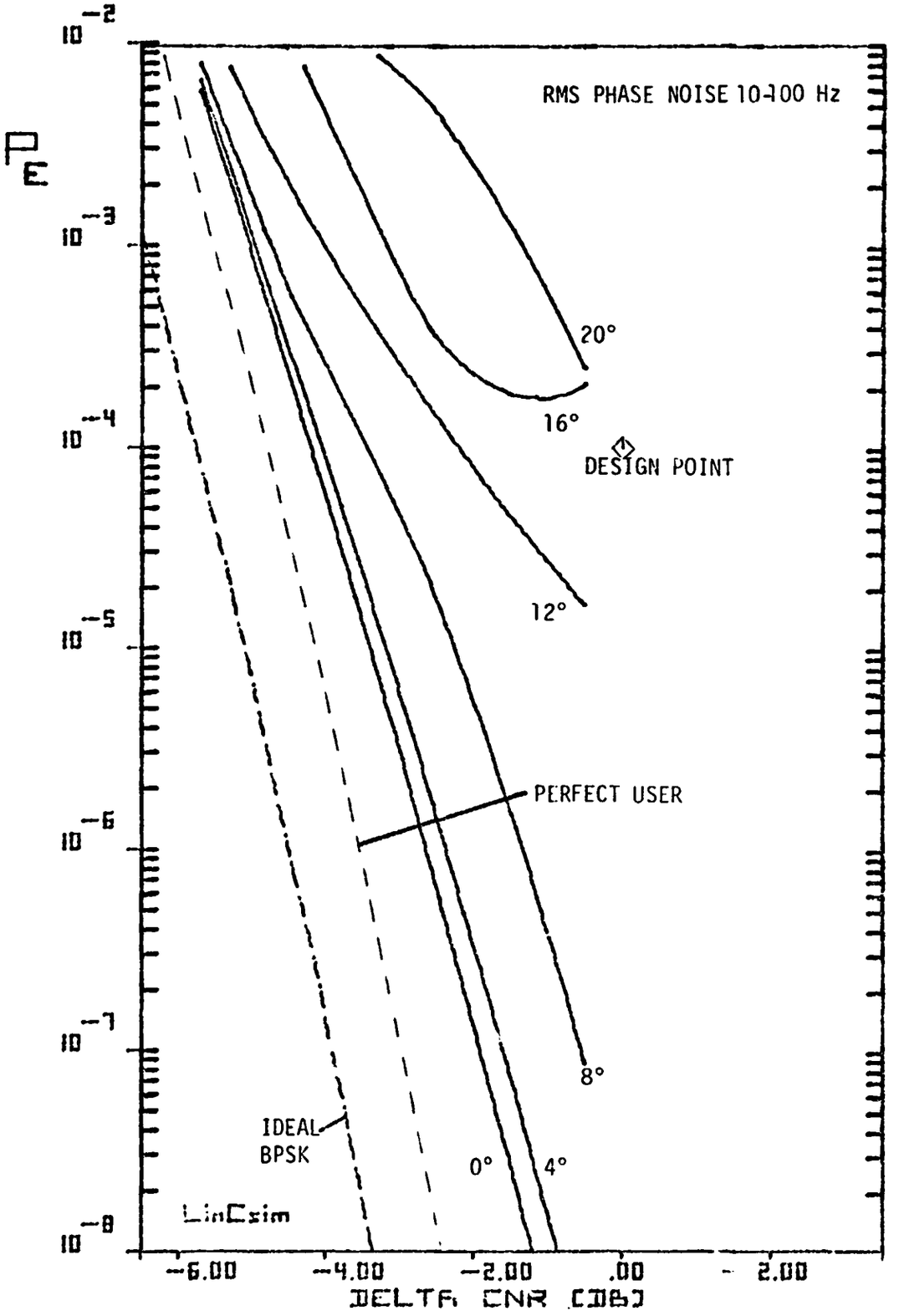

Figure 2.19.BER Plot for Low Frequency Phase Noise.

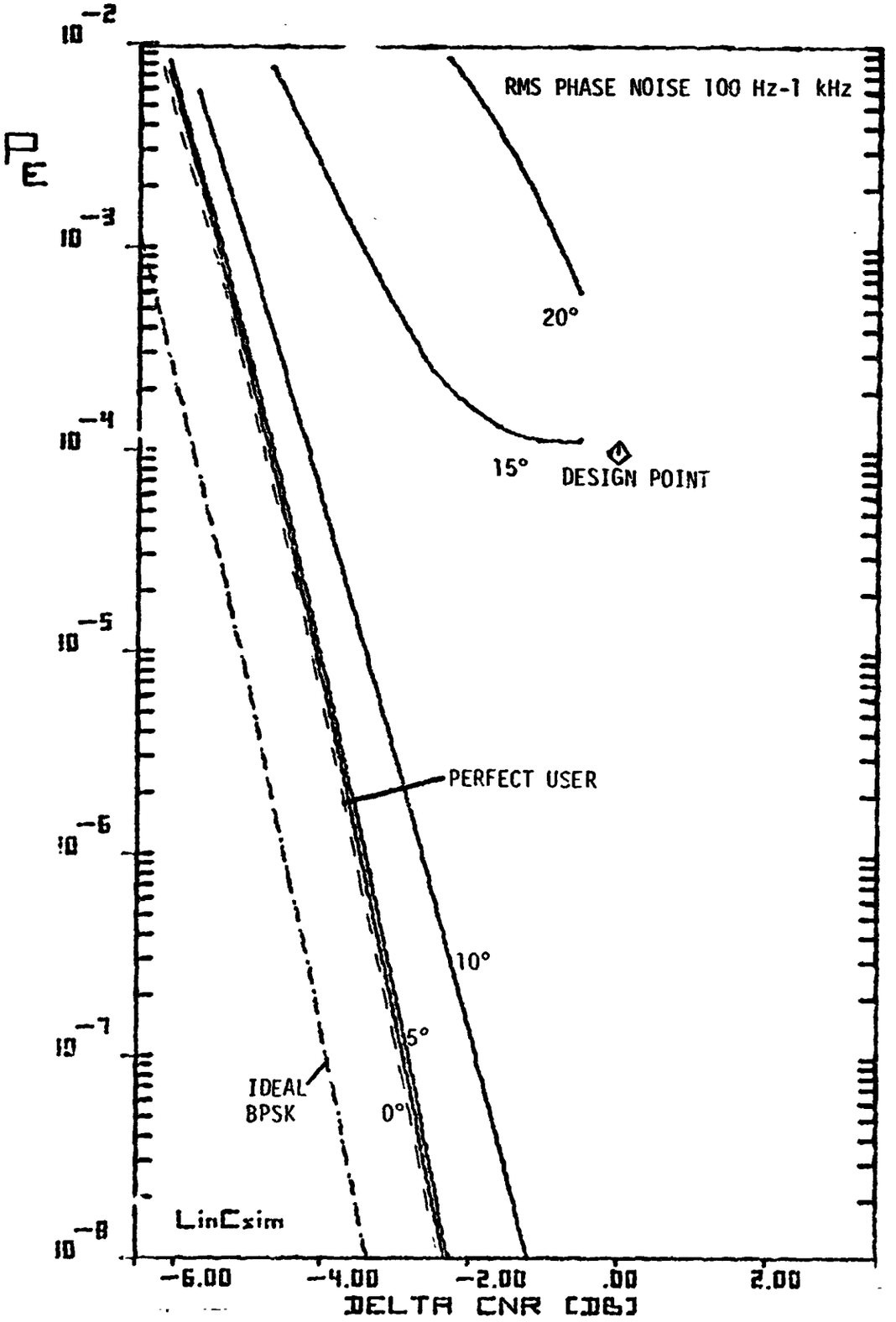

Figure 2.20. BER Plot for Medium Frequency Phase Noise.

79 0868

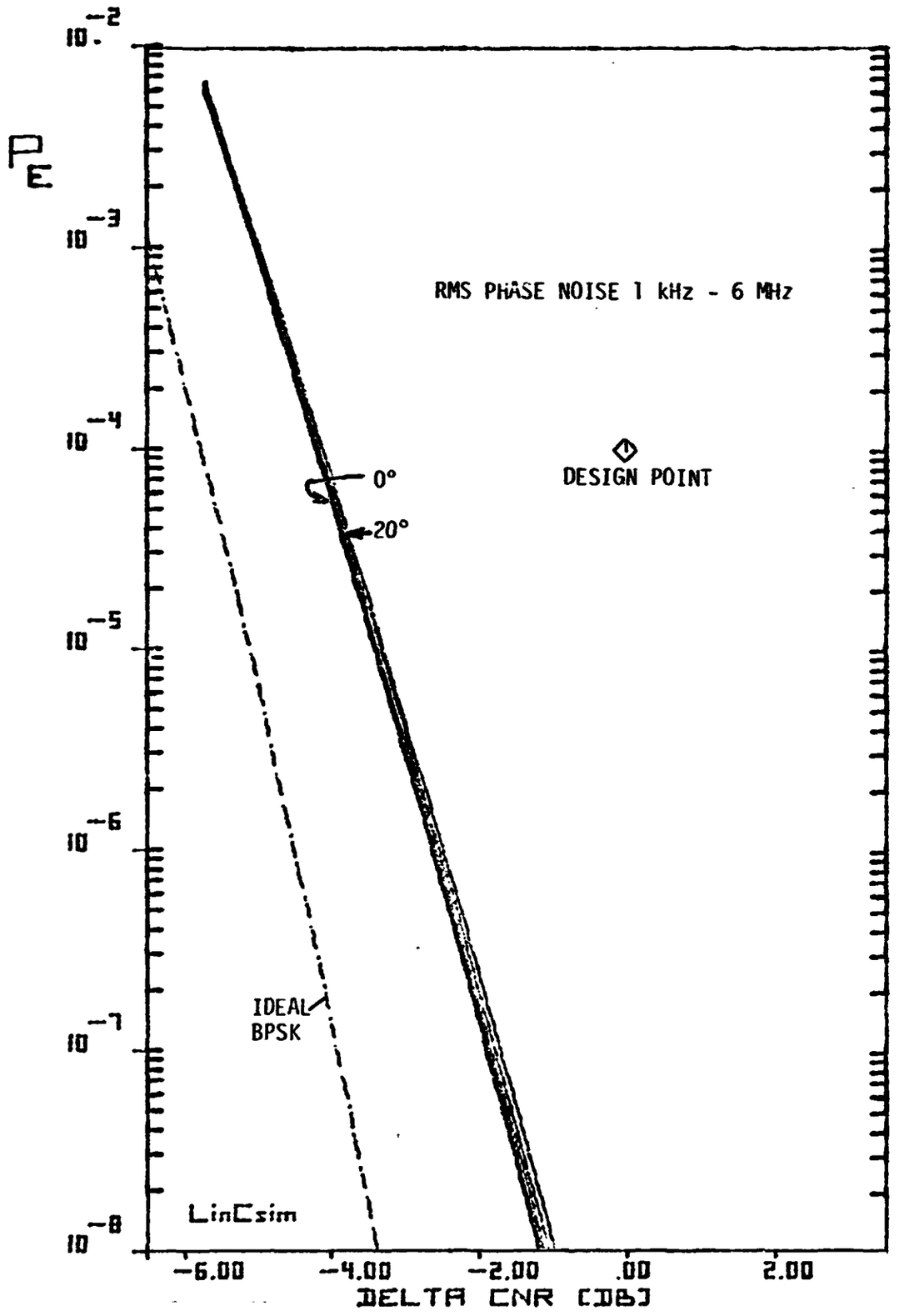

Figure 2.21. BER Plot for High Frequency Noise.

79 0069

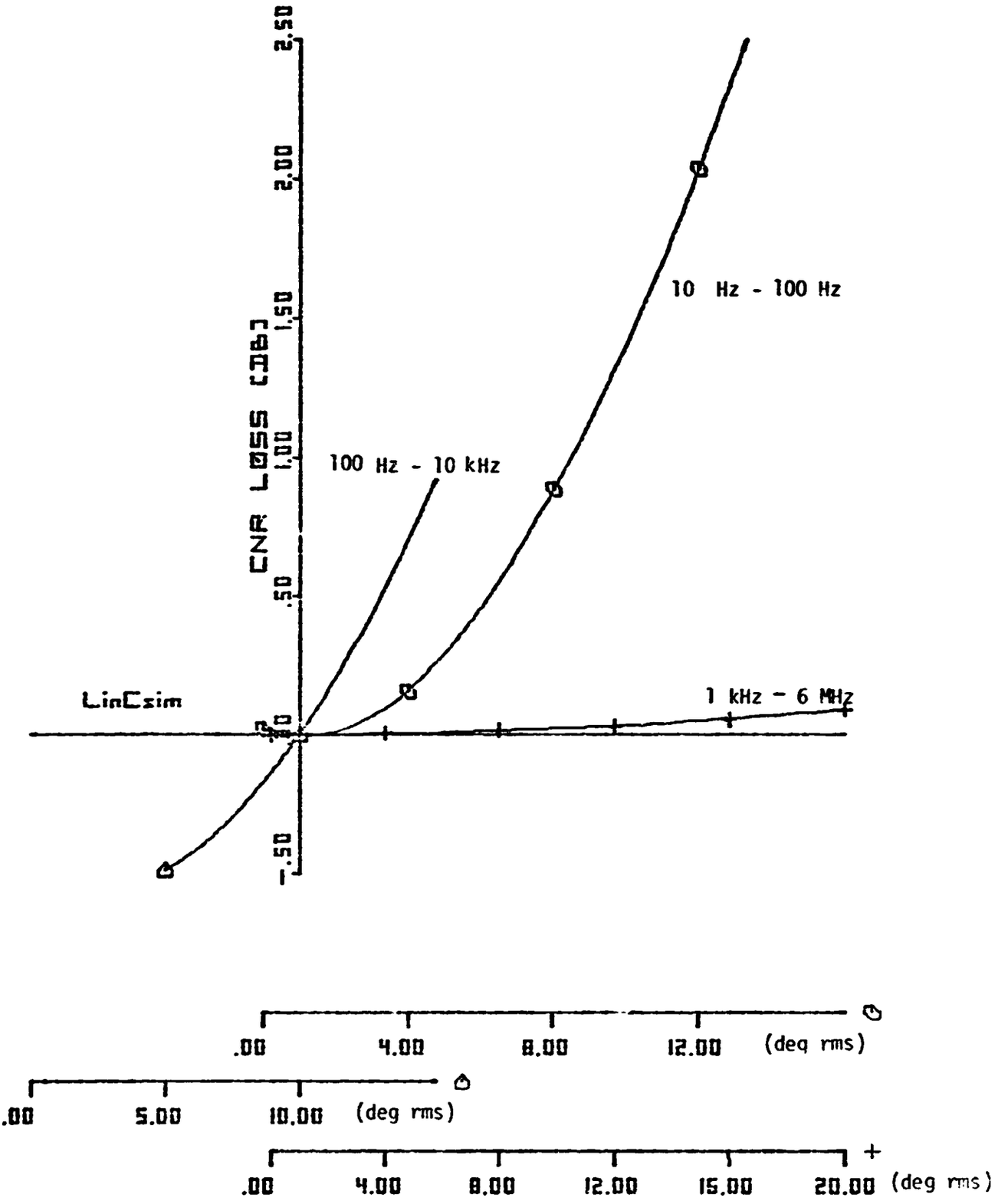

Figure 2.22. Sensitivity Curves for Phase Noise.

79 0070

2.3 Performance Prediction for Snuttle Ku-Band Return Link, Mode 1

This section presents the sensitivity of the Shuttle/TDRSS Ku-band return link BER performance to variations of the user constraint values. The all-digital mode 1 is considered and results are given for all three data channels. The link characteristics assumed are summarized in Table 2.7. The nominal values of the user constraints are listed in Table 2.8. They agree with the expected Shuttle values whereever such data were available from JSC. The link dubget is reproduced in Table 2.9; it is based on Ref. 2. Table 2.10 lists the user constraints whose effect on performance was studied.

The results are shown in two different forms. The BER plots show the bit error probability as a function of the Shuttle-to-TDRS link carrier-to-noise ratio (CNR) variation around the nominal link budget of Table 2.9. The horizontal distance between the bit error rate curve and the design point shown represents the margin in carrier-to-noise ratio which can be allocated to the various subsystems for hardware degradations. The sensitivity curves show the increase in Shuttle-to-TDRSS CNR needed to offset the performance degradation (relative to the nominal performance) due to the variation of a single parameter at the design error rate of 10^{-6}.

The error rate curves in Figs. 2.23, 2.40 and 2.57 represent the BER performance of channels 1, 2, and 3, respectively, for a Shuttle transponder transmitting a perfect signal (i.e. all user constraints are set to zero). The CNR loss shown (Table 2.11) can be attributed to the TDRS and the ground station. This BER curve is reproduced on all other BER plots and labeled "Perfect Shuttle." The horizontal distance

between this curve and one of the other BER curves represents the CNR loss due to the combined effect of all the user constraints. For the nominal conditions this loss is shown in Table 4.11. Table 4.12 lists the major contributors to this loss for each of the three channels.

Table 4.13 contains a complete list of all nominal system parameters used in LinCsim, including those pertaining to the TDRS and TDRSS ground station.

Table 2.7. Shuttle Ku-Band Return Link Characteristics Used for LinCsim.

Data Rate	Channel 1	192 kb/sec
	Channel 2	2 Mb/sec
	Channel 3	50 Mb/sec
Data Format	Channel 1	Bi-phase
	Channel 2	NRZ
	Channel 3	NRZ
Coding	Channel 1	none
	Channel 2	none
	Channel 3	rate 1/2
Carrier		Noncoherent with Forward Link
Subcarrier		Square Wave
Design Error Rate		10^{-6}

Table2.8. Nominal User Constraint Values Used for LinCsim

Relative Phase Between I and Q Channels	2°
Data Asymmetry	10%
Modulator Gain Imbalance	.5 dB
Gain Flatness	.3 dB
Gain Slope	.01 dB/MHz
Phase Nonlinearity	7°
AM/PM	5°/dB
Data Bit Jitter	.01% rms
3 dB Bandwidth	200 MHz
Carrier Phase Noise	
100 Hz - 1 kHz	17° rms
1 k Hz - 150 MHz	3° rms
Subcarrier Phase Noise	1° rms

Table 2.9. Shuttle Ku-Band Return Link Power Budget.

Shuttle-to-TDRS	
Shuttle EIRP	48.1 dBW
Space Loss	208.5 dB
Polarization Loss	.3 dB
TDRS G/T	22.6 dB/°K
TDRS-to-Ground Link	
TDRS TWT max Output Power	12.5 dBW
TWT Output Backoff	.5 dB
TDRS Hardware Losses	1.2 dB
TDRS Antenna Gain	41.3 dB
Pointing Loss	.7 dB
Space Loss	207.7 dB
Polarization Loss	.1 dB
Atmospheric Loss	.8 dB
Ground Station G/T	40.3 dB/°K

Table 2.10. Parameters Studied.

Carrier Power Split

Modulator Gain Imbalance

Relative Phase Between I and Q Channels

Data Asymmetry

Data Bit Jitter

Transmitter AM/AM

Transmitter AM/PM

Carrier Phase Noise

Gain Flatness

Gain Slope

Phase Nonlinearity

Table 2.11.CNR Loss.

CHANNEL	CNR LOSS (dB)		
	PERFECT SHUTTLE	NOMINAL SHUTTLE	USER CONSTRAINTS
1	1.9	3.9	2.0
2	2.0	4.6	2.6
3	1.2	2.3	1.1

Table 2.12Major Contributors to CNR Loss.

Channel 1:	
Modulator Gain Imbalance	.25 dB
AM/AM	.5 dB
Data Asymmetry	.7 dB
Subcarrier Power Split Error	.9 dB
Channel 2:	
Modulator Gain Imbalance	.55 dB
Carrier I/Q Relative Phase	.5 dB
AM/AM	.6 dB
AM/PM	.75 dB
Data Asymmetry	2.0 dB
Channel 3:	
Modulator Gain Imbalance	.1 dB
Carrier I/Q Relative Phase	.1 dB
Data Asymmetry	.25 dB
AM/PM	.2 dB
Phase Nonlinearity	.4 dB
Gain Flatness	.2 dB
Gain Slope	.2 dB

Table 2.13. Complete List of Simulation Parameters.

PARAMETER	PRESENT VALUE	WHERE OBTAINED	DATE OBTAINED	OLD VALUE	SOURCE OLD VALUE
DATA RATE - 1 Ch.1 Ch.2 Ch.3				192 Kb/s 2 Mb/s 50 Mb/s	S-805-1
POWER SPLIT				20: 4: 1	S-805-1
MODULATOR PHASE IMBALANCE (BPSK)	5°	JSC	11/78	±3°	S-805-1
REL. PHASE BETWEEN I&Q CHANNELS	2°	JSC	11/78	±3°	S-805-1
DATA ASYMMETRY	10%	JSC	11/78	±3%	S-805-1
PN ASYMMETRY				N/A	S-805-1
DATA SKEW				N/A	S-805-1
PN SKEW				N/A	S-805-1
MODULATOR GAIN IMBALANCE	.5 dB	JSC	11/78	±0.25 dB	S-805-1
XTR GAIN FLATNESS				±0.3 dB	S-805-1
XTR GAIN SLOPE	.01 dB/MHz	JSC	11/78	±0.1dB/MHz	S-805-1
XTR PHASE NON-LINEARITY	7°	JSC	11/78	±3°	S-805-1
XT FILTER BW	200 MHz	JSC	11/78	225 MHz	LinCom Estimate
XT FILTER ORDER				4	LinCom estimate
XT FILTER RIPPLE				0.1	LinCom estimate
XTR AM/AM				1 dB/dB	LinCom estimate
XTR AM/PM	5°/dB	JSC	11/78	12°/dB	S-805-1
TDRS TWT MAX AM/PM				10°/dB	LinCom estimate
TDRS TWT AM/AM				0 dB/dB	LinCom estimate
TDRS TWT AM/PM				6°/dB	LinCom estimate
TDRS FRONT END FILTER BW				225 MHz	WU Proposal, 7/76
ORDER				4	LinCom estimate
RIPPLE				0.1	LinCom estimate
TDRS TRANSMIT FILTER BW				225 MHz	LinCom estimate
ORDER				4	LinCom estimate
RIPPLE				0.2	LinCom estimate
PN TIMING OFFSET				±1%	LinCom estimate
PN TIMING JITTER				1 %peak	S-805-1
DATA TIMING OFFSET				1%	LinCom estimate
DATA TIMING JITTER	.01% rms	JSC	11/78	1% peak	S-805-1

Table 2.1.3 (Cont'd)

PARAMETER	PRESENT VALUE	WHERE OBTAINED	DATE OBTAINED	OLD VALUE	SOURCE OLD VALUE
	LINK BUDGET				
XTR EIRP				43.1 dBW	SSRF Circuit Margin, 1/77
SPACE LOSS				208.5 dB	SSRF Circuit Margin, 1/77
POLARIZATION LOSS				-0.3 dB	SSRF Circuit Margin, 1/77
ATMOSPHERIC LOSS				0 dB	SSRF CircuitMargin 1/77
TDRS G/T				22.6 dB/°K	SSRF Circuit Margin 1/77
TDRS TWT MAX OUTPUT POWER				12.5 dB	WU Proposal, 7/76
TDRS TWT OUTPUT BACKOFF				Composite,7.dB Dedicated,.5dB	WU Proposal, 7/76
POWER ALLOCATION	-2.5 dB	TPM#8	3/78	-2.4 dB	WU Proposal, 7/76
CHANNEL POWER				Composite,8.0dBW Dedicated,12dBW	WU Proposal, 7/76
TDRS HARDWARE LOSS				1.2 dB	LinCom estimate
TDRS ANTENNA GAIN				41.3 dB	WU Proposal, 7/76
POINTING LOSS				0.7 dB	WU Proposal, 7/76
SPACE LOSS				207.7 dB	TDRSS Users Guide #3
POLARIZATION LOSS				0.1 dB	TDRSS Users Guide #3
ATMOSPHERIC LOSS				0.8 dB	TDRSS Users Guide #3
RX ANTENNA G/T				40.3 dB	TDRSS Users Guide #3
	PHASE NOISE BUDGET				
TX OSC, NONCOHERENT TURNAROUND					
1 to 10 Hz				15° rms	S-805-1
10 to 100 Hz				7.5° rms	S-805-1
100 Hz to 1 kHz	17° rms	JSC	11/78	2° rms	S-805-1
1 kHz to 150 MHz	3° rms	JSC	11/78	2° rms	S-805-1
TDRS OSCILLATORS	3.4°	TPM#8	3/78	3°	S-805-1
RX OSCILLATORS				1°	S-805-1
RX CARRIER TRACKING LOOP					
STATIC PHASE ERROR				3°	LinCom Estimate
BANDWIDTH				1000 Hz	TRW, 8/77
DAMPING				2	LinCom Estimate
SQUARING LOSS				DG1: 2 dB DG2: 8 dB	LinCom Estimate
SUBCARRIER PARAMETERS:					
POWER SPLIT ERROR	1 dB	JSC	11/78		
PHASE NOISE	1° rms	JSC	11/78		

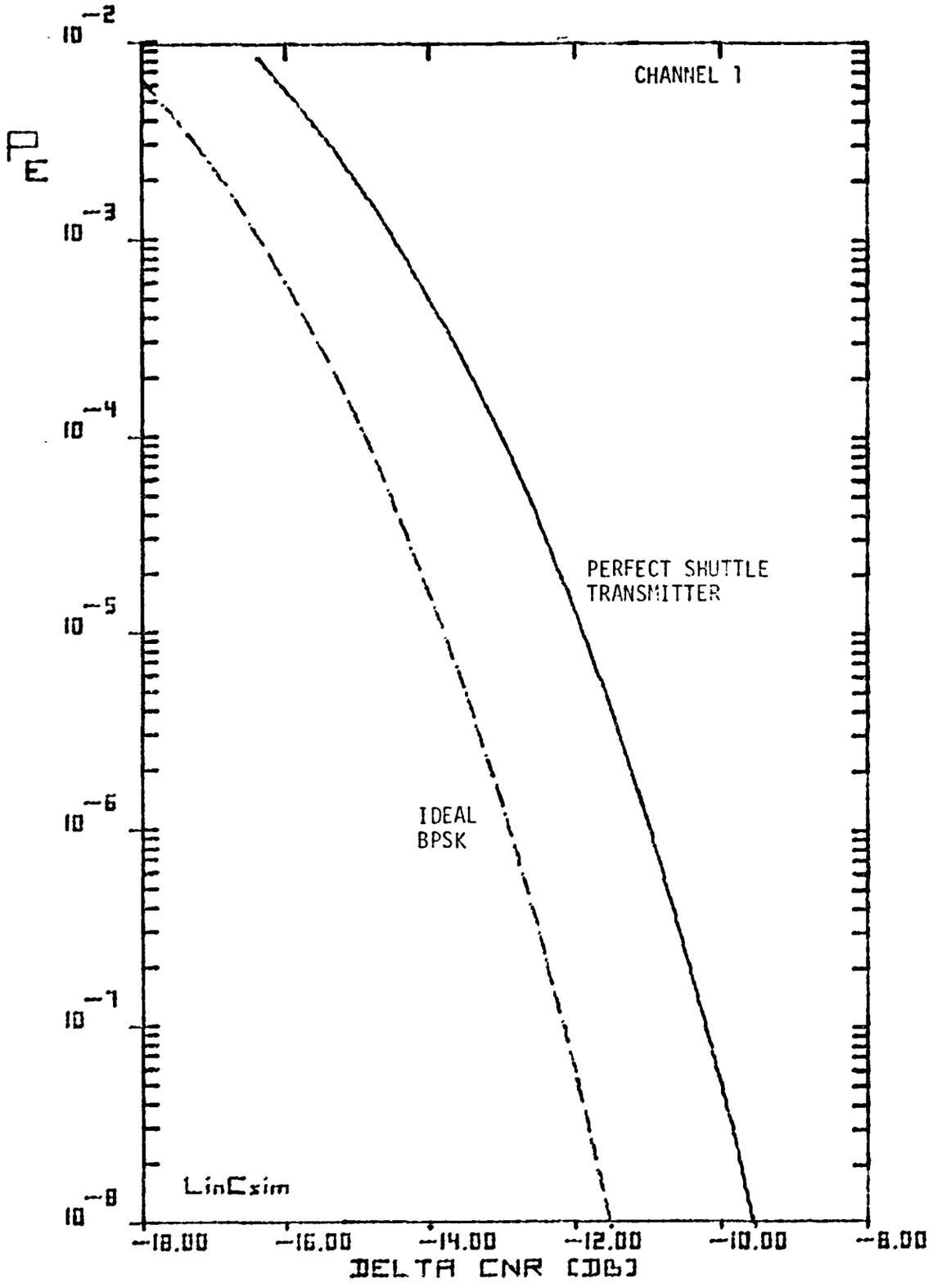

Figure 2.23 BER Plot for Perfect Shuttle Transmitter.

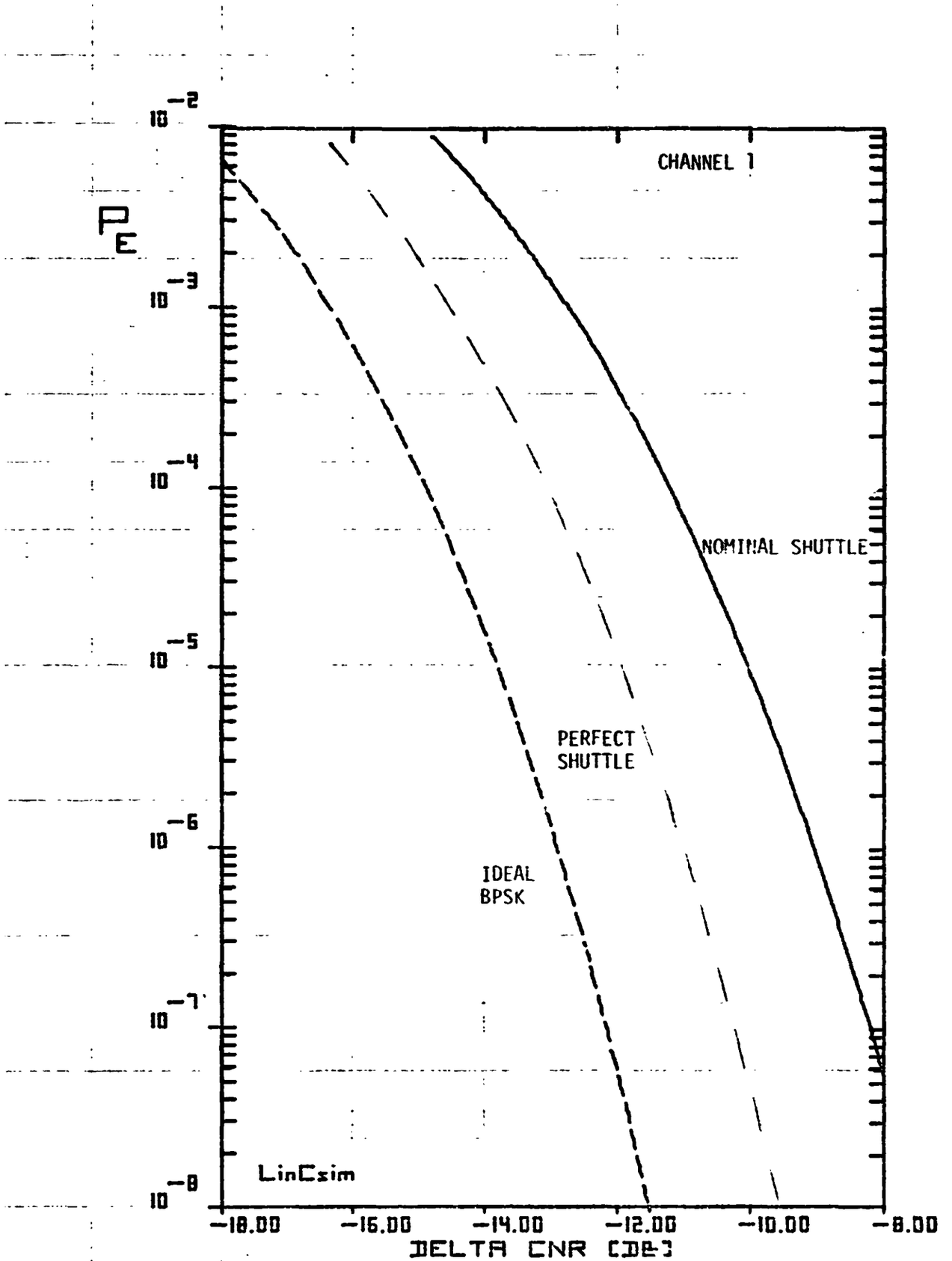

Figure 2.24 BER Plot for Nominal Shuttle Transmitter.

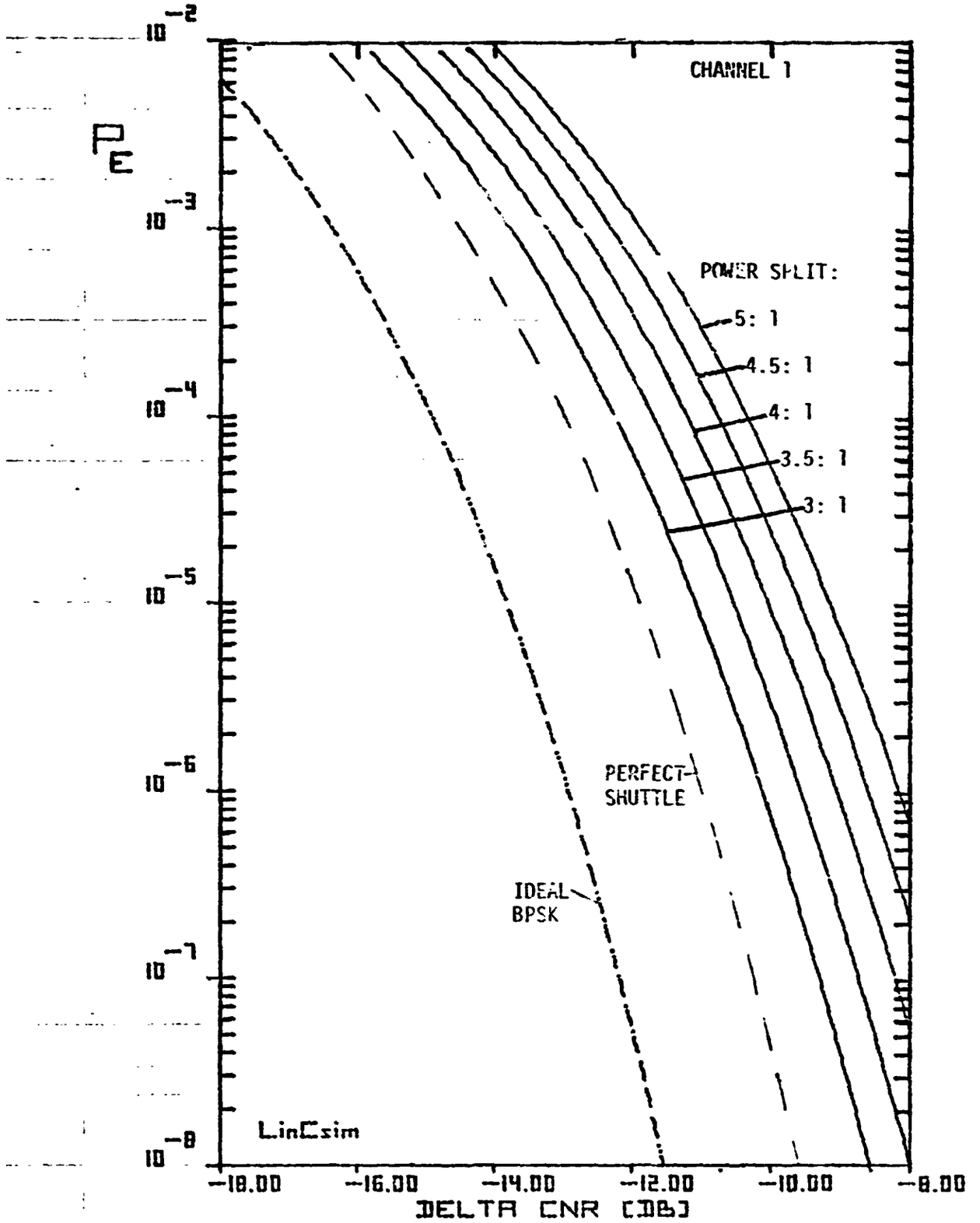

Figure 2.25.BER Plot for Carrier Power Split.

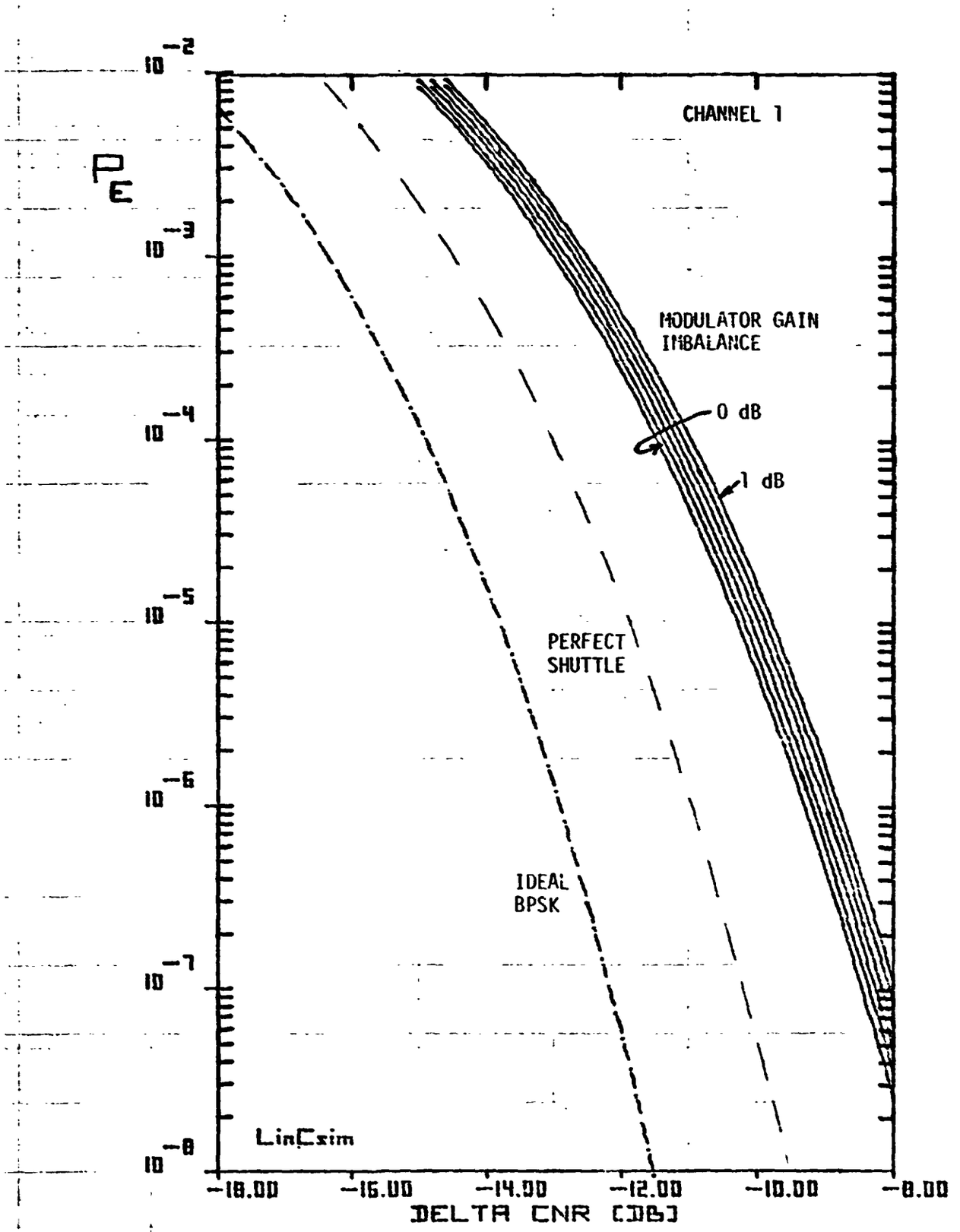

Figure 2.26. BER Plot for Carrier Modulator Gain Imbalance.

79 0200

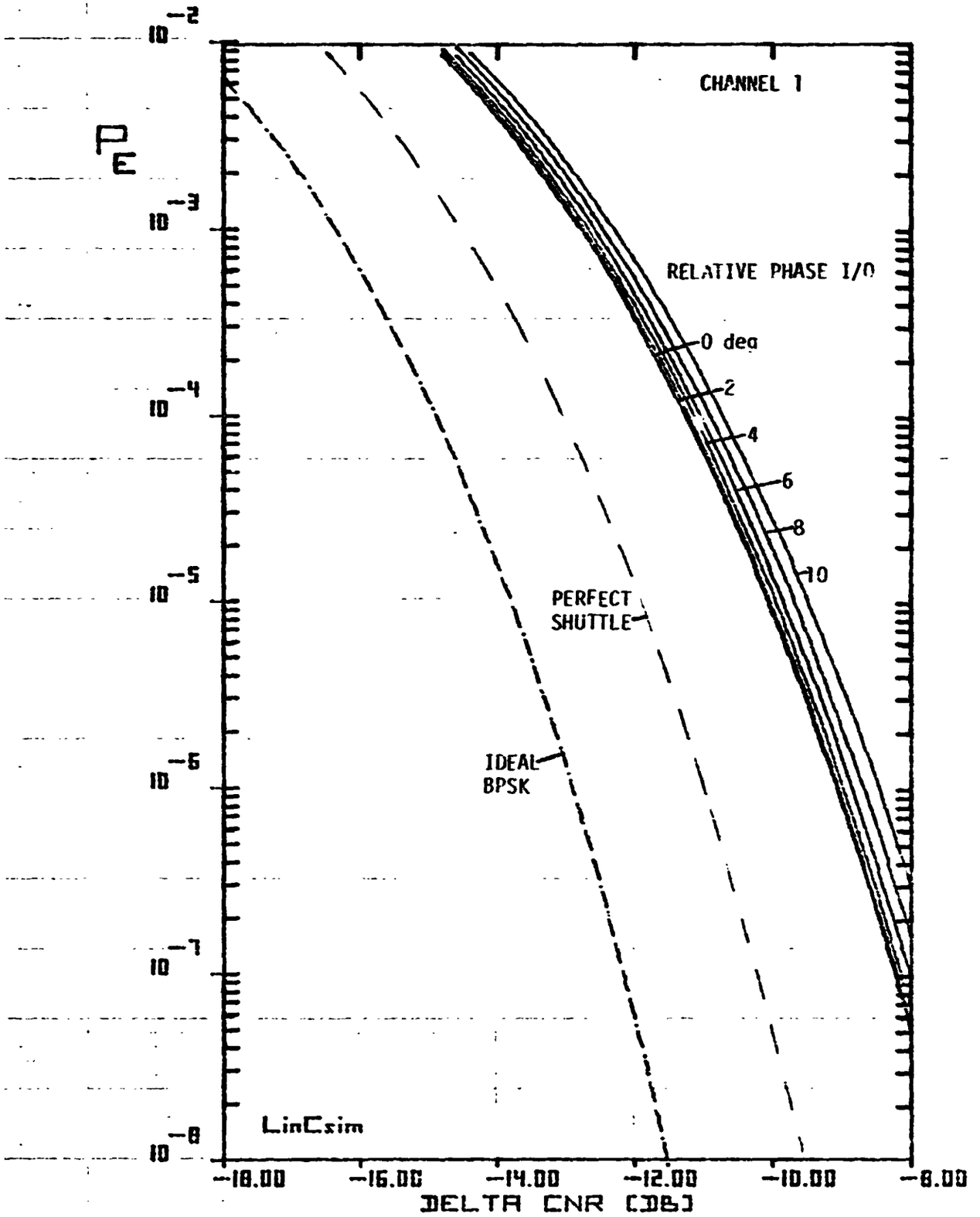

Figure 2.27. BER Plot for Relative I/Q Carrier Phase.

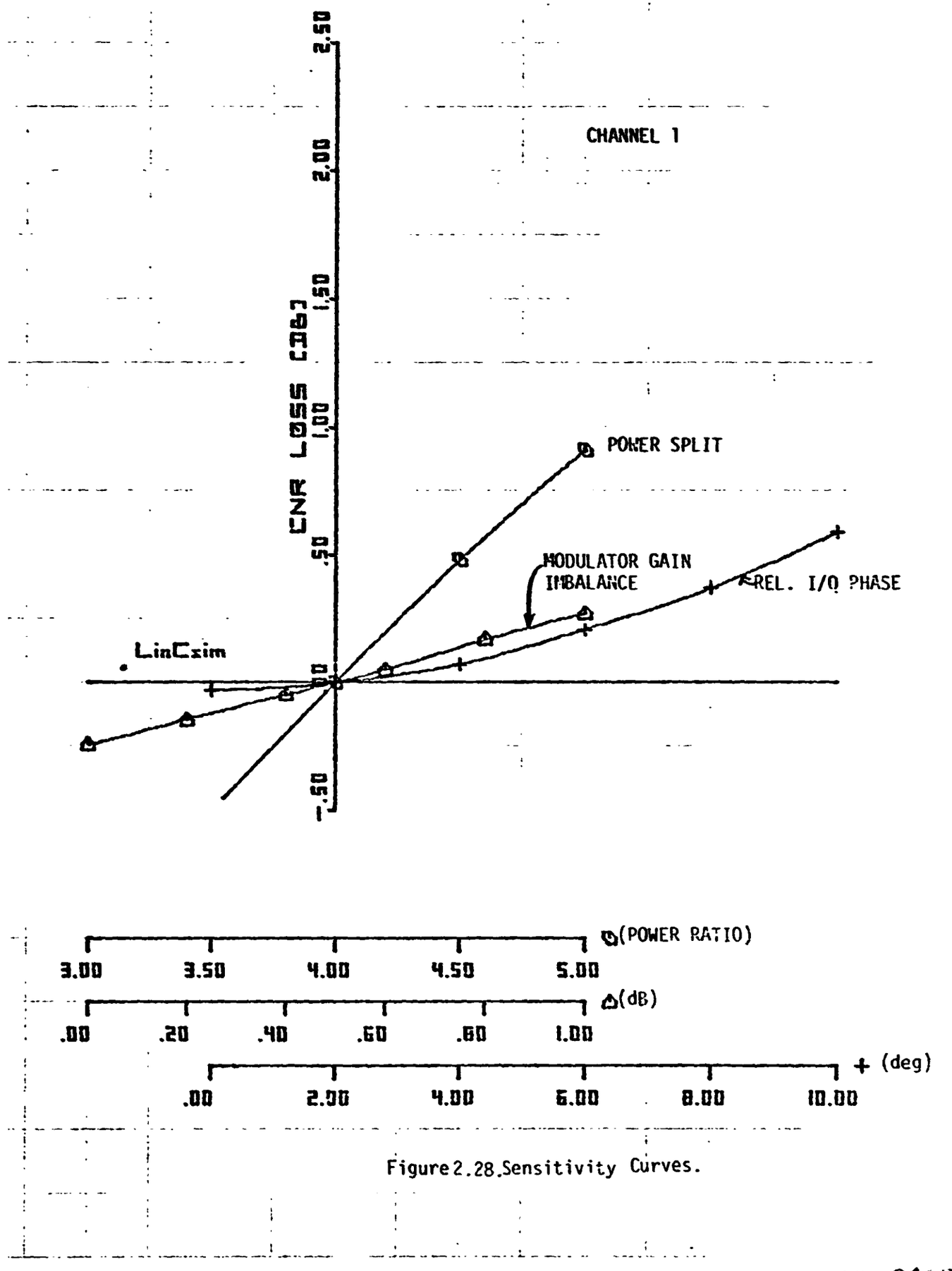

Figure 2.28 Sensitivity Curves.

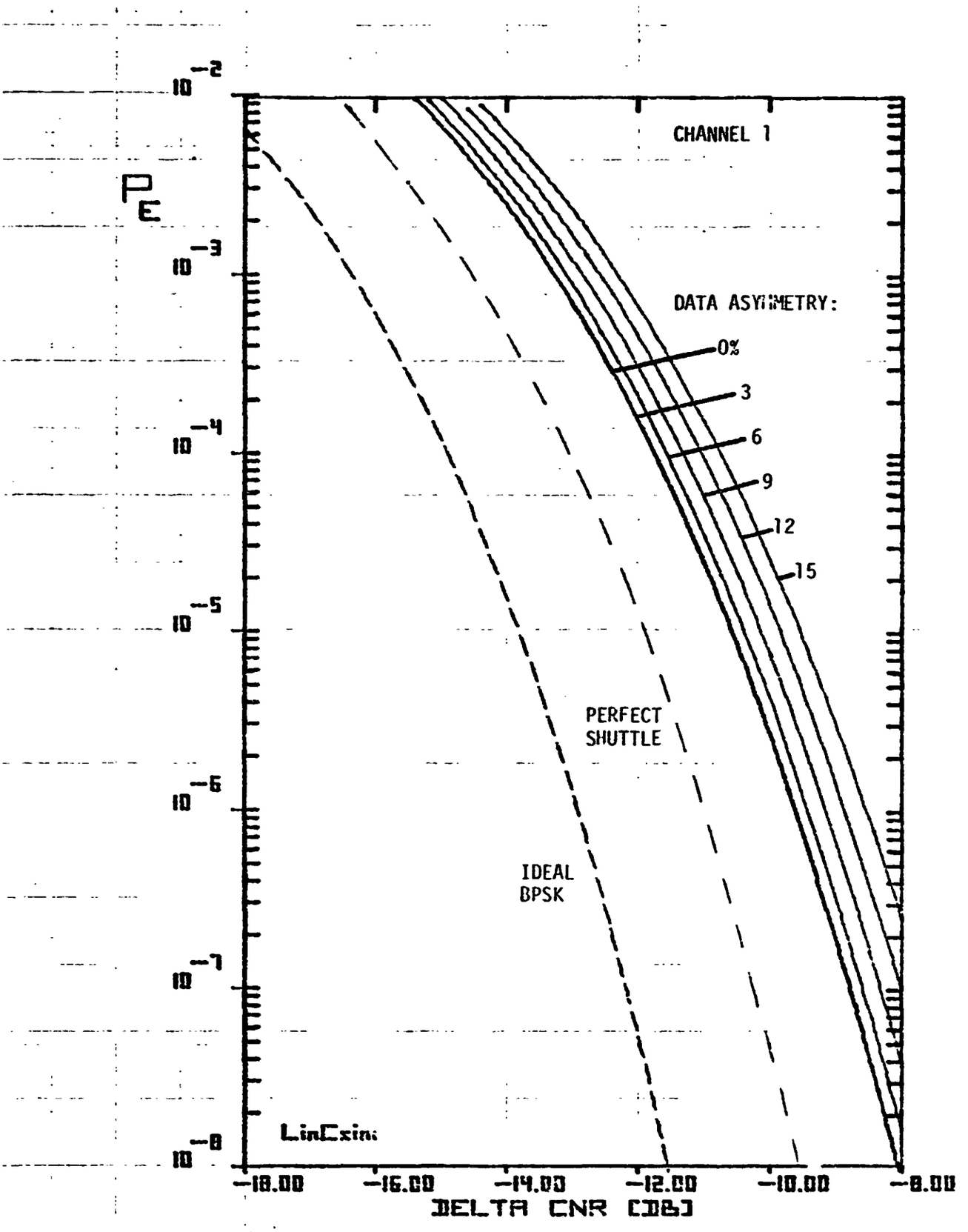

Figure 2.29.BER Plot for Data Asymmetry.

79 0193

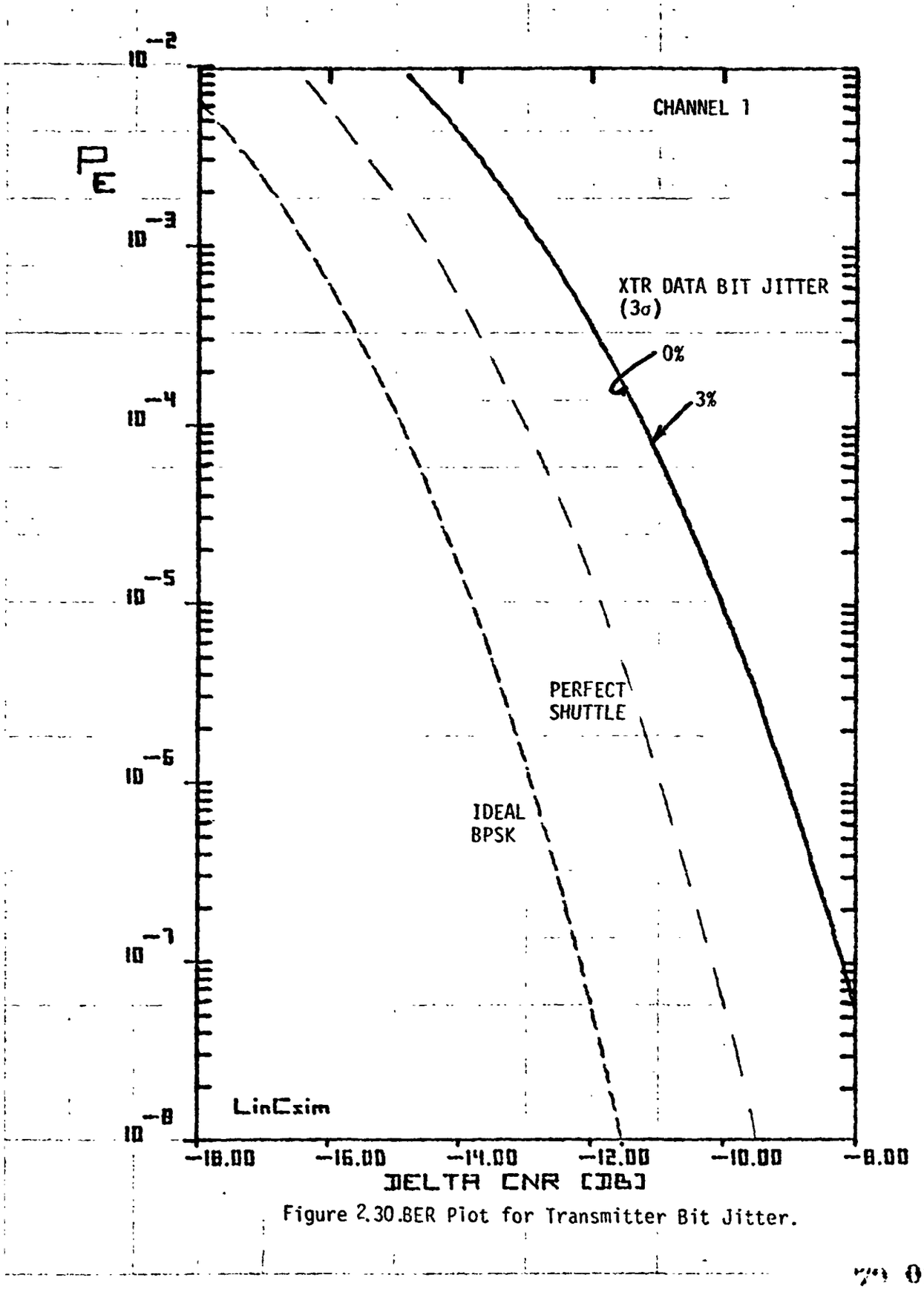

Figure 2.30.BER Plot for Transmitter Bit Jitter.

0104

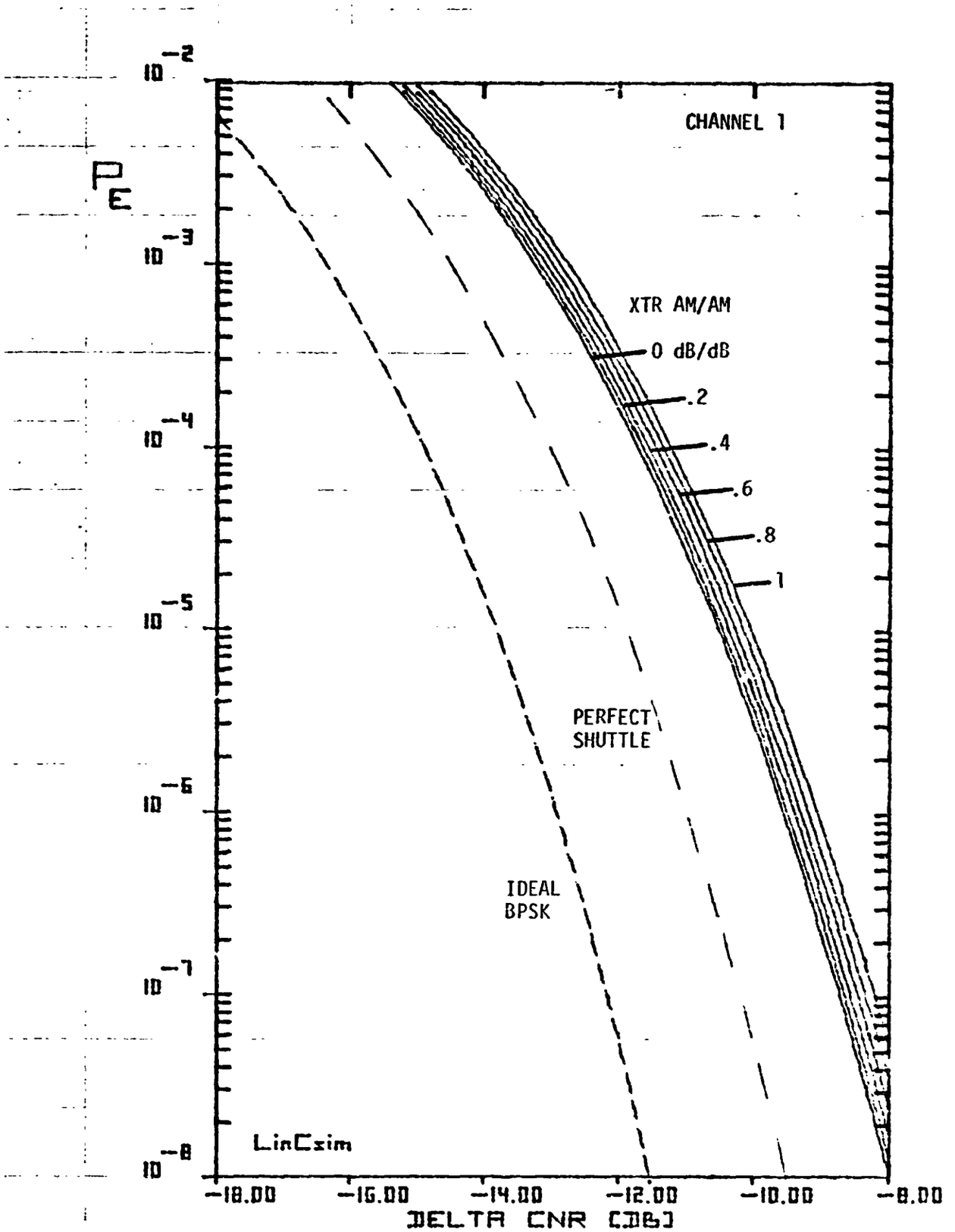

Figure 2.31. BER Plot for Transmitter AM/AM.

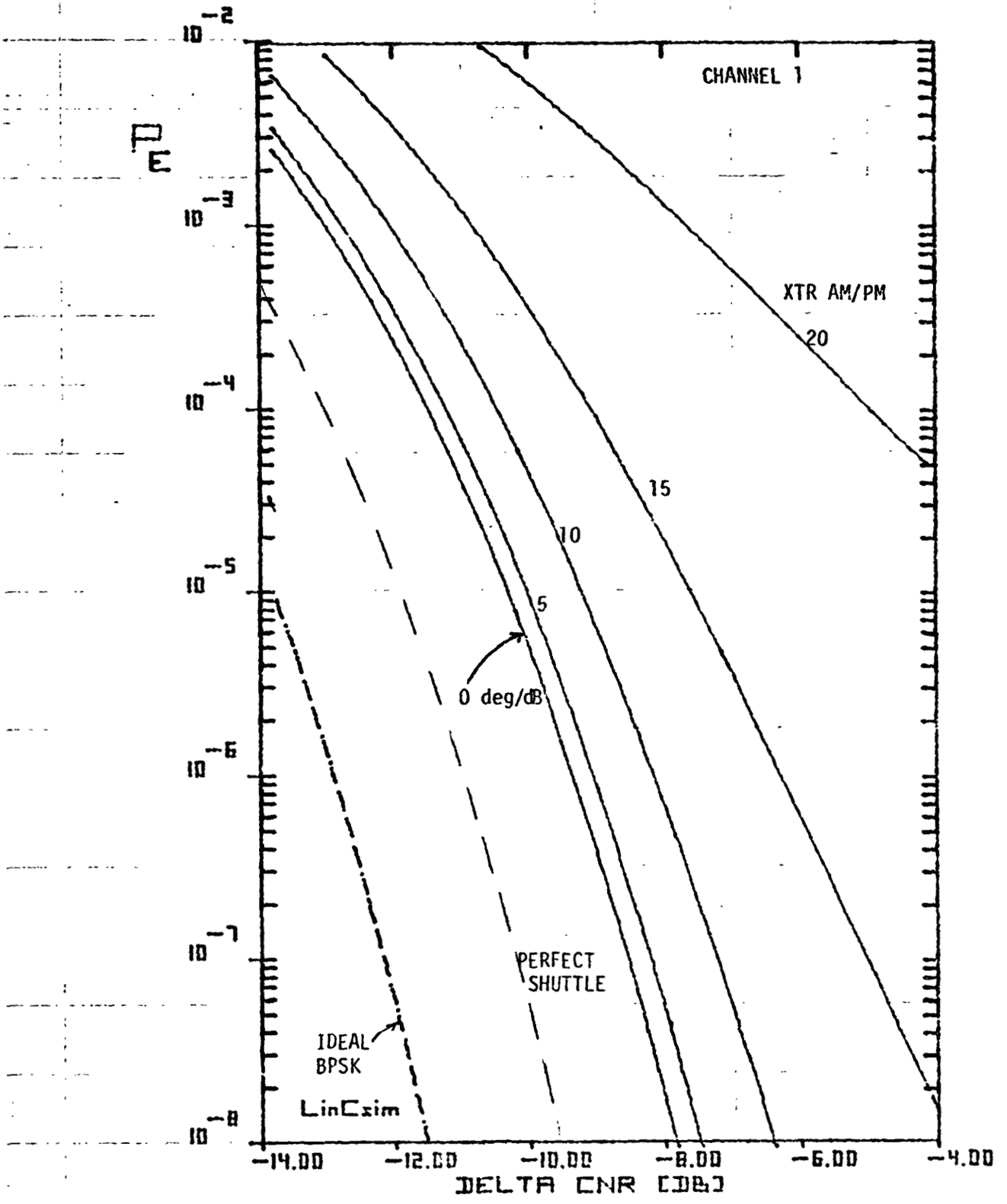

Figure 2.32.BER Plot for Transmitter AM/PM.

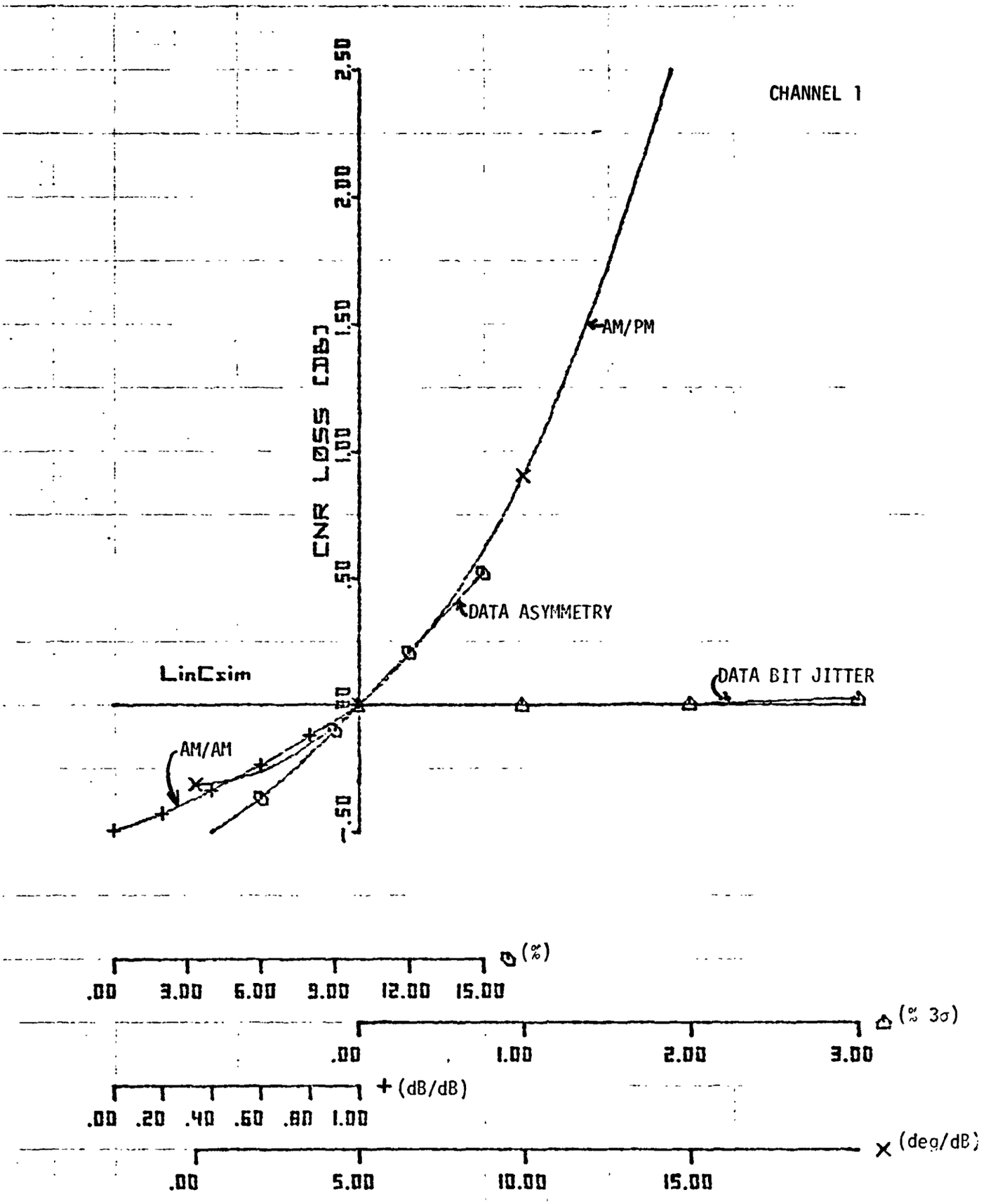

Figure 2.33. Sensitivity Curves.

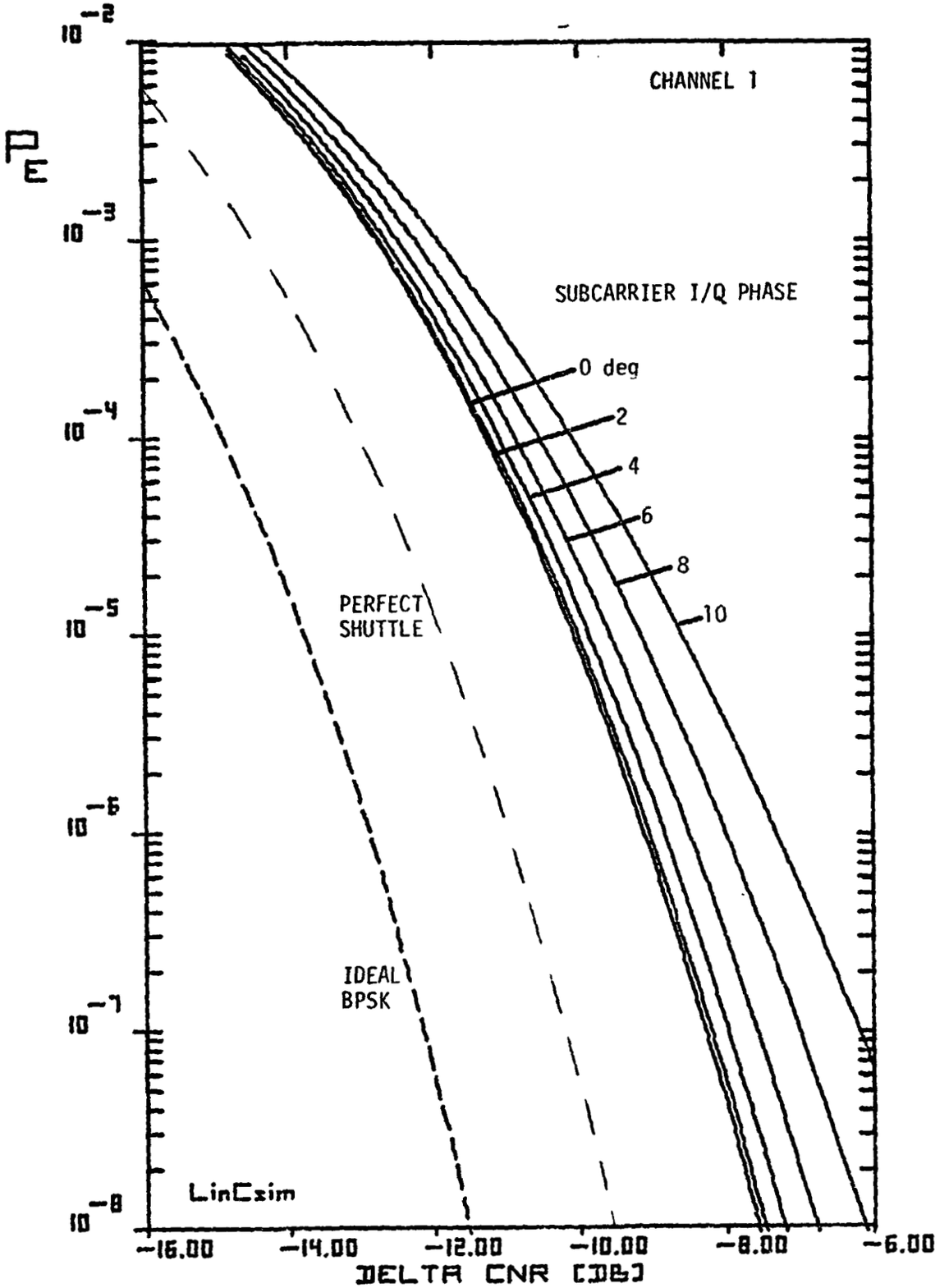

Figure 2.34. BER Plot for Subcarrier I/Q Phase.

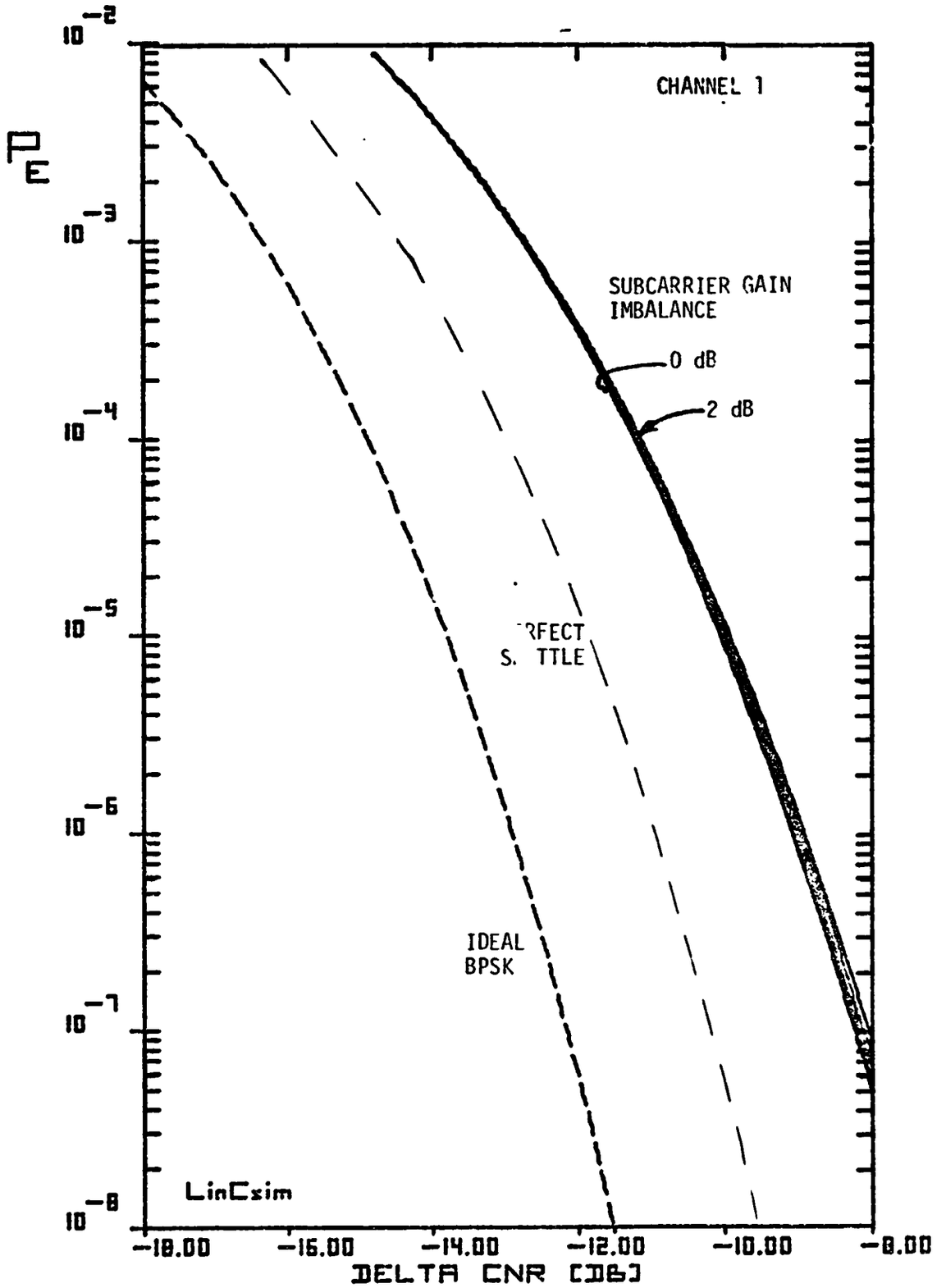

Figure2.35. BER Plot for Subcarrier Gain Imbalance.

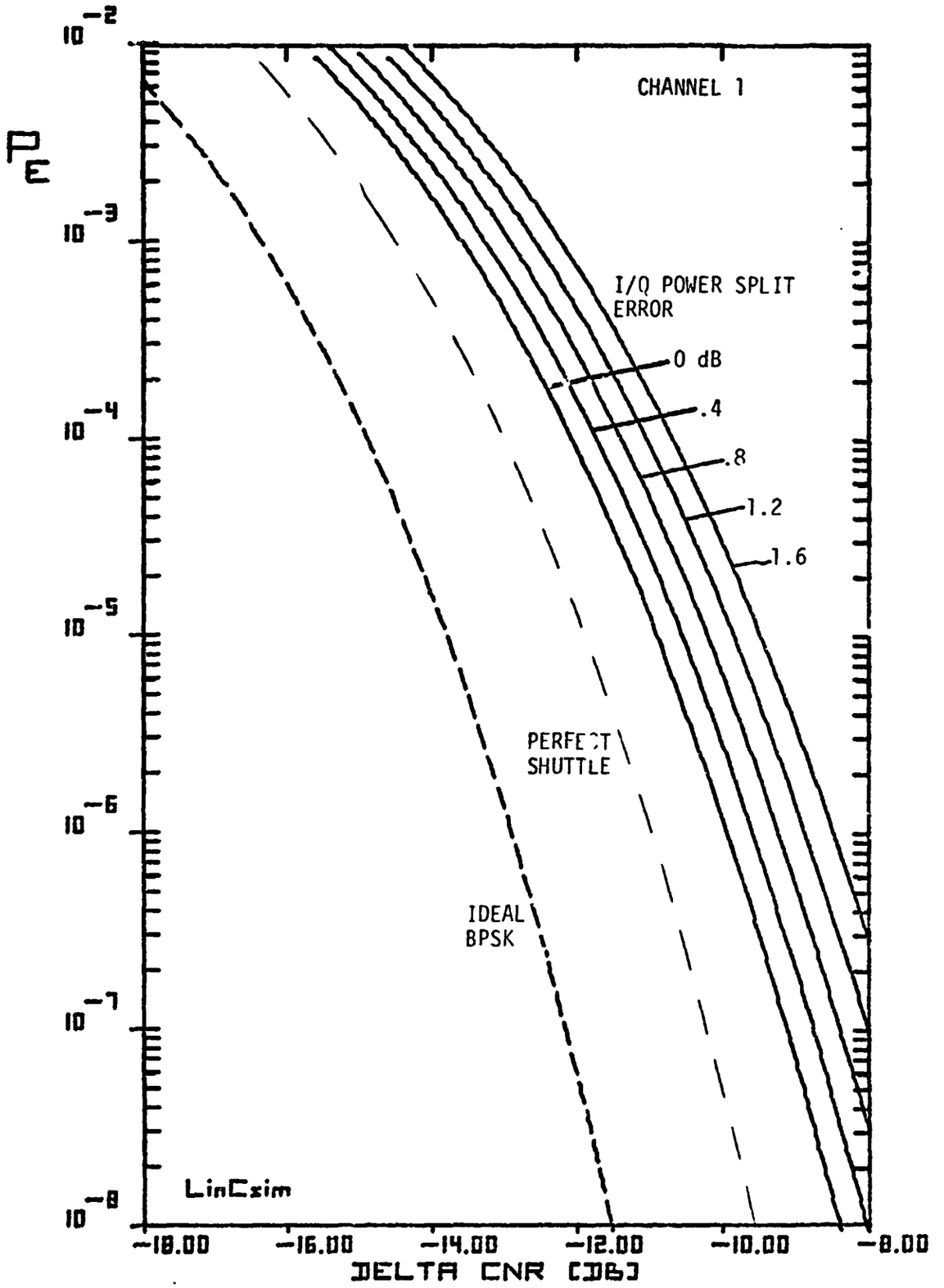

Figure 2.36. BER Plot for Subcarrier Power-Split Error.

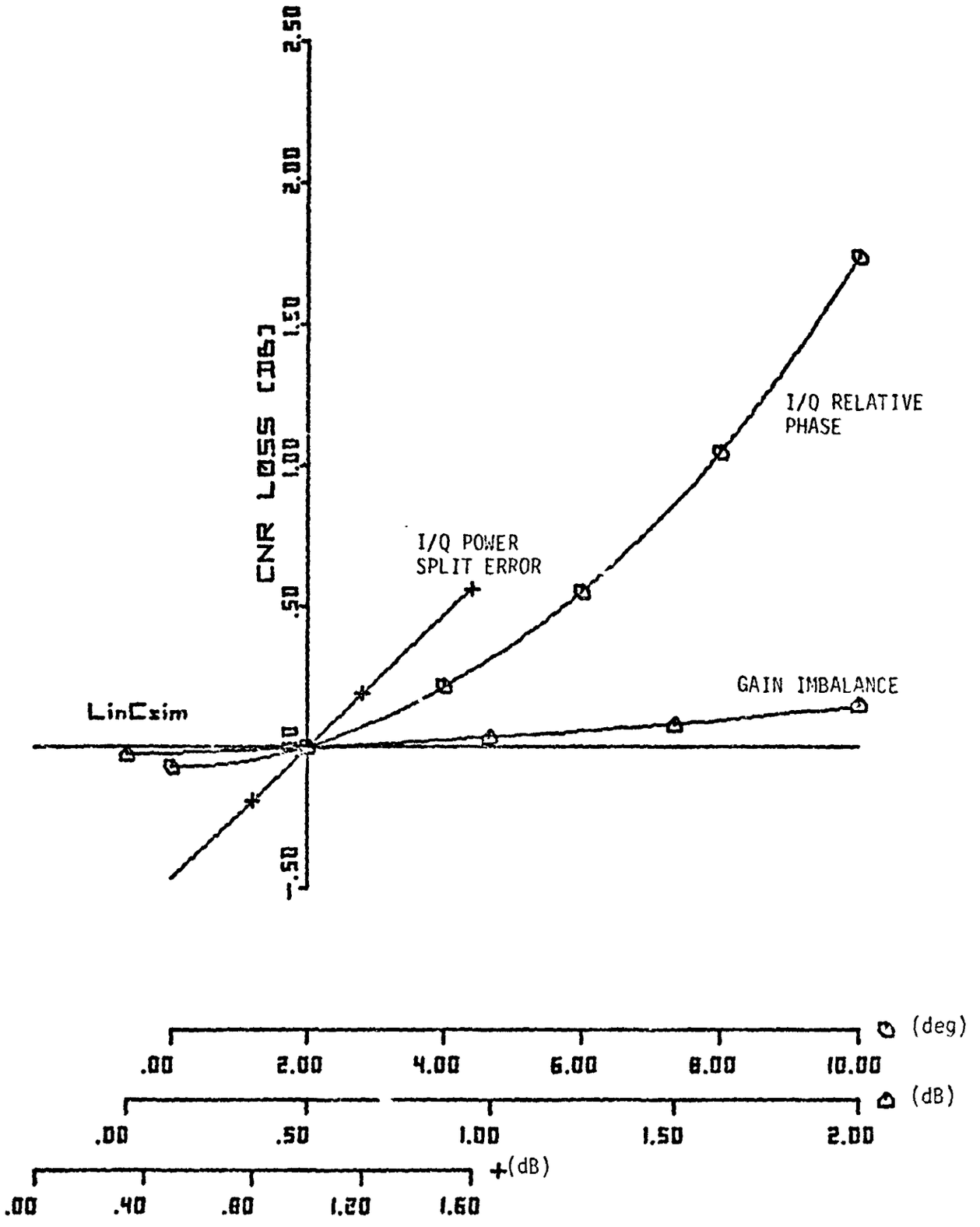

Figure 2.37 Sensitivity Curves for Subcarrier Modulator Parameters.

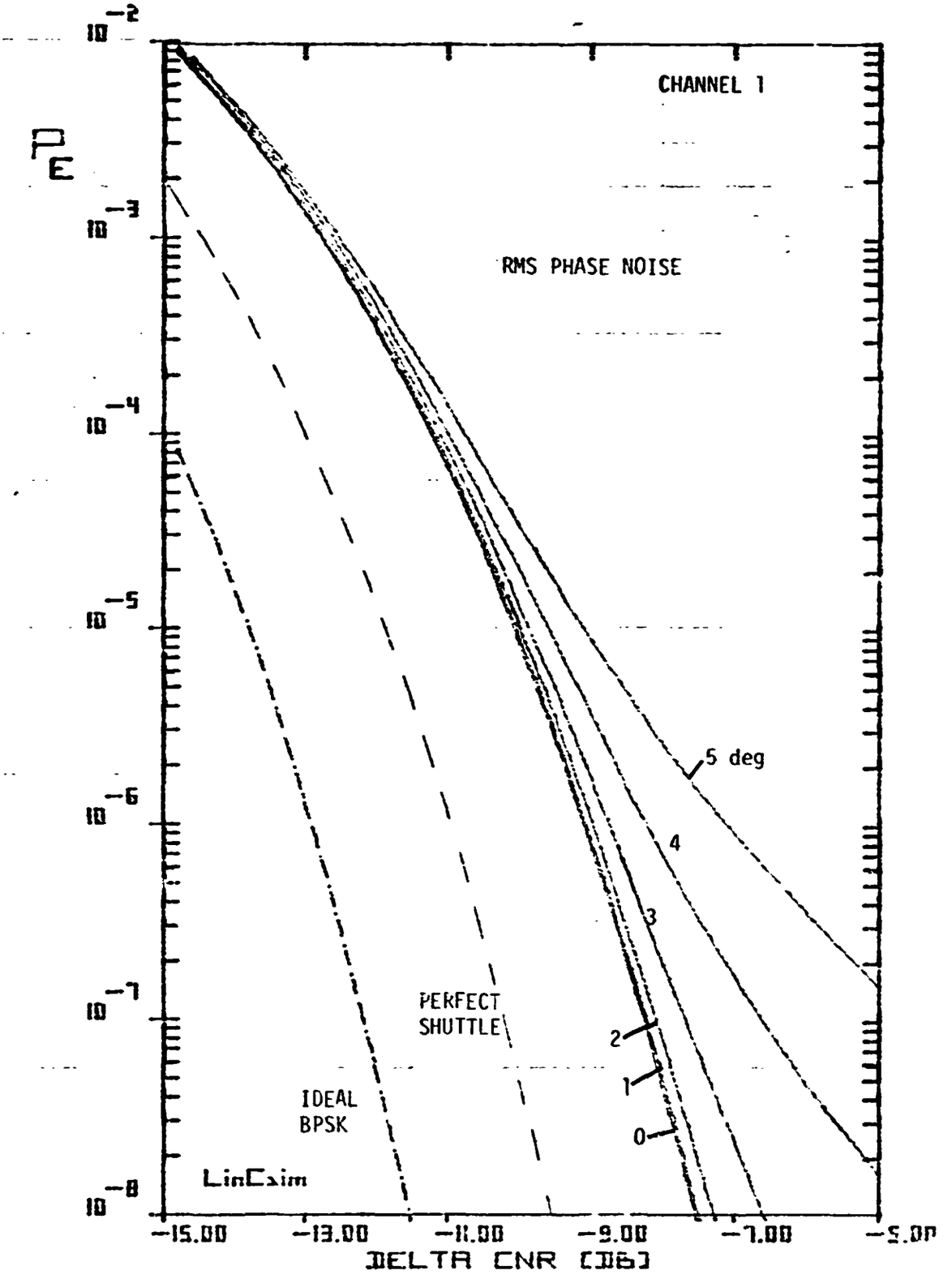

Figure2.38. BER Plot for Subcarrier Phase Noise.

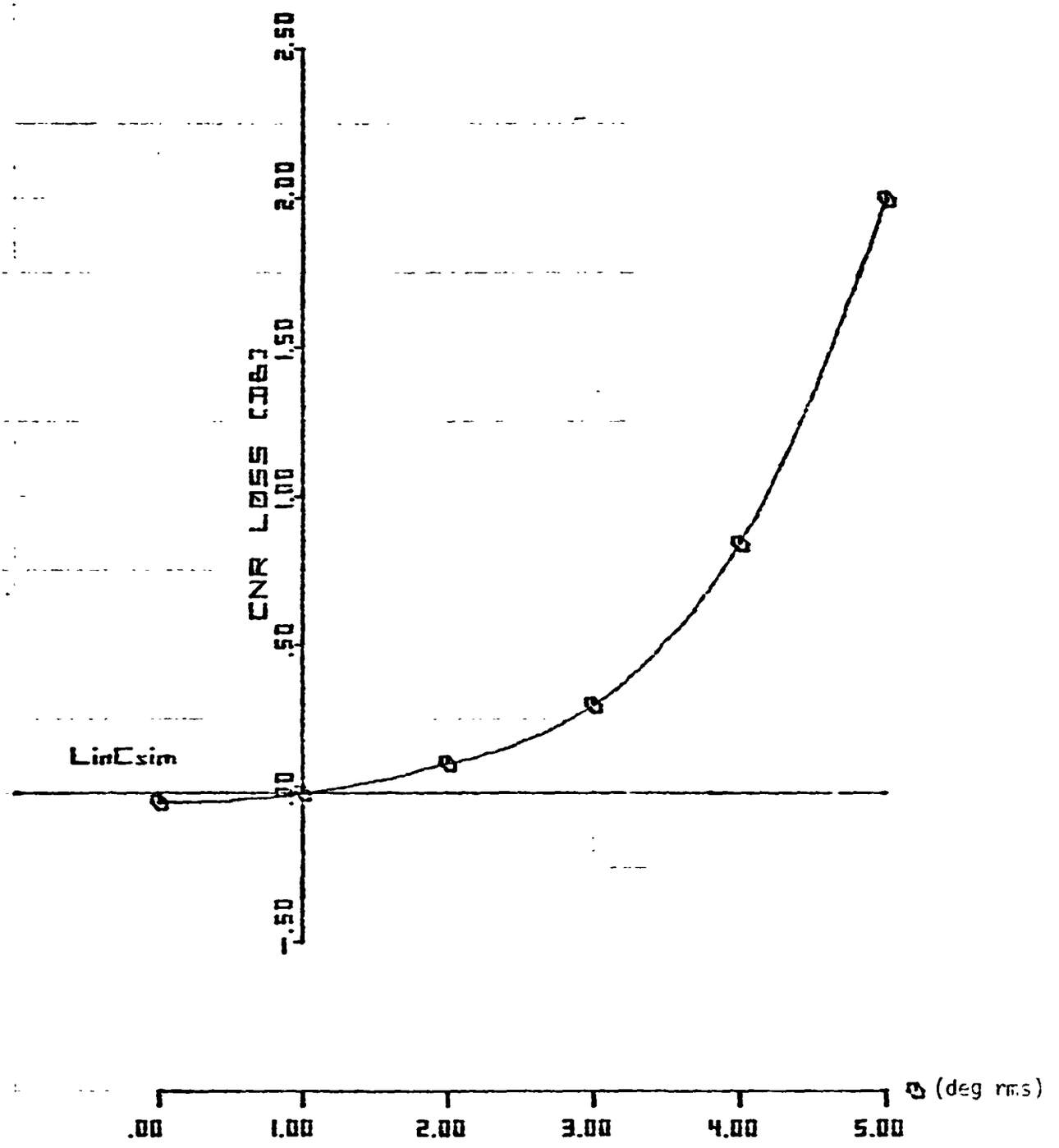

Figure 2.39. Sensitivity Curve for Subcarrier Phase Noise.

79 0[illegible]

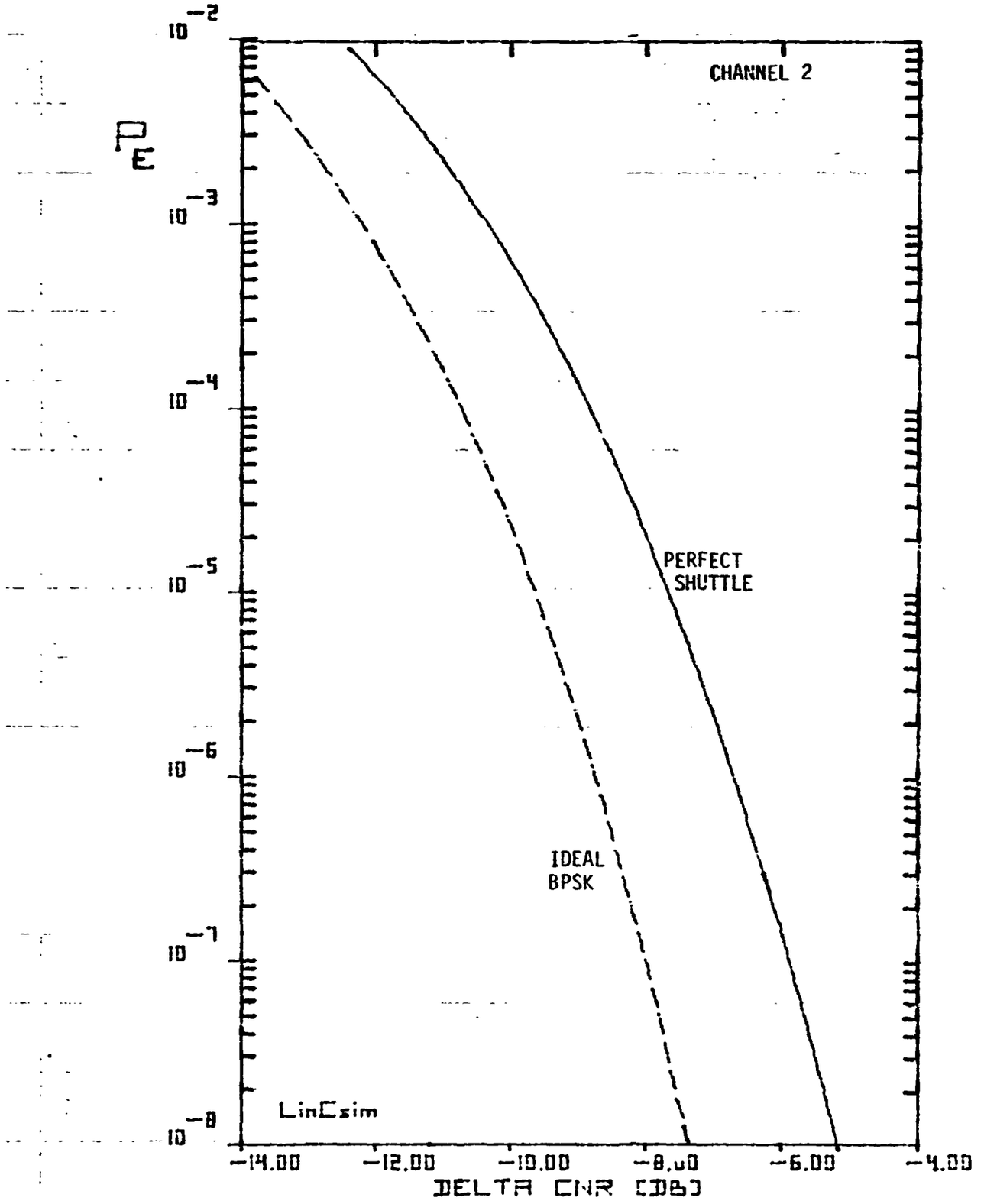

Figure 2.40.BER Plot for Perfect Shuttle Transmitter.

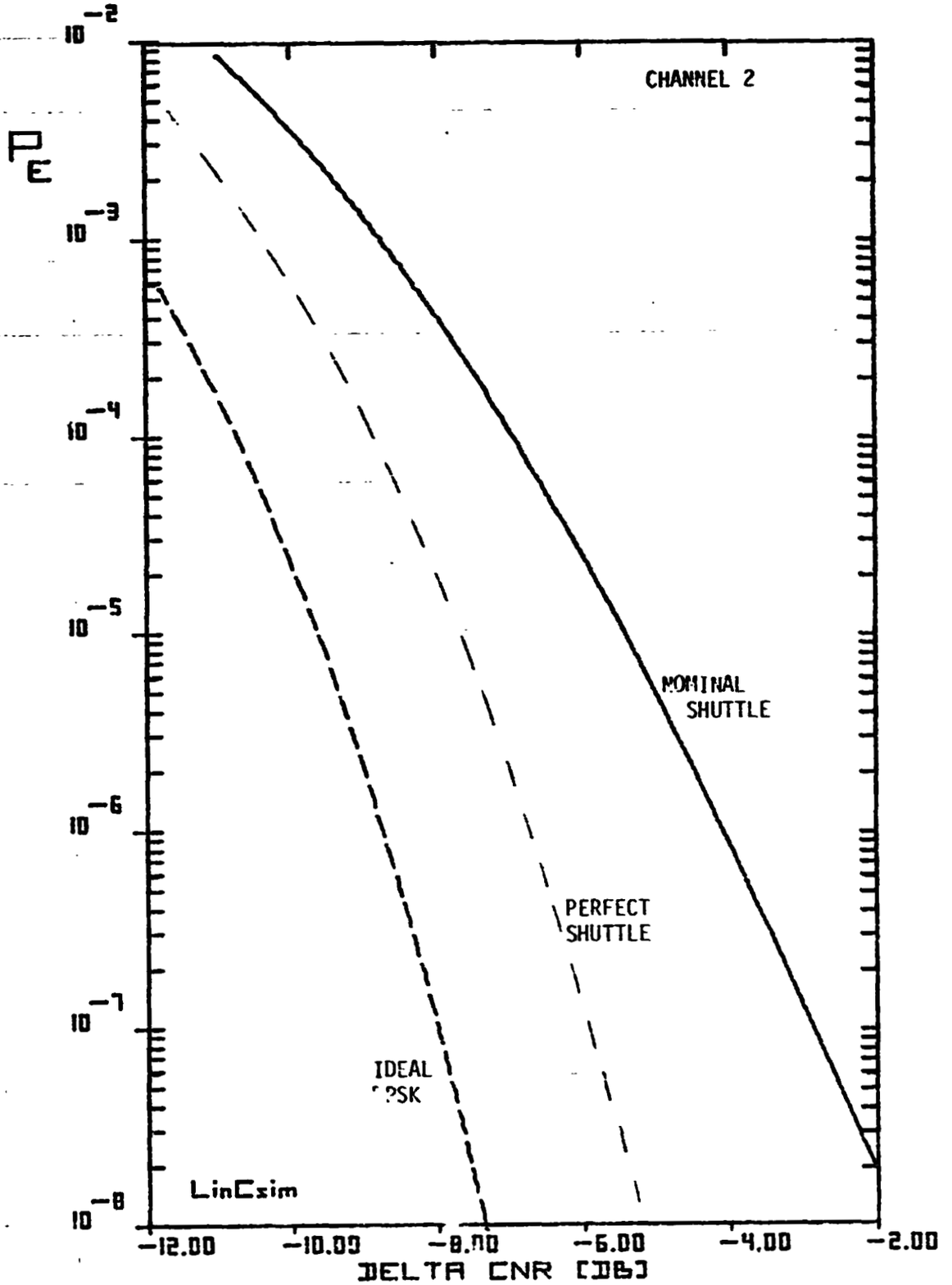

Figure 2.41. BER Plot for Nominal Shuttle Transmitter.

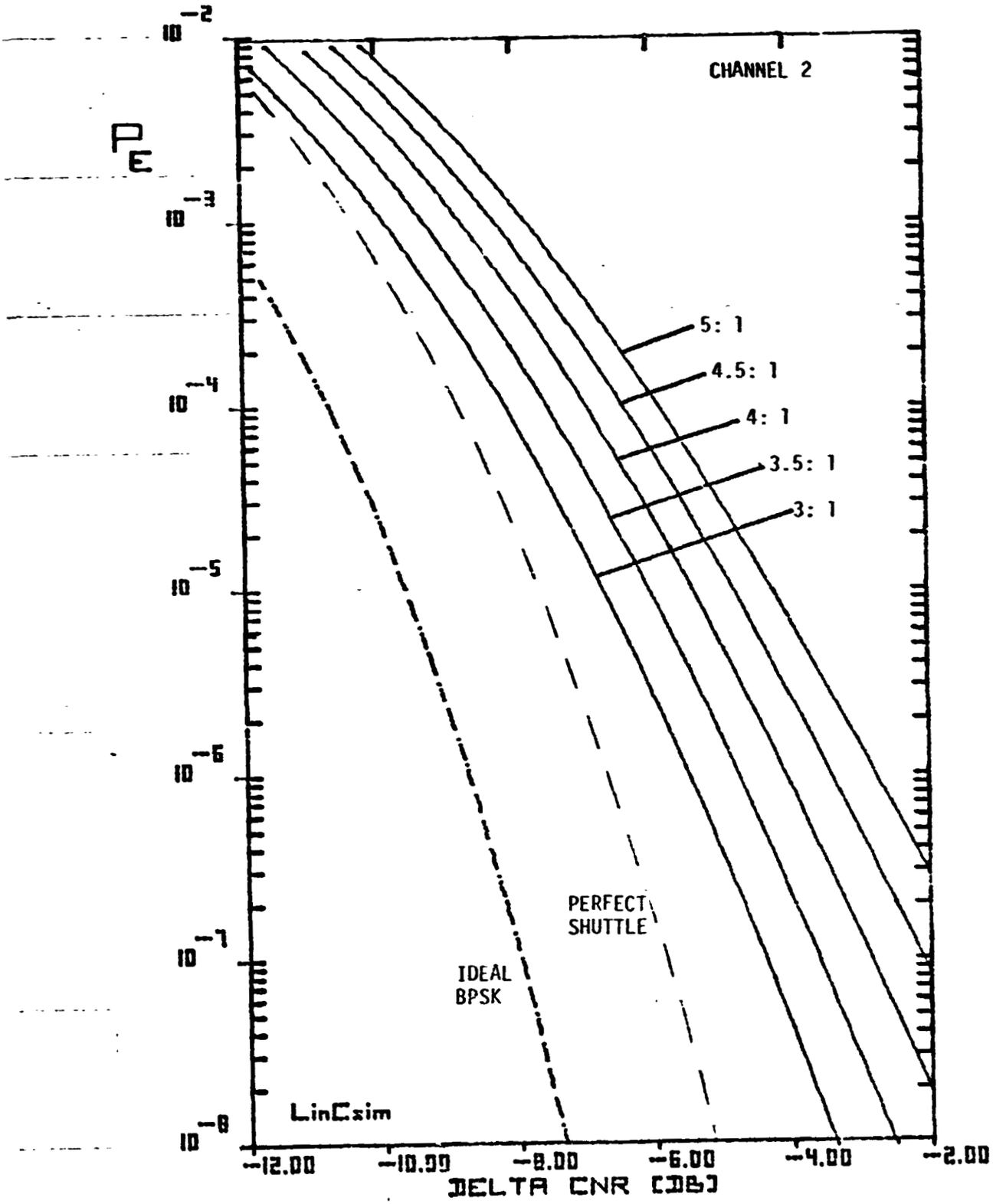

Figure 2.42. BER Plot for Carrier Power Split.

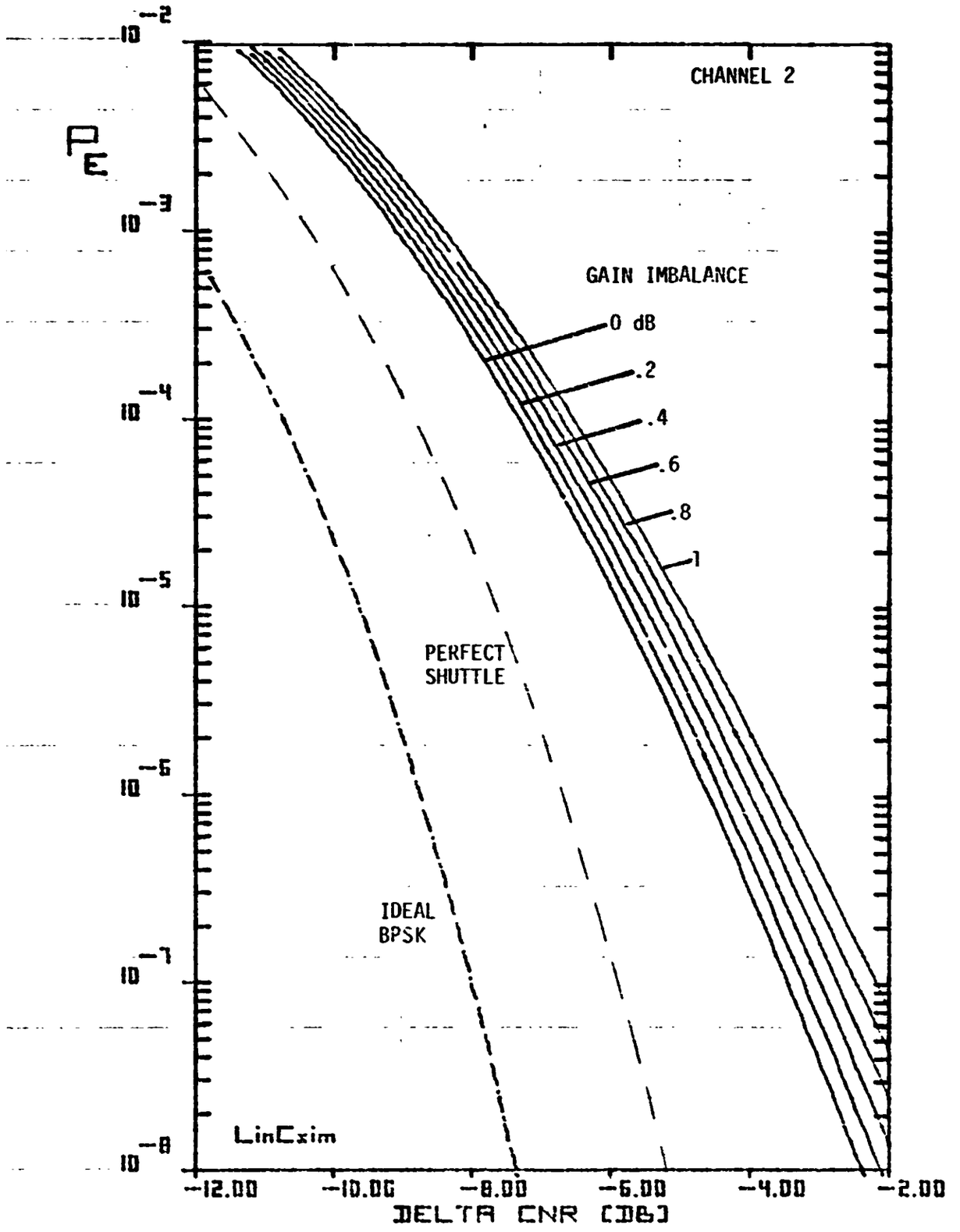

Figure 2.43. BER Plot for Modulator Gain Imbalance.

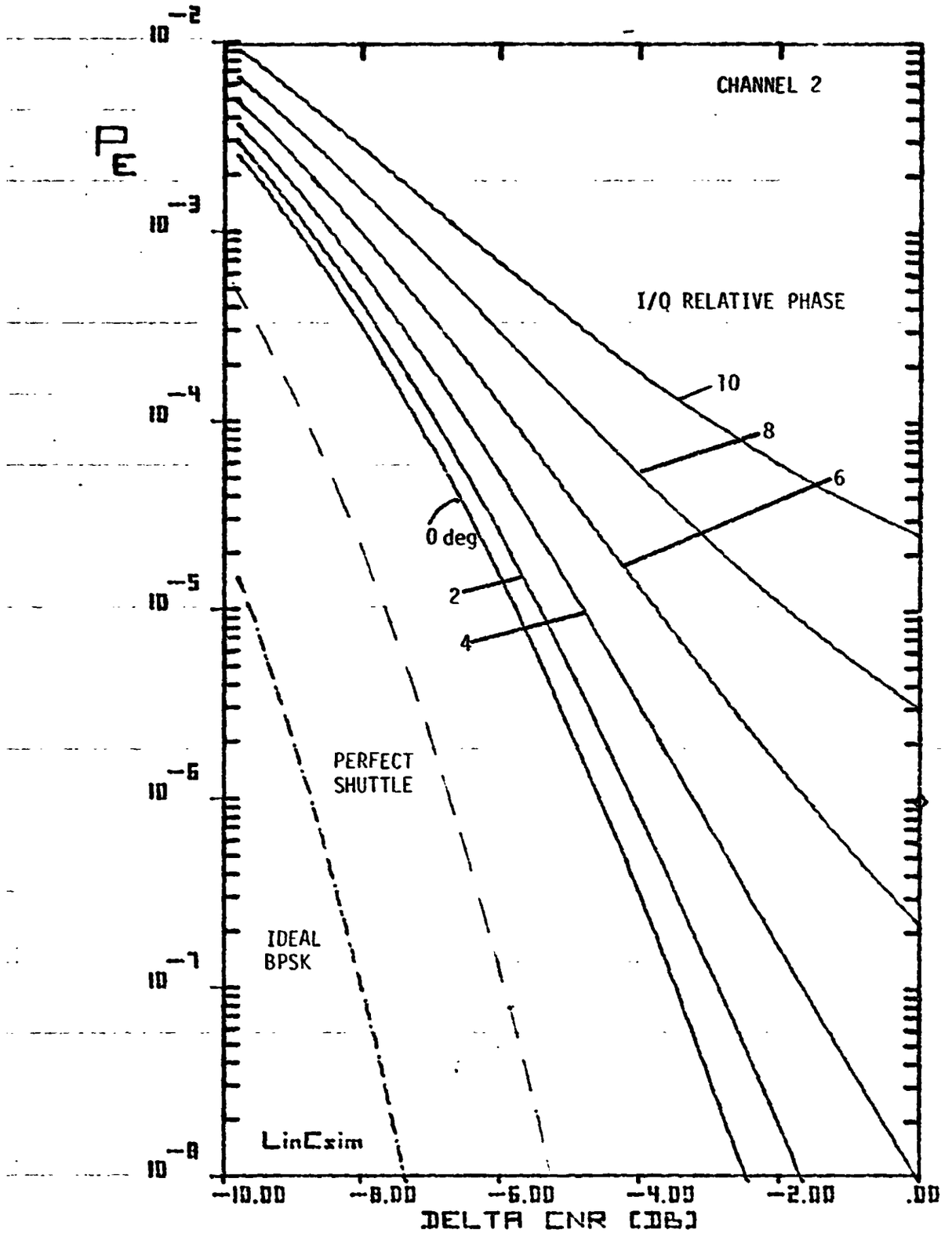

Figure 2.44. BER Plot for Relative I/Q Carrier Phase.

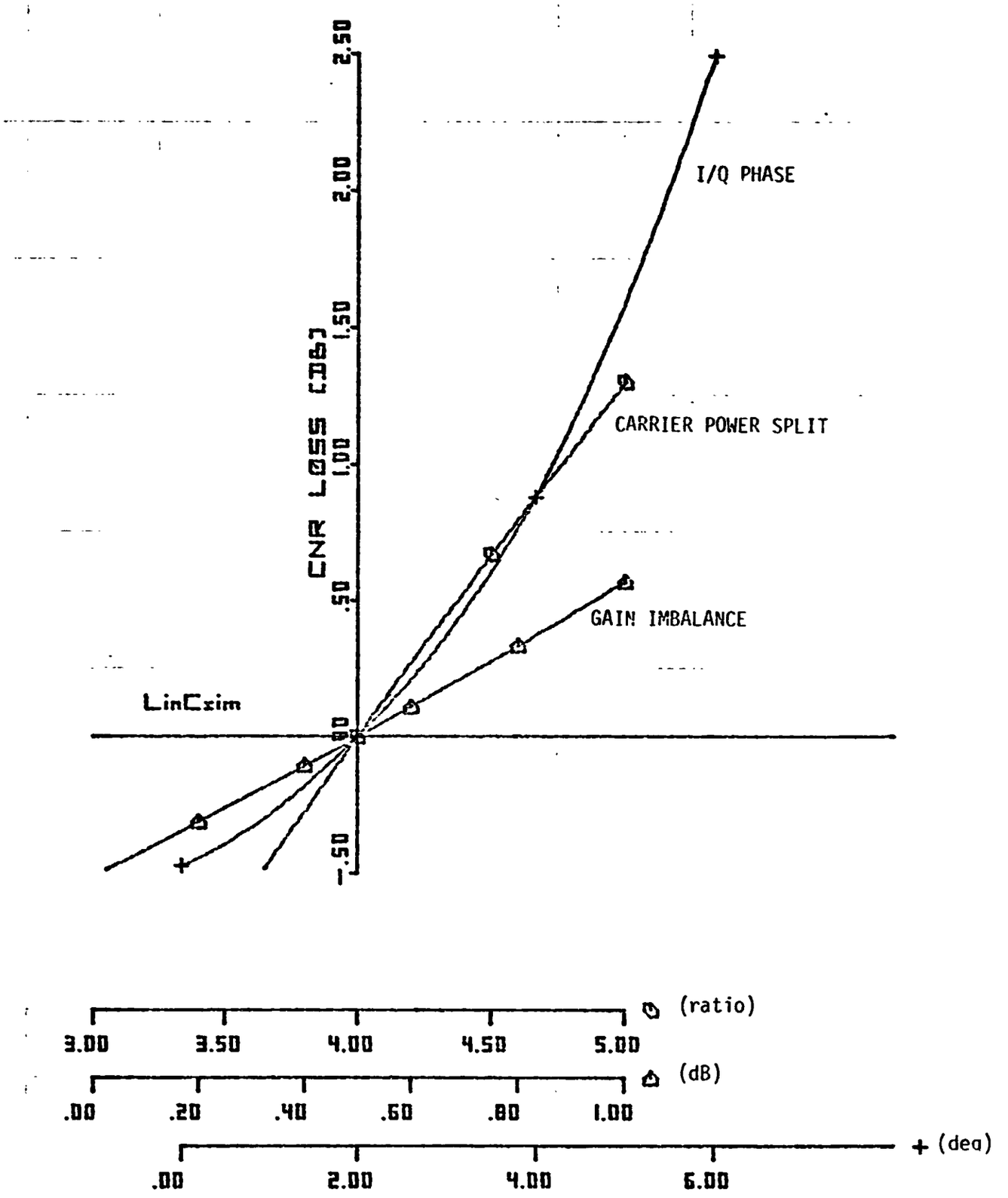

Figure 2.45. Sensitivity Curves.

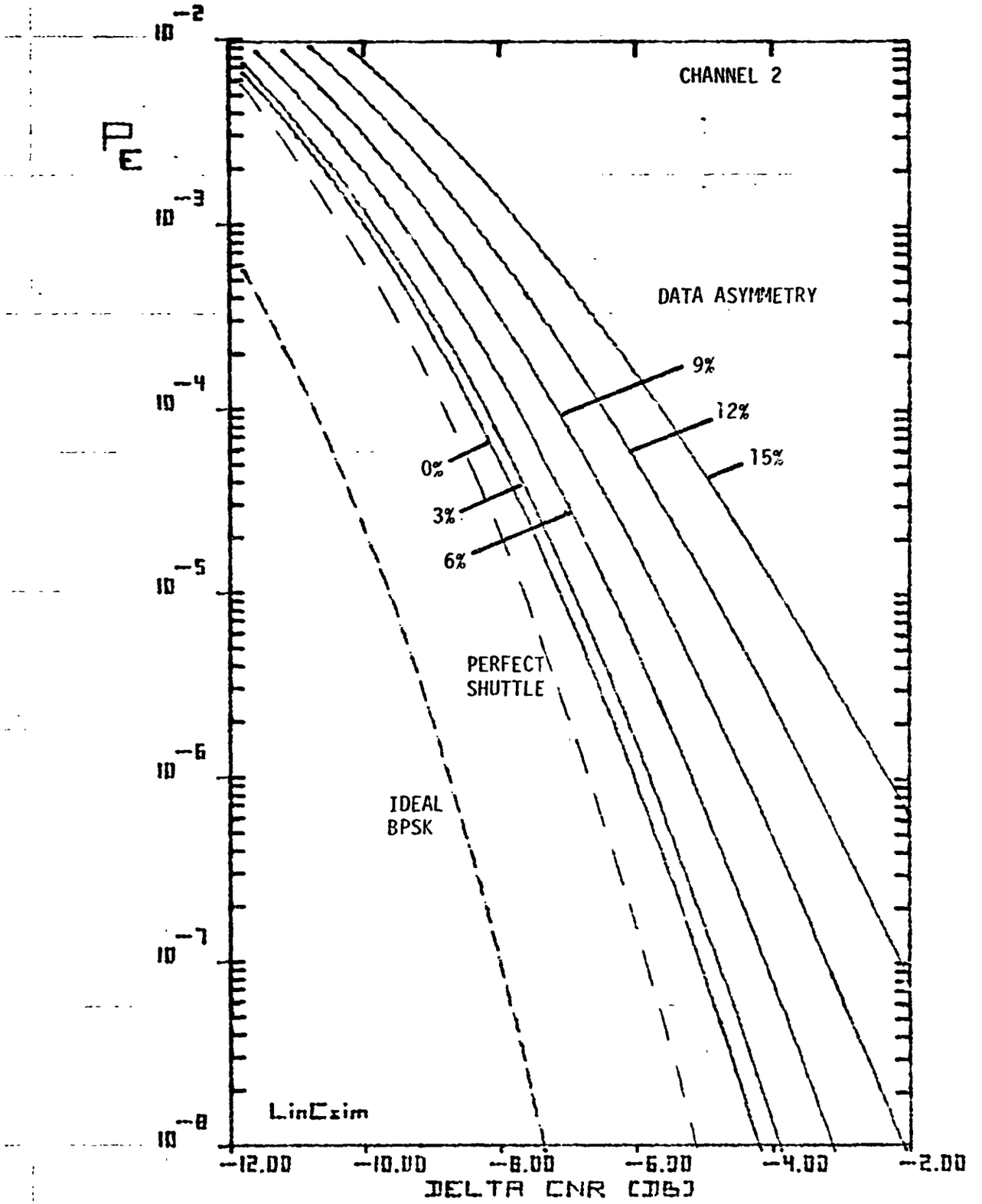

Figure 2.46. BER Plot for Data Asymmetry.

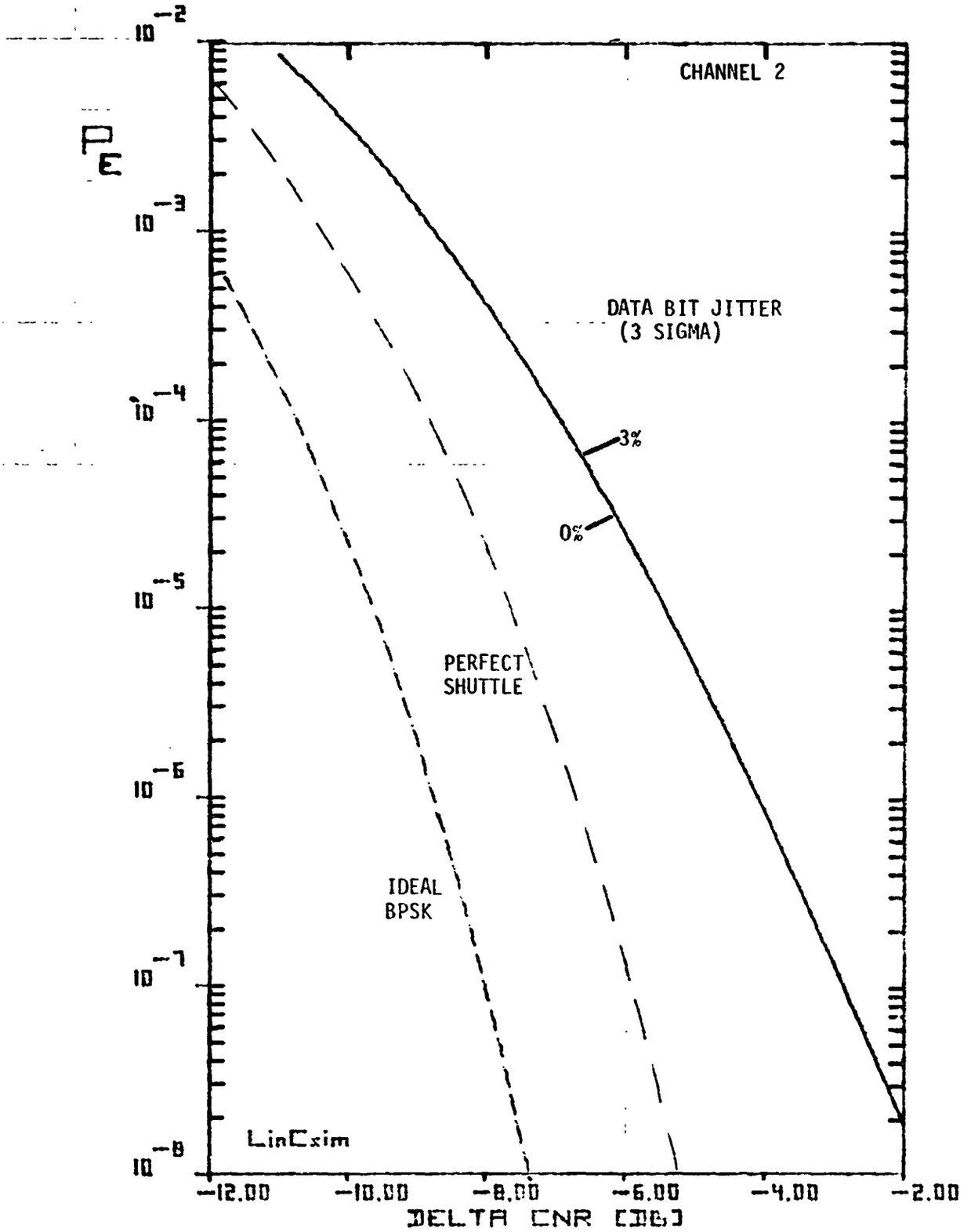

Figure 2.47. BER Plot for Data Bit Jitter.

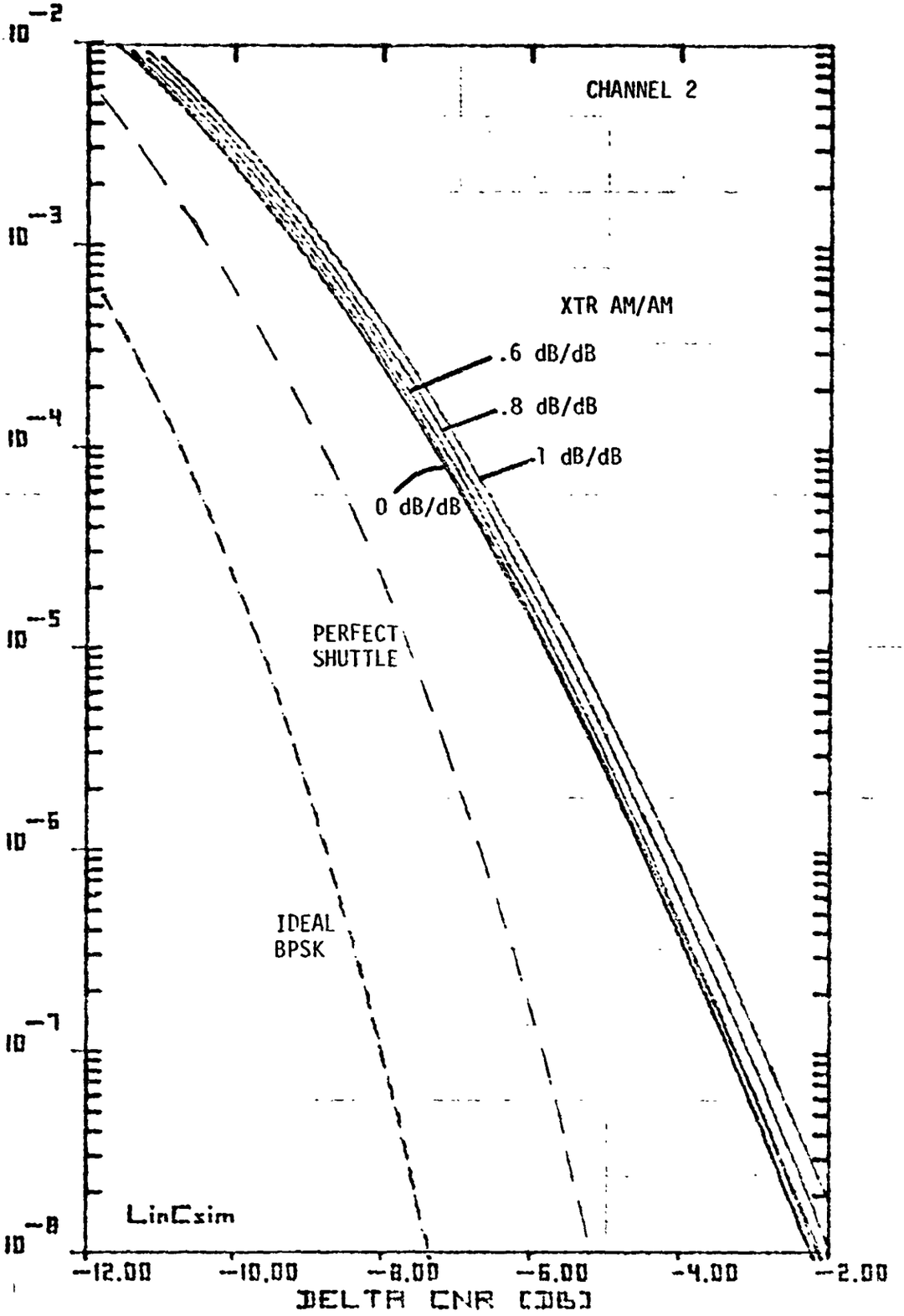

Figure 2.48.BER Plot for Transmitter AM/AM.

79 0122

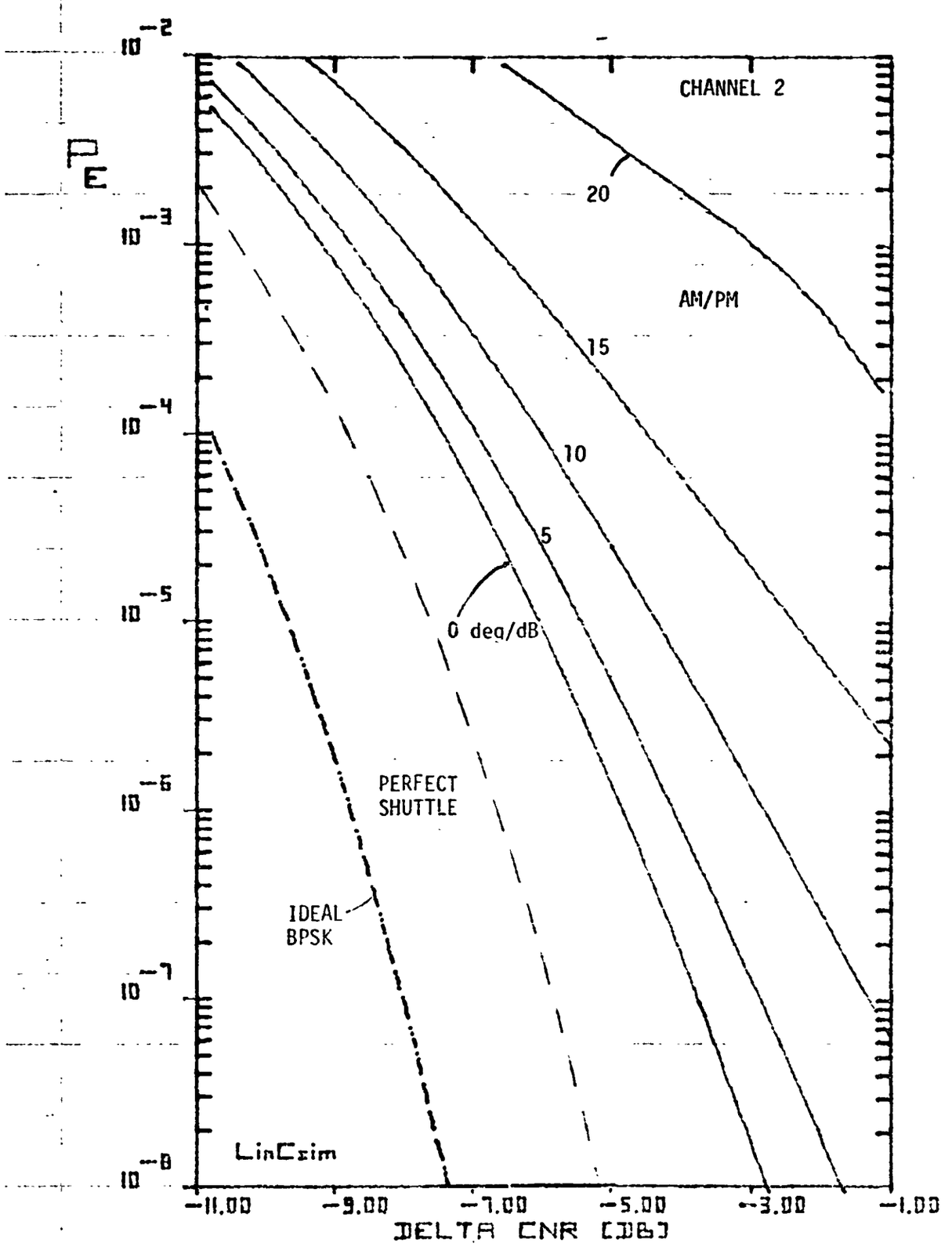

Figure 2.49. BER Plot for Transmitter AM/PM.

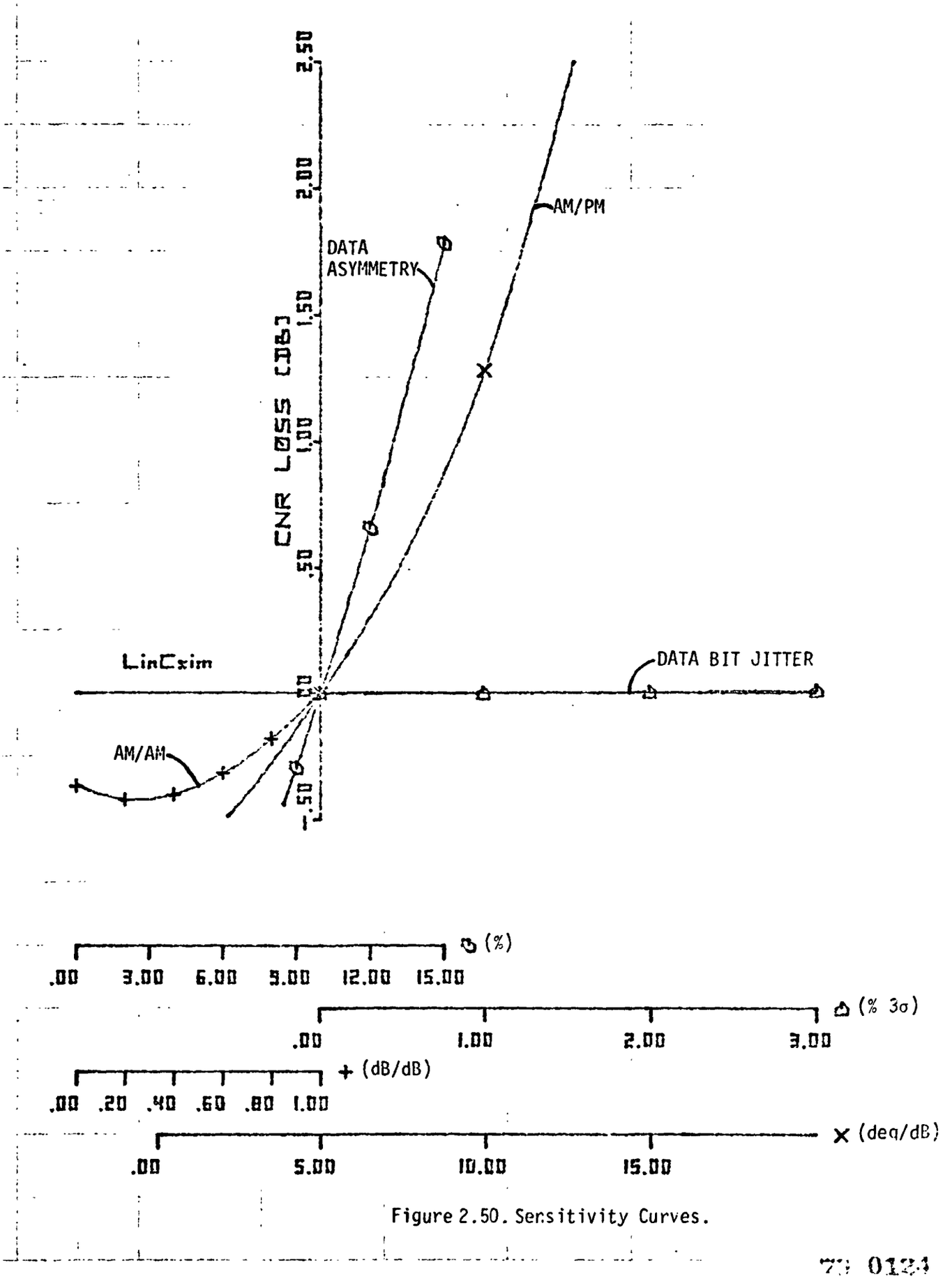

Figure 2.50. Sensitivity Curves.

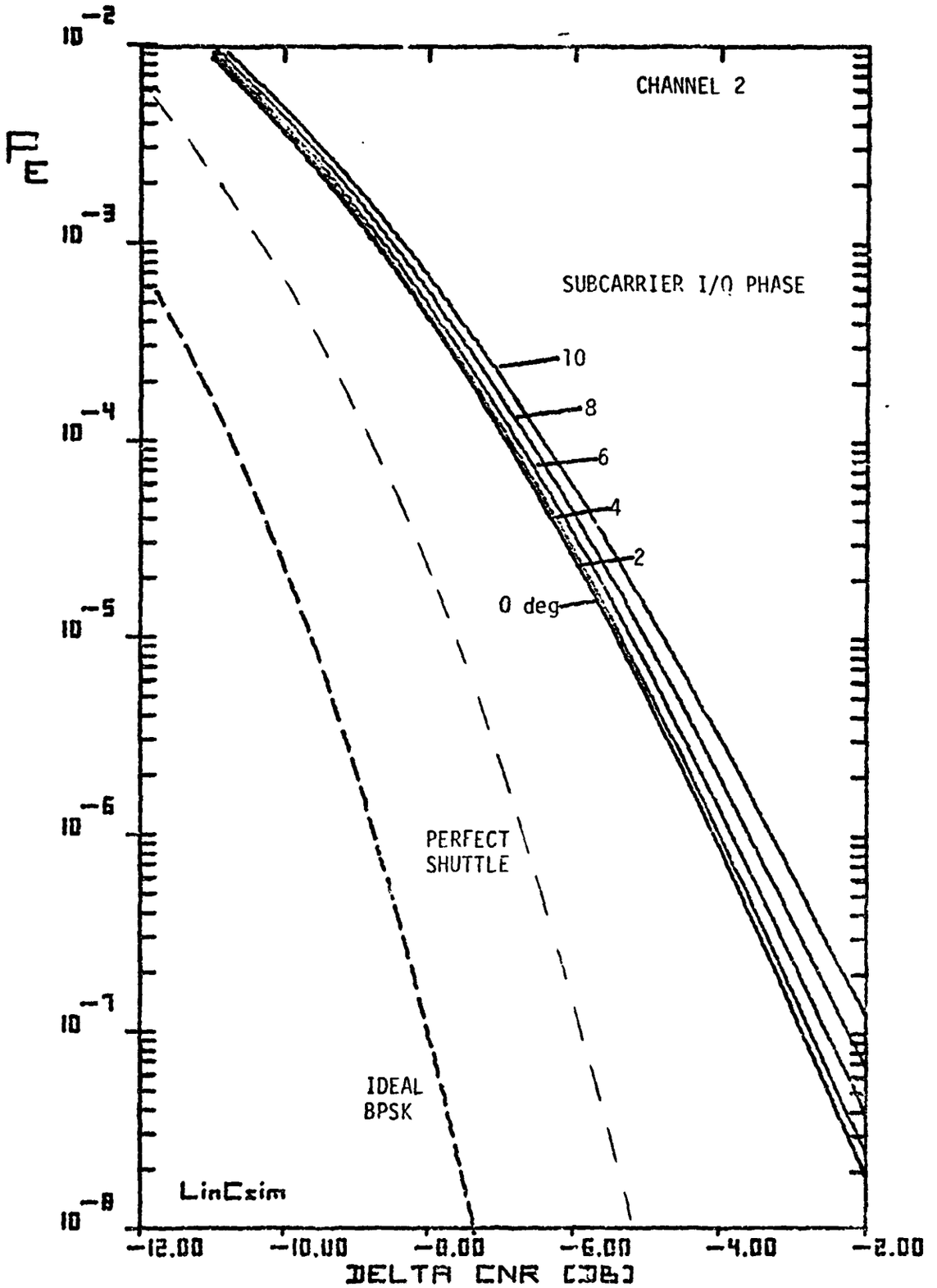

Figure 2.51. BER Plot for Subcarrier I/Q Phase.

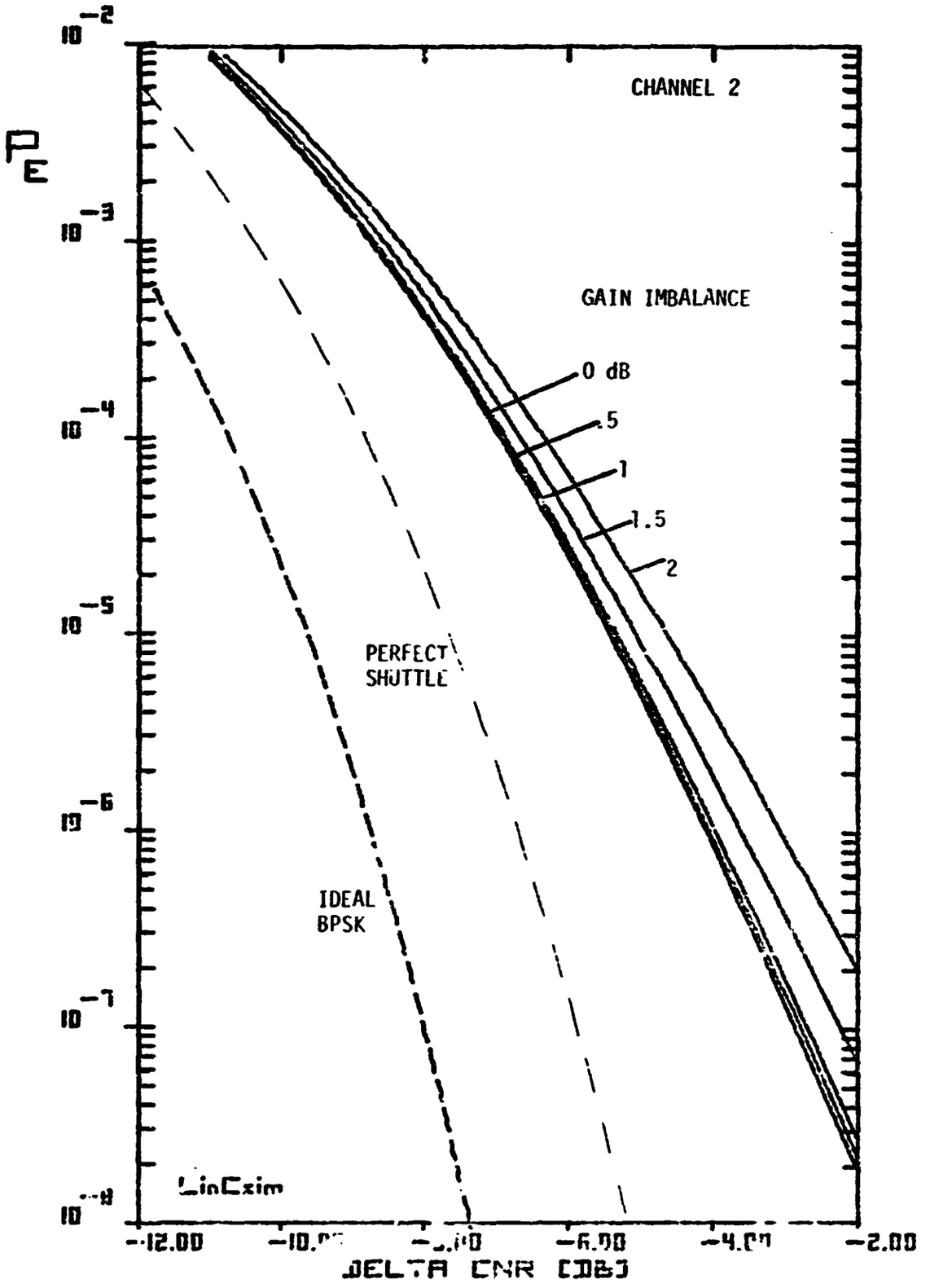

Figure 2.52.BER Plot for Subcarrier Modulator Gain Imbala

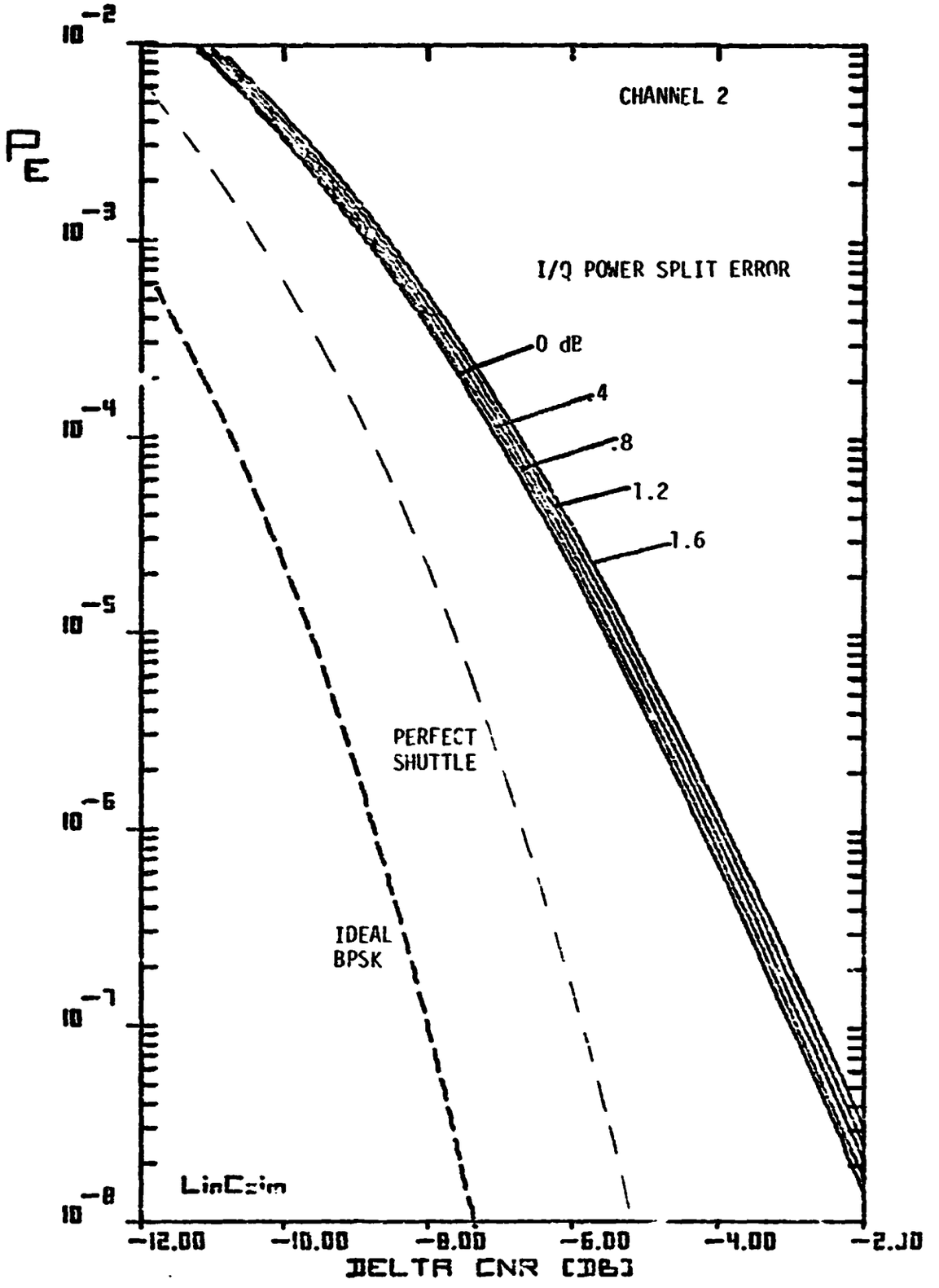

Figure 2.53. BER Plot for Subcarrier Power Split Error.

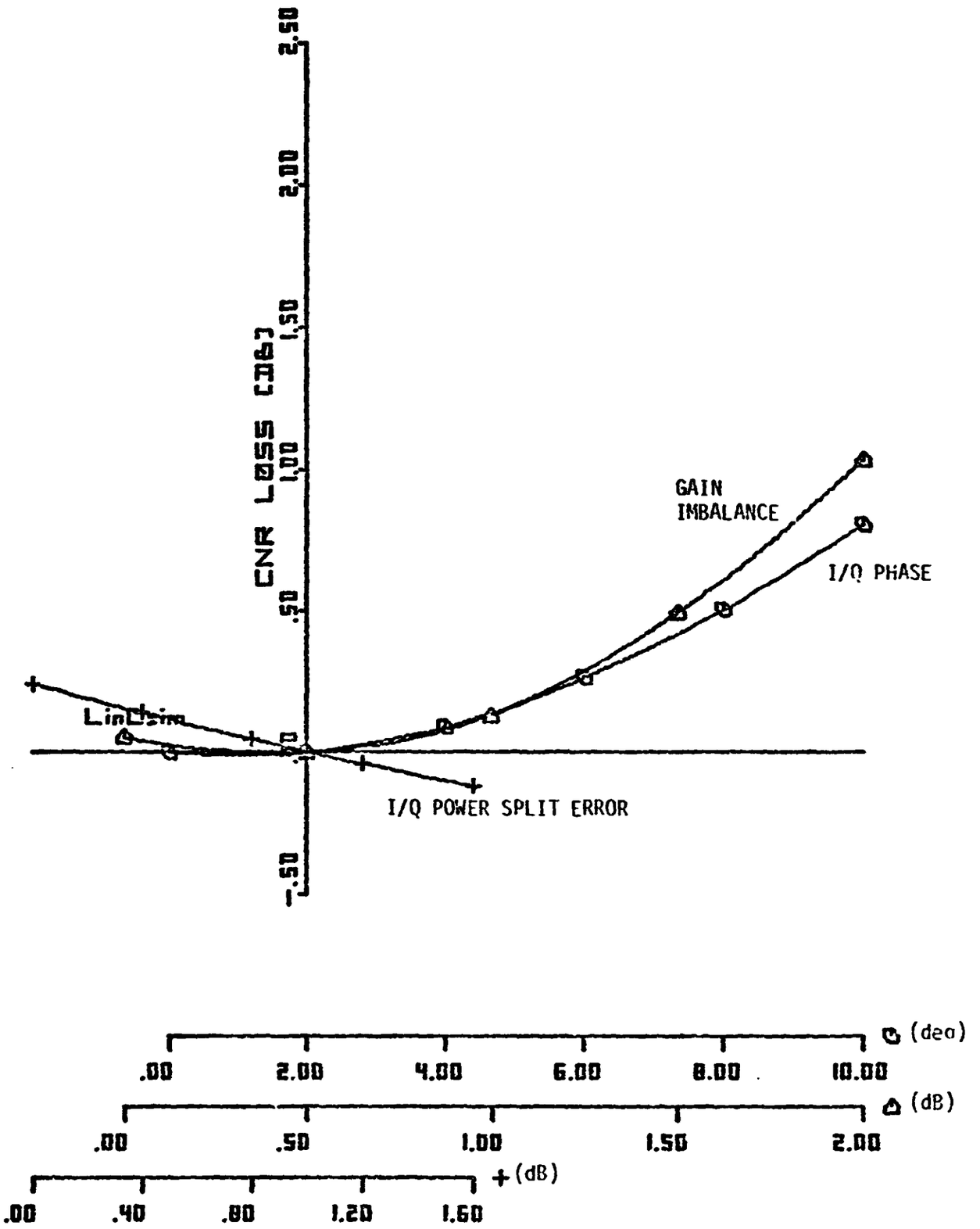

Figure 2.54.Sensitivity Curves for Subcarrier Parameters.

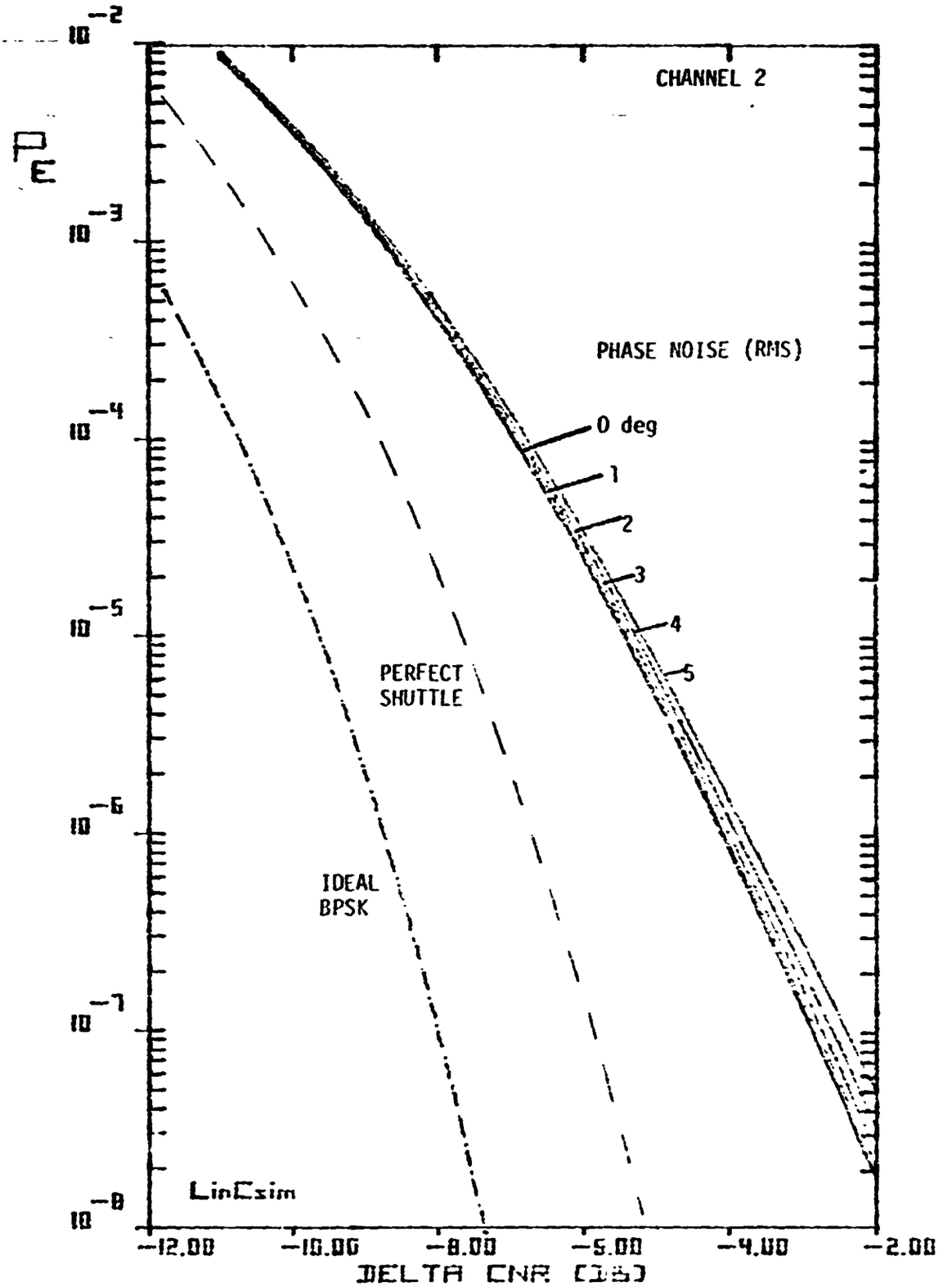

Figure 2.55. BER Plot for Subcarrier Phase Noise.

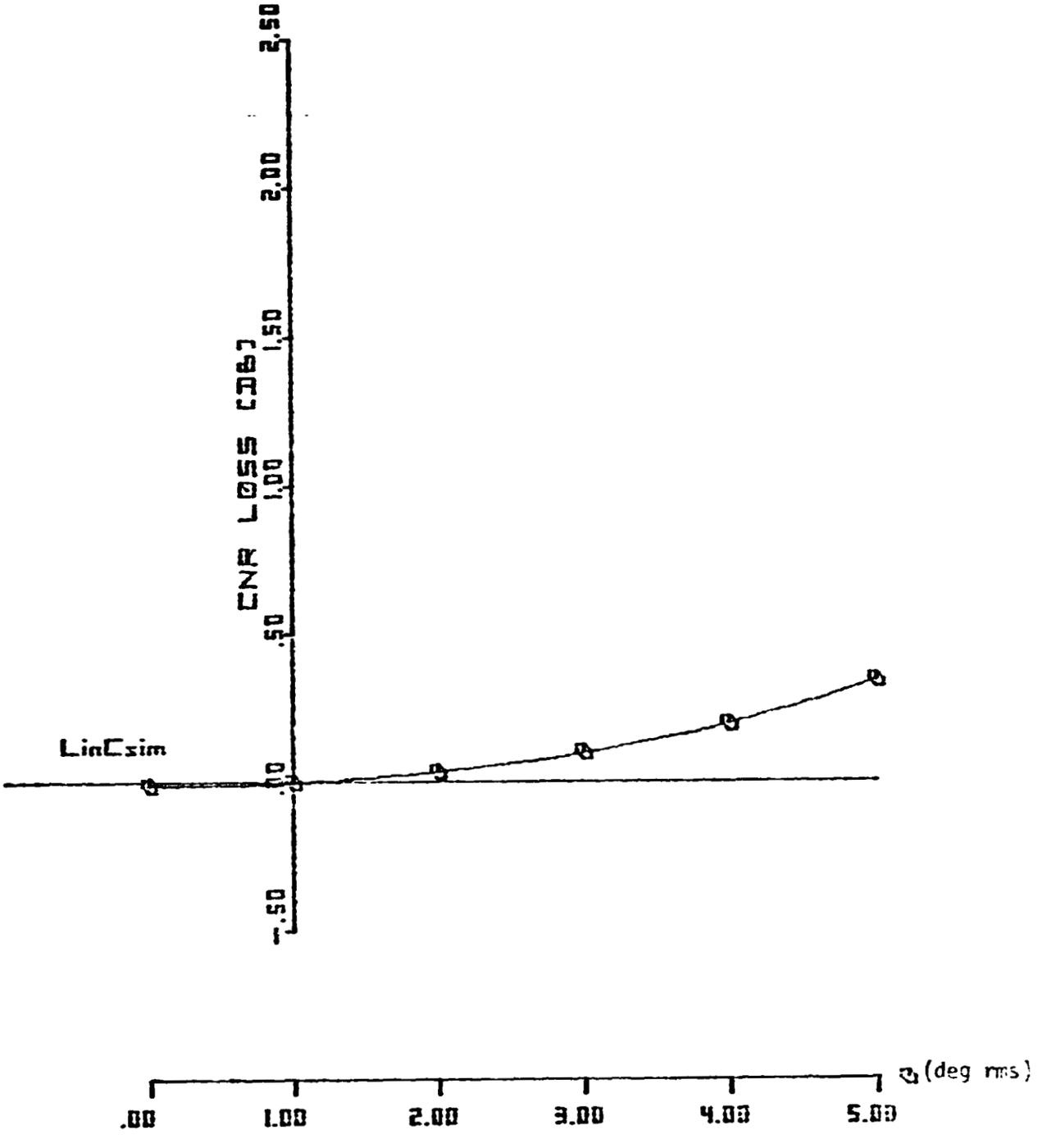

Figure 2.56. Sensitivity Curve for Subcarrier Phase Noise.

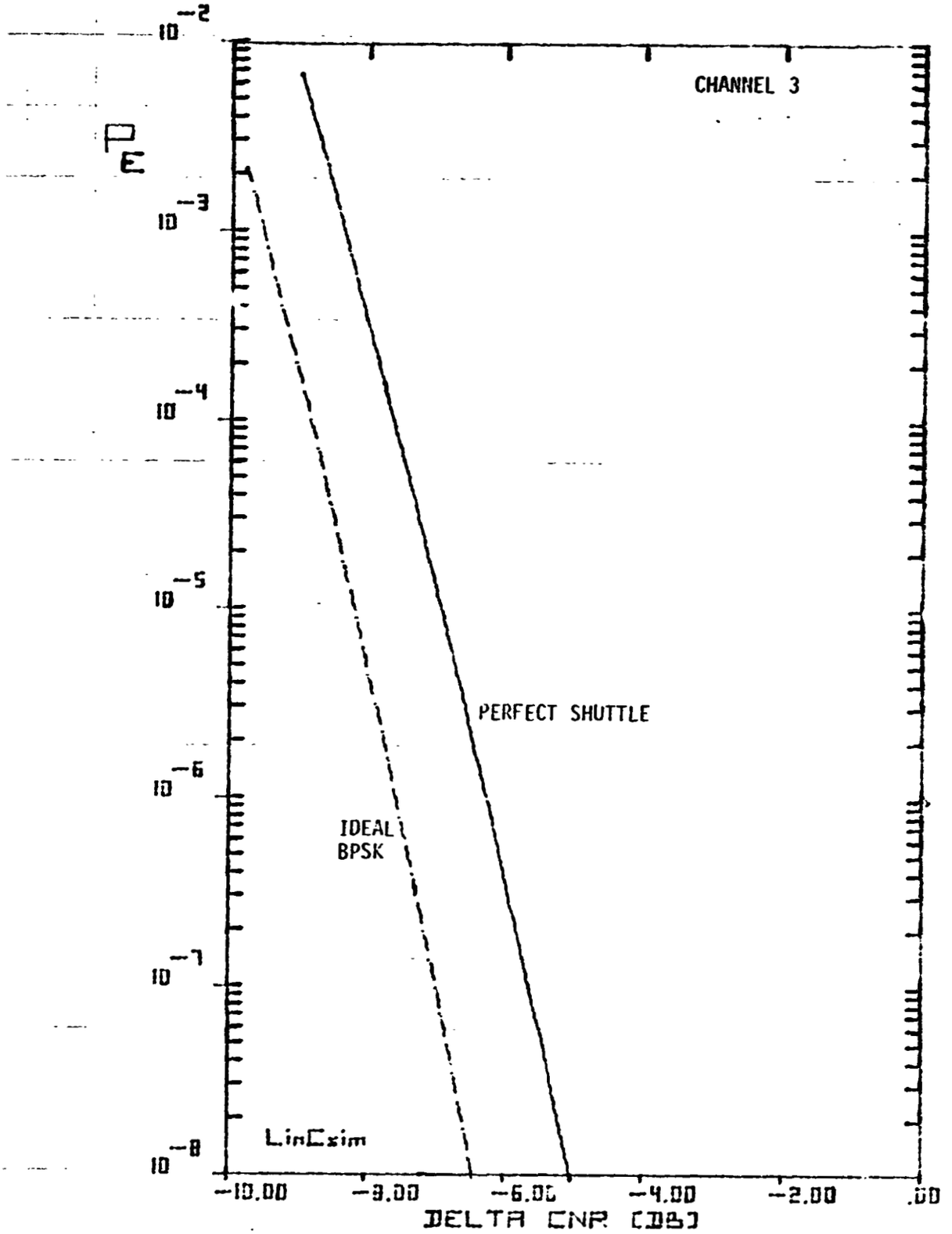

Figure 2.57. BER Plot for Perfect Shuttle Transmitter.

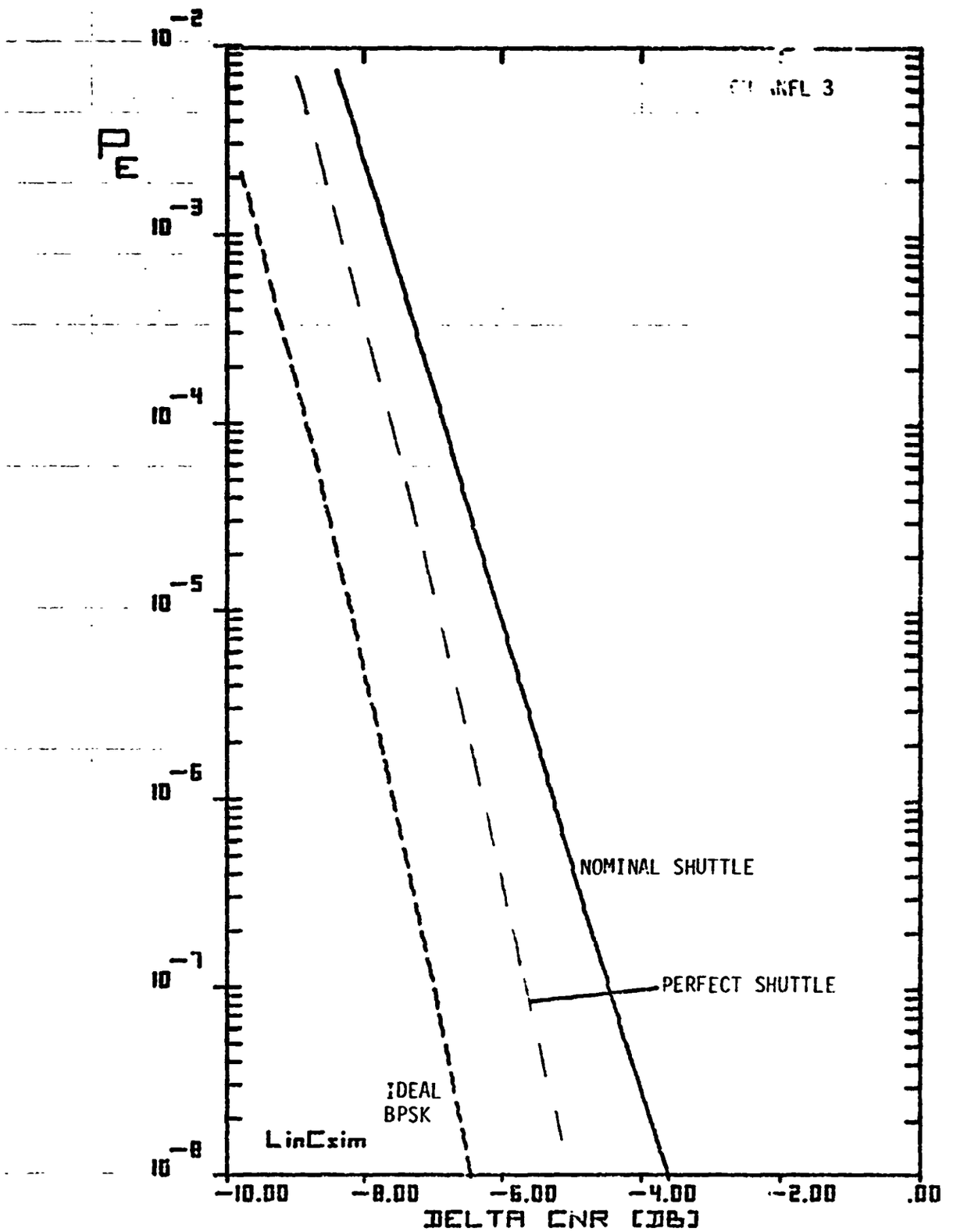

Figure 2.58. BER Plot for Nominal Shuttle Transmitter.

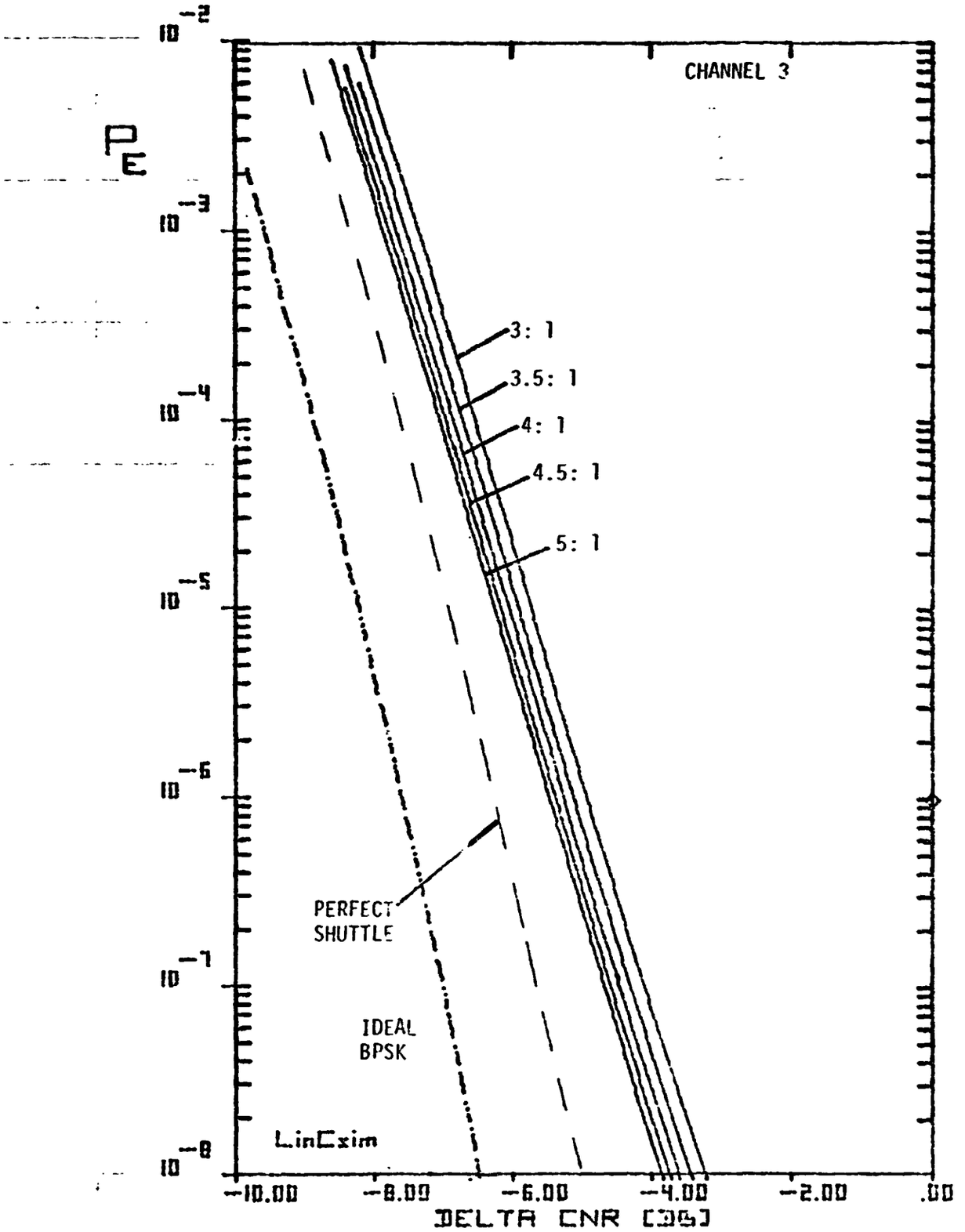

Figure 2.59. BER Plot for Carrier Power Split.

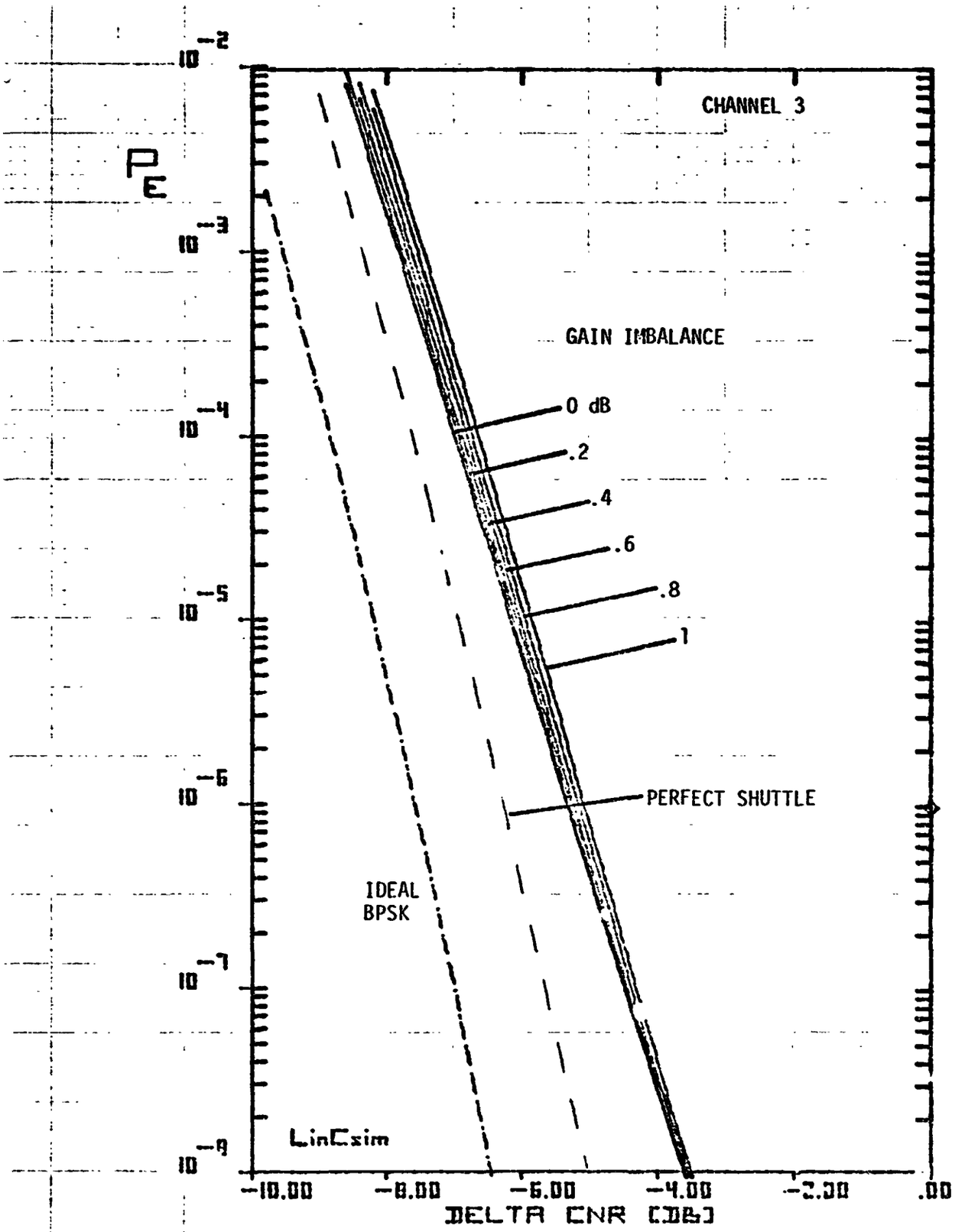

Figure 2.6c. BER Plot for Modulator Gain Imbalance.

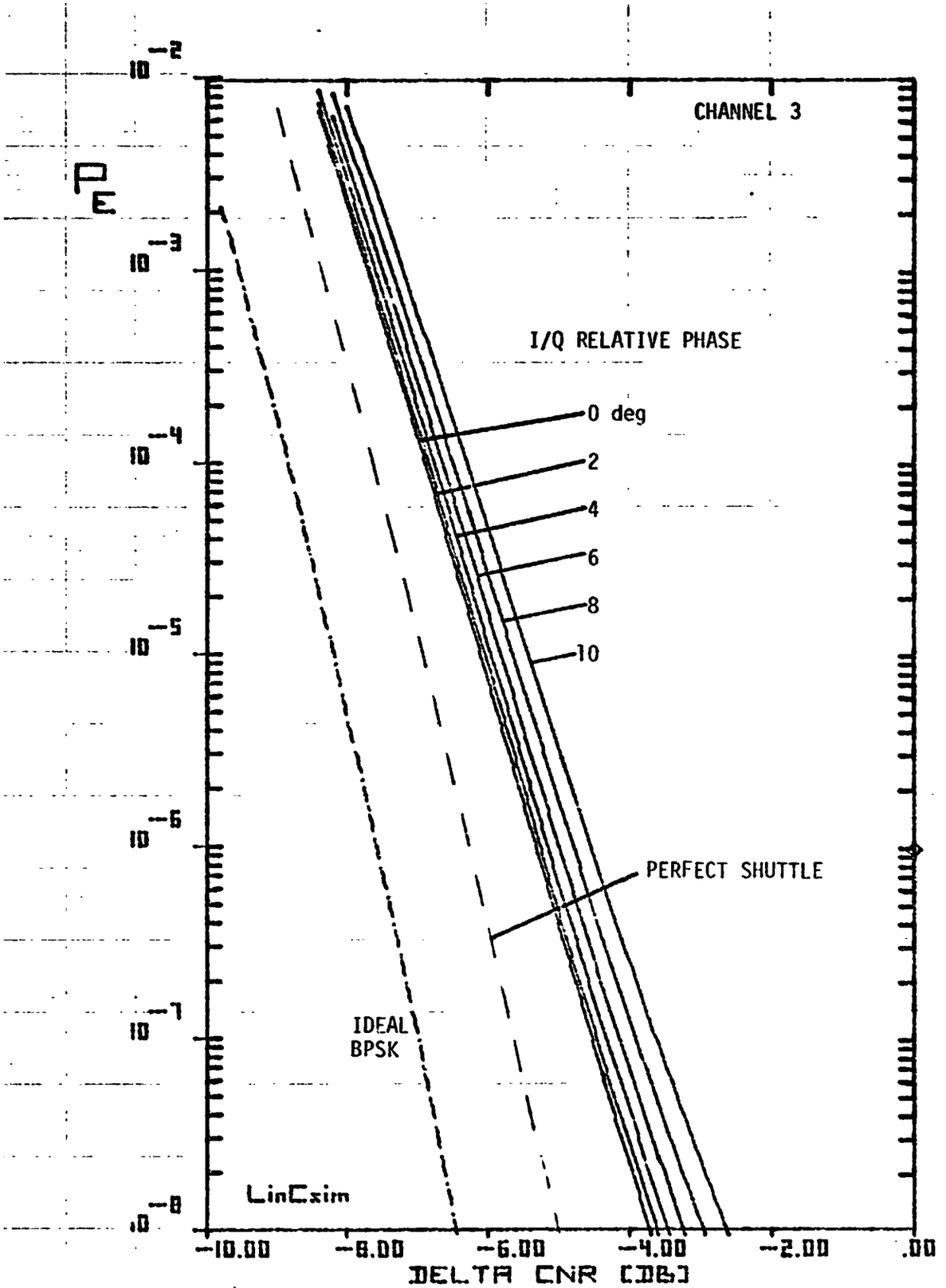

Figure 2.61.BER Plot for Relative I/Q Carrier Phase.

79 0136

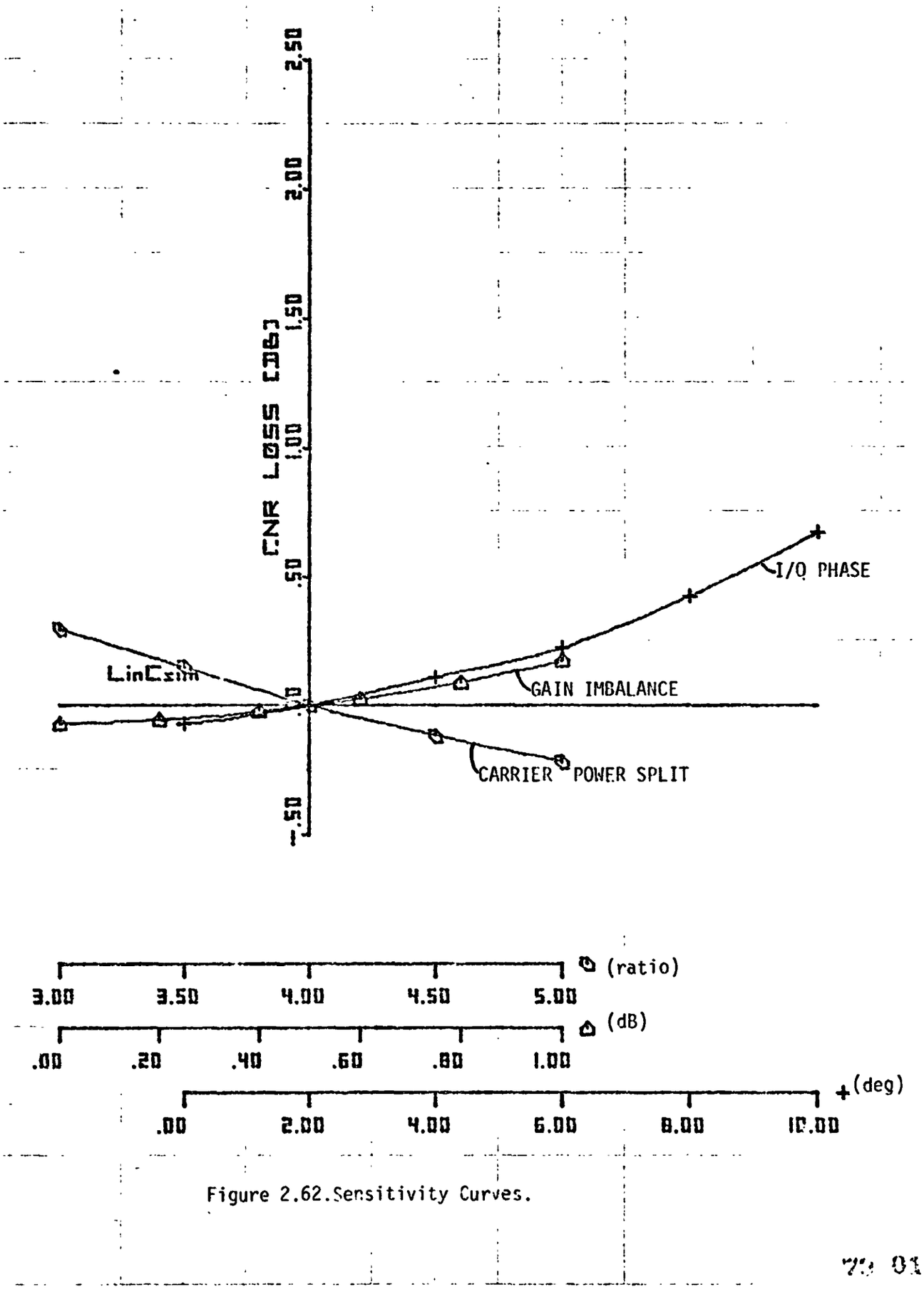

Figure 2.62. Sensitivity Curves.

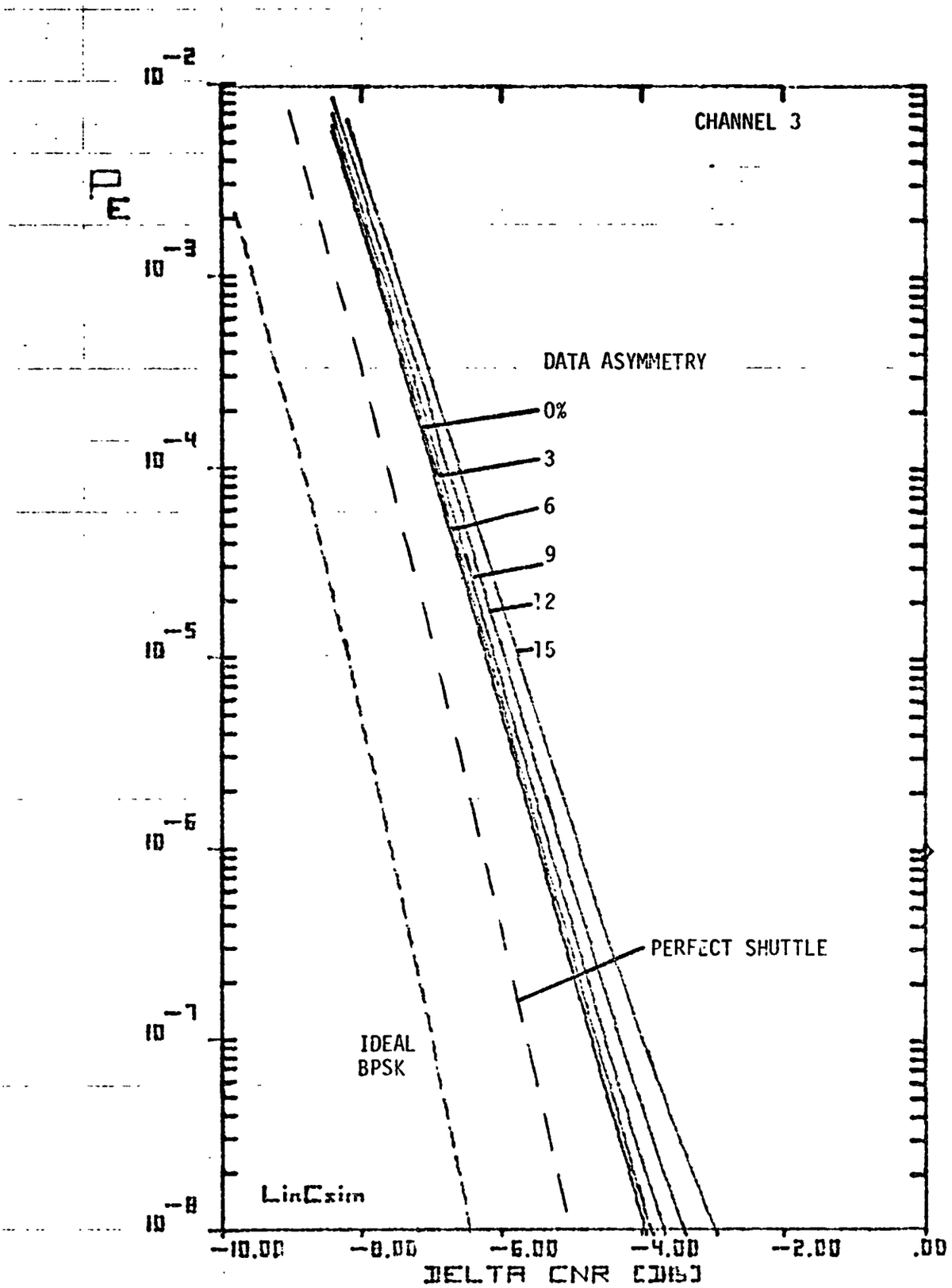

Figure 2.63. BER Plot for Data Asymmetry.

79 0137

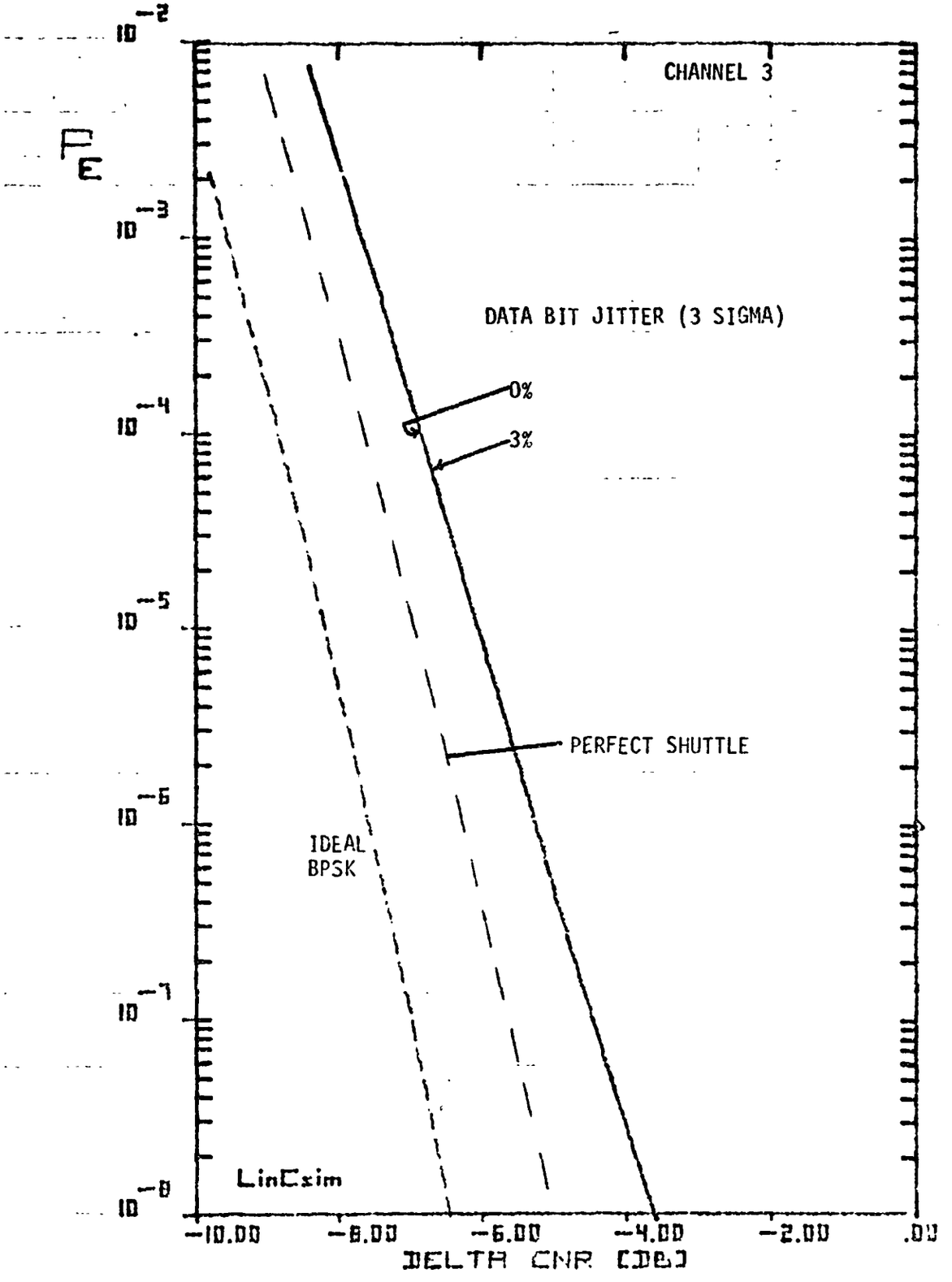

Figure 2.64. BER Plot for Data Bit Jitter.

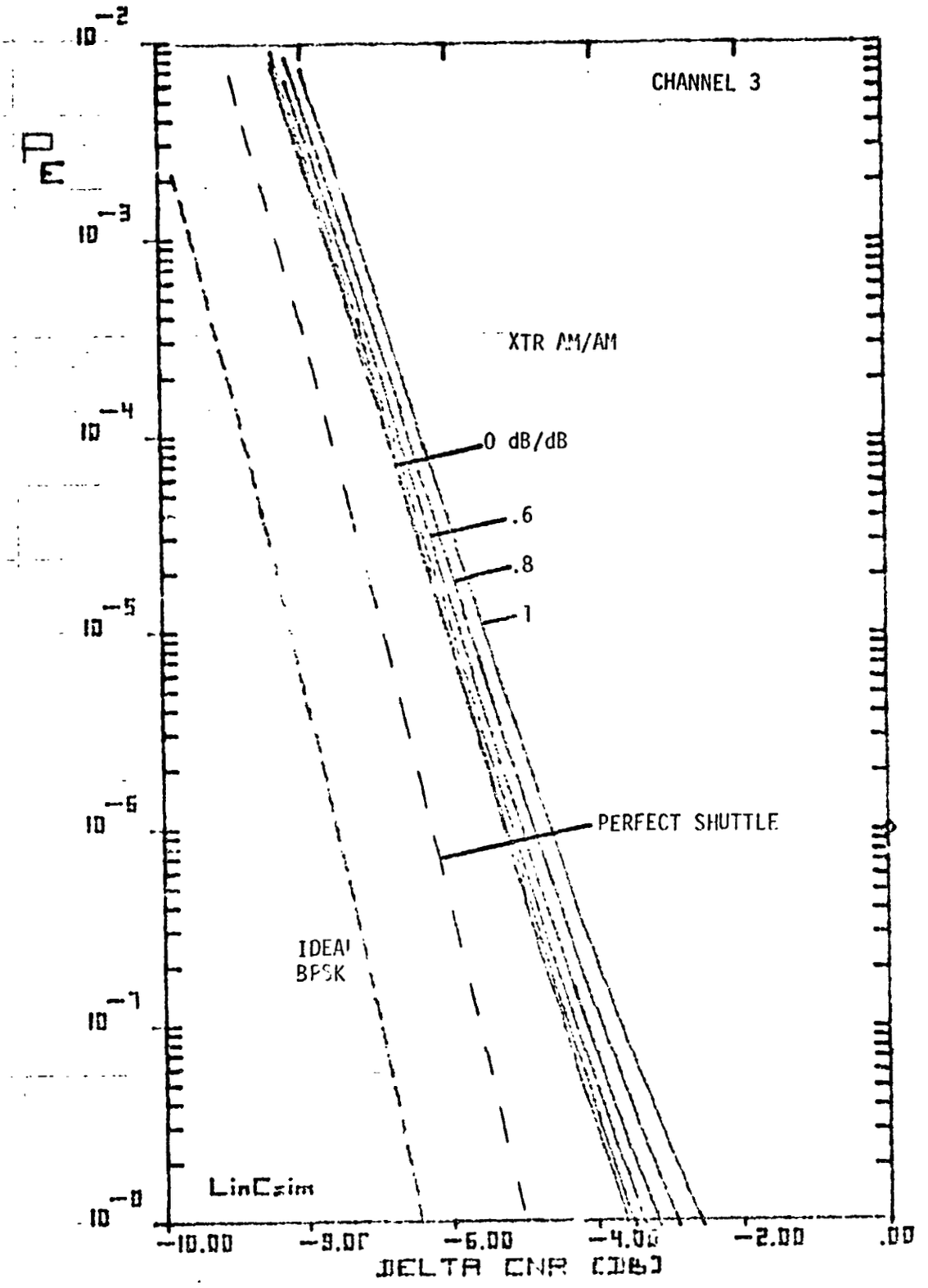

Figure 2.65. BER Plot for Transmitter AM/AM.

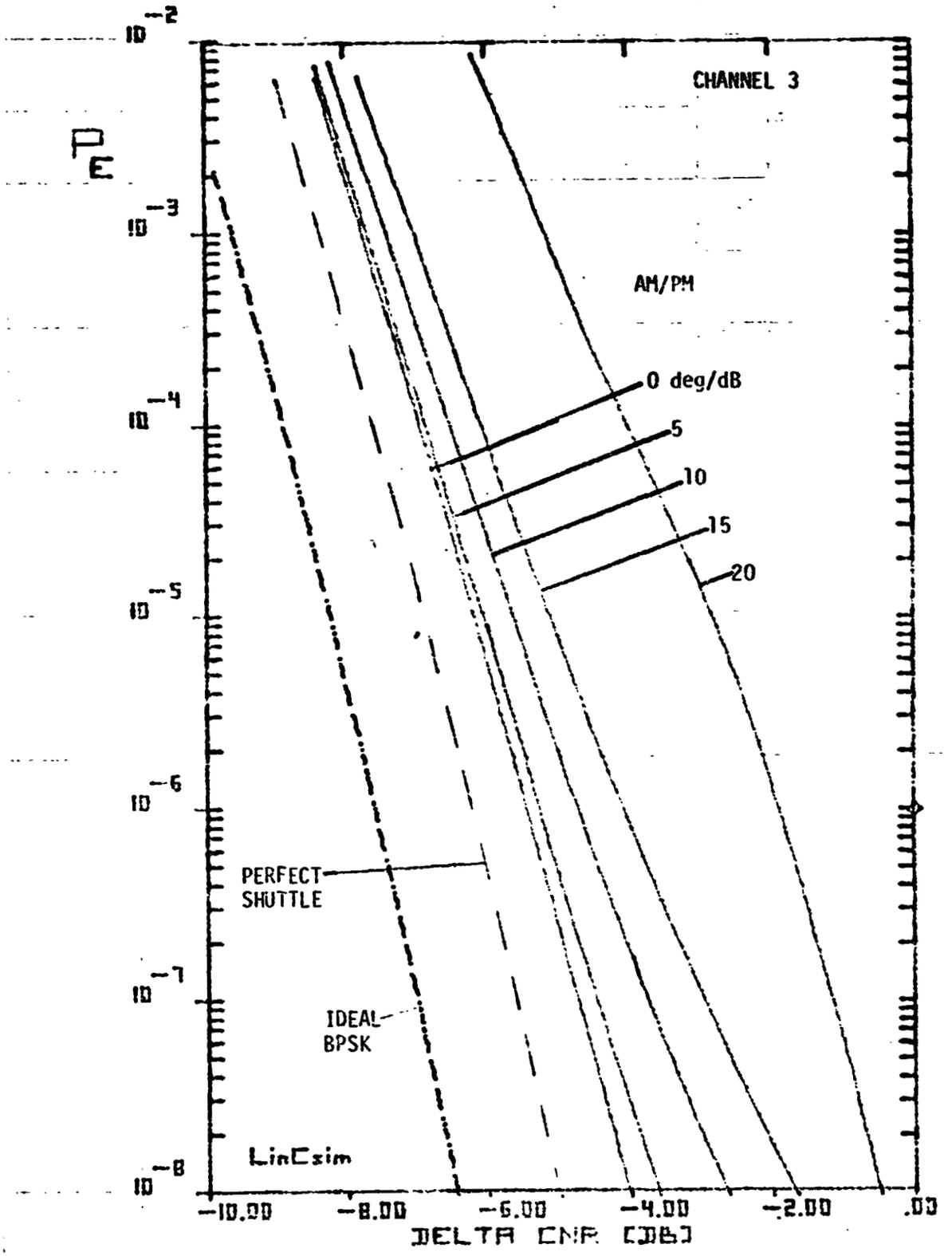

Figure 2.66.BER Plot for Transmitter AM/PM.

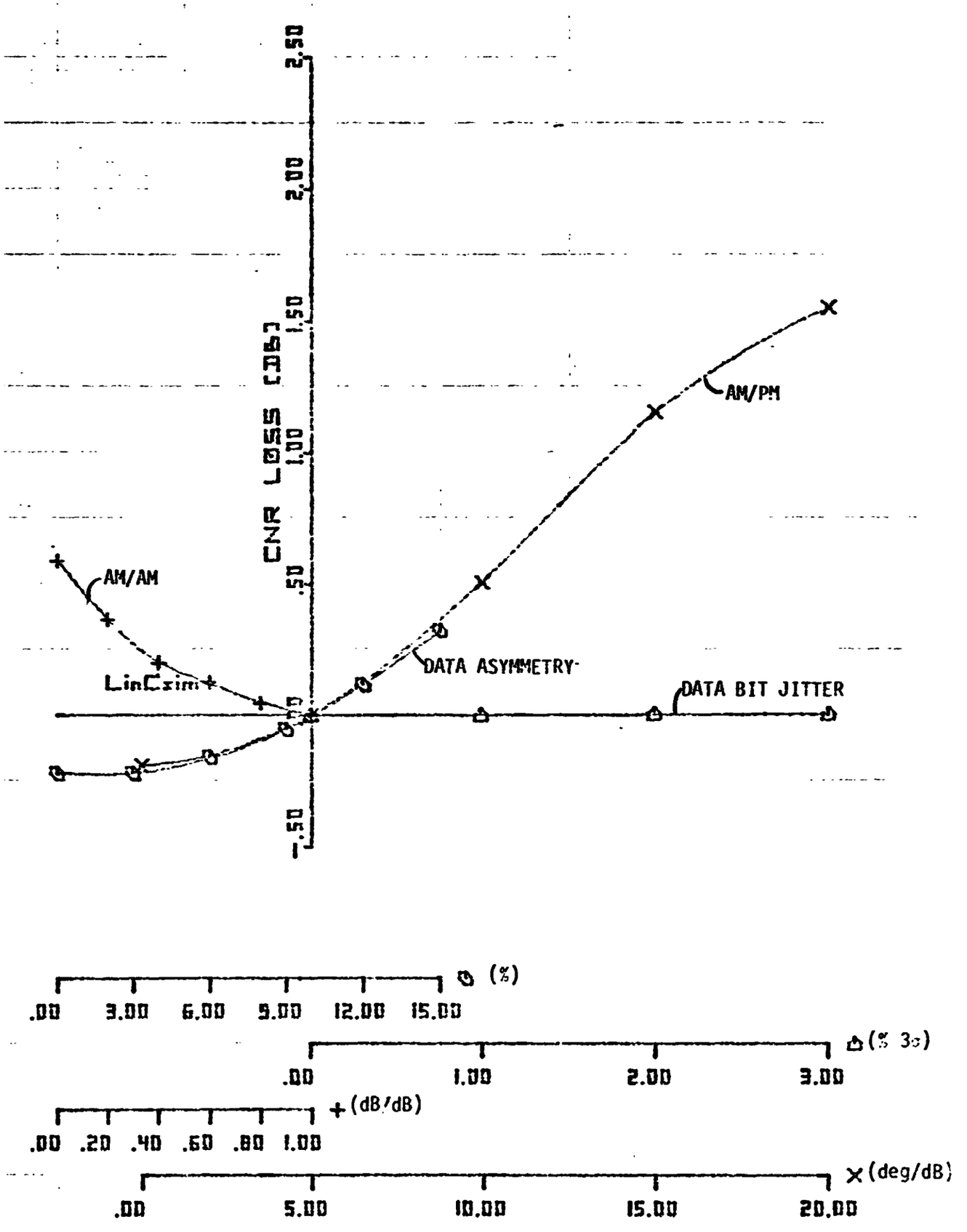

Figure 2.67. Sensitivity Curves.

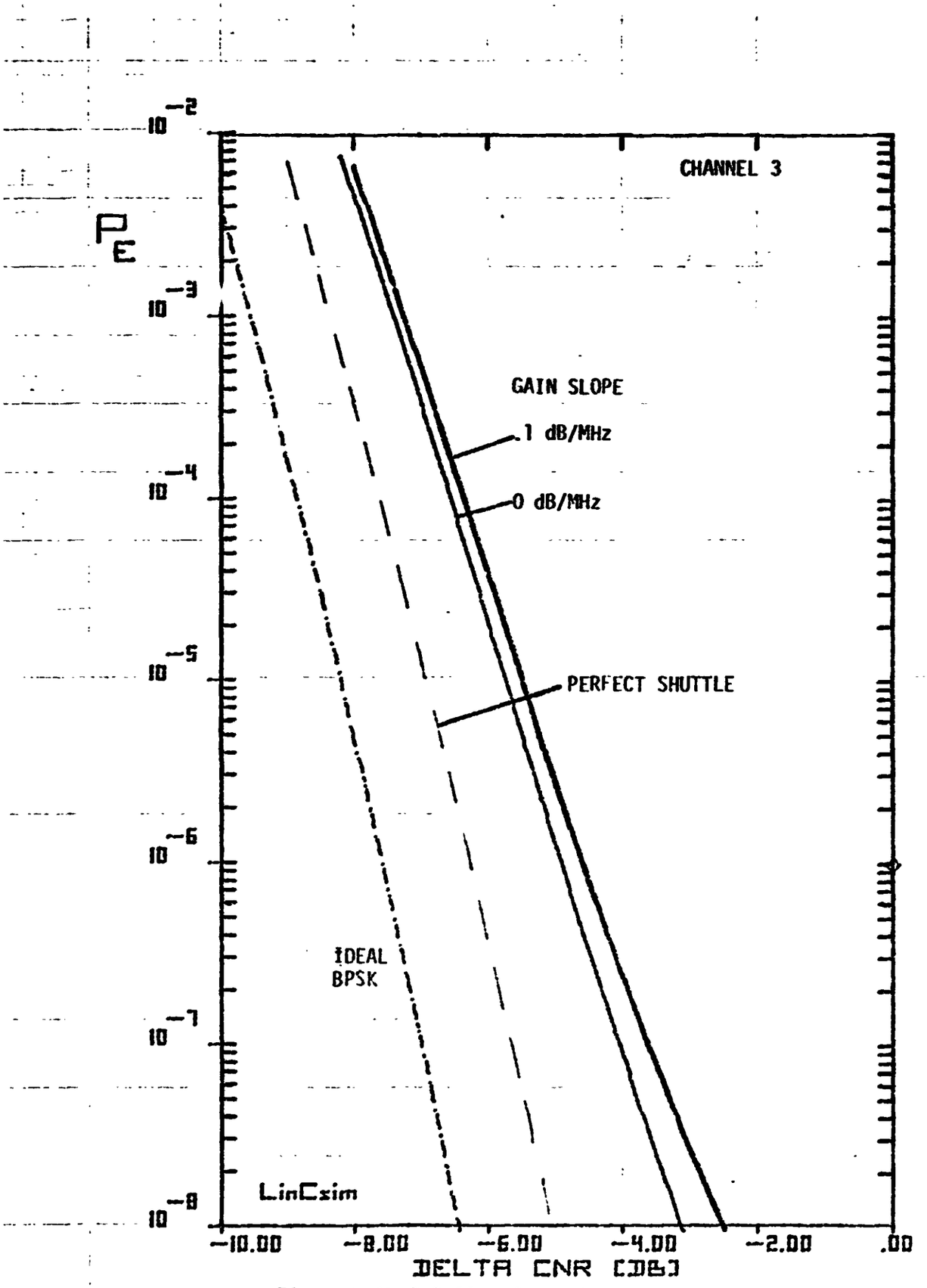

Figure 2.68. BER Plot for Gain Slope.

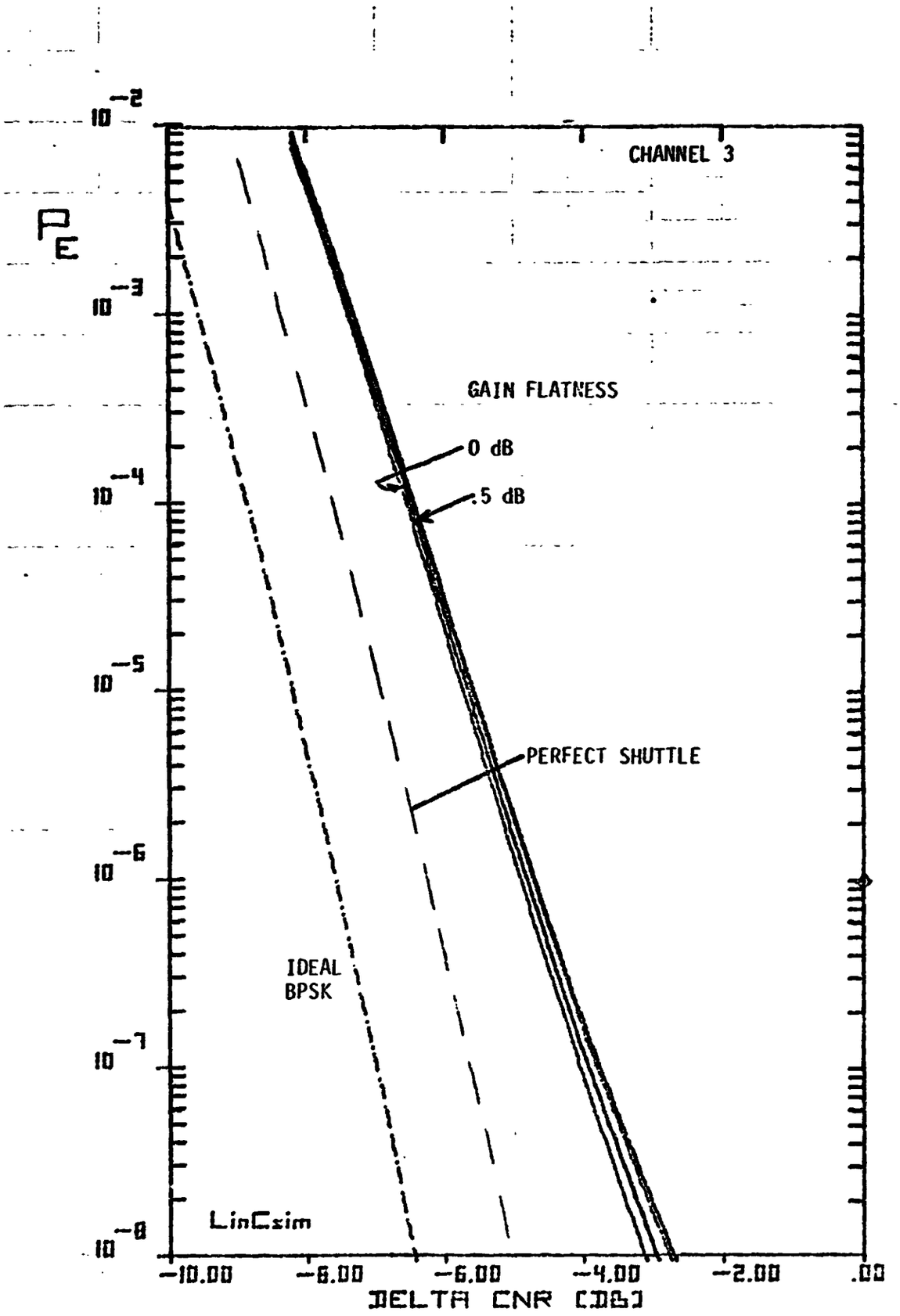

Figure 2.69. BER Plot for Gain Flatness.

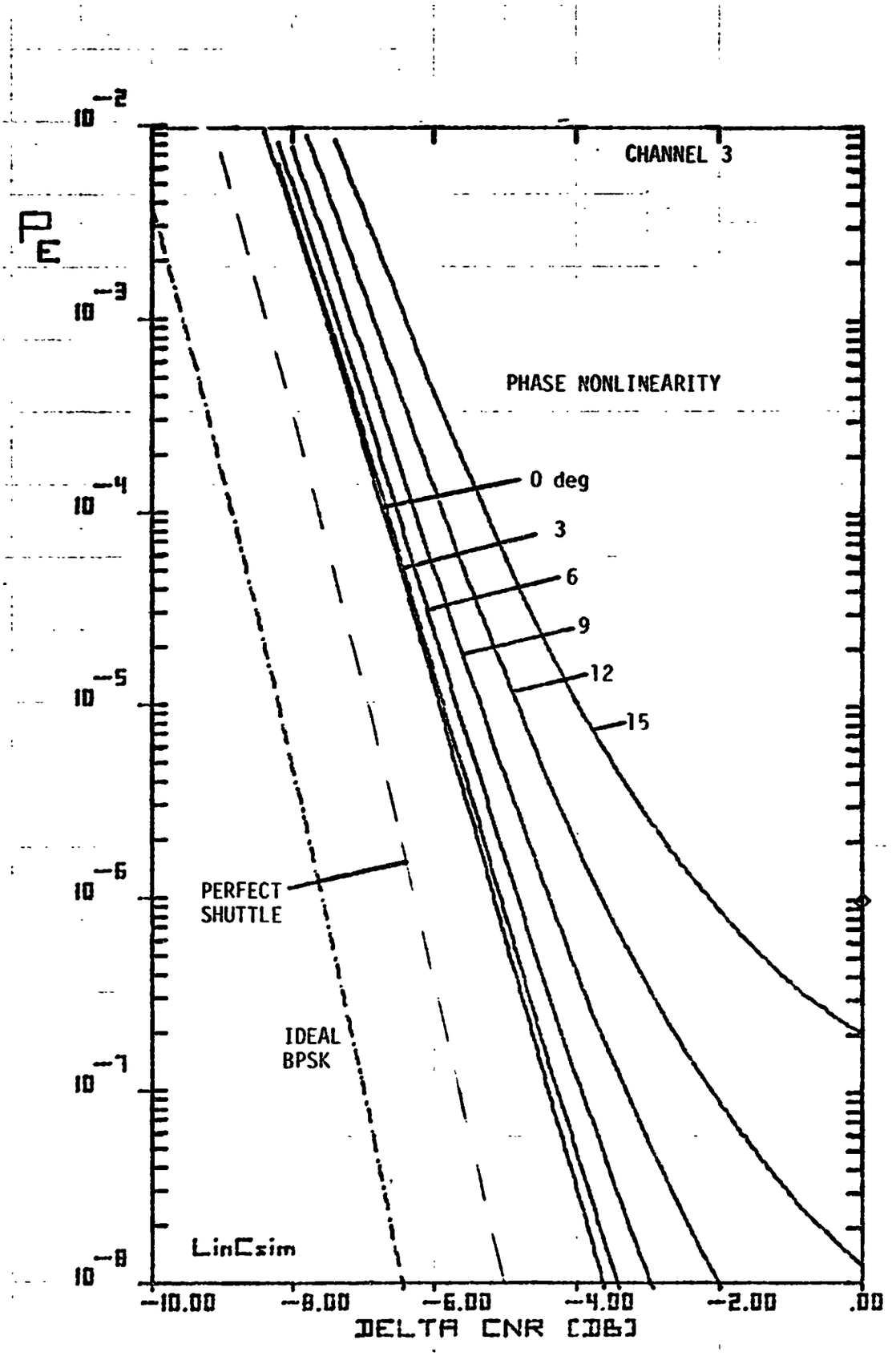

Figure 2.70. BER Plot for Phase Nonlinearity.

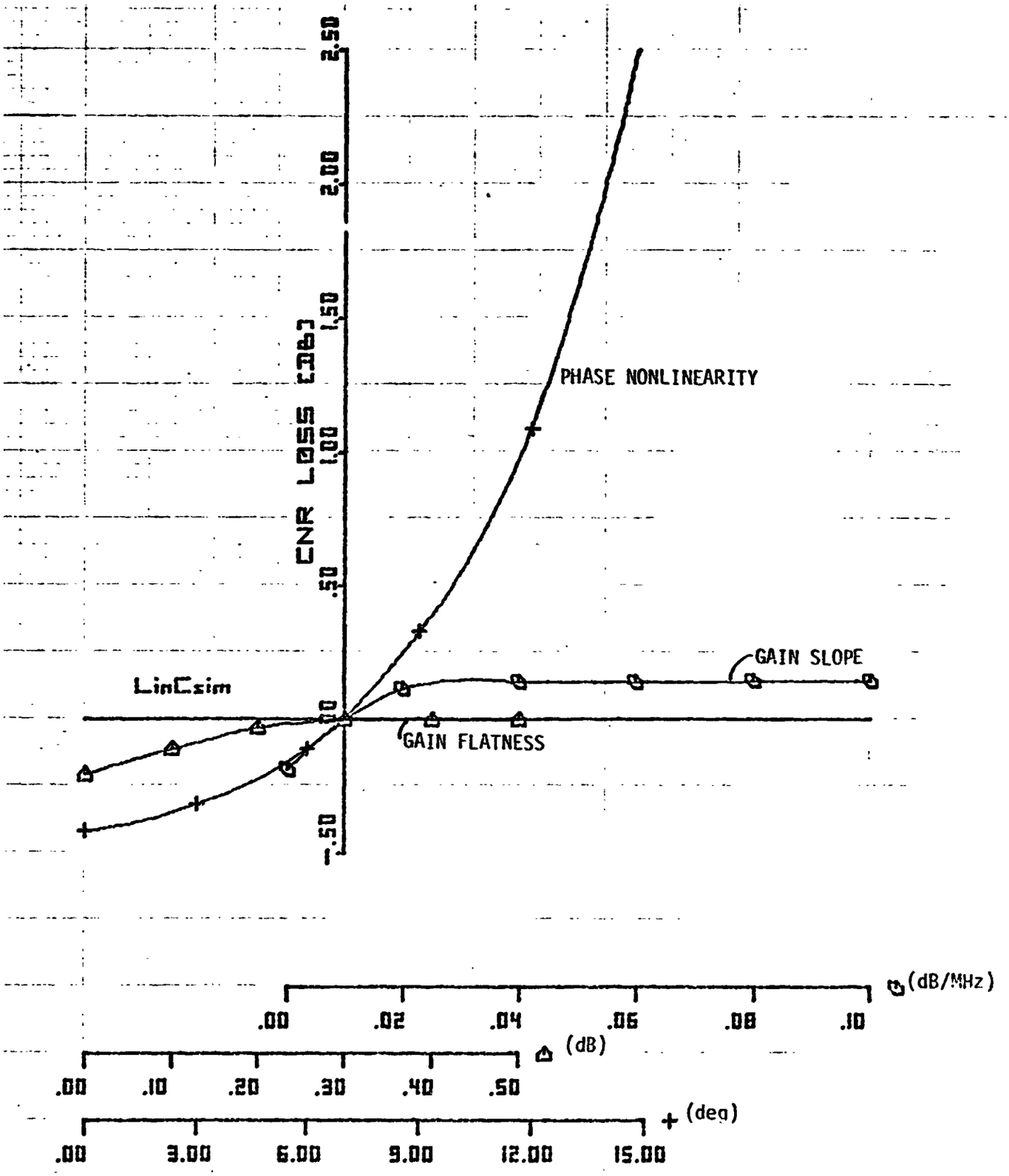

Figure 2.71. Sensitivity Curves.

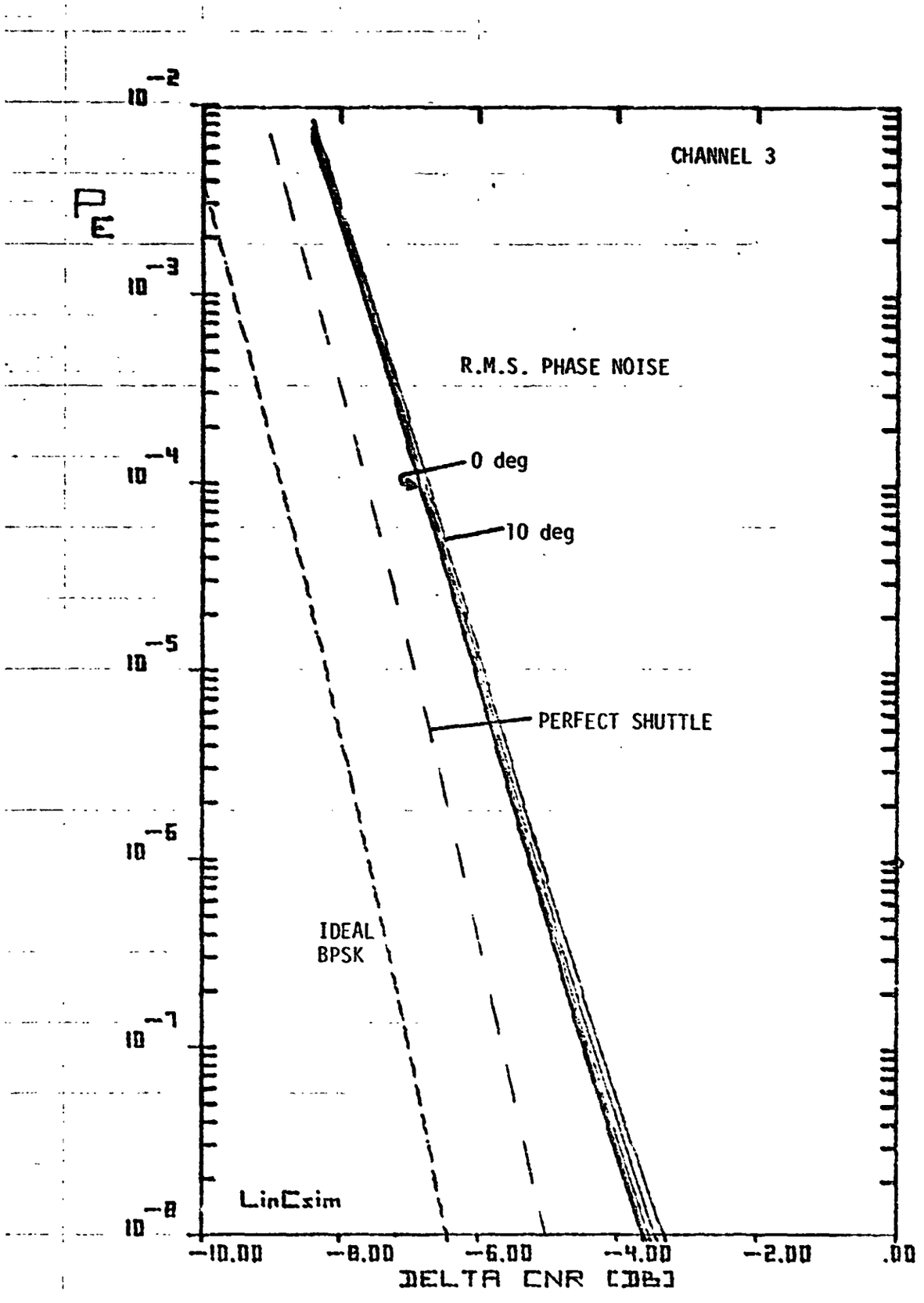

Figure 2.72. BER Plot for Carrier Phase Noise (1 kHz to 150 MHz).

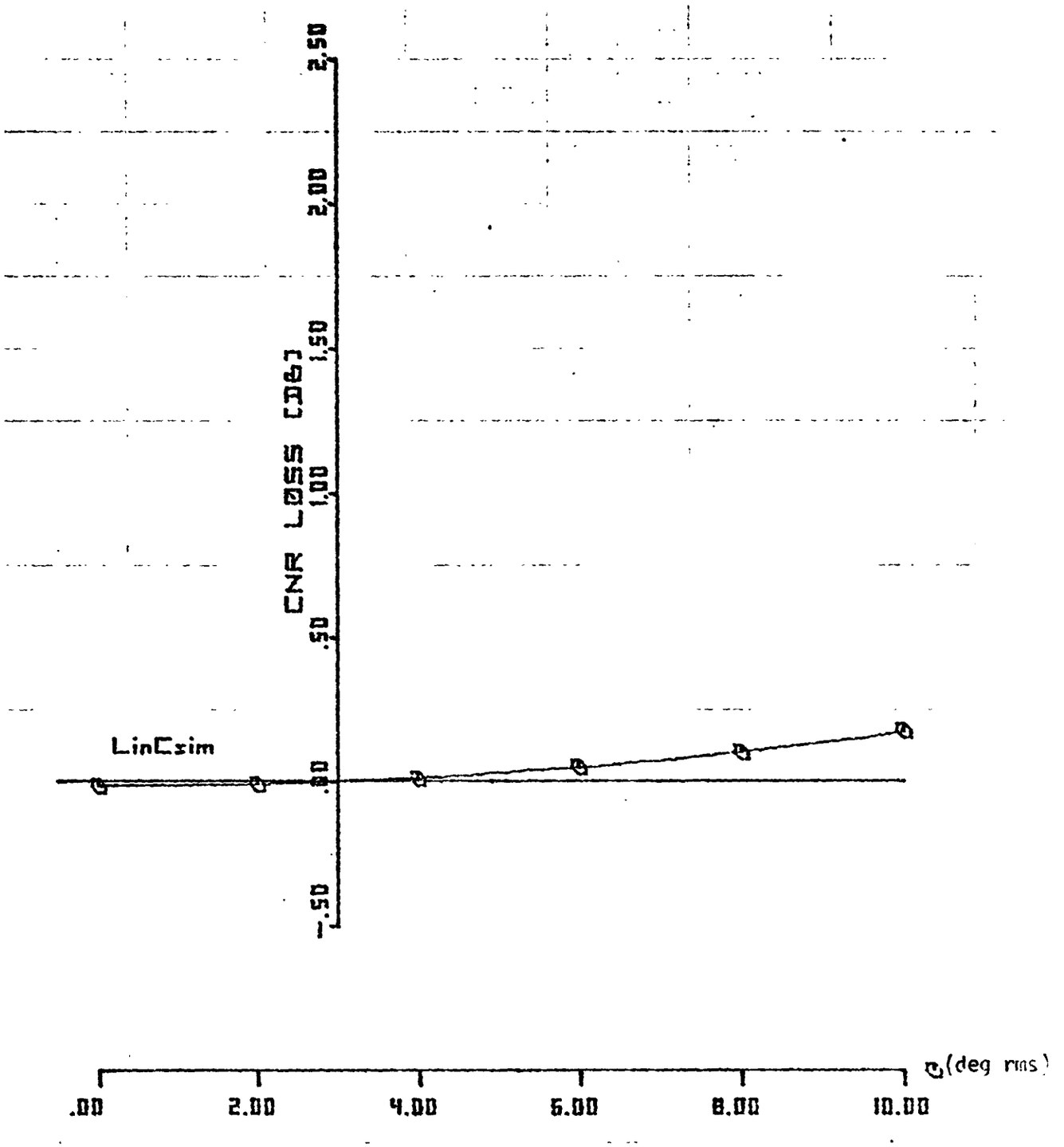

Figure 2.73. Sensitivity Curve for Carrier Phase Noise.

REFERENCES

[1] Tracking and Data Relay Satellite System (TDRSS) Users' Guide, Revision 3, STDN No. 101.2, Goddard Space Flight Center, Greenbelt, MD, January, 1978.

[2] Space Shuttle RF Link Circuit Margins, Jan. 1977.

3. LinCsim MODELING OF CARRIER AND TIMING RECOVERY

3.1 Introduction

This chapter presents models of carrier and timing recovery for the Shuttle/TDRSS S-band and Ku-band mode 1 return links in the absence of radio-frequency interference (RFI). The generalized nonlinear link is described in Section 3.2. Sections 3.3 and 3.4 present expressions for the S-curve and r.m.s. recovered phase error for the S-band and Ku-band mode 1, respectively. Two sections are taken for carrier recovery because the two links use different loops. The carrier is assumed to have constant phase and frequency. Section 3.5 presents expressions for the S-curve and normalized r.m.s. recovered timing error for both NRZ and biphase (i.e., Manchester) symbols.

The chapter following this one gives models for the RFI effects on the loops and gives numerical results in the form of curves for both no-RFI and RFI situations, assuming some typical link parameter values.

3.2 Generalized Link Description

In order to study the phase and symbol-timing recovery, we must characterize the signal at the input to the White Sands ground station. The general link diagram used herein for both S-band and Ku-band mode 1 return links is shown in Figure 3.1. For S-band, only one symbol stream is present. The three symbol streams on the Ku-band return link are handled by treating channel 3 and the modulated square-wave subcarrier as one UQPSK signal and then channels 2 and 1 as another.

Let us start by assuming that the Shuttle transmits the signal

$$y_1(t) = \sqrt{2P_1}\,d_1(t)\cos \omega t - \sqrt{2P_2}\,d_2(t) \sin \omega t \qquad (1)$$

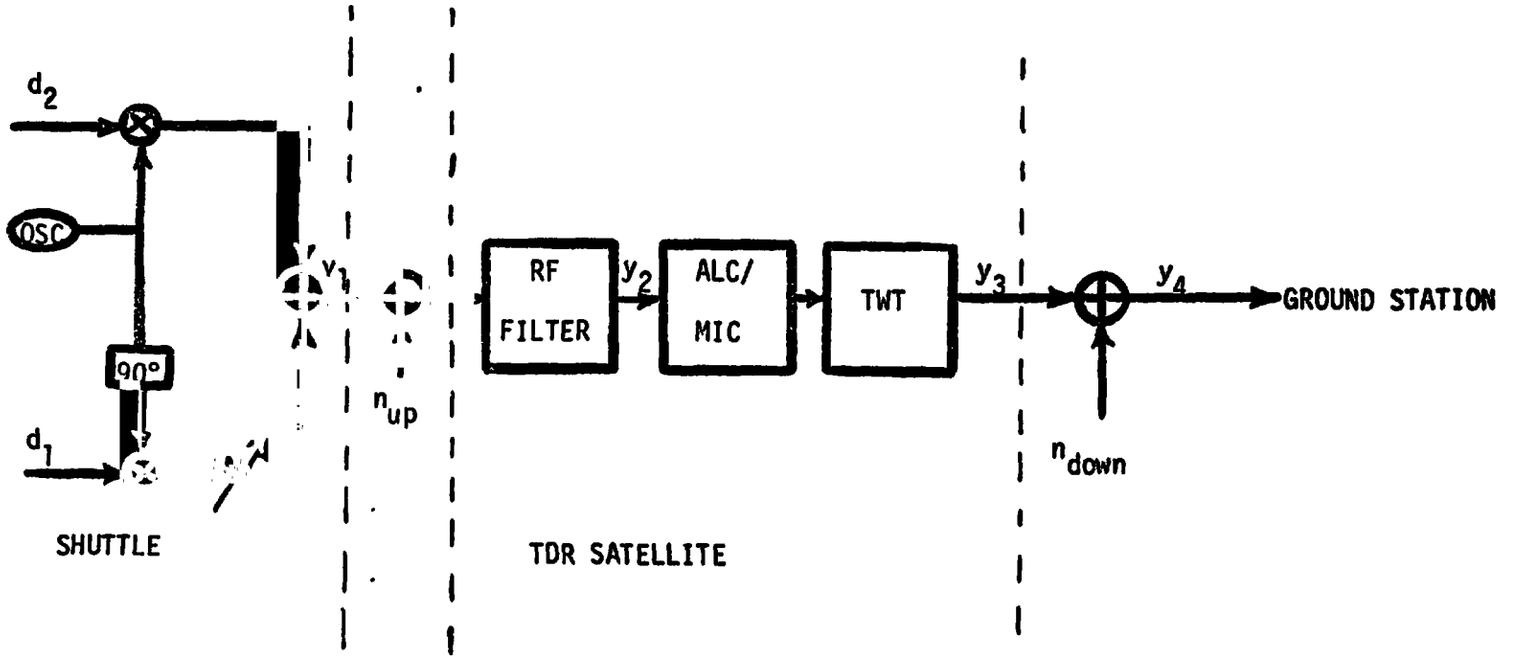

Figure 3.1. Generalized Link Diagram.

where

d_i = unit-power stream of NRZ or biphase symbols, i = 1,2
(It may be the output of an encoder. Nonetheless, any two symbols are assumed independent and are equally likely to have either polarity.)

P_i = power of $i^{\underline{th}}$ symbol stream, i = 1,2

ω = radian carrier frequency

Also, $P_1 \geq 0$ and $P_2 > 0$.

The TDR satellite filters the modulated carrier plus uplink thermal noise. The bandwidth of this filter is wide enough to pass the data undistorted; thus, the signal at the output can be written

$$y_2(t) = y_1(t) + n_u(t) \tag{2}$$

where

$$n_u(t) = \sqrt{2}\, n_{u1}(t)\cos \omega t - \sqrt{2}\, n_{u2}(t)\sin \omega t \tag{3}$$

and n_{u1}, n_{u2} are independent, identically distributed, baseband Gaussian processes. y_2 can be rewritten

$$\begin{aligned} y_2(t) &= \sqrt{2}\, \mathrm{Re}\{[(\sqrt{P_1}d_1+n_{u1}) + j(\sqrt{P_2}d_2+n_{u2})]e^{j\omega t}\} \\ &= \sqrt{2}\, \mathrm{Re}[r(t)e^{j(\nu(t)+\omega t)}] \end{aligned} \tag{4}$$

where

$$r^2(t) = (\sqrt{P_1}d_1+n_{u1})^2 + (\sqrt{P_2}d_2+n_{u2})^2 \tag{5}$$

$$\sin \nu(t) = \frac{\sqrt{P_2}d_2+n_{u2}}{r}, \quad \cos \nu(t) = \frac{\sqrt{P_1}d_1+n_{u1}}{r} \tag{6}$$

Still in the TDR satellite, the signal goes through a bandpass nonlinearity characterized by AM-AM and AM-PM distortion functions f(r) and g(r), respectively. The nonlinearity consists of an ALC/MIC clipper followed by a TWT amplifier. The signal at the output can be written

$$y_3(t) = \sqrt{2}\,\mathrm{Re}[f(r(t))e^{j(v(t)+g(r(t))+\omega t)}]$$

$$= \sqrt{2}\,\mathrm{Re}\{[h_1(r(t)) + jh_2(r(t))]r(t)e^{j(v(t)+\omega t+\delta)}\} \quad (7)$$

where

$$h_1(r) + jh_2(r) = \frac{f(r)}{r}\,e^{j(g(r)-\delta)} \quad (8)$$

The latter equation is a characterization of the nonlinearity, where δ is an average phase shift introduced by g. It should be noted that if the nonlinearity is linear, then $h_2 = 0$.

The signal at input to the ground station is

$$y_4(t) = y_3(t) + n_d(t) \quad (9)$$

where n_d, the downlink thermal noise, is expressed

$$n_d(t) = \sqrt{2}\,n_{d1}(t)\cos(\omega t+\delta) - \sqrt{2}\,n_{d2}(t)\sin(\omega t+\delta) \quad (10)$$

The input signal has quadrature components x_1 and x_2; i.e.,

$$y_4(t) = \sqrt{2}\,\mathrm{Re}\{[x_1(t)+jx_2(t)]e^{j(\omega t+\delta)}\} \quad (11)$$

The appropriate characterization of x_1 and x_2 depends on the loop under consideration.

3.3 Carrier Tracking with Costas Loop

3.3.1 Introduction

The first loop we'll study is the Costas loop for use on the S-band return link with its BPSK signal.

3.3.2 Further Characterization of Link

Since Ku-band mode 1 return link will not use the Costas loop, we can specialize the signal to the S-band characteristics. The transmitted signal is given by (1), where now $P_1 = 0$ and d_2 is a stream of biphase symbols. The symbol stream has two possible rates R_2, 288 Ksps (mode 1) and 576 Ksps (mode 2). These rates are three times the data-bit rates since the data bits are convolutionally encoded at rate 1/3.

The best way to write the quadrature components x_1 and x_2 of the ground station input signal is as follows:

$$\begin{aligned} x_1 &= -(Eh_2(r))\sqrt{P_2}d_2 + N_1 \\ x_2 &= (Eh_1(r))\sqrt{P_2}d_2 + N_2 \end{aligned} \tag{12}$$

where

$$\begin{aligned} N_1 &= -(h_2(r)-Eh_2(r))\sqrt{P_2}d_2 + v_1 + n_{d1} \\ N_2 &= (h_1(r)-Eh_1(r))\sqrt{P_2}d_2 + v_2 + n_{d2} \\ v_1+jv_2 &= (h_1(r)+jh_2(r))(n_{u1}+jn_{u2}) \end{aligned} \tag{13}$$

We see that x_2 contains most of the data and x_1 just a little. Since most of the power entering the TDRS bandpass nonlinearity is due to noise and not data and the noise is a much faster process than d_2, then the r process defined in (5) is practically independent of d_2. Similarly, $h_i(r)d_2$ is practically independent of d_2, i=1,2. Thus,

we will assume that the noise part N_i of x_i is independent of d_2, i=1,2. However, N_1 and N_2 are not independent.

We will obtain some statistics of the processes that will be useful later, namely, the correlation functions. They are given as follows:

$$R_{d_2}(t) = \begin{cases} 1-3R_2|t|, & |t| \le 1/2R_2 \\ R_2|t|-1, & 1/2R_2 \le |t| \le 1/R_2 \\ 0, & |t| \ge 1/R_2 \end{cases} \quad (14)$$

$$R_{N_i}(t) \doteq R_{h_{3-i}}(t)P_2 + R_{v_i}(t) + \frac{N_{0d}}{2}\delta(t), \quad i=1,2 \quad (15)$$

$$R_{v_i}(t) = R_{h_1 n_{ui}}(t) + R_{h_2 n_{u,3-i}}(t), \quad i=1,2 \quad (16)$$

$$R_{N_1,N_2}(t) \doteq -P_2 R_{h_1,h_2}(t) + R_{v_1,v_2}(t) \quad (17)$$

$$R_{v_1,v_2}(t) = R_{h_1 n_{u1},h_2 n_{u1}}(t) - R_{h_1 n_{u2},h_2 n_{u2}}(t) \quad (18)$$

Now that we know all about the signal that enters the loop, we are prepared to see what the loop does.

3.3.3 Costas Loop Operation

The Costas loop is shown in Figure 3.2. Input is the signal y_4 with quadrature components x_1 and x_2. After multiplication by $\sin(\omega t+\hat{\theta}(t))$ and $\cos(\omega t+\hat{\theta}(t))$, where $\hat{\theta}(t)$ is the loop's phase estimate, the signal in each arm goes through the arm filter G, which has bandwidth on the order of the symbol rate. When RFI is absent the power spectral densities (psd's) of N_1 and N_2 are much wider than G, so that after filtering by G, N_1 and N_2 are practically Gaussian and thus not too hard to handle. The method of analysis of the loop is to study a continuous-wave (CW) phase-locked loop with the same dynamic phase error

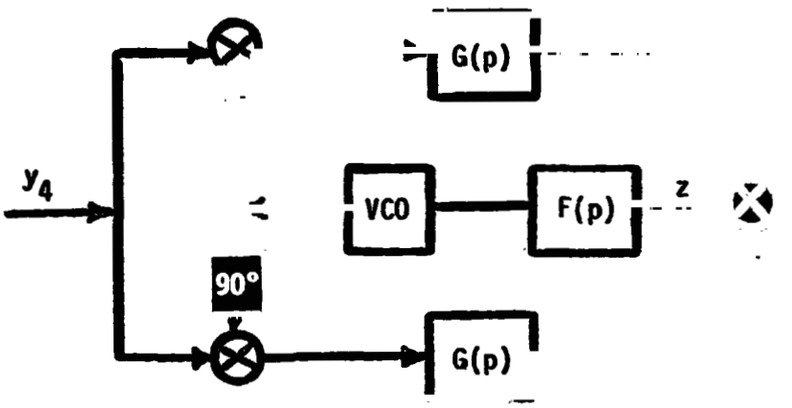

Figure 3.2. Costas Loop.

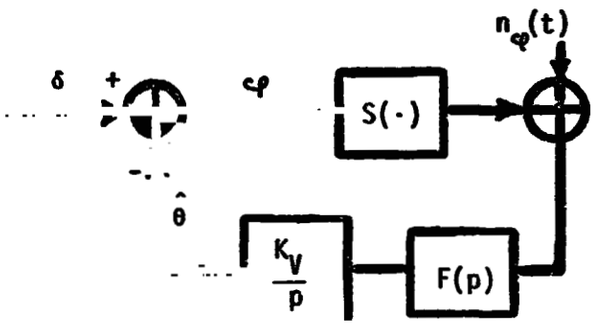

Figure 3.3. Equivalent CW Phase-Locked Loop.

process z entering the loop filter F as we have here.

The phase error φ is defined by

$$\varphi(t) = \delta - \hat{\theta}(t) \tag{19}$$

It is the difference between the actual (constant) phase δ and the loop estimate. Since φ varies slowly, the z process can be broken up into two parts:

$$z(t) = S(\varphi) + n_\varphi(t) \tag{20}$$

where

$$S(\varphi) \equiv E[z(t)|\varphi] \qquad \text{(S-curve)}$$

$$n_\varphi(t) \equiv z(t) - S(\varphi),\ \varphi \text{ fixed} \qquad \text{(equivalent noise)} \tag{21}$$

The equivalent loop is shown in Figure 3.3.

$S(\varphi)$ is given by

$$S(\varphi) = \frac{1}{2}\sin(2\varphi)E[\bar{x}_2^2(t)-\bar{x}_1^2(t)]-\cos(2\varphi)E[\bar{x}_1(t)\bar{x}_2(t)] \tag{22}$$

where we define for any signal a,

$$\bar{a}(t) = G(p)a(t) \tag{23}$$

The second term in the S-curve definition is 0 if φ has been properly defined so that $S(0) = 0$. This requirement allows us to calculate δ, as we will do later. The S-curve is needed for nonlinear analysis of the loop, which will not be pursued here.

Our main goal is to obtain the variance σ_φ^2 of phase error. To do so, we assume that $|\varphi|$ is almost always small so that the equivalent loop can be linearized. Since [1] gives full details of how this is done, we need only say that

$$\varphi(t) = H(p)\frac{n(t)}{S'(0)} \tag{24}$$

where H is a filter and $n \equiv n_0$. Then when the psd of n is much wider than the bandwidth of H, we have

$$\sigma_\varphi^2 = B_L N_0'/(S'(0))^2 \tag{25}$$

where B_L is the one-sided noise bandwidth of H and N_0' is the one-sided psd of n. Therefore, to calculate σ_φ^2 we need S'(0) and N_0', which we will later express in terms of statistics of $\bar{x}_1$ and $\bar{x}_2$.

3.3.4 Statistics of $\bar{x}_1$ and $\bar{x}_2$

We recall (cf. (12)) that each of $\bar{x}_1$ and $\bar{x}_2$ consists of some of the filtered symbol stream $\bar{d}_2$ plus an independent noise part, $\bar{N}_1$ and $\bar{N}_2$, respectively, the important statistics of which are given below.

$$R_{\bar{d}_2}(t) = G^*(p)G(p)R_{d_2}(t) \tag{26}$$

$$R_{\bar{N}_i,\bar{N}_k}(t) \doteq S_{N_i,N_k}(0)G^*(p)G(p)\delta(t), \quad i,k = 1,2 \tag{27}$$

$$S_{N_i,N_k}(0) = \int_{-\infty}^{\infty} R_{N_i,N_k}(t)dt, \quad i,k = 1,2 \tag{28}$$

The expression for $R_{\bar{N}_i,\bar{N}_k}(t)$ is valid only when thermal noise is the only interference in the link.

3.3.5 Expression for δ

Before we go on to express S'(0) and N_0', let us first find the angle δ. It has been defined as that angle which allows S(0) = 0, which ensures that the loop has been linearized near the lock-up point. From (22) we find

$$S(0) = -E[\bar{x}_1(t)\bar{x}_2(t)] \tag{29}$$

so from (12), (26), (27), (28), (17), and (18), the requirement is seen to be that

$$(Eh_1)(Eh_2)P_2R_{\bar{d}_2}(0) = 2B_G S_{N_1,N_2}(0) \tag{30}$$

where B_G is the one-sided noise bandwidth of the G filter.

This equation is solved below for δ in terms of statistics obtained by assuming $\delta=0$.

The first step is to note from (8) that

$$h_1(r) = \frac{f(r)}{r}\cos(g(r)-\delta) = \cos\delta\cdot h_{10}(r) + \sin\delta\cdot h_{20}(r)$$

$$h_2(r) = \frac{f(r)}{r}\sin(g(r)-\delta) = \cos\delta\cdot h_{20}(r) - \sin\delta\cdot h_{10}(r) \tag{31}$$

where

$$h_{10}(r) + jh_{20}(r) \equiv f(r)/r\cdot\exp(jg(r)) \tag{32}$$

Then

$$(Eh_1)(Eh_2) = \cos(2\delta)(Eh_{10})(Eh_{20}) - \sin(2\delta)\tfrac{1}{2}((Eh_{10})^2-(Eh_{20})^2) \tag{33}$$

$$S_{h_1,h_2}(0) = \cos(2\delta)S_{h_{10},h_{20}}(0) - \sin(2\delta)\tfrac{1}{2}(S_{h_{10}}(0)-S_{h_{20}}(0)) \tag{34}$$

$$S_{v_1,v_2}(0) = \cos(2\delta)[S_{h_{10}n_{u1},h_{20}n_{u1}}(0) - S_{h_{10}n_{u2},h_{20}n_{u2}}(0)] - \sin(2\delta)\tfrac{1}{2}[S_{h_{10}n_{u1}}(0) - S_{h_{20}n_{u1}}(0) - S_{h_{10}n_{u2}}(0) + S_{h_{20}n_{u2}}(0)] \tag{35}$$

Writing $S_{v_1,v_2}(0)$ as

$$S_{v_1,v_2}(0) = \cos(2\delta)A - \sin(2\delta)\tfrac{1}{2}B \tag{36}$$

where the definitions of A and B are obvious, then one finds

$$\tan(2\delta) = \{2B_G[A-P_2S_{h_{10},h_{20}}(0)]-P_2R_{\bar{d}_2}(0)(Eh_{10})(Eh_{20})\}/\{B_G[B-P_2(S_{h_{10}}(0)$$

$$- S_{h_{20}}(0))] - \frac{1}{2} P_2R_{\bar{d}_2}(0)((E_{h_{10}})^2-(E_{h_{20}})^2)\} \qquad (37)$$

3.3.6 Expressions for $S'(0)$ and N_0'

Now that we have the δ that properly defines φ, we may proceed to obtain the quantities $S'(0)$ and N_0' needed in the calculation of the phase error variance σ_φ^2 given in (25). Since now

$$S(\varphi) = \frac{1}{2}\sin(2\varphi)E[\bar{x}_2^2(t)-\bar{x}_1^2(t)] \qquad (38)$$

then the derivative at 0 is

$$S'(0) = R_{\bar{x}_2}(0) - R_{\bar{x}_1}(0)$$

$$\doteq ((Eh_1)^2-(Eh_2)^2)P_2R_{\bar{d}_2}(0) + (S_{N_2}(0)-S_{N_1}(0))2B_G \qquad (39)$$

The equivalent noise $n(t)$ and its two-sided psd $N_0'/2$ are given by

$$n(t) = -\bar{x}_1(t)\bar{x}_2(t)$$

$$\doteq (Eh_2)\sqrt{P_2}\,\bar{d}_2(t)\bar{N}_2(t) - (Eh_1)\sqrt{P_2}d_2(t)\bar{N}_1(t)$$

$$-\bar{N}_1(t)\bar{N}_2(t) + (Eh_1)(Eh_2)P_2\bar{d}_2^2(t) \qquad (40)$$

$$N_0'/2 \doteq P_2R_{\bar{d}_2}(0)[(Eh_1)^2S_{N_1}(0)+(Eh_2)^2S_{N_2}(0)-2(Eh_1)(Eh_2)S_{N_1,N_2}(0)]$$

$$+ S_{\bar{N}_1\bar{N}_2}(0) \qquad (41)$$

Since in the absence of RFI $\bar{N}_1$ and $\bar{N}_2$ are usually not very correlated and since the G filter is RC-type, it is sufficient to approximate $S_{\bar{N}_1\bar{N}_2}(0)$ by

$$S_{N_1N_2}(0) \triangleq B_G S_{N_1}(0) S_{N_2}(0) \qquad (42)$$

3.4 Carrier Tracking with Two-Channel Costas Loop

3.4.1 Introduction

The Shuttle Ku-band mode 1 return link will use a two-channel (i.e., quadriphase) Costas loop with hard-limiters to track each of the carrier and subcarrier. In order to study both cases with the same model, we keep the full generality of the link model shown in Figure 3.1 and of the signal characterization given in Section 3.2.

3.4.2. Further Characterization of Link

Since now both symbol streams d_1 and d_2 are to be used for carrier tracking, the most useful expressions for the quadrature components x_1 and x_2 of the loop input signal are different from before; they are

$$\begin{aligned} x_1 &= (Eh_1)\sqrt{P_1}d_1 + N_1 \\ x_2 &= (Eh_1)\sqrt{P_2}d_2 + N_2 \\ N_1 &= (h_1(r)-Eh_1)\sqrt{P_1}d_1 - h_2(r)\sqrt{P_2}d_2 + v_1 + n_{d1} \\ N_2 &= (h_1(r)-Eh_1)\sqrt{P_2}d_2 + h_2(r)\sqrt{P_1}d_1 + v_2 + n_{d2} \end{aligned} \qquad (43)$$

where v_i, h_i, $i = 1,2$, are as defined before in (8) and (13) and now δ is defined by

$$\delta = \tan^{-1}[E(f(r)/r \cdot \sin g(r))/E(f(r)/r \cdot \cos g(r))] \qquad (44)$$

so that

$$Eh_2(r) = 0 \qquad (45)$$

It will be shown later that this definition of δ is adequate.

Just as for the Costas loop, we assume that the symbol streams d_1 and d_2 are independent of N_1 and N_2. For channels 2 and 1 (those on the subcarrier) this is practically true by the same reasoning as for the Costas loop used at S-band. This applies also to roughly half of the transmission on channel 3 (on the carrier), the most powerful channel. For the highest data rates or for the highest values of E_b/N_{ou} (data-bit energy to one-sided psd of uplink noise) which will be used for any particular data rate on channel 3, we must appeal to the argument that $h_1(r)-Eh_1$ and $h_2(r)$ are small in order to justify the assumption.

We will need later the correlation functions of d_i and N_i, given below.

$$R_{d_i}(t) = \begin{cases} 1-R_i|t|, & |t| \le 1/R_i \\ 0, & |t| \ge 1/R_i \end{cases} \quad \text{(NRZ)}$$

$$= \begin{cases} 1-3R_i|t|, & |t| \le 1/2R_i \\ R_i|t|-1, & 1/2R_i \le |t| \le 1/R_i \\ 0, & |t| \ge 1/R_i \end{cases} \quad \text{(Biphase)} \qquad (46)$$

$$R_{N_i}(t) \doteq R_{h_{3-i}}(t)P_2 + R_{h_i}(t)P_1 + R_{v_i}(t) + \frac{N_{0d}}{2}\delta(t), \quad i=1,2 \qquad (47)$$

$$R_{N_1,N_2}(t) \doteq (P_1-P_2)R_{h_1,h_2}(t) + R_{v_1,v_2}(t) \qquad (48)$$

where R_i is the symbol rate of d_i, $i = 1,2$, and where correlation functions of v_1 and v_2 are the same as given in (16) and (18).

We now know what the signal is that enters the loop, so we can start to look at the loop.

3.4.3 Operation of Two-Channel Costas Loop

The two-channel (i.e., quadriphase) Costas loop with hard-limiters that will be in the ground station is shown in Figure 3.4. As opposed to a more optimal implementation [1], this implementation uses the same filter G in all the arms. The ratio C_2/C_1 will be 2 when $P_2/P_1 = 4$. Just as for the Costas loop, the method of analysis is to study an equivalent CW phase-locked loop with the same dynamic phase error process ε input to the loop filter F.

Since the operation of this loop is fully described in [1], we will go over it only briefly. The phase error φ is defined as in (19). The ε process is the sum of two others, as shown in Figure 3.4:

$$\varepsilon = -\varepsilon_1 + \varepsilon_2 \tag{49}$$

The S-curve $S(\varphi)$ and the equivalent noise $n_\varphi(t)$ are given by the following:

$$S(\varphi) = E(\varepsilon|\varphi) \tag{50}$$

$$n_\varphi(t) = \varepsilon(t) - S(\varphi) \text{ for fixed } \varphi \tag{51}$$

We obtain below the S-curve and the quantities $S'(0)$ and N_0' for the equivalent loop. The latter two are used to calculate the variance of φ using (25). All are expressed in terms of statistics of $\bar{x}_1$ and $\bar{x}_2$.

3.4.4 Properties of $\bar{x}_1$ and $\bar{x}_2$

The bandwidth of the G filter is chosen to pass most of the power of both d_1 and d_2. Unlike for the Costas loop, we need to assume here that the effect of G on d_1 and on d_2 is merely to reduce their power; i.e.,

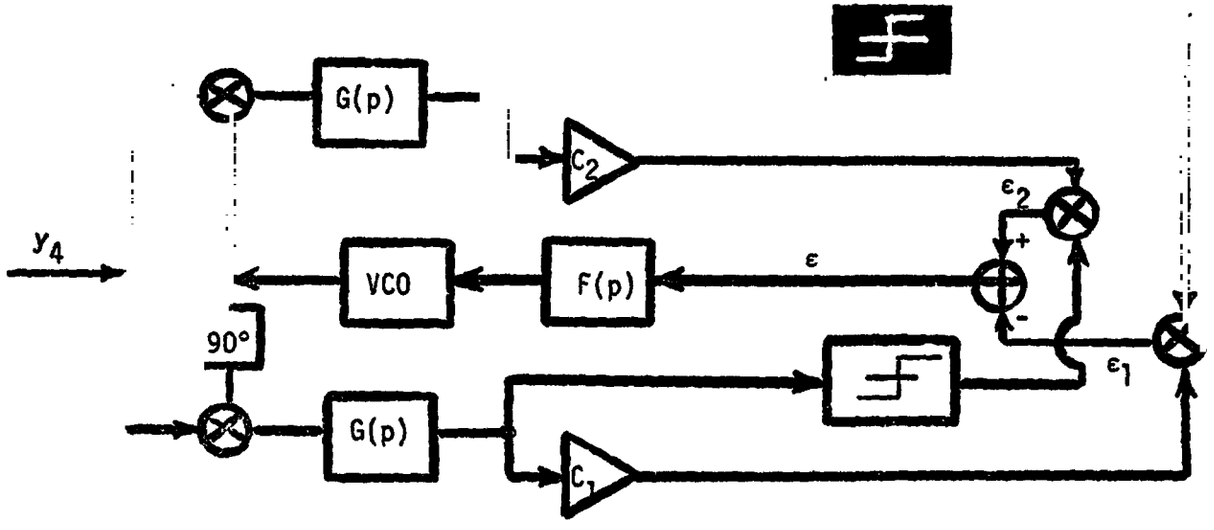

Figure 3.4. Two-Channel Costas Loop With Hard-Limiters.

$$\bar{x}_i(t) = A_i d_i + \bar{N}_i$$

$$A_i = \sqrt{n_i}(Eh_1)\sqrt{P_i}$$

$$n_i = R_{\bar{d}_i}(0) \qquad (52)$$

In the absence of RFI $\bar{N}_1$ and $\bar{N}_2$ are approximately Gaussian. The correlation functions of $\bar{d}_i$ and $\bar{N}_k$ are as given in Section 3.3.4.

3.4.5 S-Curve $S(\varphi)$

Now we are able to write an expression for $S(\varphi)$, which from (49) is seen to be the sum of two terms.

$$S(\varphi) = -S_1(\varphi) + S_2(\varphi)$$

$$S_i(\varphi) \equiv E[\varepsilon_i(t)|\varphi] \qquad (53)$$

From [1] we obtain

$$\begin{aligned}\varepsilon_1/C_1 \doteq\ & [-\sin\varphi\cdot(A_1 d_1 + \bar{N}_1) - \cos\varphi\cdot(A_2 d_2 + \bar{N}_2)]\,\mathrm{sgn}[\cos\varphi\cdot(A_1 d_1 + \bar{N}_1) \\ & - \sin\varphi\cdot(A_2 d_2 + \bar{N}_2)] \\ =\ & [-\sin\varphi\cdot A_1 d_1 - \cos\varphi\cdot A_2 d_2 + (-\sin\varphi\cdot\bar{N}_1 - \cos\varphi\cdot\bar{N}_2)] \\ & \cdot \mathrm{sgn}[\cos\varphi\cdot A_1 d_1 - \sin\varphi\cdot A_2 d_2 + (\cos\varphi\cdot\bar{N}_1 - \sin\varphi\cdot\bar{N}_2)] \qquad (54)\end{aligned}$$

so that for correlated $\bar{N}_1$ and $\bar{N}_2$,

$$S_1(\varphi)/C_1 = -\frac{1}{2}(\sin\varphi\cdot A_1 + \cos\varphi\cdot A_2)\,\mathrm{erf}\left(\frac{\cos\varphi\cdot A_1 - \sin\varphi\cdot A_2}{\sqrt{2}\sigma_1}\right) - \frac{1}{2}(\sin\varphi\cdot A_1 - \cos\varphi\cdot A_2)\,\mathrm{erf}\left(\frac{\cos\varphi\cdot A_1 + \sin\varphi\cdot A_2}{\sqrt{2}\sigma_1}\right)$$

$$+\frac{\frac{1}{2}\sin(2\varphi)(\sigma^2_{\bar{N}_2}-\sigma^2_{\bar{N}_1})-\cos(2\varphi)R_{\bar{N}_1,\bar{N}_2}(0)}{\sigma_1}\ \frac{1}{\sqrt{2\pi}}$$

$$\cdot\left[e^{-(\cos\varphi\cdot A_1-\sin\varphi\cdot A_2)^2/2\sigma_1^2}+e^{-(\cos\varphi\cdot A_1+\sin\varphi\cdot A_2)^2/2\sigma_1^2}\right] \tag{55}$$

where

$$\sigma_1^2 = \cos^2(\varphi)\sigma^2_{\bar{N}_1}+\sin^2(\varphi)\sigma^2_{\bar{N}_2}-\sin(2\varphi)R_{\bar{N}_1,\bar{N}_2}(0)$$

and the facts have been used that for Gaussiar. random variables u,v and constant A,

$$E\ \mathrm{sgn}(A+u) = \mathrm{erf}\left(\frac{A}{\sqrt{2}\sigma_u}\right) \tag{56}$$

$$E[v\ \mathrm{sgn}(A+u)] = \frac{E(u\,v)}{\sigma_u}\sqrt{\frac{2}{\pi}}\ e^{-A^2/2\sigma_u^2} \tag{57}$$

$$\mathrm{erf}(x) \equiv \frac{2}{\sqrt{\pi}}\int_0^x e^{-y^2}dy \tag{58}$$

Similarly, ε_2 is given by

$$\varepsilon_2/C_2 \doteq [\cos\varphi\cdot(A_1\ d_1+\bar{N}_1)-\sin\varphi\cdot(A_2\ d_2+\bar{N}_2)]\mathrm{sgn}[-\sin\varphi\cdot(A_1\ d_1+\bar{N}_1)-\cos\varphi\cdot(A_2\ d_2+\bar{N}_2)] \tag{59}$$

so that

$$S_2(\varphi)/C_2 = -\frac{1}{2}(\cos\varphi\cdot A_1-\sin\varphi\cdot A_2)\mathrm{erf}\left(\frac{\sin\varphi\cdot A_1+\cos\varphi\cdot A_2}{\sqrt{2}\sigma_2}\right)$$

$$-\frac{1}{2}(\cos\varphi\cdot A_1+\sin\varphi\cdot A_2)\mathrm{erf}\left(\frac{\sin\varphi\cdot A_1-\cos\varphi\cdot A_2}{\sqrt{2}\sigma_2}\right)$$

$C_1A_1+C_2A_2$ and $S(0)$ is much less.

3.4.6 Psd N_0' of Equivalent Noise

Still needed to evaluate (25) for the phase error variance is the one-sided psd N_0' of $n(t) \equiv n_0(t)$. One finds

$$n(t) = -\varepsilon_1 + \varepsilon_2 + S_1(0) - S_2(0)$$

$$\doteq C_1(A_2d_2+\bar{N}_2)\mathrm{sgn}(A_1d_1+\bar{N}_1) - C_2(A_1d_1+\bar{N}_1)\mathrm{sgn}(A_2d_2+\bar{N}_2)$$

$$+ S_1(0) - S_2(0) \qquad (64)$$

$$N_0'/2 = \int_{-\infty}^{\infty} R_{\varepsilon_1}(t)dt + \int_{-\infty}^{\infty} R_{\varepsilon_2}(t)dt - 2\int_{-\infty}^{\infty} R_{\varepsilon_1,\varepsilon_2}(t)dt \qquad (65)$$

The expression for N_0' in the case of $\bar{N}_1,\bar{N}_2$ uncorrelated is given in (79) of [1].

3.5 Symbol Tracking with Digital Data-Transition Tracking Loop

3.5.1 Introduction

The digital data-transition tracking loop (DTTL) will be used for both NRZ and biphase symbol synchronization on the Shuttle/TDRSS S-band and Ku-band mode 1 return li . The loop input is one of the quadrature components x_1 and x_2 of ..e ground station input y_4, given by (12) for S-band and by (43) for Ku-band mode 1. Figure 3.5 shows the loop, the exact operation of which is described in [2]. The input to the loop is of the form $Ad(t+\varepsilon)+w(t)$, where d is a unit-power stream of NRZ or biphase symbols and w is white Gaussian noise of one-sided power spectral density (psd) N_0. We obtain below the S-curve and the noise psd for an equivalent CW phase-locked loop, shown in Figure 3.3; then we compute the sigma of the normalized timing error

$$+\frac{\frac{1}{2}\sin(2\varphi)(\sigma_{\bar{N}_2}^2-\sigma_{\bar{N}_1}^2)-\cos(2\varphi)R_{\bar{N}_1,\bar{N}_2}(0)}{\sigma_2}\ \frac{1}{\sqrt{2\pi}}$$

$$\cdot\left[e^{-(\sin\varphi\cdot A_1+\cos\varphi\cdot A_2)^2/2\sigma_2^2}+e^{-(\sin\varphi\cdot A_1-\cos\varphi\cdot A_2)^2/2\sigma_2^2}\right] \tag{60}$$

where

$$\sigma_2^2 = \sin^2(\varphi)\sigma_{N_1}^2+\cos^2(\varphi)\sigma_{N_2}^2+\sin(2\varphi)\cdot R_{\bar{N}_1,\bar{N}_2}(0)$$

The derivative of the S-curve at $\varphi=0$ is, therefore,

$$S'(0) \equiv -S_1'(0)+S_2'(0)$$

$$\doteq C_1\left\{A_1\ \operatorname{erf}\left(\sqrt{\frac{\alpha_1}{2}}\right)-\left[\frac{A_2^2+\sigma_{\bar{N}_2}^2-\sigma_{\bar{N}_1}^2}{\sigma_{\bar{N}_1}}-\left(\frac{R_{\bar{N}_1,\bar{N}_2}(0)}{\sigma_{\bar{N}_1}^2}\right)\sigma_{\bar{N}_1}\ (\alpha_1-1)\right]\sqrt{\frac{2}{\pi}}\,e^{-\alpha_1/2}\right\}$$

$$+C_2\left\{A_2\ \operatorname{erf}\left(\sqrt{\frac{\alpha_2}{2}}\right)-\left[\frac{A_1^2+\sigma_{\bar{N}_1}^2-\sigma_{\bar{N}_2}^2}{\sigma_{\bar{N}_2}}-\left(\frac{R_{\bar{N}_1,\bar{N}_2}(0)}{\sigma_{\bar{N}_2}^2}\right)\sigma_{\bar{N}_2}\ (\alpha_2-1)\right]\sqrt{\frac{2}{\pi}}\,e^{-\alpha_2/2}\right\} \tag{61}$$

where the signal-to-noise ratios α_i have been defined by

$$\alpha_i \equiv A_i^2/\sigma_{\bar{N}_i}^2 \qquad , \quad i=1,2 \tag{62}$$

In order that the range of values of φ where $|\varphi|$ is small include the loop lock-up point, it is necessary that $S(0)/S'(0)$ be small. This has previously been assumed to follow when δ is as defined in (44). Let us now check it. With this δ, $S(0)$ is

$$S(0) \doteq C_1\ \frac{R_{\bar{N}_1,\bar{N}_2}(0)}{\sigma_{\bar{N}_1}}\sqrt{\frac{2}{\pi}}\ e^{-\alpha_1/2}-C_2\ \frac{R_{\bar{N}_1,\bar{N}_2}(0)}{\sigma_{\bar{N}_2}}\sqrt{\frac{2}{\pi}}\ e^{-\alpha_2/2} \tag{63}$$

If $\bar{N}_1(t),\bar{N}_2(t)$ are little correlated, as is the case, then $S(0)/S'(0)$ is small. It is also small if α_1,α_2 are large because then $S'(0) \doteq$

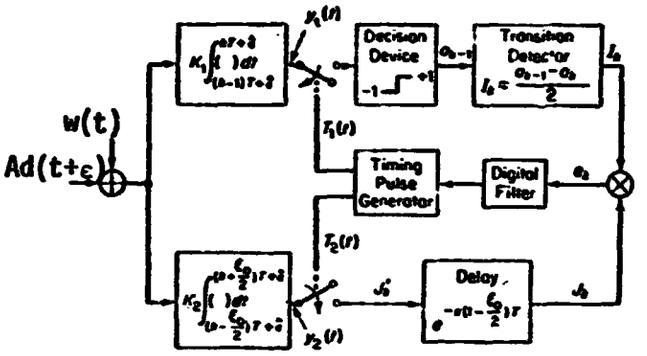

Figure 3.5. DTTL.

for the linearized equivalent loop.

3.5.2 Tracking NRZ Symbols

The performance of the DTTL on NRZ symbols is extensively analyzed in [3]. The S-curve and equivalent-noise psd expressions given below come from that source.

The normalized timing error λ is defined by

$$\lambda = (\varepsilon-\hat{\varepsilon})/T \tag{66}$$

where λ is the timing of the data signal, $\hat{\varepsilon}$ is the timing estimate produced in the loop, and T is the symbol time. The S-curve $g(\lambda)$ of the equivalent loop is defined by

$$g(\lambda) = E[e_k|\lambda] \tag{67}$$

and is given by

$$\frac{g(\lambda)}{K_2 AT} \equiv g_n(\lambda) = \begin{cases} \lambda \operatorname{erf}(\sqrt{R_s}(1-2\lambda)) - \frac{1}{8}[\xi_0-2\lambda] \\ \quad \cdot[\operatorname{erf}(\sqrt{R_s}) - \operatorname{erf}(\sqrt{R_s}(1-2\lambda))] & \text{for } \lambda \le \frac{\xi_0}{2} \\ \frac{\xi_0}{2}\operatorname{erf}(\sqrt{R_s}(1-2\lambda)) & \text{for } \frac{\xi_0}{2} \le \lambda \le \frac{1}{2} \end{cases} \tag{68}$$

where

$$R_s = A^2 T/N_0 \tag{69}$$

The two-sided psd of the equivalent noise when $\lambda = 0$ is given by

$$S(0,0) = TE[e_k^2|\lambda=0] + 2T\sum_{m=1}^{\infty} E[e_k e_{k+m}|\lambda=0] \tag{70}$$

$$h(0) = \frac{S(0,0)}{K_2^2 \xi_0 \frac{N_0 T^2}{4}} = 1 + \frac{\xi_0}{2} R_s - \frac{\xi_0}{\pi} \exp^2(-R_s)$$

$$- \frac{\xi_0}{\sqrt{\pi}} \sqrt{R_s} \exp(-R_s)\mathrm{erf}(\sqrt{R_s}) - \frac{\xi_0}{2} R_s \mathrm{erf}^2(\sqrt{R_s}) \tag{71}$$

From (68), we see that

$$g_n'(0) = \mathrm{erf}(\sqrt{R_s}) - \frac{\xi_0}{2\sqrt{\pi}} \sqrt{R_s} \exp(-R_s) \tag{72}$$

so we find that for the linearized loop

$$\sigma_\lambda = \frac{\sqrt{S(0,0)2B_L}}{g'(0)}$$

$$= \frac{\sqrt{\frac{\xi_0 h(0) B_L T}{2R_s}}}{g_n'(0)} \tag{73}$$

where B_L is the one-sided loop bandwidth. In order to compare later the loop's performance for NRZ and biphase symbols, we note that

$$\lim_{R_s \to \infty} \sigma_\lambda = \sqrt{\frac{\xi_0 B_L T}{2R_s}} \tag{74}$$

3.5.3 Tracking Biphase Symbols

We assume that the DTTL tracks a stream of biphase symbols as if it were a stream of double-rate NRZ symbols. Figure 3.5 still shows the loop operation if T is replaced by T/2 and if now ξ_0 is a fraction of T/2, the duration of half a biphase symbol.

The normalized timing error λ is still defined as in (66). The S-curve $g(\lambda)$ now has period 1/2. Starting from Equation (A-14) in [3] we find the S-curve:

$$\frac{g(\lambda)}{K_2 AT/2} \equiv g_n(\lambda) = \begin{cases} \left(\frac{\lambda}{2} - \frac{\xi_0}{8}\right) \operatorname{erf}\left(\sqrt{\frac{R_s}{2}}\right) + \left(\frac{5\lambda}{2} + \frac{\xi_0}{8}\right) \operatorname{erf}\left(\sqrt{\frac{R_s}{2}}\,(1-4\lambda)\right), & 0 \le \lambda \le \frac{\xi_0}{4} \\ \frac{3\xi_0}{4} \operatorname{erf}\left(\sqrt{\frac{R_s}{2}}\,(1-4\lambda)\right), & \frac{\xi_0}{4} \le \lambda \le \frac{1}{4} \end{cases} \tag{75}$$

Its derivative at zero is given by

$$g_n'(0) = 3 \operatorname{erf}\left(\sqrt{\frac{R_s}{2}}\right) - \frac{\xi_0}{\sqrt{\pi}} \sqrt{\frac{R_s}{2}}\, e^{-R_s/2} \tag{76}$$

From Equations (B-37) and (B-42) in [3] after some work we obtain

$$E[e_k e_{k+m} | \lambda=0] = 0 \text{ for all } m \ge 1 \tag{77}$$

so that the psd of the equivalent noise for $\lambda = 0$ is given by

$$S(0,0) = \frac{T}{2} E[e_k^2 | \lambda=0] \tag{78}$$

From Equation (B-30) in [3] we obtain

$$h(0) \equiv \frac{S(0,0)}{K_2^2 \xi_0 \frac{N_0 T^2}{16}} = 1 + \frac{R_s}{2}\frac{\xi_0}{2} - \frac{\xi_0}{\pi}\exp(-R_s)$$

$$-\left(\frac{1}{2} - \frac{R_s}{2}\frac{\xi_0}{2}\right)\mathrm{erf}^2\left(\sqrt{\frac{R_s}{2}}\right) - \sqrt{\frac{R_s}{2}}\frac{3\xi_0}{2\sqrt{\pi}}\exp\left(-\frac{R_s}{2}\right)\mathrm{erf}\left(\sqrt{\frac{R_s}{2}}\right) \quad (79)$$

where R_s is defined as in (69). Then σ_λ is given by (73).

In the case of low noise, for the same values of ξ_0, R_s, and $B_L T$ biphase symbols will give a smaller timing sigma than NRZ symbols will, as can be seen from (74) and the fact that for biphase symbols

$$\lim_{R_s \to \infty} \sigma_\lambda = \sqrt{\frac{\xi_0 B_L T}{2R_s}} \cdot \frac{1}{\sqrt{6}} \quad (80)$$

REFERENCES

1. Braun, Walter R., and Lindsey, W. C., "Carrier Synchronization Techniques for Unbalanced QPSK Signals--Part II," IEEE Trans. on Communications, September 1978.

2. Lindsey, W. C., and Simon, M. K., Telecommunication Systems Engineering, Prentice-Hall, Englewood Cliffs, N.J., 1973.

3. Simon, M. K., "An Analysis of the Steady-State Phase Noise Performance of a Digital Data-Transition Tracking Loop," Jet Propulsion Laboratory Technical Memo 3341-65-815, November 21, 1968.

4. RFI EFFECTS ON SHUTTLE/TDRSS LINK

4.1 Introduction

The Russian air defense system uses large numbers of powerful radars whose carrier frequencies coincide with the TDRSS SSA return link frequency band. The TDRSS payload and ground station hardware had to be redesigned to minimize the deleterious effect of the radio frequency interference (RFI) resulting from these radars. The overall effect of the RFI and the hardware changes is impaired system performance both with RFI and without.

This chapter gives a statistical description of the RFI environment and lists the hardware changes in the TDR satellites and ground station. Then analytical models are described to assess the performance impact both for the bit error probability and for carrier and data tracking. Finally, preliminary performance results are given.

4.2 RFI Environment

The radio frequency interference is caused by large numbers of high-powered radars (peak EIRP in excess of 100 dBW) in eastern Europe and Russia. The radar region as seen from the orbital locations of the two active TDRSS satellites is shown in Figs. 4.1 and 4.2. The illumination of the TDRS occurs through the radars' main, side, and backlobes, resulting in a large dynamic range of the composite RFI.

The radar pulses consist of pulsed sine waves (CW) accompanied by wideband Gaussian noise (Fig. 4.3). The pulse duration is in the 2 to 5 microsecond range. Table 4.1 shows an unclassified coarse approximation to the actual distribution of pulse power and pulse duration. The first two lines correspond to radar pulses whose CW component lies outside the TDRS input band; hence, only the wideband

noise affects performance. The remaining lines represent CW pulses within the TDRS band. Since the CW power by far exceeds the wideband noise power in this case, the latter may be neglected. The first column shows the RFI EIRP in the direction of the TDRS (for noise-like pulses it is measured in a 20 MHz bandwidth) quantized in ten-dB steps. The pulse duration has been quantized into two values, two and five microseconds. The numbers in the second and third column represent the number of pulses per second with a given power and duration. The duty cycle listed in the fourth column is the product of repetition rate (PPS) and pulse duration. The environment shown in Table 4.1 applies to the TDRS over the Pacific and for the center frequency 2217.5 MHz. It is generally referred to as the non-benign Shuttle environment [1]. The RFI environment encountered by the eastern TDRS is worse, the other Shuttle S-band frequency, 2287.5 MHz, is less severely affected on both satellites. Table 4.2 shows a more severe TDRSS SSA RFI environment which is being used for program testing.

The TDRS S-band antenna pattern can reduce the interference when the Shuttle is not too close to the RFI region. The antenna gain drops about 12 dB at 1.5 degrees off-pointing and about 24 dB at 4 degrees off-pointing (Fig. 4.4). Figs. 4.1 and 4.2 show where these off-pointing angles are reached.

4.3 TDRSS RFI Hardware Changes

The TDRSS RFI hardware modifications have the purpose of removing powerful spikes from the signal. This is accomplished by clipping the signal when it exceeds a certain level.

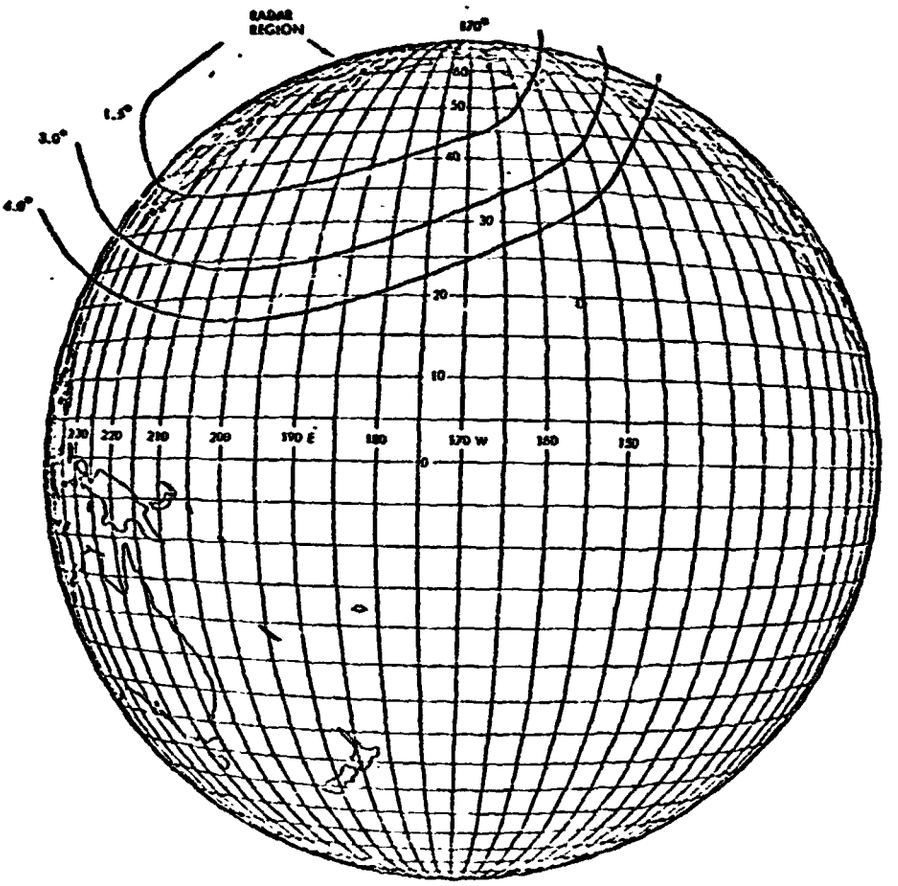

Figure 4.1. TDRS West View of Radar Interference Region.

80 0005

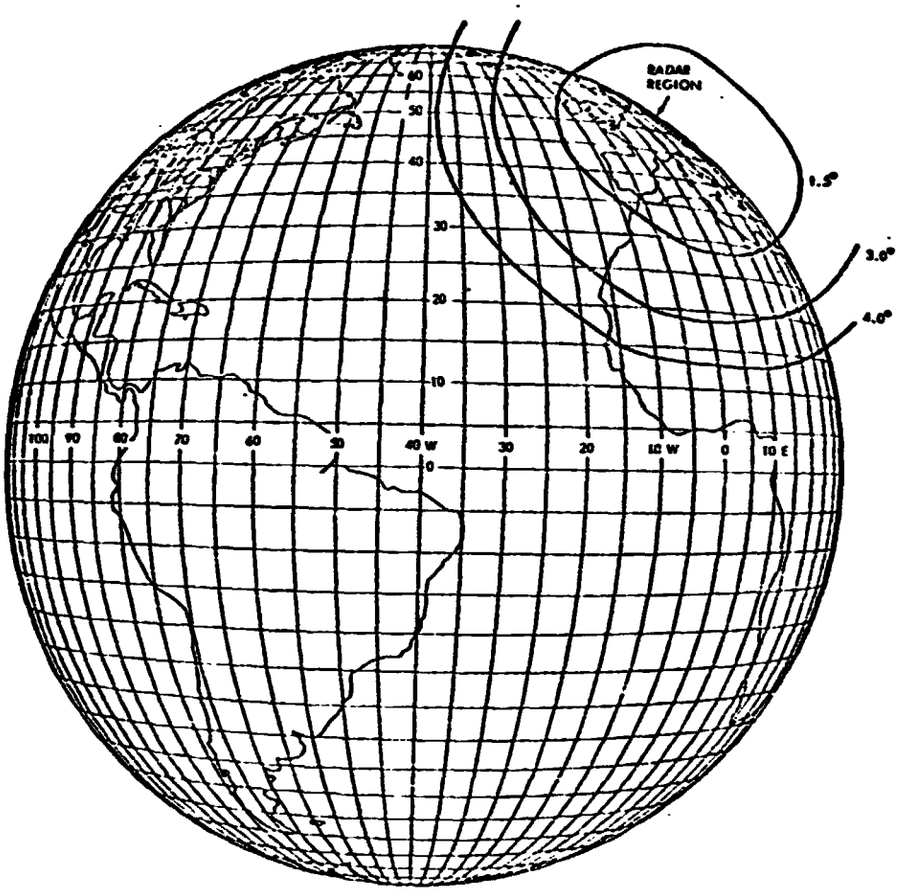

Figure 4.2. TDRS East View of Radar Interference Region.

80 0006

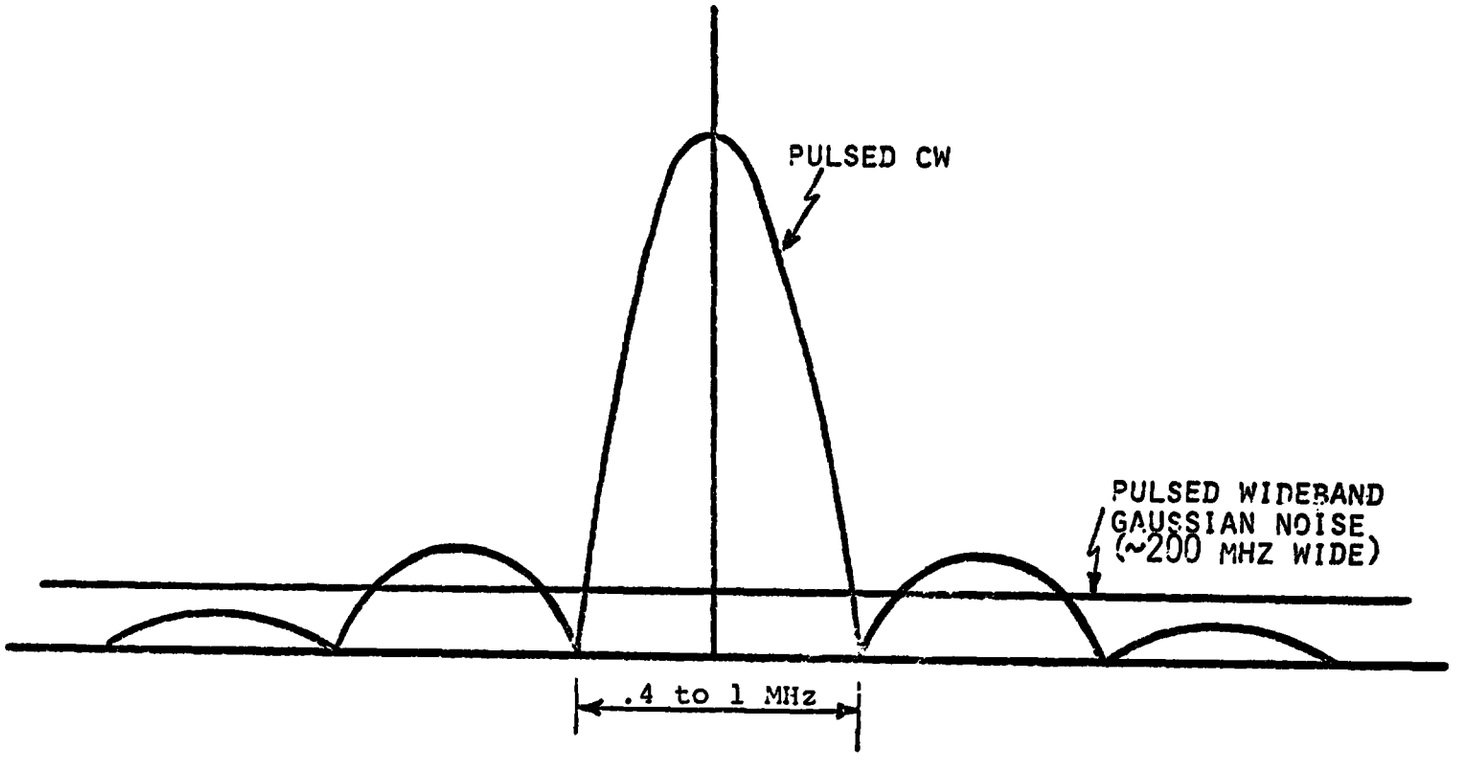

Figure 4.3. Typical RFI Pulse Spectrum.

Table 4.1. Moderate SSA RFI Environment.

SIMPLIED TEST ENVIRONMENT
(PACIFIC TDRS)

Moderate SSA (Including Non-Benign Shuttle)

Interference	PPS		Duty Cycle	Signal Type
dBW	5 μsec	2 μsec	(percent)	
25	2000	8000	2.6	Noise
35	6000	2000	3.4	Noise
45	2000	300	1.1	CW
55	2300	100	1.2	CW
65	250	50	.14	CW
75	25	5	.001	CW
110	1		N/A	CW

Table 4.2. Severe SSA RFI Environment.

SIMPLIED TEST ENVIRONMENT
(PACIFIC TDRS)

Severe SSA

Interference dBW	PPS 5 μsec	PPS 2 μsec	Duty Cycle (percent)	Signal Type
25	500	1000	0.5	Noise
35	4000	1600	2.3	Noise
45	4000	15000	5.0	CW
55	6500	3100	3.9	CW
65	600	500	0.4	CW
75	60	40	.03	CW
110	1		N/A	CW

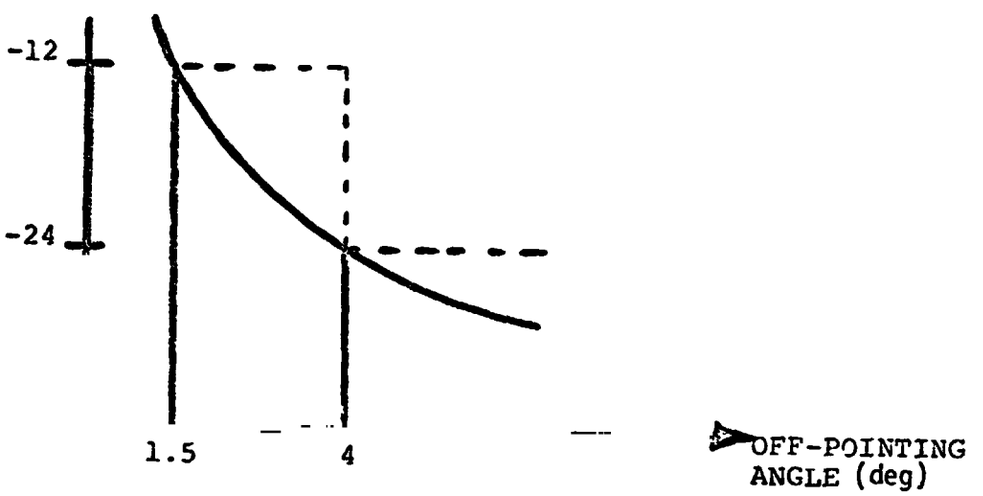

Figure 4.4. TDRS S-Band Antenna Discrimination.

80 0008

In the satellite this clipping is performed by a limiting microwave integrated circuit (MIC) amplifier located in the automatic level control (ALC) circuit. This set-up is shown in Fig. 4.5. The characteristic of the MIC amplifier (Fig. 4.6) shows good linearity below the clipping level and a sharp cutoff at this point. Presently the nominal operating level is set 6 dB below saturation but this setting can be varied between 2 and 10 dB below saturation in steps of .5 dB.

Unfortunately, the limiter also introduces nonlinear phase distortion in the form of AM/PM conversion. This characteristic is shown in Fig. 4.7.

There will also be a clipper in the TDRSS ground station. However, its characteristics and nominal operating level are not defined at present.

4.4 LinCsim Modeling of RFI Effects on Bit Error Rate

4.4.1 Introduction

This section presents the models and algorithms used in LinCsim to compute the bit error probability of the nonlinear TDRS channel in the presence of RFI.

The RFI environment as presently characterized for the TDRSS consists of RF pulses, either noise-like or pulsed CW, of approximately 2 to 5 μsec duration and a wide range of power levels. Typically, a large number of the pulses exceed the signal power level. The duty cycle of the RFI, i.e., the product of pulse duration and number of pulses per second, is used to characterize the severity of the disturbance. Typical values are between 20 and 30%.

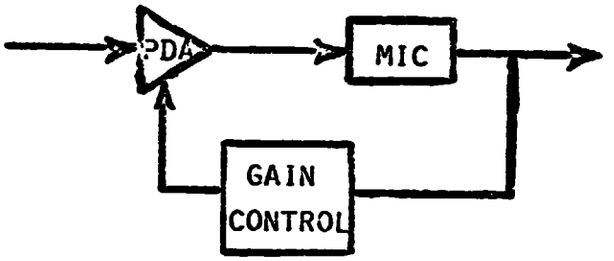

Figure 4.5. ALC with Limiting MIC Amplifier.

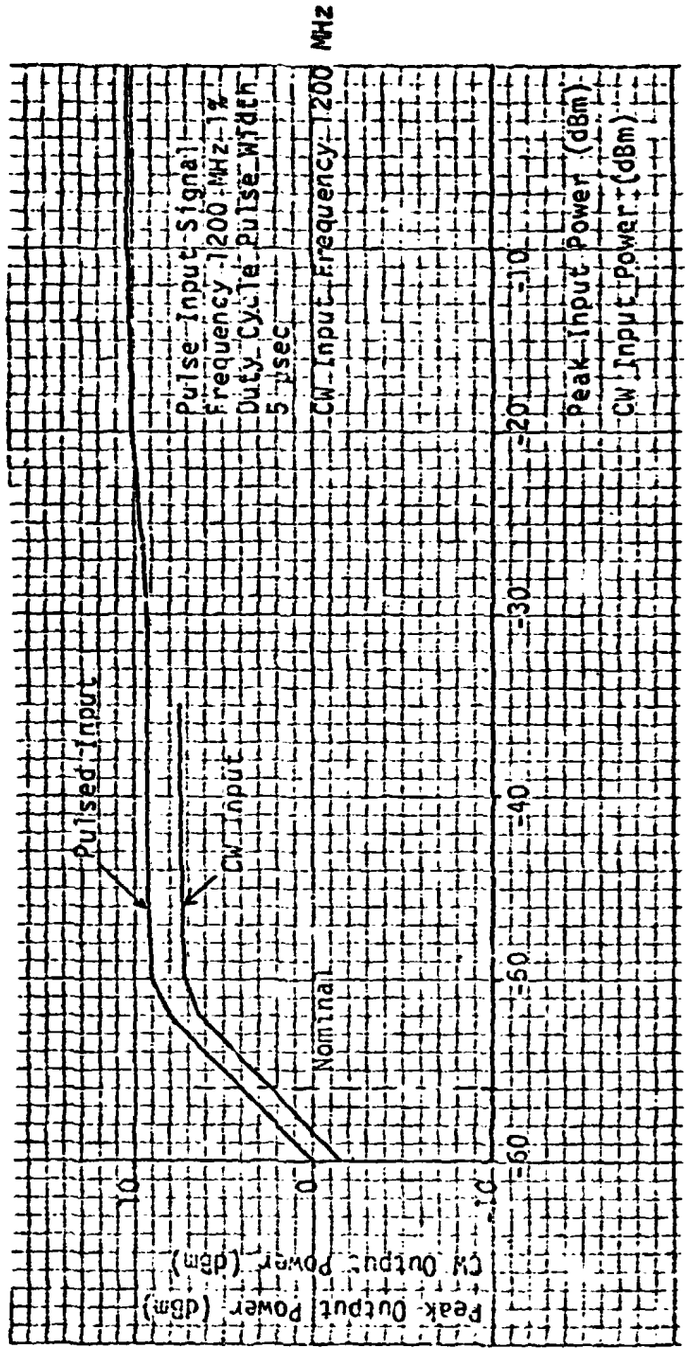

Figure 4.6. MIC Amplitude Characteristic.

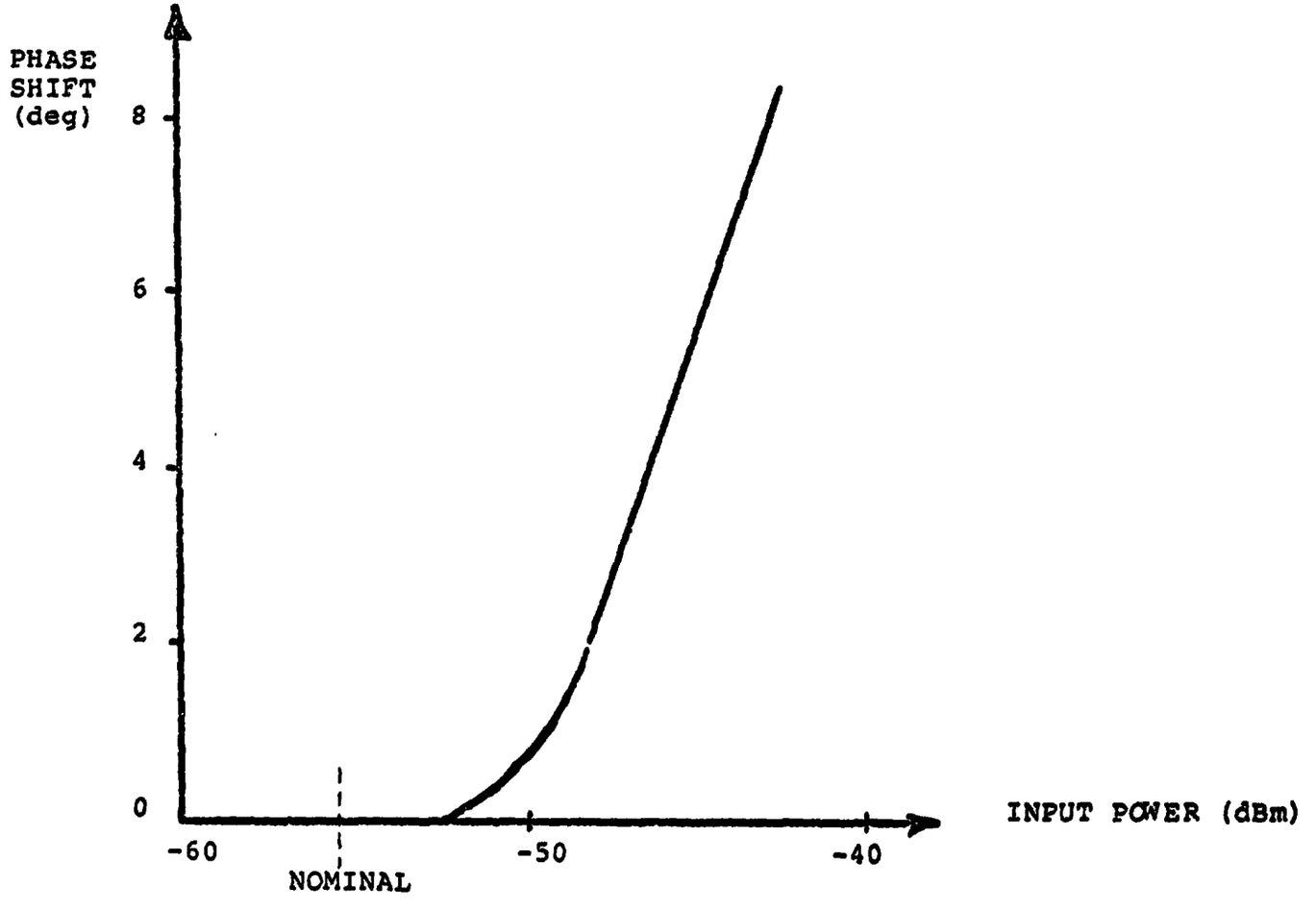

Figure 4.7. ALC/MIC AM to PM Conversion Characteristic.

The basic approach is to condition first the error probability on the satellite repeater output. (The conditioning is not done on the complete repeater output waveform but rather on a parameter which provides a sufficient statistic for the signal in the detection process. This parameter, called the decision variable Z_{IM} below, is the demodulated repeater output integrated over a symbol time.) Since the only random disturbance left is the downlink noise this conditional error rate is given by a simple expression involving the standard error function. This conditional error rate is then averaged over the statistics of the decision variable.

For this averaging of the conditional error rate different approaches are used for low and high data rates, where the break-point is the inverse of the RFI pulse duration. The first approach is to compute the probability density function (p.d.f.) of the decision variable using the classical moment technique and then to average the conditional BER over this p.d.f. This applies to the case of low data rates since the RFI pulse duration is only a fraction of the data symbol time. The second approach, used for the case of high data rates, is based on the assumption that one bit is only affected by at most one RFI pulse. The error rate is therefore computed conditioned on the presence of a particular RFI pulse characteristic and then averaged over the probability distribution of the pulse characteristics.

The detailed description of these two approaches is given in Section 4.4.3,4.4.4. Section 4.4.2 defines the models for the channel and for the RFI and defines the notation used in the remainder of the chapter. Section 4.4.5 addresses the problem of computing the moments

needed in the approximation of the decision variable p.d.f. These moments are derived from the characteristic function, in part analytically, in part through fast numerical algorithms, depending on the character of the random variable.

4.4.2 Description of Model

4.4.2.1 RFI Model

The RFI environment as seen by the TDRSS satellites consists of two classes: pulsed wideband Gaussian noise and pulsed CW tones. These two classes are further divided into groups with different power levels. The pulses from each such group are assumed to arrive at the TDRS as a Poisson process and independently from all other groups. We will however assume that no pulse overlaps occur which is true with good accuracy for duty cycles up to 30% and provides an upper bound on the error rate for higher duty cycles since effectively a larger portion of each symbol is affected by RFI. The pulsed RFI is represented as follows

$$J(t) = J_c(t) + J_g(t) \tag{1}$$

where

$$J_c(t) = \sum_{k_c=1}^{N_c} \sum_{\ell_c=1}^{n_{k_c}^t} J_{k_c} \exp(j\omega_0 t + \psi_{k_c,\ell_c}) p(t - t_{k_c \ell_c}) \tag{2a}$$

$$J_g(t) = \sum_{k_g=1}^{N_g} \sum_{\ell_g=1}^{n_{k_g}^t} J_{k_g} n(t) p(t - t_{k_g \ell_c}) \exp(j\omega_0 t) \tag{2b}$$

$n(t)$ = a complex baseband Gaussian random process with mean zero and variance 1/2.

$$p_k(t) = \begin{cases} 1 & 0 < t \leq \tau_{k_\ell} \\ 0 & \text{elsewhere} \end{cases} \tag{3}$$

τ = Pulse duration

$\left.\begin{matrix} N_c \\ N_g \end{matrix}\right\}$ = {number of groups of the RFI for CW tone and noise-like, respectively.

$\left.\begin{matrix} n^t_{k_c} \\ n^t_{k_g} \end{matrix}\right\}$ = {number of RFI pulses in group k_c (or k_g) arrived in the observation interval (t_0,t).

t_0 = the beginning of the observation time, usually the beginning of a symbol.

$t_{i\,\ell}$ = the arrival time of the ℓth RFI pulse in the ith group.

Here, the variables $n^t_{k_c}$ and $n^t_{k_g}$ are homogeneous Poisson random variables. The CW tone RFI will be further expressed as follows:

$$J_c(t) = \left\{ \sum_{k_c=1}^{N_c} \sum_{\ell_c=1}^{n_{k_c}} J_{k_c} (t-t_{k_c\ell_c}) \exp(\psi_{k_c\ell_c}) \right\} \exp(j\omega_0 t)$$

$$= |J_c| \exp j(\omega_0 t + \psi_J) \qquad (4)$$

where

$$|J_c|^2 = \left(\sum_{k_c=1}^{N_c} \sum_{\ell_c=1}^{n_{k_c}} J_{k_c} p(t-t_{k_c\ell_c}) \cos \psi_{k_c\ell_c} \right)^2 + \left(\sum_{k_c=1}^{N_c} \sum_{\ell_c=1}^{n_{k_c}} J_{k_c} p(t-t_{k_c\ell_c}) \sin \psi_{k_c\ell_c} \right)^2$$

$$\psi_J(t) = \tan^{-1} \frac{\sum_{k_c=1}^{N_c} \sum_{\ell_c=1}^{n_{k_c}} J_{k_c} p(t-t_{k_c\ell_c}) \sin \psi_{k_c\ell_c}}{\sum_{k_c=1}^{N_c} \sum_{\ell_c=1}^{n_{k_c}} J_{k_c} p(t-t_{k_c\ell_c}) \cos \psi_{k_c\ell_c}}$$

Note that $|J_c|$ and $\psi_J(t)$ are functions of time because of the pulse $p(t-t_{k_c\ell_c})$. However the variations of $|J_c|$ and $\psi_J(t)$ are much slower than the carrier frequency $\omega_0/2\pi$ and they remain constant over the RFI pulse duration τ.

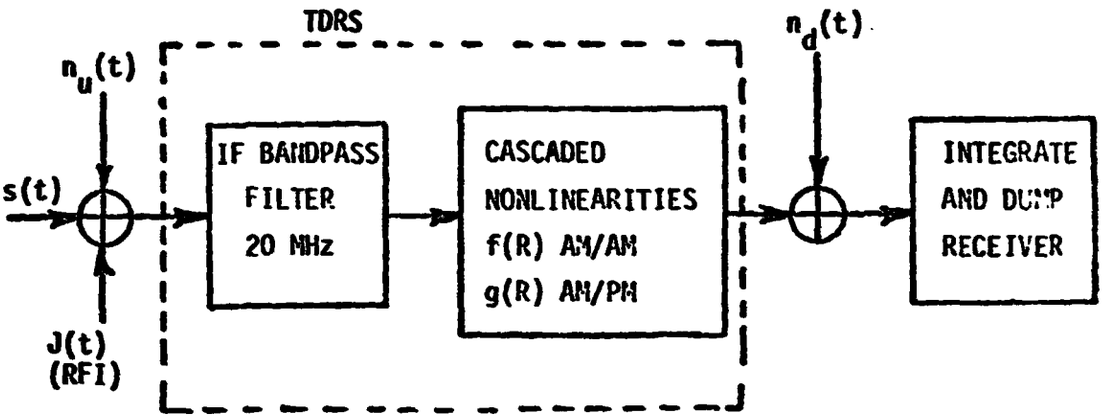

Figure 4.8. Mathematical Model for TDRS Link.

4.4.2.2 Channel Model

The mathematical model of the TDRS link is depicted in Fig. 4.8 where there is RFI in the uplink channel and Gaussian noise in the uplink and downlink channels. The signal transmitted is a BPSK signal or a QPSK signal modulated with independent inphase and quadrature data streams, so at the receiver the data messages are detected for the inphase and quadrature phase separately. In this study we shall discuss the BPSK signal case. The signal received at the satellite transponder can be expressed as

$$x(t) = V \exp(j(\omega_0 t+\theta(t)) + J(t) + n_u(t) \qquad (5)$$

where

$v^2/2$ = signal power

$\theta(t)$ = transmitted phase

$\omega_0/2\pi$ = carrier frequency

$J(t)$ = RFI, as defined by eq. (1)

$n_u(t)$ = uplink channel noise with mean zero and variance σ_u^2

Using the RFI model of eq. (1), the expression for $x(t)$ is rewritten as

$$x(t) = V \exp(j(\omega_0 t+\theta(t))) + J_c(t) + n_1(t) \qquad (6)$$

where

$$n_1(t) = n_u(t) + J_g(t)$$

Note that the noise process $n_1(t)$ still has zero mean but its variance changes with time (conditioned on the RFI arrival process) because of the presence of the noise-like RFI. By the assumption that the channel noise process and the RFI are statistically independent of

each other, the variance of $n_1(t)$ may be either equal to σ_u^2 or $\sigma_u^2 + J_{k_c}^2/2$, depending on which group of RFI is present. Here we assume that samples taken from these noise processes at the Nyquist rate are statistically independent of each other with variance σ_u^2 if no RFI is present, or $\sigma_u^2 + J_{k_g/2}^2$ if RFI of k_gth group is present.

Now the signal x(t) passes through the satellite transponder and becomes

$$y(t) = f(R)\exp(j(\omega_0 t+\theta(t) +\eta+ g(R))) \qquad (7)$$

where

R = the envelope of x(t)

η = the phase of x(t)

f(R) = AM/AM distortion

g(R) = AM/PM distortion

One can show, [see 2] that the probability density function of R and η, after averaging over the random phase of RFI, ψ_J,

$$P(R,\eta,|J_c|) = P_1(R,\eta)f(R,\eta,|J_c|) \qquad (8)$$

where

$$P_1(R,\eta) = \frac{R}{2\pi\sigma_1^2} \exp\left[-\frac{1}{2\sigma_1^2}(R^2+V^2-2RV\cos\eta)\right] \qquad (9a)$$

$$f(R,\eta,|J_c|) = \exp\left(-\frac{|J_c|}{2\sigma_1^2}\right) I_0\left(\frac{|J_c|}{\sigma_1^2}\sqrt{R^2+V^2-2RV\cos\eta}\right) \qquad (9b)$$

$$I_0(x) = \frac{1}{\pi}\int_0^{\pi} \exp(x\cos\theta)d\theta$$

If $|J_c|$ equals 0, the expression P(R,η,0) reduces to that for normal channel condition, that is

$$P(R,\eta,0) = P_1(R,\eta) . \qquad (10)$$

4.4.3 Conditional Error Probability

At the ground station, the received signal can be represented as

$$r(t) = \mathrm{Re}[y(t)] + n_d(t)$$

where $n_d(t)$ is the downlink Gaussian noise with mean zero and variance σ_d^2 in the receiver channel band. The signal is first demodulated by a local carrier $2\cos(\omega_0 t+\bar{g})$, ideally tracking the received phase of the signal and processed through an integrate-and-dump (I&D) device which gives

$$Z_I = \frac{1}{T_d}\int_0^{T_d} f(R)\cos(\theta+n+g(R)-\bar{g})dt + n_z \qquad (11)$$

where

n_z = baseband noise process whose mean is zero and variance σ_2^2 is (σ_d^2/T_d)

T_d = integration interval of the I&D, assumed to be the same as the data symbol interval.

The integral term represents the desired signal for the detection in the absence of uplink interference such as channel Gaussian noise and RFI. Denote the power associated with this term as E_d, then the downlink bit energy to noise spectral density ratio (E_b/N_0) is defined as E_d/σ_2^2 where σ_2^2 is the variance of the downlink noise in the data bandwidth.

When the uplink interference is present, the power E_d is shared by the retransmitted signal and interference. Therefore, the effect of the uplink interference is two-fold--power robbing and signal perturbation. Since the integrand in (11) is a nonlinear function of the uplink signal, noise and RFI the statistics of the associated

integral cannot be found exactly. However, this integral can be well approximated by the sum of signal samples taken at the Nyquist rate of the repeater input signal:

$$Z_I = Z_{IM} + n_z \tag{12}$$

where

$$Z_{IM} = \frac{1}{N}\sum_{i=1}^{N} a_i \tag{13}$$

N = product of the channel bandwidth B_{IF} prior to the nonlinearity and the data symbol time T_d

$$a_i = f(R_i)\cos(n_i + g(R_i) - \bar{g}) \tag{14}$$

The samples a_i, taken every B_{IF}^{-1} sec, are statistically independent of each other, but not necessarily identically distributed because of the possible presence of RFI. The impact of an RFI pulsed on the variable Z_{IM} can be classified into two cases--(1) all a_i are affected by an RFI pulse, (2) parts of the samples of Z_{IM} are affected. Denote the pulse duration of an RFI pulse by τ. If $B_{IF}\tau$ is smaller than N, i.e., the data symbol is longer than the pulse duration τ, only some of the samples a_i are affected by the RFI. We shall group those independent and identically distributed (iid) a_i into groups as follows

$$Z_{IM} = \frac{1}{N}\left\{\sum_{k_c=1}^{N_c}\sum_{r=1}^{N_{k_c}} a_r(k_c) + \sum_{k_g=1}^{N_g}\sum_{r=1}^{N_{k_g}} a_r(k_g) + \sum_{r=1}^{n_0} a_r(0)\right\} \tag{15}$$

where

$$N_{k_c} = n_{k_c}^{T_d}(\tau B_{IF}) \tag{15a}$$

$$N_{k_g} = n_{k_g}^{T_d}(\tau B_{IF}) \tag{15b}$$

$$\left.\begin{matrix} n_{k_c}^{T_d} \\ n_{k_g}^{T_d} \end{matrix}\right\} = \left\{ \begin{matrix} \text{the number of pulses from the } k_c\text{-th or } (k_g\text{-th}) \\ \text{RFI group arrived in a symbol interval } T_d \end{matrix} \right.$$

$a_r(0)$ = samples not affected by any RFI pulses

$$n_0 = N - \left(\sum_{k_\ell=1}^{N_c} N_{k_\ell} + \sum_{k_g=1}^{N_g} N_{k_g} \right)$$

For a high data rate, all of the samples are completely hit by a single RFI pulse. So the variable Z_{IM} for symbol detection is

$$Z_{IM} = \frac{1}{N} \sum_{i=1}^{N} a_i(k_\ell) \tag{16}$$

conditioned on the k_ℓth group of RFI pulses. Equations (15) and (16) point out the difference between the low and high data rate models alluded to in the introduction. In both cases the error probability conditioned on the decision variable Z_{IM} takes the form

$$P_e(Z_{IM}) = .5 \operatorname{erfc}\left(\frac{Z_{IM}}{\sqrt{2}\sigma_2}\right) \tag{17}$$

where

$$\operatorname{erfc}(x) \triangleq \frac{2}{\sqrt{\pi}} \int_x^\infty \exp(-t^2)dt$$

The averaging over Z_{IM} however is done differently in these two cases. This will be explored in the next section.

4.4.4 Bit Error Probability

Due to the different impact of RFI pulses on the decision variable Z_{IM}, two approaches are needed to evaluate the bit error probability for high and low data rates, respectively.

4.4.4.1 Low Data Rate Case

In principle, the error probability for low data rates can be obtained by averaging the conditional error probability of eq. (17) over the statistics of the variable Z_{IM}, which is not explicitly known.

$$P_e = E_{Z_{IM}}\left[0.5\ \text{erfc}\left(\frac{Z_{IM}}{\sqrt{2}\sigma_2}\right)\right] \tag{18}$$

However, we shall use the classical moment technique to construct the approximate probability density of Z_{IM}. To do this we need to evaluate the moments of Z_{IM} with respect to the statistics of the RFI pulses and their arrival distribution and the uplink channel noise. For example, the kth moment of Z_{IM} can be found in a straightforward manner as below:

$$m_k = E\left[\frac{1}{N^k}\left(\sum_{k_c=1}^{N_c}\sum_{r=1}^{N_{k_c}} a_{k_c r} + \sum_{k_g=1}^{N_c}\sum_{r=1}^{N_{k_0}} a_{k_g r} + \sum_{r=1}^{n_0} a_{0r}\right)^k\right] \tag{19}$$

One can recognize that the evaluation of the above equation is non-trivial. Thus the characteristic function will be used to evaluate the needed moments, as discussed in Section 4.4.5. Based on the calculated moments of the classical moment technique, the expectation of the error probability in eq. (18) can be written as

$$P_E = 0.5 \sum_{k=1}^{\nu} \omega_k\ \text{erfc}\left(\frac{Z_{Ik}}{\sqrt{2}\sigma_2}\right) \tag{20}$$

where (ω_k, Z_{Ik}) is a discrete probability density function (p.d.f.) approximating the continuous p.d.f. of the variable Z_{IM} and ν is the number of points Z_{1k} with nonzero probability ω_k.

4.4.4.2 High Data Rate Case

Since the duration of an RFI pulse becomes longer than the symbol duration for a high data rate, the error probability conditioned on a type of RFI pulse should be computed, then averaged over the arrival distribution of the RFI pulses. Denote by $P_e(k_\ell)$ the bit error probability conditioned on k_ℓ-th group of RFI pulses Then the overall bit error probability is (see Appendix)

$$P_e = \sum_{k_c=1}^{N_c} P(k_c)P_e(k_c) + \sum_{k_g=1}^{N_g} P(k_g)P_e(k_g) + P_0P_e(0) \quad (21)$$

where

$$\left.\begin{matrix} P(k_c) \\ P(k_g) \end{matrix}\right\} = \left\{ \begin{matrix} \text{Probability of a symbol being hit by an RFI} \\ \text{pulse of } k_c\text{-th (or } k_g\text{-th) group} \end{matrix}\right.$$

P_0 = Probability of a symbol not hit by any RFI pulse

$P_e(0)$ = Error probability conditioned on the absence of RFI pulses

One can express P_0 as below:

$$P_0 = 1 - \left(\sum_{k_c=1}^{N_c} P(k_c) + \sum_{k_g=1}^{N_g} P(k_g) \right) \quad (22)$$

The probability $P(k_\ell)$ takes the form

$$P(k_\ell) = \lambda_{k_\ell} \tau_{k_\ell} \quad (23)$$

where

λ_{k_ℓ} = Arrival rate of the k_ℓ-th group RFI pulses

τ_{k_ℓ} = Pulse duration of the k_ℓ th group RFI pulses

Here we have assumed that the overlaps between RFI pulses are negligible and that $\lambda_{k_\ell} \tau_{k_\ell}$ is small (less than one).

4.4.5 Evaluation of Moments

In computing the conditional error probability for high data rates or overall error probability for low data rates, the moments of the decision variable Z_{IM} are needed in constructing the probability density function of Z_{IM}. In this study, the characteristic function approach is used.

Denote the characteristic function to be $\Phi_{Z_{IM}}(j\omega)$

$$\Phi_{Z_{IM}}(j\omega) \equiv E[\exp(j\omega Z_{IM})] \tag{24}$$

$$= \sum_{k=0}^{\infty} m_k \frac{(j\omega)^k}{k!} \tag{25}$$

where

E = expectation taken over all random variables

m_k = k^{th} moment of Z_{IM}

A comparison between eq. (15) and (16) shows that the high-rate model can be evaluated as a simple special case of the low-rate model, hence only the averaging for the low-rate case is discussed below.

Substituting eq. (15) into eq.(24) and based on the assumption that samples in each group are statistically independent and samples among one group are iid, we can write the characteristic function as follows:

$$\Phi_{Z_{IM}}(j\omega) = \Phi_0^N(j\tfrac{\omega}{N}) \prod_{k_c=1}^{N_c} \Phi_{k_c}(j\tfrac{\omega}{N}) \prod_{k_g=1}^{N_g} \Phi_{k_g}(j\tfrac{\omega}{N}) \tag{26}$$

where

$$\Phi_0(j\omega) = E[\exp(j\omega a_r(0)] \tag{27}$$

$$ {}_{s}\Phi_{k_c}(j\omega) = \frac{1}{\Phi_0(j\omega)} E[\exp(j\omega a_r(k_c))] \tag{28a} $$

$$ {}_{s}\Phi_{k_g}(j\omega) = \frac{1}{\Phi_0(j\omega)} E[\exp(j\omega a_r(k_g))] \tag{28b} $$

$$ \Phi_{k_c}(j\omega) = E\left\{ {}_{s}\Phi_{k_c}^{N_{k_c}}(j\omega) \right\} \tag{29a} $$

$$ \Phi_{k_g}(j\omega) = E\left\{ {}_{s}\Phi_{k_c}^{N_{k_g}}(j\omega) \right\} \tag{29b} $$

Here we denote ${}_{s}\Phi_{k_c}(j\omega)$ (or ${}_{s}\Phi_{k_g}(j\omega)$) to be the characteristic function of a single sample $a_r(k_c)$ (or $a_r(k_g)$), divided by the characteristic function of a single sample $a_r(0)$, and $\Phi_{k_c}(j\omega)$ (or $\Phi_{k_g}(\omega)$) to be the resultant characteristic function averaged over the statistics of the Poisson arrival rate of the k_c-th or (k_g-th) group of RFI pulses. For a given data rate R, the total number N of samples $a_r(k_\ell)$, $k_\ell = 0,1,2,\ldots$, can be written as

$$ N = B_{IF}/R \tag{30} $$

Thus the variable n_{k_ℓ}, defined by Eqs. (15a) and (15b) can be expressed as

$$ N_{k_\ell} = (NR\tau_p) n_{k_\ell}^{T_d} \tag{31} $$

and Eqs. (29) become:

$$ \Phi_{k_c}(j\omega) = E\left\{ \left[{}_{s}\Phi_{k_c}^{NR\tau_p}(j\omega) \right]^{n_{k_c}^{T_d}} \right\} \tag{32a} $$

and

$$ \Phi_{k_g}(j\omega) = E\left\{ \left[{}_{s}\Phi_{k_g}^{NR\tau_p}(j\omega) \right]^{n_{k_g}^{T_d}} \right\} \tag{32b} $$

Here $n_{k_c}^{T}$ and $n_{k_g}^{T}$ are the only random variables and their probability distributions are characterized as Poisson processes:

$$P_{k_\ell}(n) = \frac{(P_\ell T)^n}{n!} e^{-P_\ell T} \tag{33}$$

where

P_ℓ = Pulse repetition rate of ℓth group of RFI

T = Observation period.

To simplify the notations, we denote

$$H_{k_\ell}(j\omega) \equiv {}_s\Phi_k^{NR\tau_p}(j\tfrac{\omega}{N}) \tag{34}$$

and

$$H_0(j\omega) = \Phi_0^N(j\tfrac{\omega}{N}) \tag{35}$$

Then, after taking the expectation with respect to $N_{k_c}^T$ for Eq. (32a) or to $N_{k_g}^T$ for Eq. (32b), we have

$$\Phi_{k_\ell}(j\tfrac{\omega}{N}) = \exp(\lambda_{k_\ell} T_d (H_{k_\ell}(j\omega)-1)) \tag{36}$$

In general, the functions $H_{k_\ell}(j\omega)$ can be expanded in terms of power series in $(j\omega)$ and $H_0(j\omega)$ in terms of its semi-invariants:

$$H_{k_\ell}(j\omega) = \sum_{i=0}^{\infty} m_i(k_\ell) \frac{(j\omega)^i}{i!} \tag{37a}$$

or

$$H_0(j\omega) = \exp\left(\sum_{i=1}^{\infty} \lambda_i(0) \frac{(j\omega)^i}{i!}\right) \tag{37b}$$

Note that the variable $m_i(k_\ell)$ is not the moment of some physical random variable. However it is a function of the moments of the sample $a_r(0)$ and the moments of the sum of the samples $a_r(k_\ell)$,

$$\text{either } \sum_{r=1}^{n_{k_c}} a_r(k_c) \quad \text{or} \quad \sum_{r=1}^{n_{k_g}} a_r(k_g)$$

Now using Eq. (37a) and (37b) we have

$$\Phi_{Z_{IM}}(j\omega) = \exp \sum_{i=1}^{\infty} \left(\lambda_i(0) + \sum_{k_c=1}^{N_c} P_{k_c} T_d^{m_i}(k_c) + \sum_{k_g=1}^{N_g} P_{k_g} T_d^{m_i}(k_g)\right) \frac{(j\omega)^i}{i!} \quad (38)$$

This yields the resultant i-th semi-invariant of Z_{IM}

$$\lambda_i = \lambda_i(0) + \sum_{k_c=1}^{N_c} P_{k_c} T_d^{m_i}(k_c) + \sum_{k_g=1}^{N_g} P_{k_g} T_d^{m_i}(k_g) \quad (39)$$

$$\text{for } i = 1,2,3,\ldots m$$

Therefore, the moments of Z_{IM} can be recursively computed from the set of semi-invariants λ_i as follows

$$m_k = \sum_{i=1}^{k} \binom{k-1}{i-1} \lambda_i m_{k-i} \quad k = 1,2,3,\ldots$$

$$m_0 = 1$$

where

$$\binom{n}{\ell} = \frac{n!}{\ell!(n-\ell)!}$$

4.5 LinCsim Modeling of RFI Effects on Synchronization Loops

4.5.1 Introduction

RFI will degrade carrier phase and symbol timing tracking when it is present on the Shuttle/TDRSS S-band return link. In this section the RFI environment of Table 4.1 is assumed. The duty cycles are so low that we can well assume that no pulses overlap. The way in which the RFI will affect each tracking loop depends on the relationships

among the symbol rate, RFI pulse durations, and RFI pulse repetition rates. We will give new expressions for r.m.s. phase error and timing error, to replace those presented in Chapter 3, that take RFI into account.

4.5.2 RFI Effect on Ground-Station Input Signal

Let us examine what the RFI effect is on the signal at input to the ground station. We refer to the generalized link shown in Figure 3.1. Since the correlation time of the TDRS input filter (about .05 μsec) is much less than the pulse durations, that filter passes the RFI essentially undistorted except for bandlimiting it. The nonlinearity (combination clipper and TWT) is memoryless. Thus, at the input to the ground station a set of signal statistics something like those in Section 3.3.2 can be found conditioned on each RFI situation. Since the power levels of the WGN RFI are relatively low, during no RFI or a WGN-RFI pulse the clipper doesn't have much effect. The noise power entering the TWT is just somewhat larger during a WGN-RFI pulse. However, the power levels of the CW RFI are much higher than those of the data and uplink noise, so that the clipper suppresses the data; little more than a tone enters the TWT.

We now proceed to treat the carrier and symbol tracking loops separately.

4.5.3 RFI Effect on Carrier Tracking

4.5.3.1 General Description of RFI in the Loop

We need to model the effect on the Costas loop, shown in Figure 3.2, of each RFI process. Fortunately, the general behavior is the same for all since the pulse duration and repetition rates of all bear the same relationships to the two S-band symbol rates. The meaning of this will be made clear below.

First step in the modeling is to consider the response of the arm filters G to a signal with a RFI pulse. The one-sided noise bandwidth B_G of G is .471 MHz for S-band mode 1 (symbol rate 288 Ksps) and .942 MHz for mode 2 (symbol rate 576 Ksps) [3], corresponding to a correlation time of $1/4B_G$, which is .53 μsec and .27 μsec for modes 1 and 2, respectively. This is much less than the pulse duration, especially since most of the higher-power RFI pulses, the ones that matter the most, have duration 5 μsec. Therefore, we assume that at the output of each of the arm filters, signal statistics can be obtained conditioned on each RFI situation.

The next step is to realize that since the loop merely multiplies the outputs of the arm filters to obtain the dynamic phase error process z, then the statistics of z are similarly conditioned.

Therefore, because of the definition (3-21) of the S-curve $S(\varphi)$, $S'(0)$ for use in the calculation (3-25) of phase-error variance is given by

$$\begin{aligned} S'(0) = {} & [S'(0)|\text{no RFI}]\cdot\Pr[\text{no RFI}] \\ & + \sum_{k=1}^{M_W} [S'(0)|\text{in a pulse of } k\text{th WGN-RFI process}] \\ & \quad \cdot(\text{duty cycle of } k\text{th WGN-RFI process}) \\ & + \sum_{k=1}^{M_C} [S'(0)|\text{in a pulse of } k\text{th CW-RFI process}] \\ & \quad \cdot(\text{duty cycle of } k\text{th CW-RFI process}) \end{aligned} \tag{40}$$

where it is assumed that the pulses of each RFI process occur at a constant rate and where M_W and M_C are the numbers of WGN- and CW-RFI processes, respectively. Since phase error Ψ is just scaled z passed through a filter H of very long correlation time (cf. (3-24)), then N_0' for use in (3-25) is given by a similar equation to (40).

We must now obtain conditioned quantities.

4.5.3.2 S'(0) and N_0' During No RFI or WGN RFI

The situation during a WGN-RFI pulse is like that of no RFI since WGN RFI looks like increased uplink thermal noise. Therefore, S'(0) and N_0' conditioned on one of these situations are calculated from (3-39) and (3-41) using the conditioned values of Eh_i and $S_{N_i}(0)$, $i = 1,2$, of $S_{N_1,N_2}(0)$ and of $S_{\overline{N}_1\ \overline{N}_2}(0)$. Since the clipper doesn't do much during WGN RFI, then N_1 and N_2 are still almost independent, so (3-42) can be used to approximate $S_{\overline{N}_1\ \overline{N}_2}(0)$.

4.5.3.3 S'(0) and N_0' During CW RFI

The signal arriving at the ground station during a CW pulse is essentially just a tone of constant power. This is because the RFI power is at least 15.7 dB above that of uplink thermal noise in the bandwidth of the TDRS input filter and the noise power is greater than that of the data. The TDRS clipper cuts down the power to a fixed level and the TWT amplifies the signal. The downlink noise is inconsequential.

Let us consider what the loop's arm filter G does to the tones. Since the correlation time of G is much less than the pulse durations, the tones appear to G to have infinite duration. The filtered quadrature components x_1 and x_2 of the loop input signal during the ith pulse are

$$\bar{x}_1(t) \equiv G(p)x_1(t) \doteq \sqrt{Q\eta(\omega_i)}\cos(\omega_i t+\theta_i) + \bar{n}_{d1}(t)$$

$$\bar{x}_2(t) \equiv G(p)x_2(t) \doteq \sqrt{Q\eta(\omega_i)}\cos(\omega_i t+\theta_i) + \bar{n}_{d2}(t) \qquad (41)$$

where

$$\eta(\omega_i) \equiv \left|G\left(\frac{\omega_i}{2\pi}\right)\right|^2 = \frac{1}{1+[(\omega_i/2\pi)/2B_G/\pi)]^2} \qquad (42)$$

B_G is the one-sided noise bandwidth of G, Q is the maximum power out of the TDR satellite, $\omega_i/2\pi$ and θ_i are chosen with uniform pdf's on [-10 MHz, 10 MHz] and $[0,2\pi]$, respectively, and n_{d1} and n_{d2} are the quadrature components of the downlink noise. 10 MHz is half the bandwidth of the TDRS input filter.

The contribution of the CW pulses to S'(0) is given by

$$[S'(0)|\text{in a pulse of CW RFI}] = 0 \qquad (43)$$

This is because during such a pulse of a tone characterized by ω_i and θ_i,

$$E[\bar{x}_2^2(t)-\bar{x}_1^2(t)] = -Q\eta(\omega_i)\frac{\sin \omega_i\tau_0}{\omega_i\tau_0}\cos(\omega_i\tau_0+2\theta_i) \qquad (44)$$

where τ_0 = 5 μsec is pulse duration. Averaging over ω_i and θ_i yields zero.

Now let us obtain N_0' conditioned on the presence of CW RFI. N_0' is the one-sided psd of n, which is the same as the z process when $\varphi = 0$. During the ith pulse n is given by

$$n(t) = -\bar{x}_1(t)\bar{x}_2(t) = -Q\eta(\omega_i)\frac{1}{2}\sin 2(\omega_i t+\theta_i) \qquad (45)$$

where we have neglected downlink noise. Since $\tau_0 << 1/2B_L$ (the correlation time of the H filter), then n during the pulse looks like

a δ-function input to H of area $-Q\eta(\omega_i)\frac{\tau_0}{2}\frac{\sin\omega_i\tau_0}{\omega_i\tau_0}\sin(\omega_i\tau_0+2\theta_i)$. The first zero crossing of $\frac{\sin\omega_i\tau_0}{\omega_i\tau_0}$ is at $\omega_i/2\pi = 1/2\tau_0 = .1$ MHz, while $\eta(\omega_i)$ is still close to one for $\omega_i/2\pi$ several times greater than that. So the operation of integrating over a pulse duration passes only a small fraction of the tones that G does. If we assume that the H filter integrates over intervals of length $1/2B_L$ and multiplies the result by $2B_L$, then the output of H due to CW RFI is $-2B_L\, Q\frac{\tau_0}{2}\sum_{\lambda=1}^{\lambda/2B_L}\eta(\omega_i)\frac{\sin\omega_i\tau_0}{\omega_i\tau_0}\sin(\omega_i\tau_0+2\theta_i)$ where λ is the repetition rate of the CW RFI process. Since $\lambda >> B_L$ we can assume that in any interval of length $1/2B_L$ the distribution of the ω_i's and θ_i's of the tones is about the same as the statistical distribution of ω_1 and θ_1, say. So the variance of that part of H(p)n(t) due to CW RFI is given by

$$\text{Var} = B_L\lambda\tau_0 Q^2\frac{\tau_0}{2}E_{\omega_1,\theta_1}\left[\eta(\omega_1)\frac{\sin\omega_1\tau_0}{\omega_1\tau_0}\sin(\omega_1\tau_0+\theta_1)\right]^2$$

$$= B_L\lambda\tau_0 Q^2\frac{\tau_0}{4}E_{\omega_1}\left[\eta(\omega_1)\frac{\sin\omega_1\tau_0}{\omega_1\tau_0}\right]^2 \qquad (46)$$

where $\omega_1/2\pi$ is uniformly distributed on [-10 MHz, 10 MHz]. But we have

$$E_{\omega_1}\left[\eta(\omega_1)\frac{\sin\omega_1\tau_0}{\omega_1\tau_0}\right]^2 \doteq \frac{1}{2}\cdot\frac{1}{2\tau_0}\cdot\frac{1}{10\text{ MHz}} \qquad (47)$$

Therefore, the conditioned N_0' is

$$[N_0' \mid \text{in pulse of CW RFI}] \doteq Q^2\cdot\frac{1}{16}\cdot\frac{1}{10\text{ MHz}} \qquad (48)$$

In the evaluations of phase error for S-band done in Section 4.6.3, the contribution to the sum N_0' made by CW RFI is an order of magnitude greater than that made by the more powerful of the two WGN RFI

processes and on the same order as that made by the no-RFI situation, which has much larger duty cycle.

4.5.4 RFI Effect on Symbol Tracking

4.5.4.1 General Description of RFI in the Loop

We need to obtain a model for the RFI in the digital-transition tracking loop (DTTL) shown in Figure 3.5 and then a new expression for timing-error variance. The loop handles the stream of biphase symbols as if it were a stream of double-rate NRZ symbols. Just as for the carrier loop, the modeling for RFI effects depends on the particular S-band symbol rates and RFI environment. The relationships among the important parameters aren't as favorable here as for the carrier loop, so this model is probably not as good as that one. The parameters we consider at this point are two: T, the duration of half a biphase symbol which has value 1.736 μsec (mode 1) or .868 μsec (mode 2); and pulse duration, which is 5 μsec for almost all the more powerful RFI pulses.

In order to analyze this loop in a way similar to the carrier loop, we make this loop be continuous-time by considering step functions I, J, and e which take on, respectively, the values I_k, J_k, and e_k (shown in Figure 3.5) on intervals of length T. Then e is just the dynamic phase error process, like the z process for the Costas loop. The correlation times of I and J are, respectively, 2T and T, so that the correlation time of e lies between those values. Now, $2T \doteq 3.5$ μsec or 1.7 μsec. We will assume, not with great accuracy, that pulse durations are enough greater than the correlation time of e so that e has two types of characteristics; one during no RFI or a pulse of WGN RFI and the other during a pulse of CW RFI.

Then (40) holds for S'(0) and so does a similar equation for N_0'. S'(0) = g'(0) and N_0' = 2S(0,0) in the notation of Section 3.5. We must obtain the conditioned quantities.

4.5.4.2 S'(0) and N_0' During No RFI or WGN RFI

Just as for the carrier loop, the situation during a WGN-RFI pulse is like that of no RFI except for an increase in uplink thermal noise. So the conditioned values of S'(0) and of N_0' are just obtained from (3-76) and (3-79) using conditioned values of symbol r.m.s. voltage A and one-sided noise psd N_0. It should be noted that "T" in those equations refers to biphase symbol duration.

4.5.4.3 S'(0) and N_0' During CW RFI

Just as for the carrier loop, we combine the CW RFI processes into one with pulse duration τ_0 = 5 μsec and say that during the ith pulse the loop input is merely a tone $\sqrt{Q}\cos(\omega_i t+\theta_i)$, where Q is the maximum power out of the TDR satellite and $\omega_i/2\pi$ and θ_i are chosen with uniform pdf's over [-10 MHz, 10 MHz] and [0,2π], respectively. Then the important loop quantities have the values given below:

$$I_k = \frac{1}{2}\left[\text{sign}\left(\frac{\sin(\omega_i T/2)}{\omega_i T/2}\right)\right]\left[\text{sign}\cos(\omega_i(k-\tfrac{1}{2})T+\theta_i) - \text{sign}\cos(k+\tfrac{1}{2})T+\theta_i)\right] \quad (49)$$

$$J_k = K_2\sqrt{Q}\,\xi_0 T\,\frac{\sin(\xi_0\omega_i T/2)}{\xi_0\omega_i T/2}\cos(\omega_i kT+\theta_i) \quad (50)$$

$$e_k = I_k J_k \quad (51)$$

The contribution to g'(0) is zero for the CW RFI.

We must find an equivalent N_0' conditioned on the occurrence of CW RFI. It must be recalled that in the linearized CW phase-

locked loop equivalent to the DTTL, a filter H filters the scaled equivalent noise process n to yield timing error. The n process equals the e process when timing error is zero. Since $\tau_0 << 1/2B_L$, where B_L is the one-sided loop bandwidth (of H), then the ith pulse looks like a δ-function input to H of area $T \sum_{k=1}^{M} e_k$, where $M = \tau/T = 2.9$ (mode 1) or 5.8 (mode 2). If H corresponds to integration over an interval of length $1/2B_L$ and multiplication by $2B_L$, then the variance of the filter output due to the CW RFI is $2B_L \lambda T^2 E_{\omega_i,\theta_i} \left(\sum_{k=1}^{M} e_k \right)^2$, where λ is the CW pulse repetition rate, so that the equivalent N_0' value is $\frac{2T^2}{\tau_0} E_{\omega_i,\theta_i} \left(\sum_{k=1}^{M} e_k \right)^2$.

In the evaluations of r.m.s. timing error for the S-band done in Section 4.6.3, the contribution to the sum N_0' made by CW RFI is about the same as that made by the more powerful of the two WGN RFI processes.

4.6 Preliminary LinCsim Performance Predictions

4.6.1 Introduction

Sections 4.6.1 and 4.6.2 have been omitted pending clarification of NASA Headquarters TWX 1/0083 of 2 January 1980 which pertained to the handling of information related to TDRSS vulnerability information analysis, data, etc.

Pages 160 through 168 missing

4.6.3 Predicted Synchronization Performance

Parts of this section have been omitted pending clarification of NASA Headquarters TWX 1/0083 of 2 January 1980 which pertained to the handling of information related to kDRSS vulnerability information analysis, data, etc.

This section gives the predicted performance of the ground-station carrier/subcarrier phase and symbol-timing recovery for the Shuttle Ku-band mode 1 and S-band return links. Results were obtained from analytical models implemented as computer programs for the two-channel Costas loop with hard-limiters, single-channel Costas loop, and data transition tracking loop. Plots of the r.m.s. phase error due to noise are given for the carrier and square-wave subcarrier of Ku-band mode 1 and for the S-band carrier for the allowable range of data rates and symbol types (NRZ or biphase). Plots of the r.m.s. timing error due to noise are given for all three channels of Ku-band mode 1 and the one S-band channel for the allowable range of data rates and symbol types. For S-band, results are shown both with and without the RFI model given in Table4.1. Tables 4.5,4.6 and 4.7 list the link parameter values assumed.

One conclusion that can be drawn from the plots is that for Ku-band subcarrier recovery, NRZ and biphase symbols in channel 2 give practically the same results, for any data rate.

LIST OF FIGURES

	Figure Numbers
•For Carrier of Ku-Band Return Link	
Mode 1--	
•R.M.S. Carrier Phase Error with Channel-3 Data Rate = 2,10,50 Mbps	15,16,17
•Normalized R.M.S. Timing Error for Channel 3 with Channel-3 Data Rate = 2,10,50 Mbps	18,19,20
•For Subcarrier of Ku-Band Return Link	
Mode 1--	
•R.M.S. Subcarrier Phase Error with Channel-2 Data Rate = 16,192,600 Kbps (NRZ and Biphase Symbols), 2 Mbps (NRZ), 1024 Kbps (Biphase)	21-25
•Normalized R.M.S. Timing Error for Channels 1 and 2 with Channel-2 Data Rate = 16,192,600, 2000 Kbps (NRZ)	26-29
•Normalized R.M.S. Timing Error for Channels 1 and 2 with Channel-2 Data Rate = 16,192,1024 Kbps (Biphase)	30,31,32
•For S-Band Return Link--	
•R.M.S. Carrier Phase Error, With and Without RFI	33
•Normalized R.M.S. Timing Error, With and Without RFI	34

CARRIER OF KU-BAND RETURN LINK MODE 1

Table 4.5 . LinCsim Parameter Values for Figures 4.16 through 4.20 .

Link: Ku-band mode 1 dedicated return link

Signal Modulation: UQPSK

Power Split (I/Q): 4/1

I Channel (Representing Channel 3):

Data rate = 2 Mbps to 50 Mbps, NRZ symbols,

unspread, convolutionally encoded at rate 1/2

Q Channel: Modulated square-wave subcarrier

TDRS Front-End Filter Bandwidth: 225 MHz

TDRS TWT: max AM/PM = 10°/dB, input backoff=10 dB

E_b/N_0 on Downlink: $\geq$ 30 dB

Receiver Carrier-Recovery Loop:

Two-channel loop with hard limiters and amplitude

ratio 2/1; arm filters noise bandwidth = $\frac{\pi}{2} \times \frac{1}{\sqrt{2}} \times$

max{ 2xI-channel data rate, 22.666 MHz }; one-sided loop

bandwidth = 1 KHz

Receiver Symbol-Timing Recovery Loop:

Data transition tracking loop with ξ_0 = .25 and with

(loop bandwidth)/(2xI-channel data rate)

$$= \begin{cases} .267\%, \text{ 2 Mbps} \leq \text{I-channel data rate} \leq \text{37.5 Mbps} \\ \text{200 KHz/(2xI-channel data rate),} \\ \quad \text{37.5 Mbps} \leq \text{I-channel data rate} \end{cases}$$

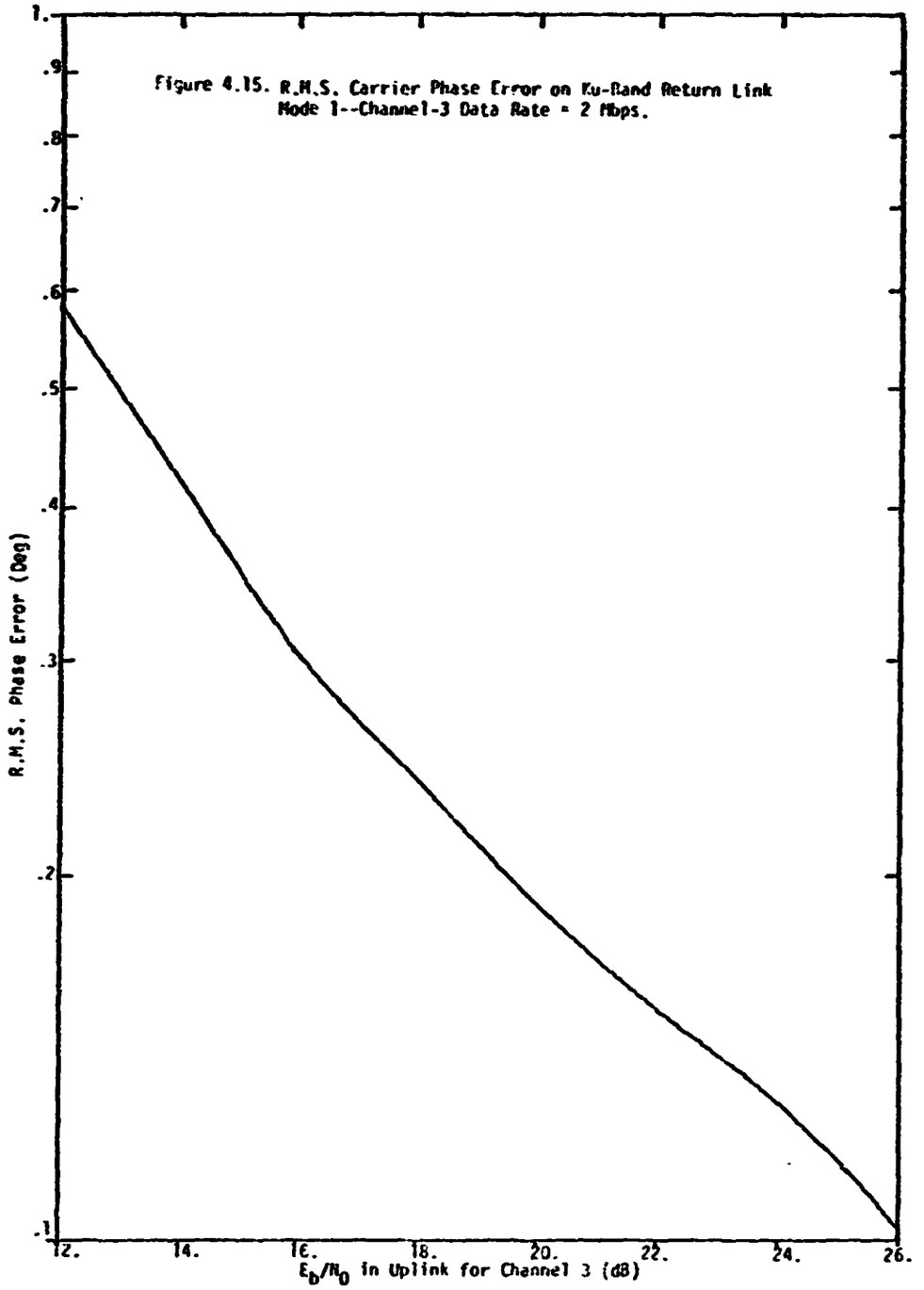

Figure 4.15. R.M.S. Carrier Phase Error on Ku-Band Return Link
Mode 1--Channel-3 Data Rate = 2 Mbps.

80 0013

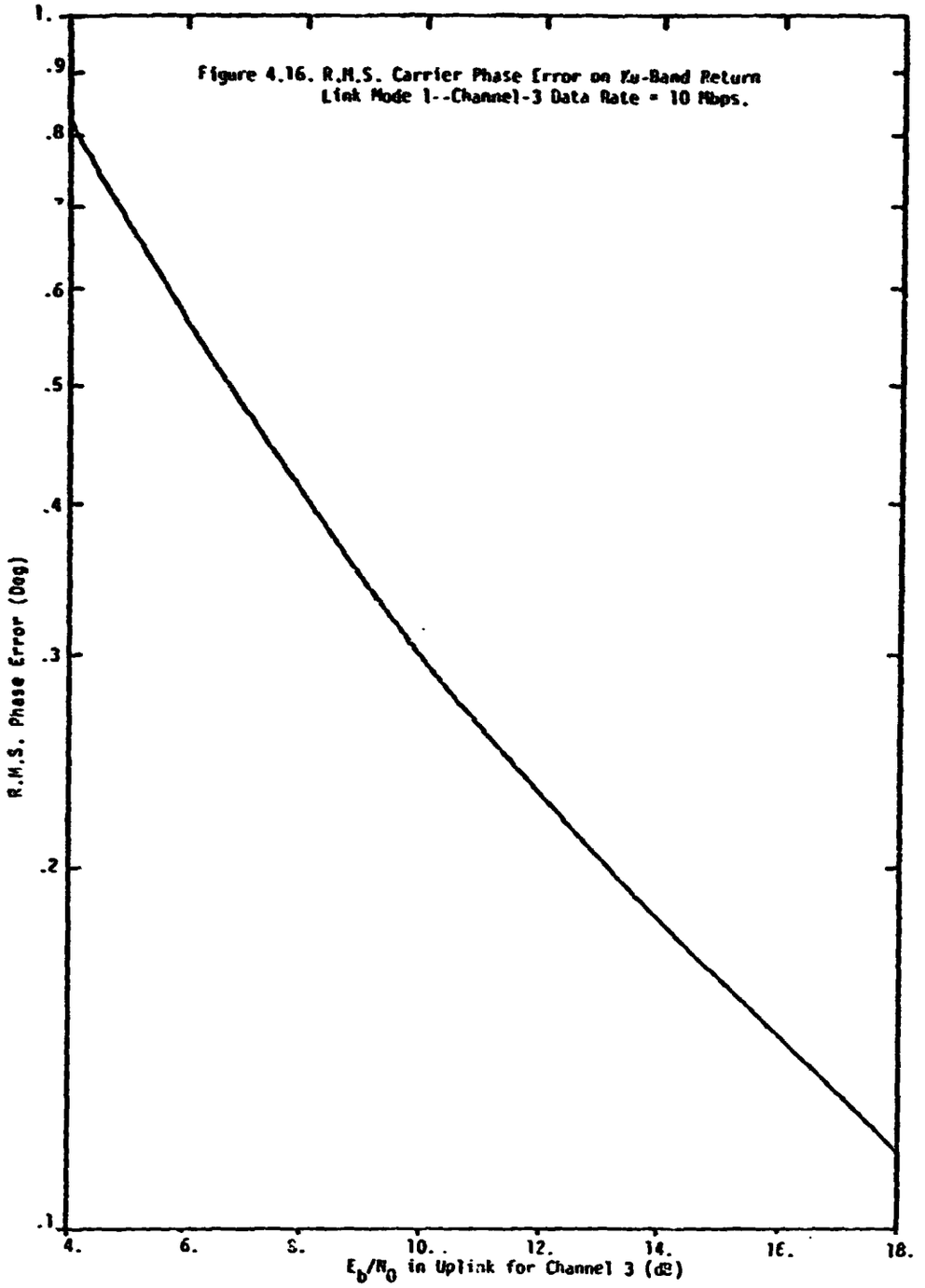

Figure 4.16. R.M.S. Carrier Phase Error on Ku-Band Return Link Mode 1--Channel-3 Data Rate = 10 Mbps.

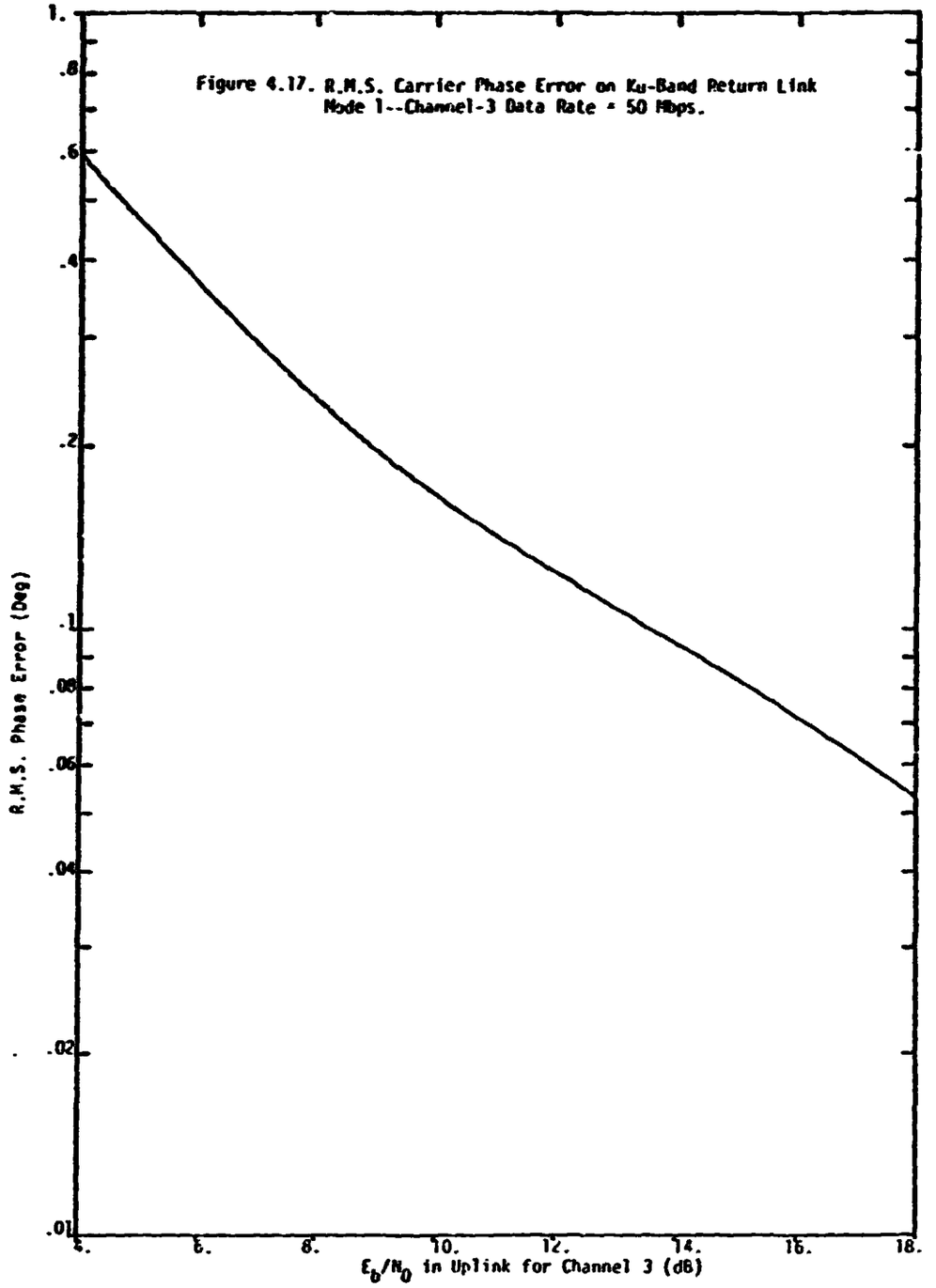

Figure 4.17. R.M.S. Carrier Phase Error on Ku-Band Return Link Mode 1--Channel-3 Data Rate = 50 Mbps.

80 0015

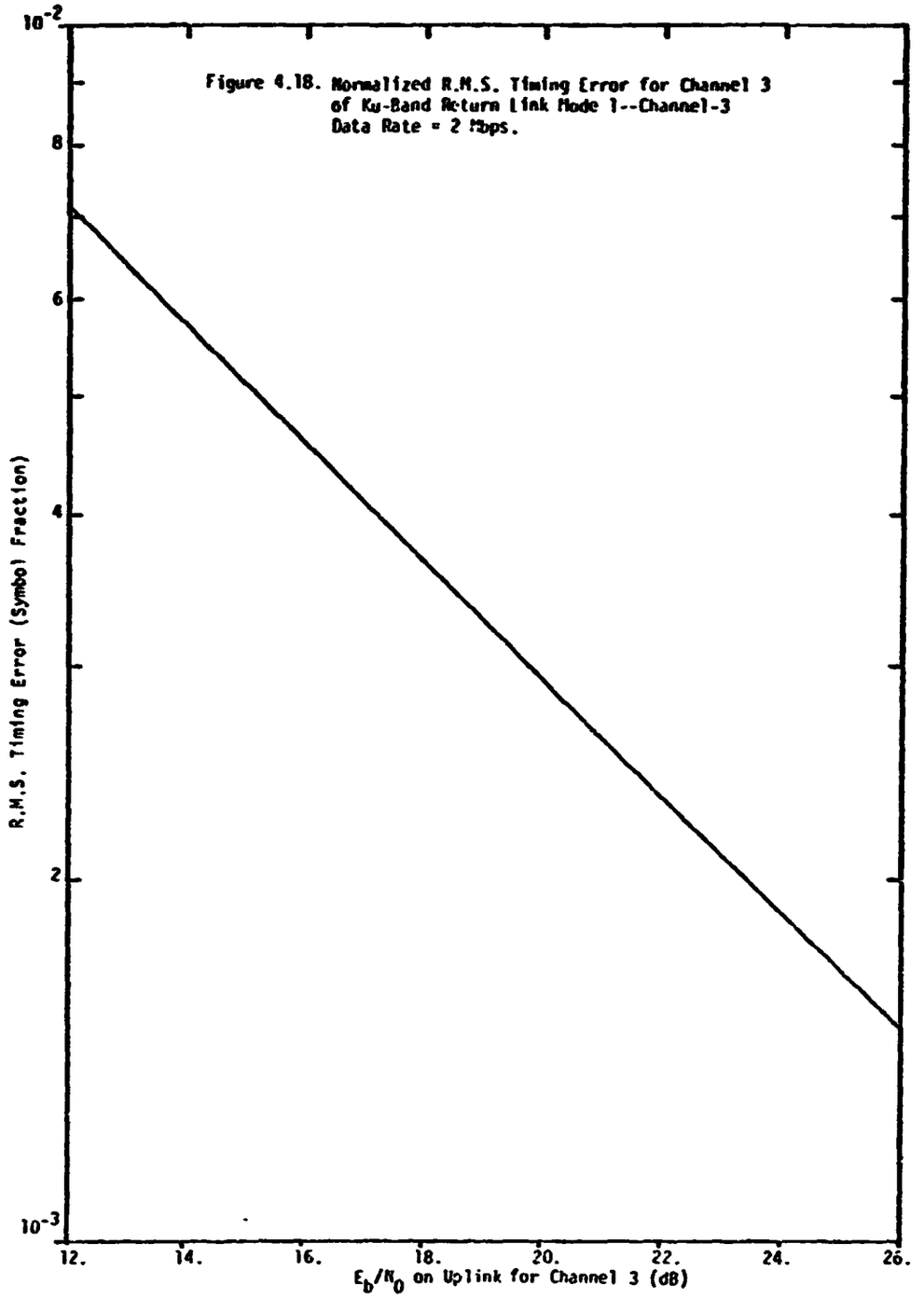

Figure 4.18. Normalized R.M.S. Timing Error for Channel 3 of Ku-Band Return Link Mode 1--Channel-3 Data Rate = 2 Mbps.

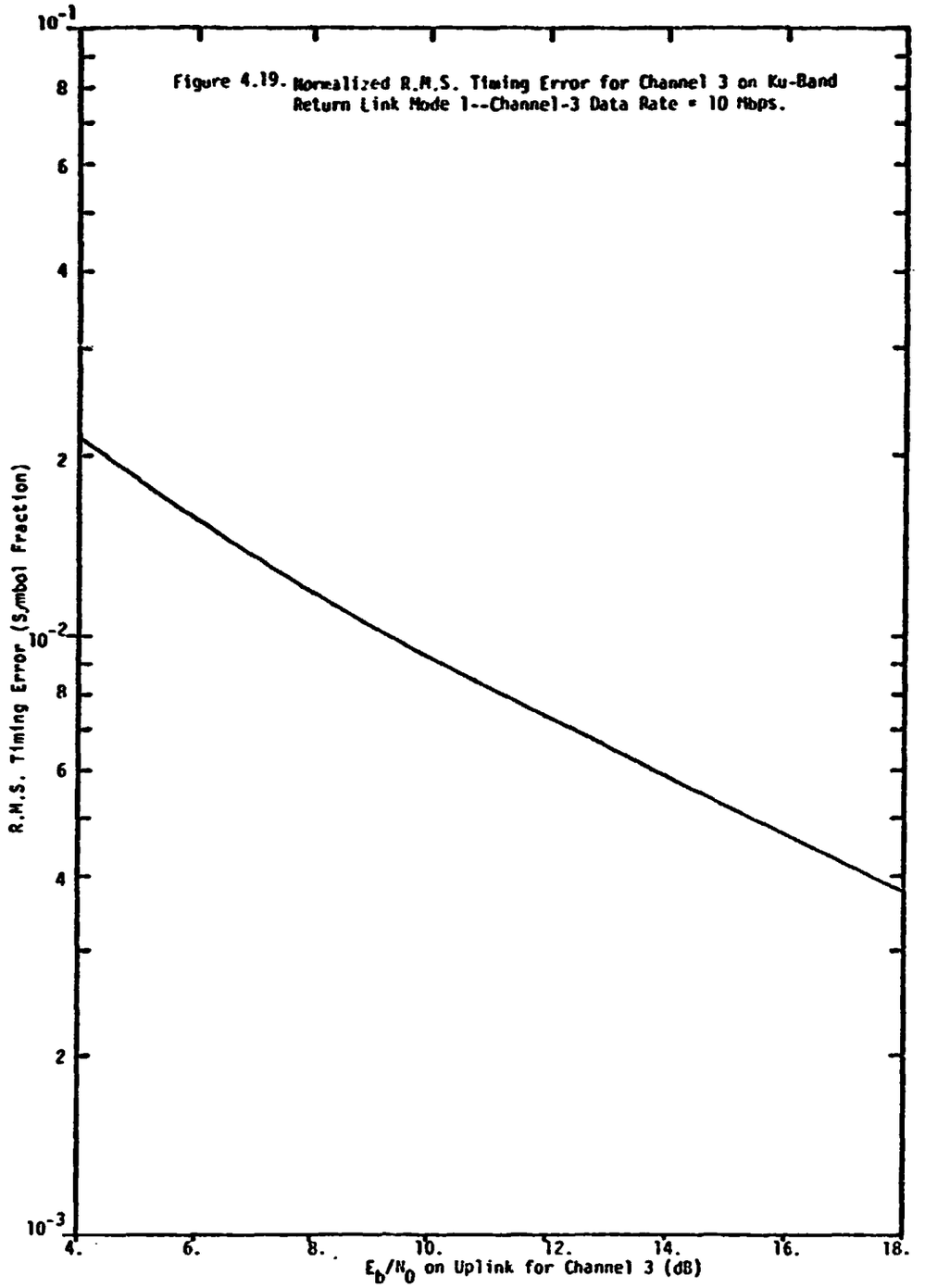

Figure 4.19. Normalized R.M.S. Timing Error for Channel 3 on Ku-Band Return Link Mode 1--Channel-3 Data Rate = 10 Mbps.

80 0017

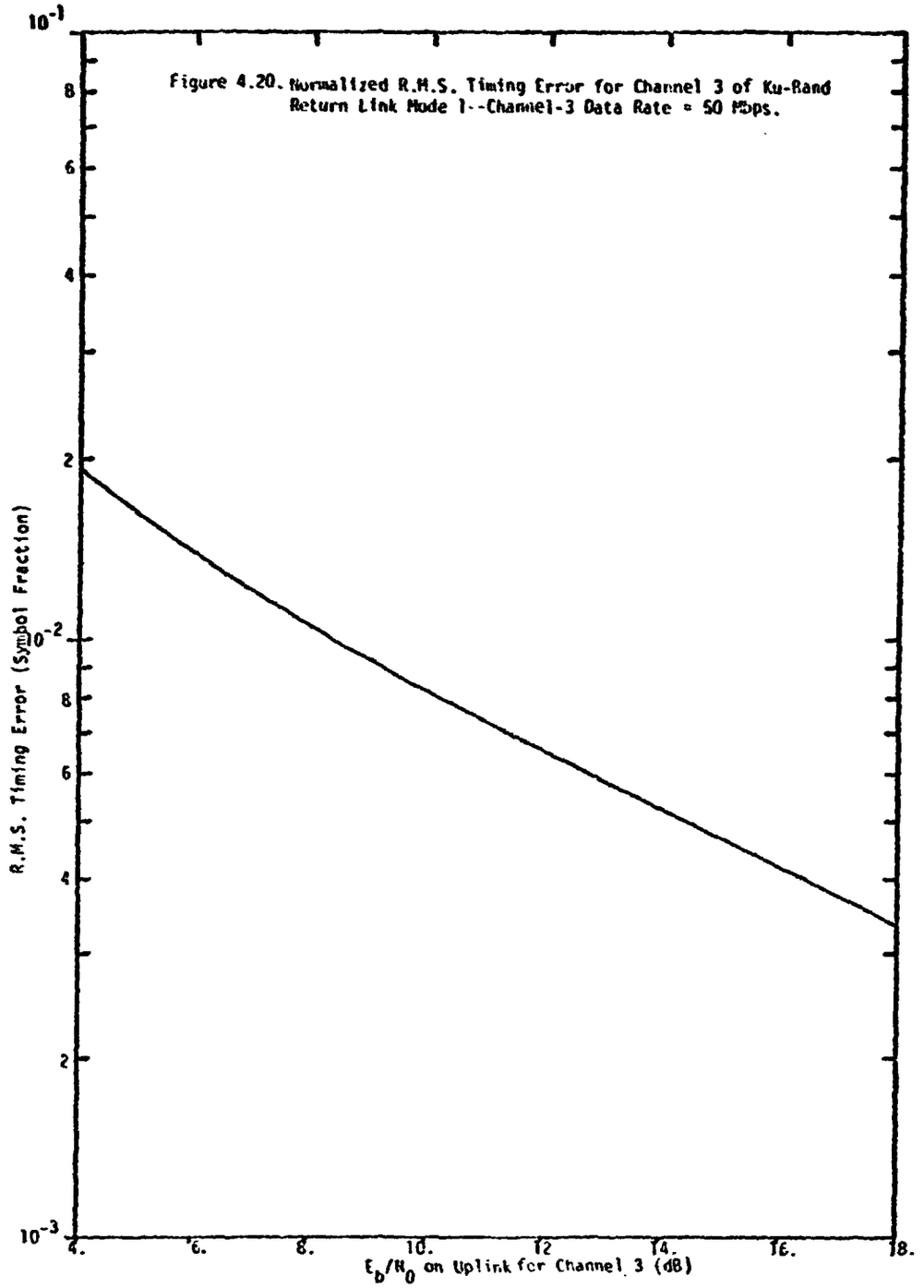

Figure 4.20. Normalized R.M.S. Timing Error for Channel 3 of Ku-Band Return Link Mode 1--Channel-3 Data Rate = 50 Mbps.

SUBCARRIER OF KU-BAND RETURN LINK MODE 1

Table 4.6. LinCsim Parameter Values for Figures 4.21 through 4.32.

Link: Ku-band mode 1 dedicated return link

Signal Modulation: UQPSK

Power Split (I/Q): 4/1

I Channel (Representing Channel 2):

Data rate = 16 Kbps to 2 Mbps (NRZ) or 16 Kbps to 1024 Kbps (biphase), NRZ or biphase symbols, unspread, uncoded

Q Channel (Representing Channel 1):

Data rate = 192 Kbps, biphase symbols, unspread, uncoded

TDRS Front-End Filter Bandwidth: 225 MHz

TDRS TWT: max AM/PM = 10°/dB, input backoff = 10 dB

E_b/N_0 on Downlink: $\geq$ 30 dB

Signal Power is Reduced in Receiver (by multiplying it by $8/\pi^2$) to Reflect Effect of Demodulating the Square-Wave Subcarrier with a Sine Wave.

Receiver Carrier-Recovery Loop:

Two-channel loop with hard-limiters and amplitude ratio 2/1;

$$\text{arm-filters noise b.w. in MHz} = \frac{\pi}{2} \times \begin{cases} .3,\ 300\ \text{Kbps} \leq R_{max} \leq 600\ \text{Kbps} \\ .6,\ 600\ \text{Kbps} \leq R_{max} \leq 1.5\ \text{Mbps} \\ 1.2,\ 1.5\ \text{Mbps} \leq R_{max} \leq 3\ \text{Mbps} \end{cases}$$

$$\text{where } R_{max} \equiv \begin{cases} \max\{384\ \text{Kbps},\ \text{I-channel data rate}\},\ \text{I NRZ} \\ \max\{384\ \text{Kbps},\ 2\text{x I-channel data rate}\},\ \text{I biphase}; \end{cases}$$

one-sided loop b.w. = 1 KHz

Receiver Symbol-Timing Recovery Loop:

Data transition tracking loop with $\xi_0 = .25$ and with loop bandwidth/data rate = .01% for channels I and Q.

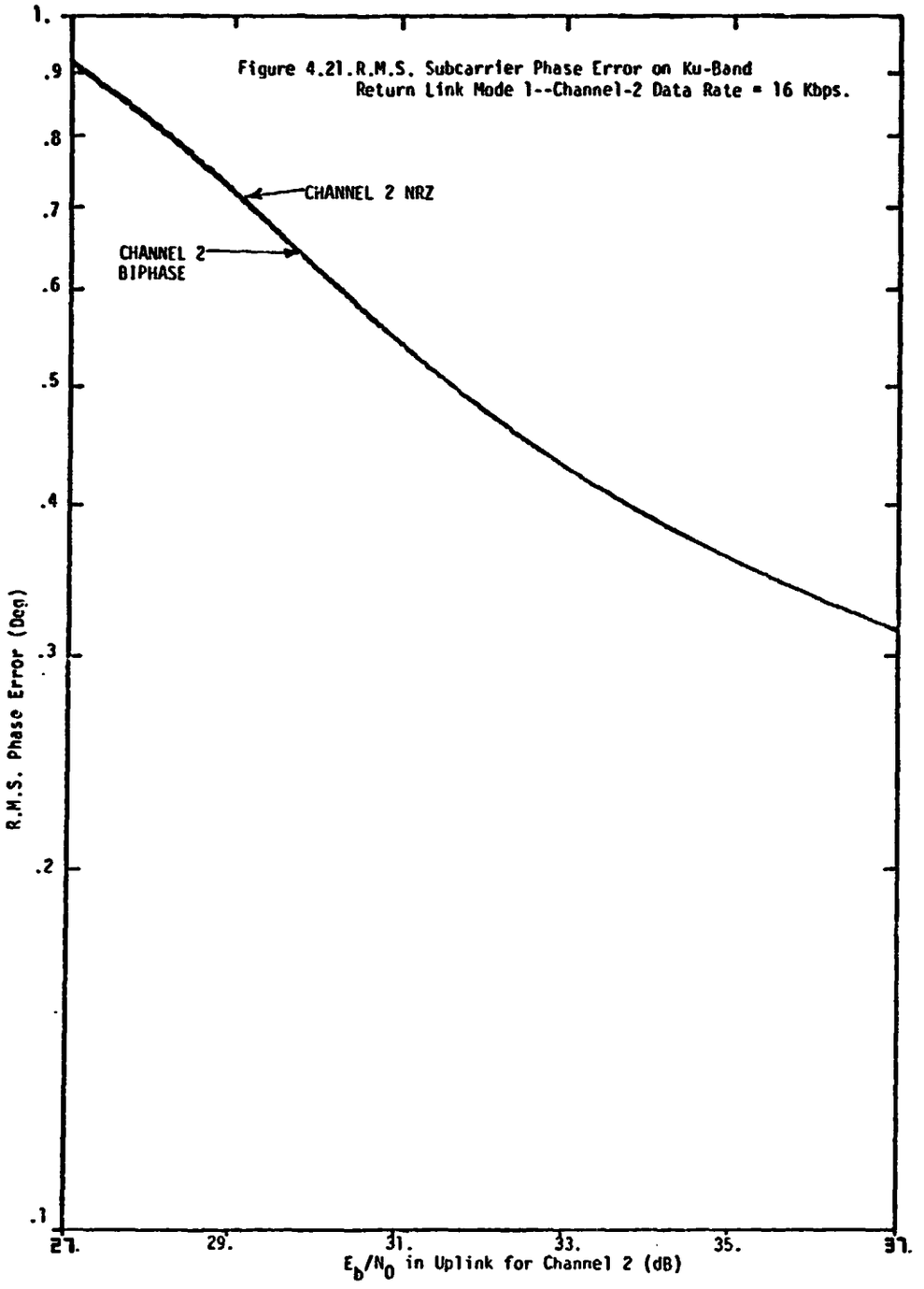

Figure 4.21. R.M.S. Subcarrier Phase Error on Ku-Band Return Link Mode 1--Channel-2 Data Rate = 16 Kbps.

80 0019

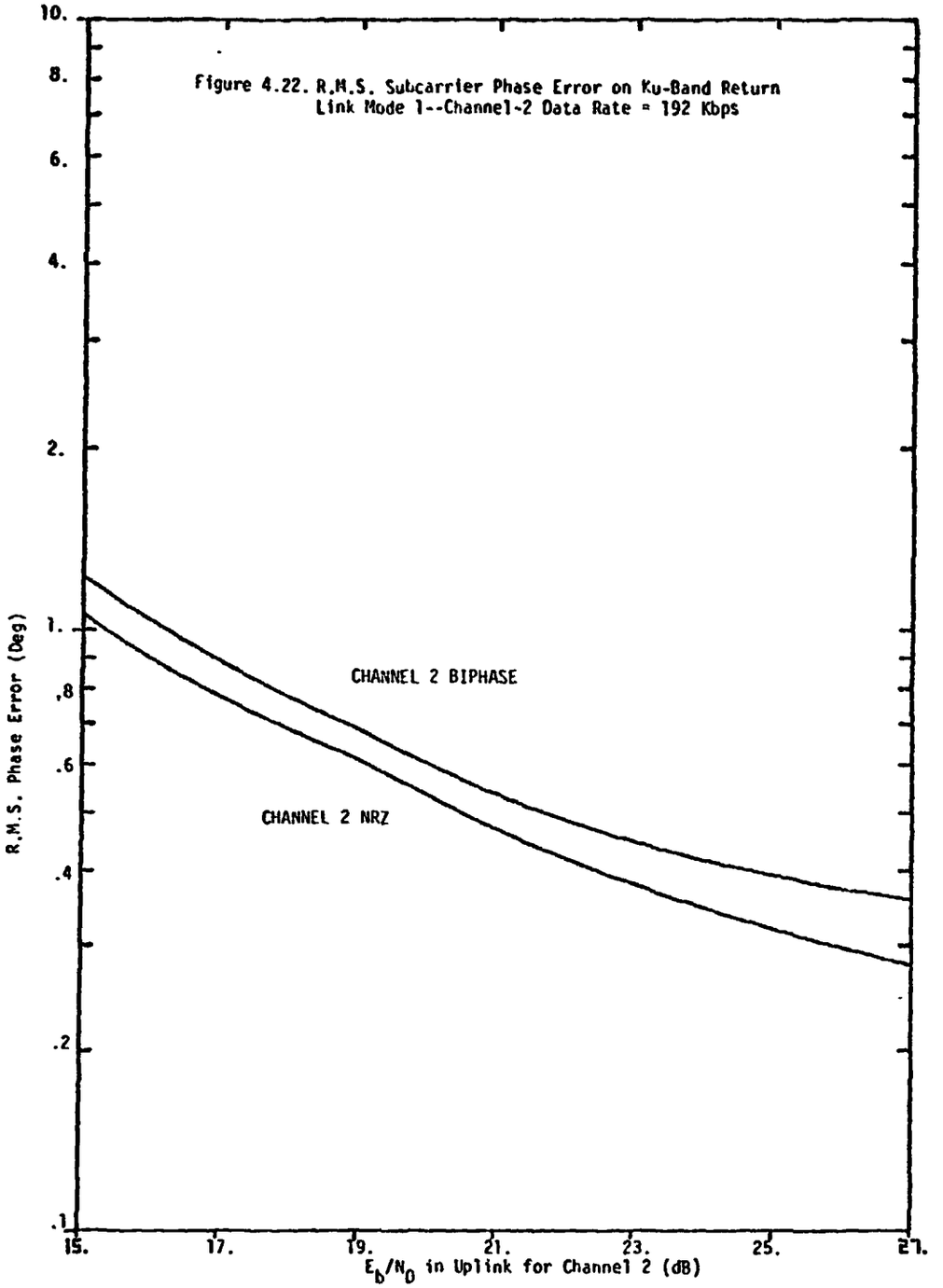

Figure 4.22. R.M.S. Subcarrier Phase Error on Ku-Band Return Link Mode 1--Channel-2 Data Rate = 192 Kbps

80 0020

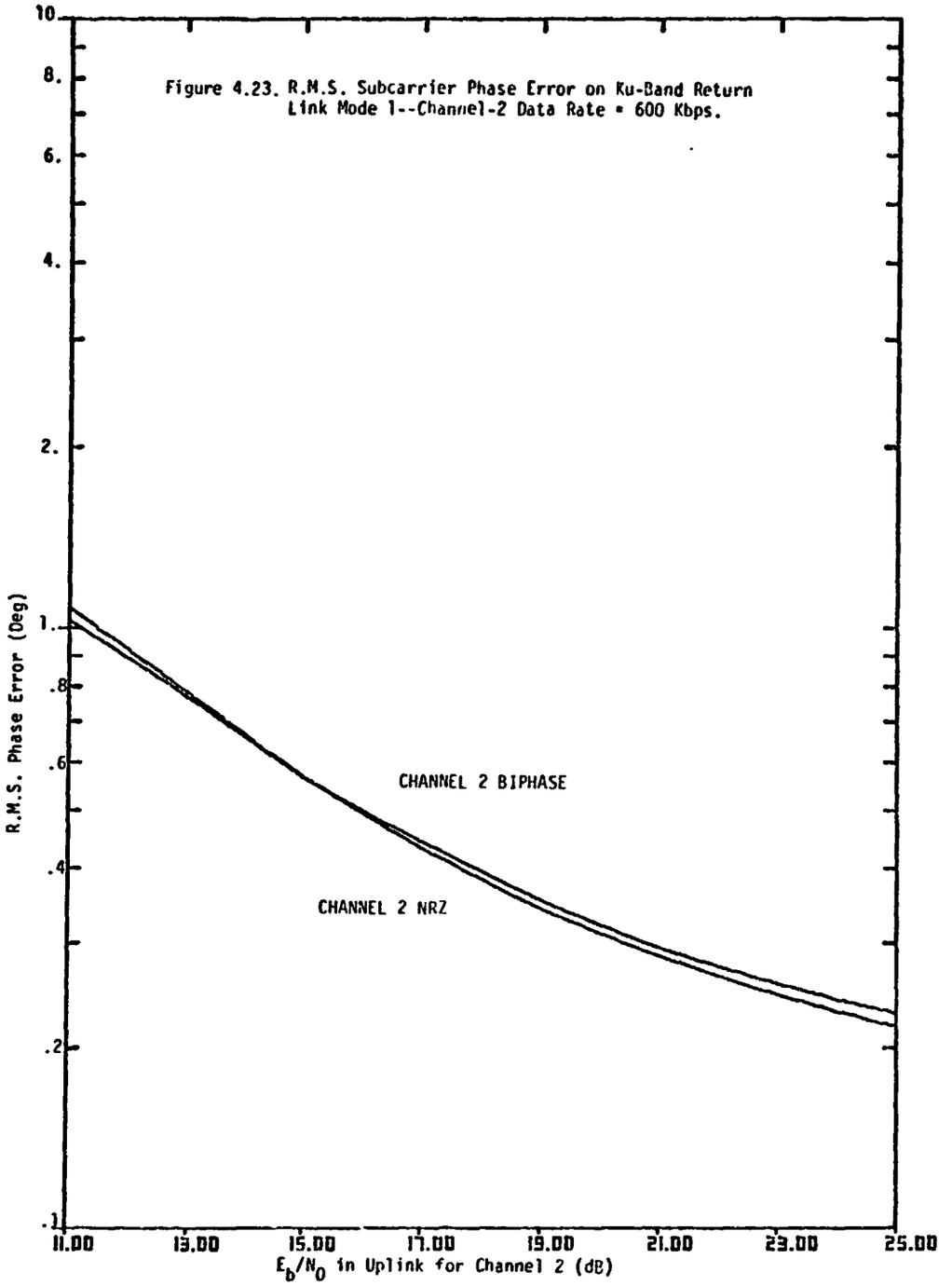

Figure 4.23. R.M.S. Subcarrier Phase Error on Ku-Band Return Link Mode 1--Channel-2 Data Rate = 600 Kbps.

80 0021

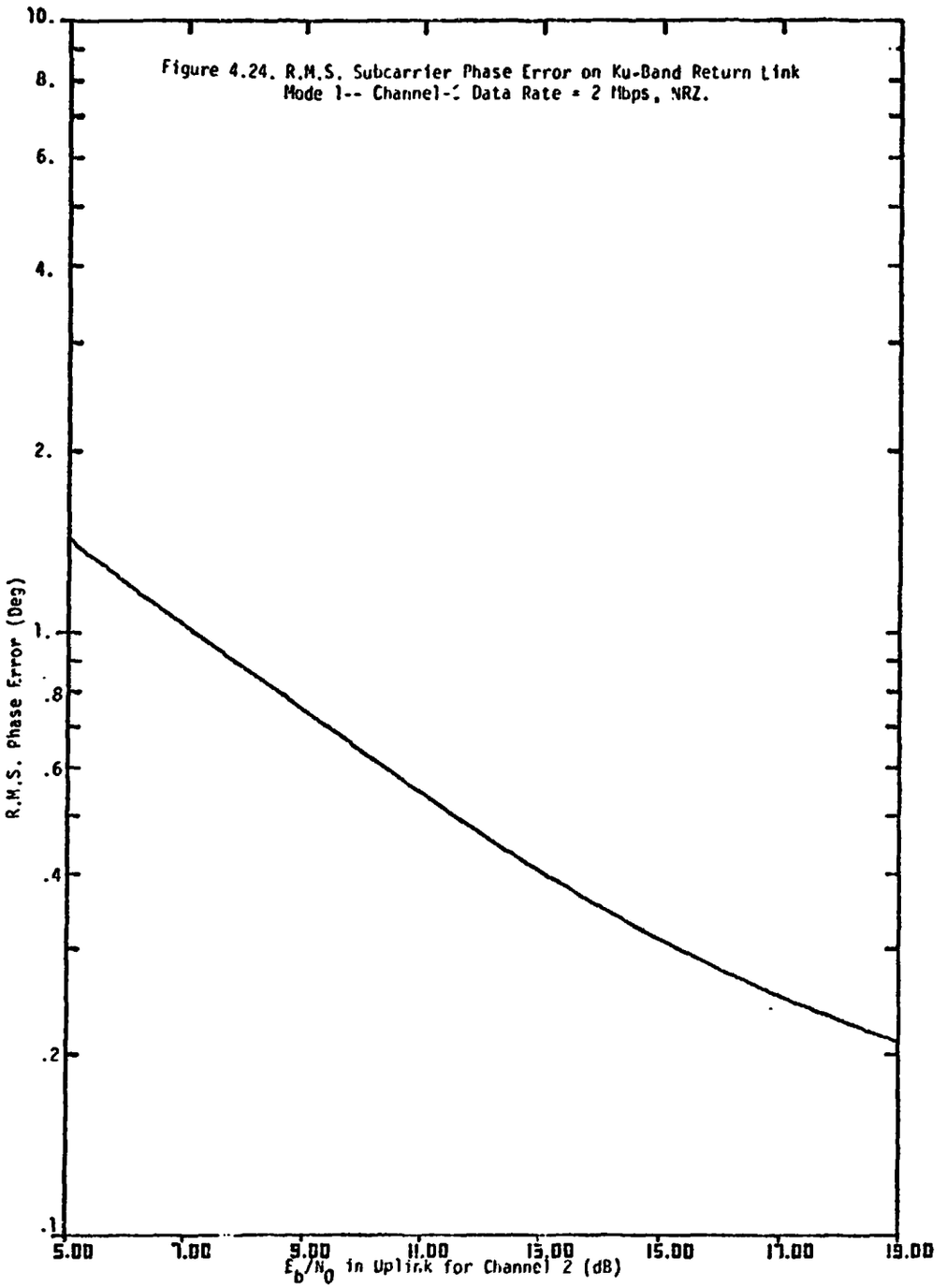

Figure 4.24. R.M.S. Subcarrier Phase Error on Ku-Band Return Link
Mode 1-- Channel-2 Data Rate = 2 Mbps, NRZ.

80 0022

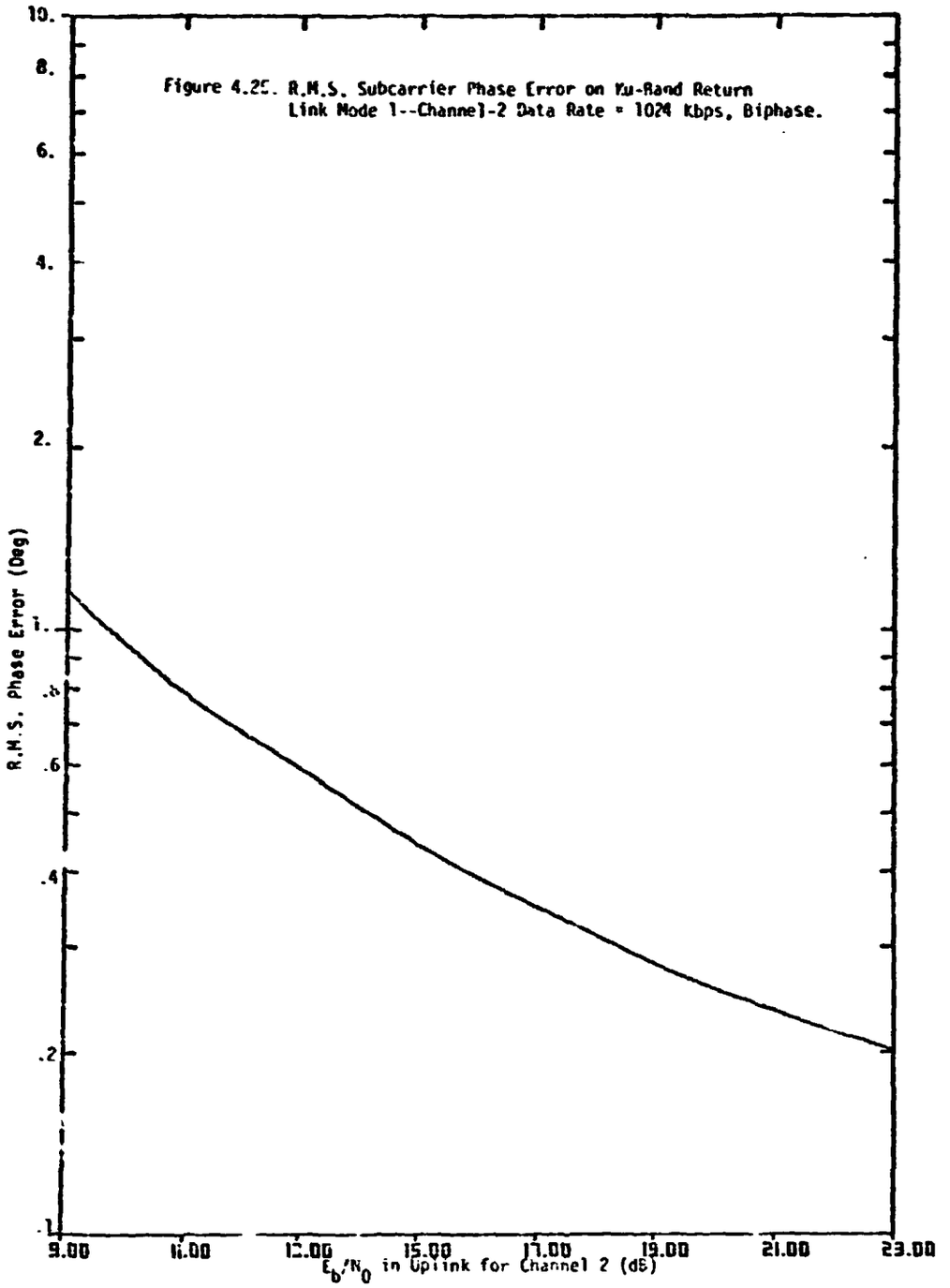

Figure 4.25. R.M.S. Subcarrier Phase Error on Ku-Band Return Link Mode 1--Channel-2 Data Rate = 1024 Kbps, Biphase.

80 0023

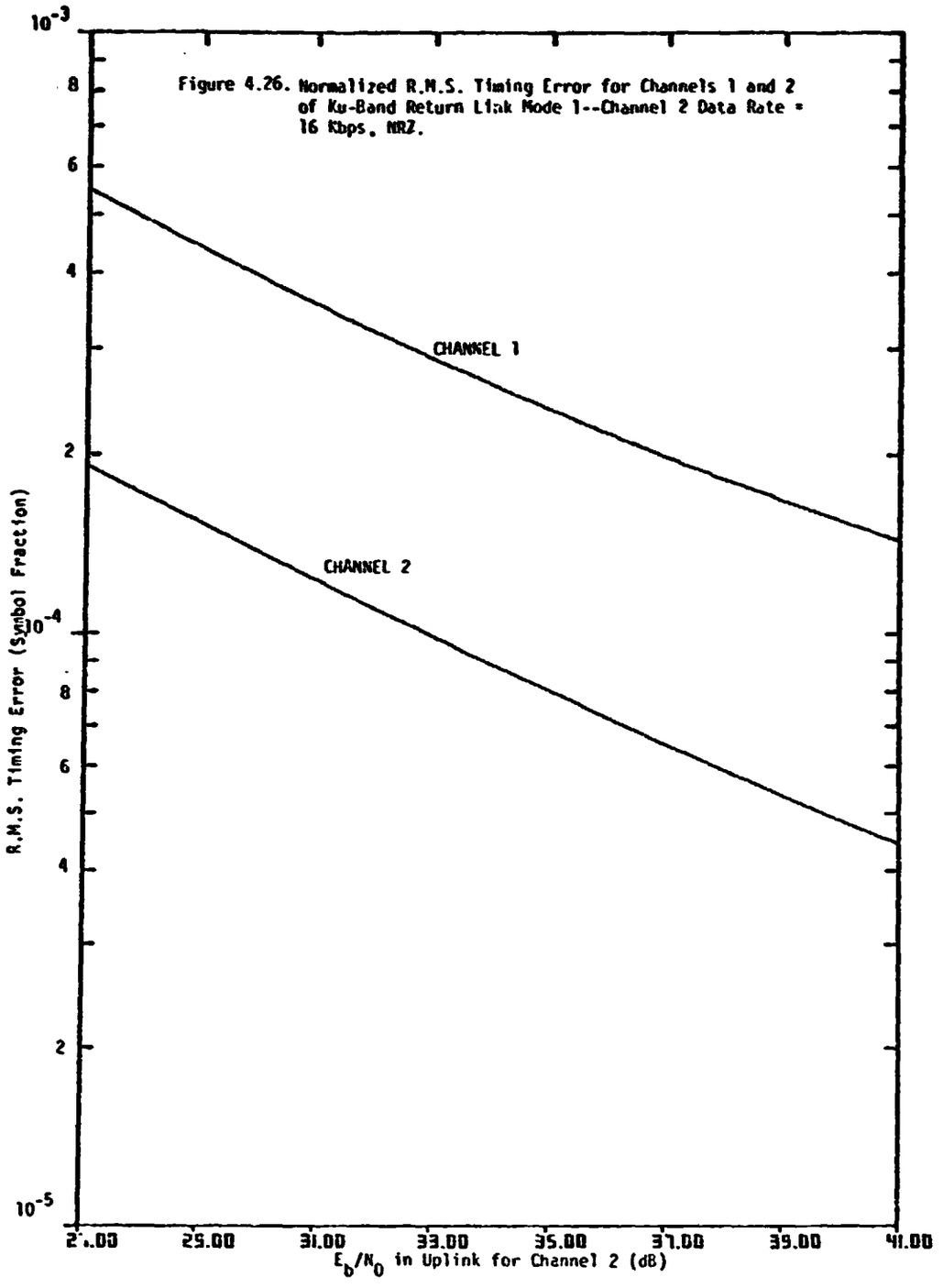

Figure 4.26. Normalized R.M.S. Timing Error for Channels 1 and 2 of Ku-Band Return Link Mode 1--Channel 2 Data Rate = 16 Kbps, NRZ.

80 0021

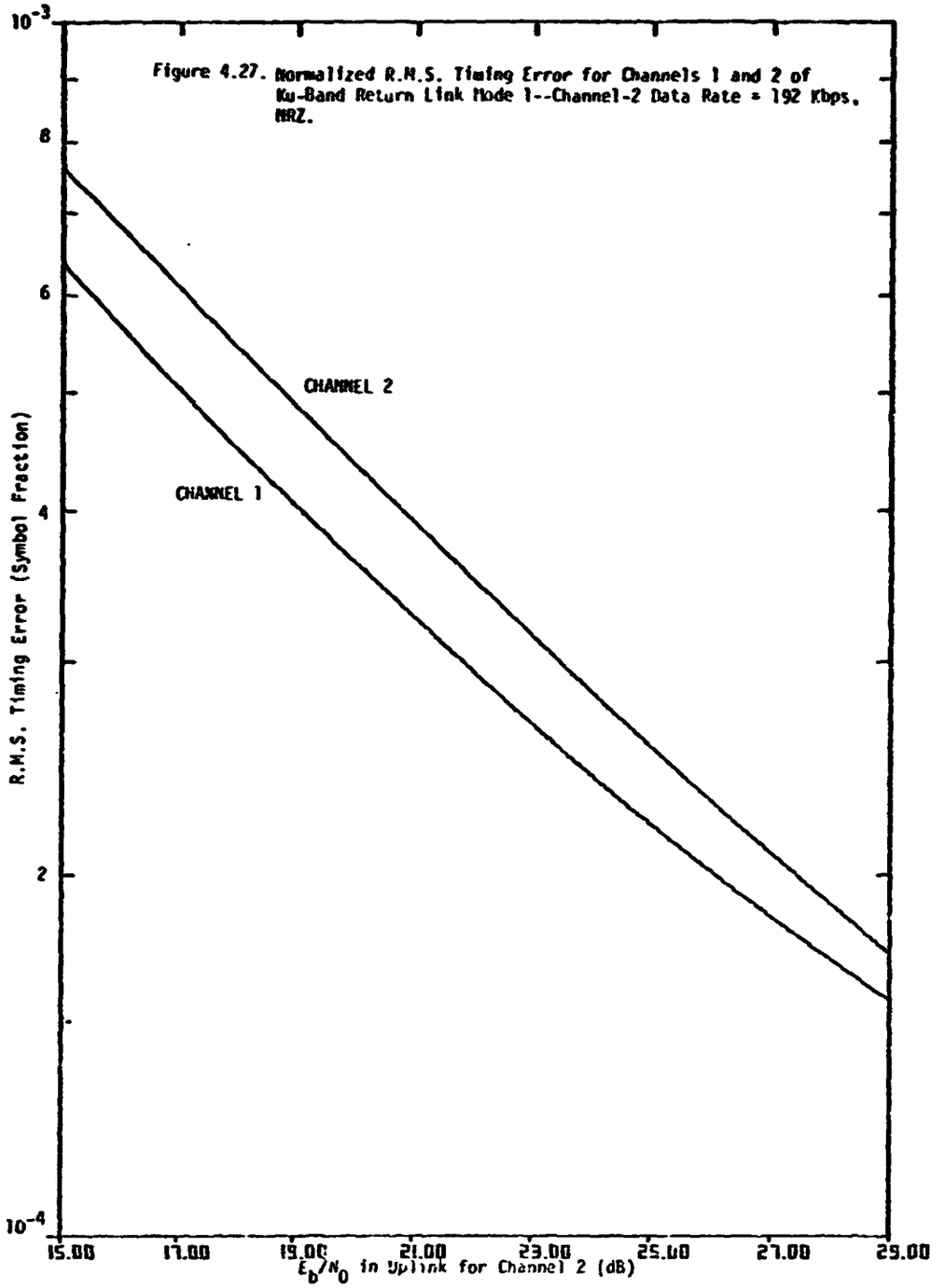

Figure 4.27. Normalized R.M.S. Timing Error for Channels 1 and 2 of Ku-Band Return Link Mode 1--Channel-2 Data Rate = 192 Kbps, NRZ.

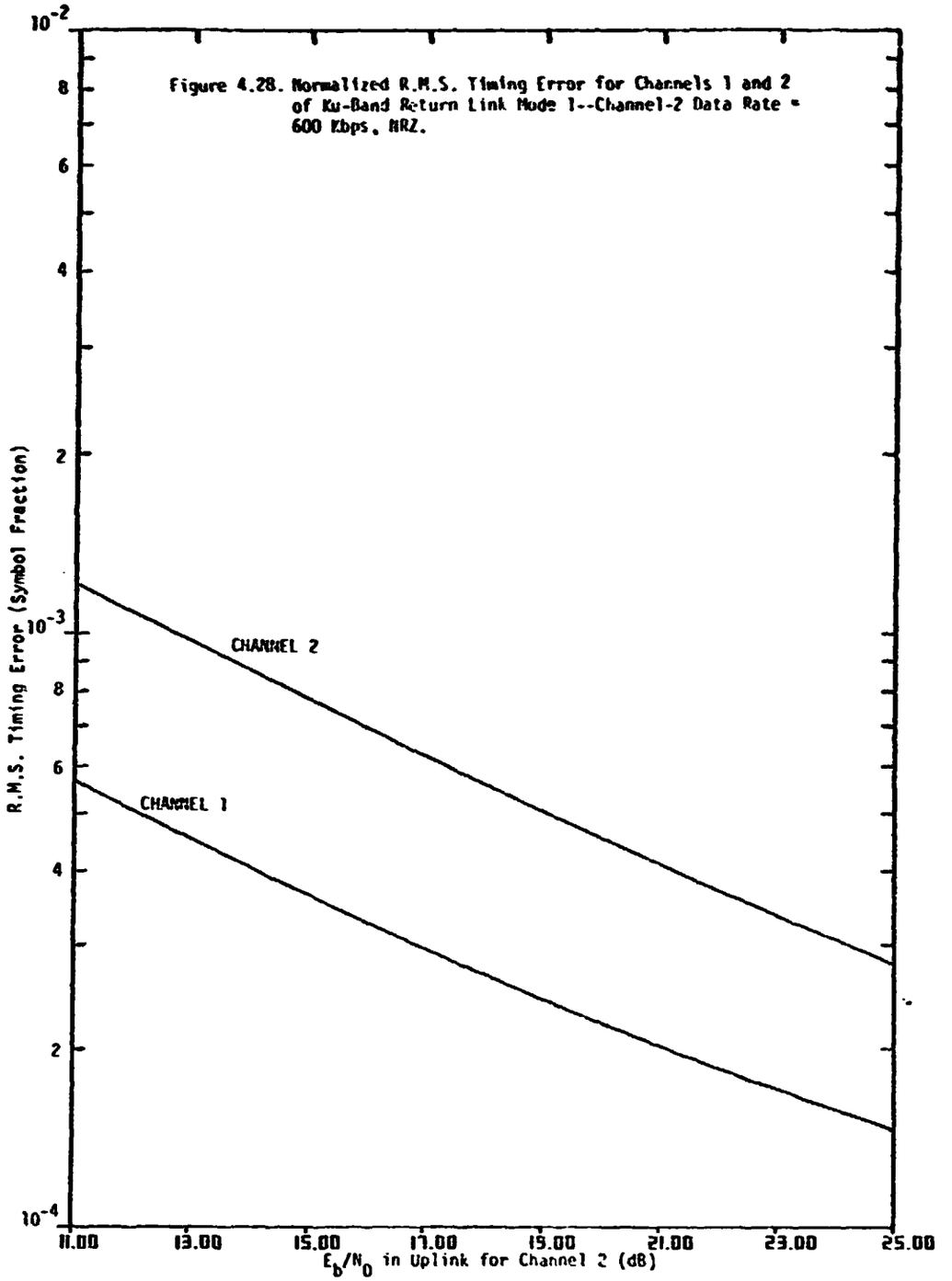

Figure 4.28. Normalized R.M.S. Timing Error for Channels 1 and 2 of Ku-Band Return Link Mode 1--Channel-2 Data Rate = 600 Kbps, NRZ.

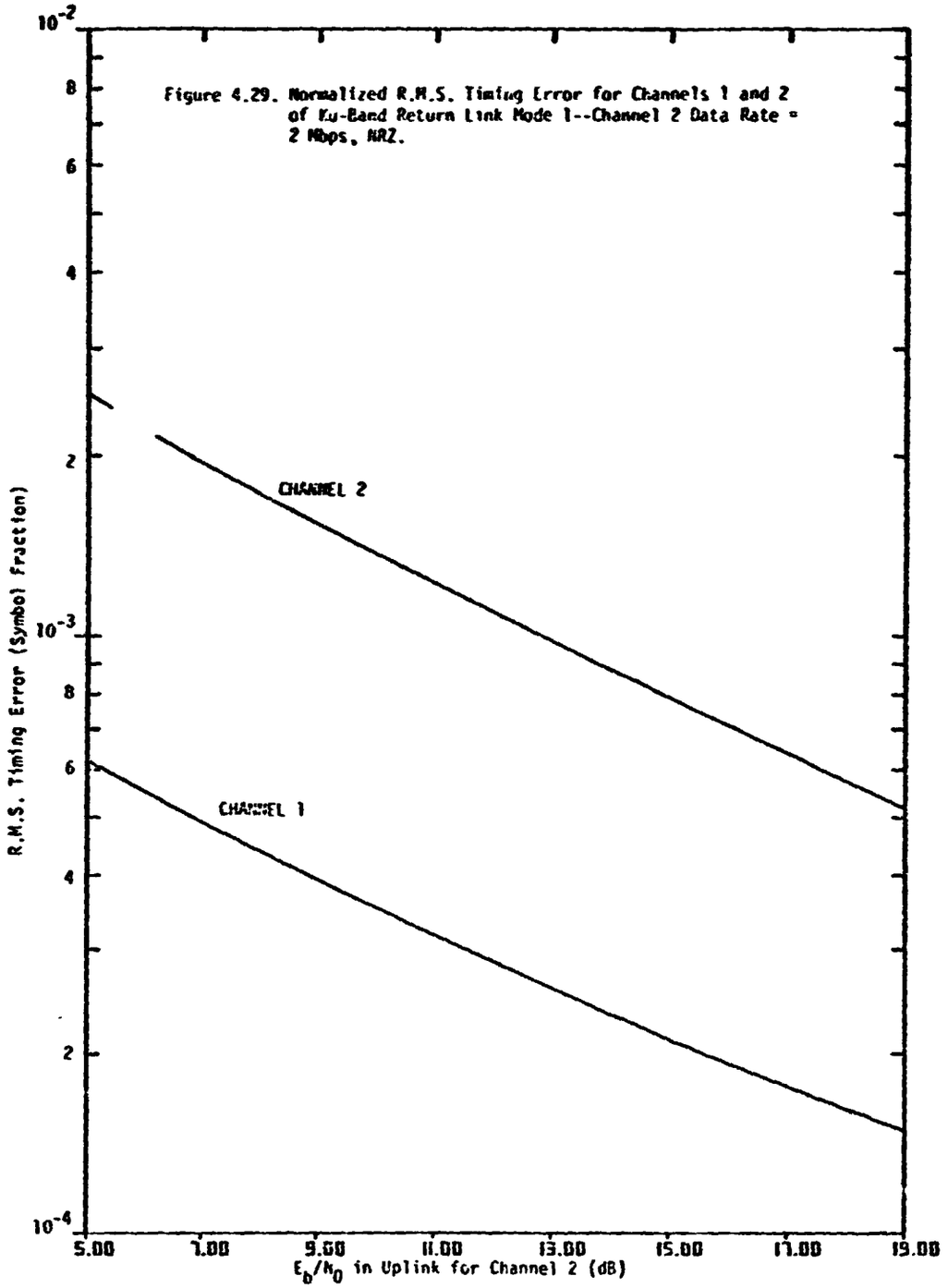

Figure 4.29. Normalized R.M.S. Timing Error for Channels 1 and 2 of Ku-Band Return Link Mode 1--Channel 2 Data Rate = 2 Mbps, NRZ.

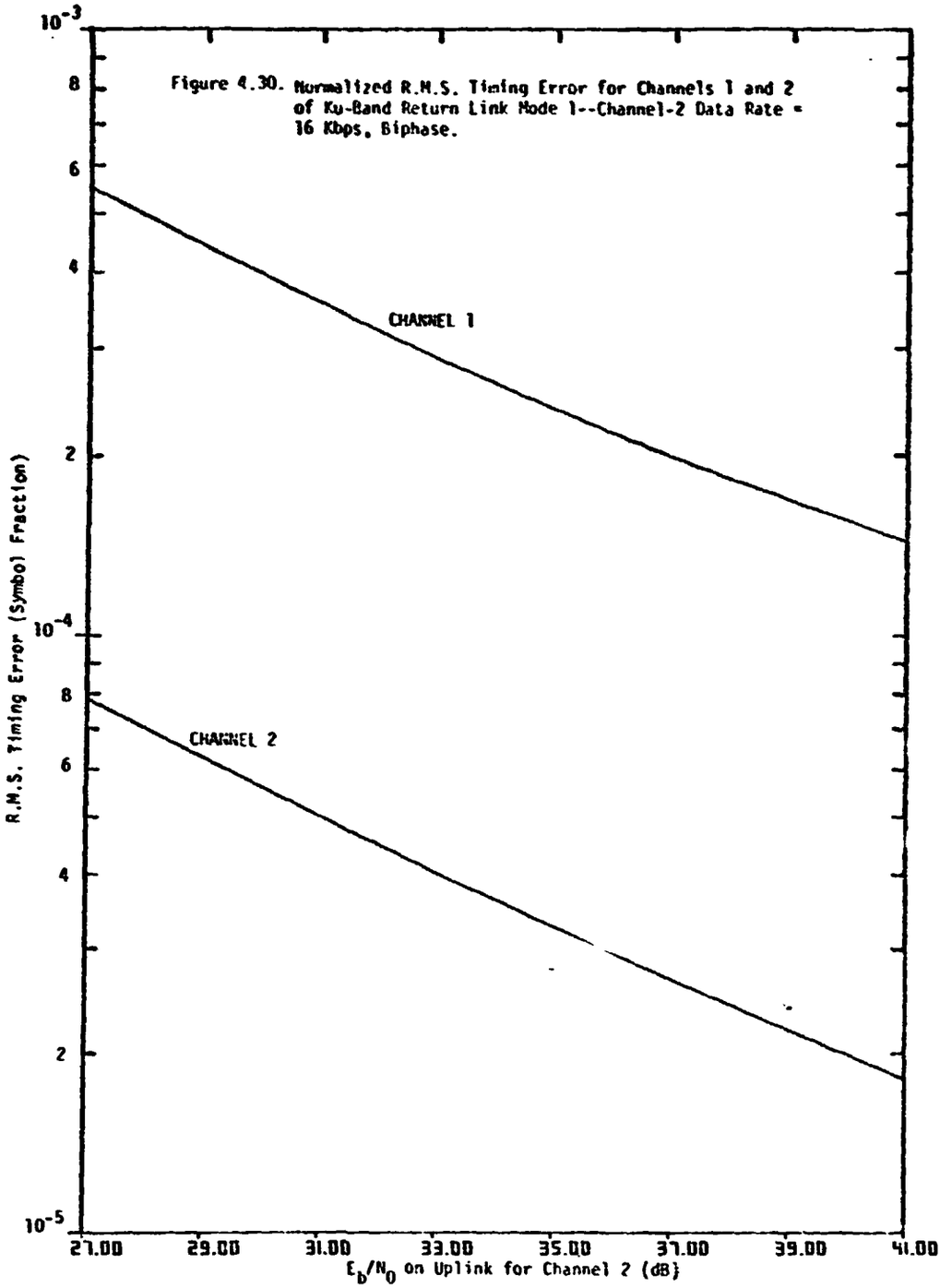

Figure 4.30. Normalized R.M.S. Timing Error for Channels 1 and 2 of Ku-Band Return Link Mode 1--Channel-2 Data Rate = 16 Kbps, Biphase.

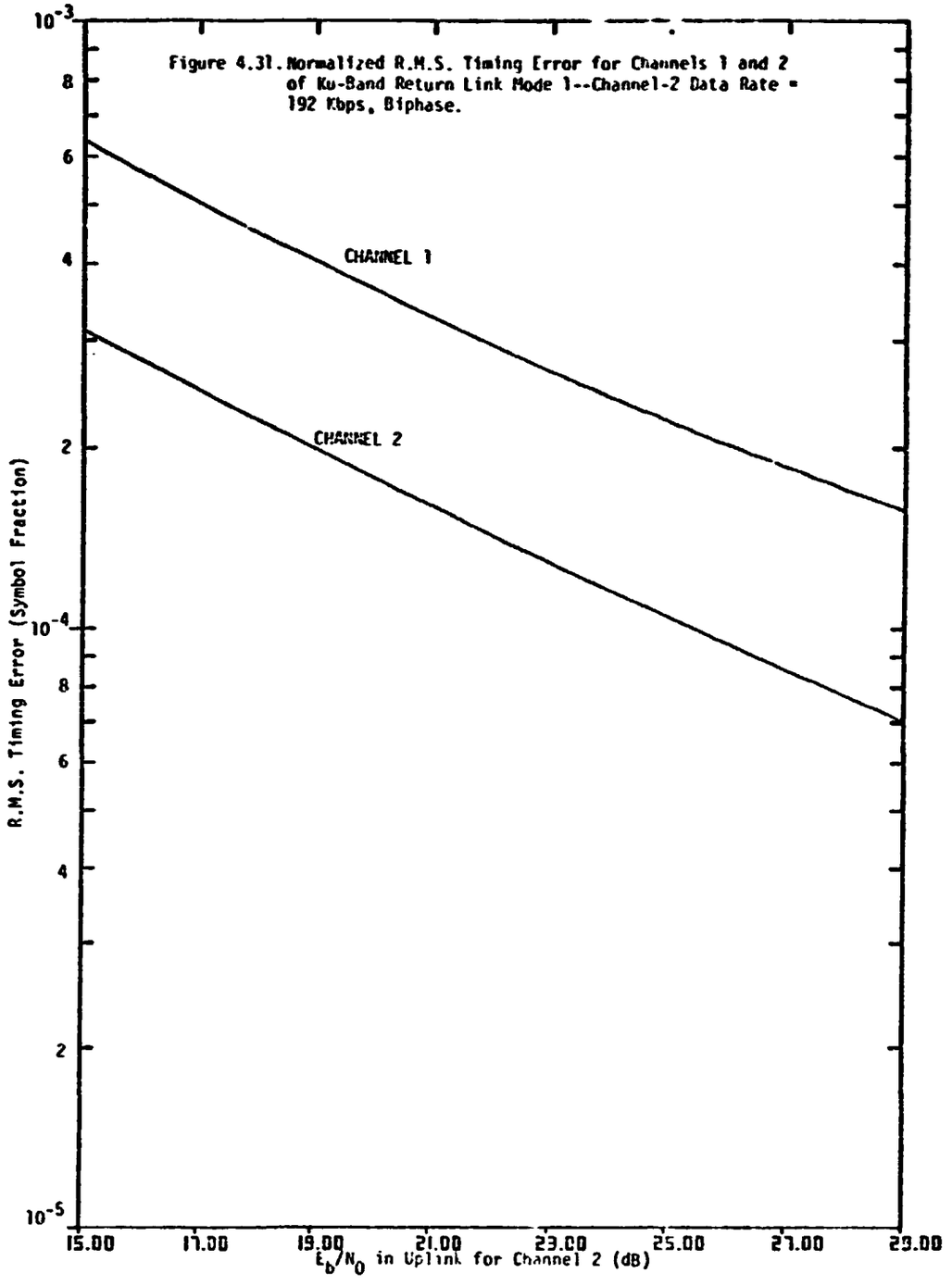

Figure 4.31. Normalized R.M.S. Timing Error for Channels 1 and 2 of Ku-Band Return Link Mode 1--Channel-2 Data Rate = 192 Kbps, Biphase.

80 0029

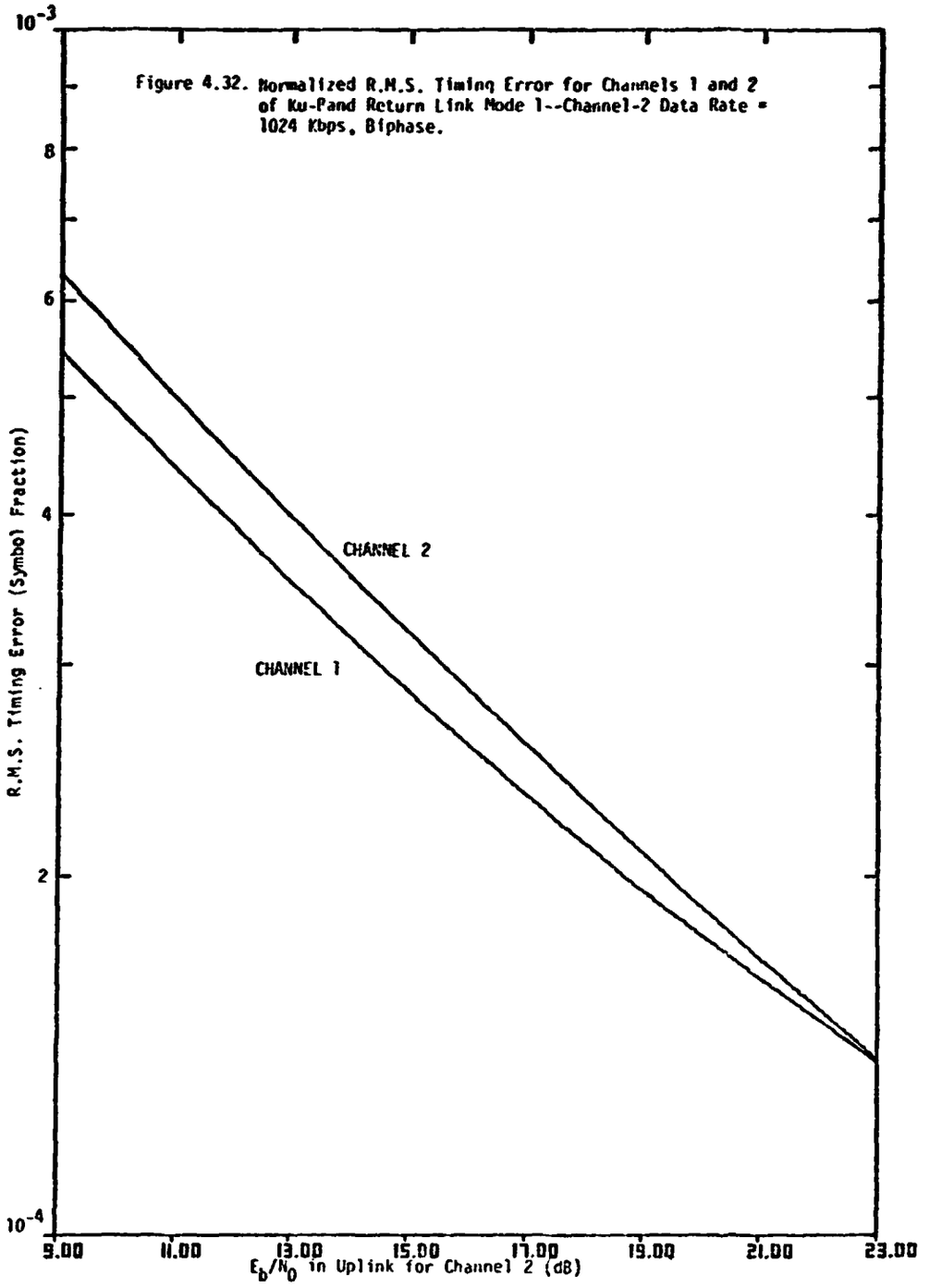

Figure 4.32. Normalized R.M.S. Timing Error for Channels 1 and 2 of Ku-Band Return Link Mode 1--Channel-2 Data Rate = 1024 Kbps, Biphase.

80 0030

APPENDIX

A DERIVATION IF EQ. (21)

Here we derive the eq. (21) of the text. Suppose that we observe the stream of received data over T sec during which period there are $N_s = TR$ symbols. The average error probability over N_s symbols can be written as

$$P_e(N_s) = \frac{1}{N_s}\left\{\sum_{k_c=1}^{N_c} n_{k_c}^T\left(\frac{\tau_{k_c}}{T_d}\right)P_e(k_c) + \sum_{k_g=1}^{N_g} n_{k_g}^T\left(\frac{\tau_{k_g}}{T_d}\right)P_e(k_g) + N_0(N_s)P_e(0)\right\} \tag{A.1}$$

where

$$N_0(N_s) = N_s - \sum_{k_c=1}^{N_c} n_{k_c}^T\left(\frac{\tau_{k_c}}{T_c}\right) - \sum_{k_g=1}^{N_g} n_{k_g}^T\left(\frac{\tau_{k_g}}{T_d}\right) \tag{A.2}$$

Note that we have assumed $N_0(N_s) > 0$ and also allowed to have non-integer values for the ratios (τ_{k_ℓ}/T_d). In practice, it is always possible to choose T sufficiently large so that $N_0(N_s)$ is larger than 0. The noninteger (τ_{k_ℓ}/T_d) implies that the symbol partially hit by a RFI pulse is counted as the symbol error caused by the RFI pulse weighted with the fractional part of the ratio (τ_{k_ℓ}/T_d). This will yield a slightly pessimistic result when the ratio (τ_{k_ℓ}/T_d) is near unity. And it becomes insignificant for $(\tau_{k_\ell}/T_d) > 1$. Rewriting eq. (A.1) we have

$$P_e(N_s) = 1 + \sum_{k_c=1}^{N_c}\left(\frac{n_{k_c}^T}{T}\right)\tau_{k_c}(P_e(k_c) - P_e(0)) + \sum_{k_g=1}^{N_g}\left(\frac{n_{k_g}^T}{T}\right)\tau_{k_c}(P_e(k_g) - P_e(0)) \tag{A.3}$$

By the assumption that the variables $n_{k_c}^T$ and $n_{k_g}^T$ are random processes with a Poisson distribution

$$p_i(n) = \frac{(\lambda_i T)^n}{n!} \exp(-\lambda_i T) \tag{A.4}$$

where

λ_i = pulse repetition rate of $i^{\underline{th}}$ group of the RFI

T = observation period.

We average the $P_e(N_s)$ over the statistics of $n_{k_c}^T$ and $n_{k_g}^T$

$$P_e(N_s) = 1 + \sum_{k_c=1}^{N_c} P_{k_c}\tau_{k_c}(P_e(k_c)-P_e(0)) + \sum_{k_g=1}^{N_g} P_{k_g}\tau_{k_g}(P_e(k_g)-P_e(0)) \tag{A.5}$$

which is independent of T. Implicitly, we have assumed that T is sufficiently large such that the statistics of the variables $n_{k_c}^T$ and $n_{k_g}^T$ satisfy the eq. (A.4). Therefore, we conclude that

$$P_e = \lim_{T\to\infty} P_e(N_s) = \sum_{k_c=1}^{N_c} P_{k_c}\tau_{k_c}P_e(k_c) + \sum_{k_g=1}^{N_g} P_{k_g}\tau_{k_g}P_e(k_g) + P_0P_e(0) \tag{A.6}$$

where

$$P_0 = 1 - \sum_{k_c=1}^{N_c} P_{k_c}\tau_{k_c} - \sum_{k_c=1}^{N_g} P_{k_c}\tau_{k_c} \tag{A.7}$$

and also that eqs. (22) and (23) of the text hold.

REFERENCES

[1] G. Kinal, ORI, "Simplified Test Environments for Pacific TDRS," 12 April 1979.

[2] T. C. Huang and W. C. Lindsey, "Performance of PN Spread Spectrum Signals Through a Nonlinear Satellite Channel," presented at NTC'78, DEc. 1978.

[3] Miller, K. E., "SSARE MRD Design and Performance Summary," TDRSS Ground Segment Technical Memo No. TG-119, Harris Corp., 5 April 1978.

5. PROPOSED ESTL RFI TESTING

5.1 Introduction

Since NASA/JSC has a complete hardware simulation system for the non-RFI Shuttle/TDRSS Link it is certainly worthwhile to extend this simulation capability to RFI environments by adding an RFI test generator. For the design of such an RFI test generator several things must be taken into account. First the available data on the RFI sources have to be reviewed and all useful statistical data must be extracted. Then the link performance sensitivity to these RFI features must be estimated in order to decide which statistical parameters must be modeled in the simulator for reasonably accurate performance predictions. The third consideration would be the complexity of the resulting simulator.

Section 5.2 reviews some of the features which might be found in the RFI signal and which, from our experience with LinCsim may substantially affect the overall link performance. Section 5.3 presents a simple RFI test generator implementation based solely on the statistical information contained in the RFI test environments. It is in our opinion the simplest test generator which might still give meaningful results.

5.2 Desirable Features for RFI Simulator

The RFI test generator should duplicate all those known RFI characteristics which affect the overall Shuttle/TDRSS link performance. This includes the following features:

(1) Type of interference. There is a significant difference in the effect of wideband Gaussian noise and pulsed CW interference on BER performance, even if both have the same power. Therefore,

both interference types must be generated.

(2) Power level. The wide range of power levels could be approximated by the histogram defined by the unclassified RFI test environments discussed in Chapter 4. The realism of the simulation can be improved however by approximating the actual distributions with steps smaller than 10 dB.

(3) Pulse duration. The actual pulse length distribution can be approximated by the two values used in the RFI test environment or, preferably, by a discrete distribution over more sample points.

(4) CW frequency. The p.d.f. of the center frequency of the CW pulses should be known and modeled.

(5) Periodicity. If there is any correlation between the RFI pulse arrival times it should be modeled if the correlated pulses are separated by less than the demodulator memory time.

(6) Modulation. If the radar pulses have signatures such as chirp or phase coding their modeling as CW pulses may be very pessimistic. In certain cases it might be more appropriate to use a narrowband Gaussian noise to simulate such modulated pulses.

(7) Pulse overlaps. The simultaneous presence of more than one CW pulse might be worth simulating because of the intermodulation effects. However,the probability of such overlaps should be compared to the accuracy of the pulse rate estimates before such a decision is made.

5.3 Proposed ESTL RFI Simulator

The RFI simulator design to be proposed is based on the considerations listed in the previous section, on the RFI test environment discussed in Section 4.2 and on the assumptions listed there.

For the RFI generator design it was decided that no effort should be made to model the overlap of pulses. This is based on the following reasons: If pulses with different power levels interact, the resulting intermodulation levels are so much smaller than the larger of the two signals that they may be neglected. The overlap of two pulses of the same power level on the other hand has negligible probability.

The proposed RFI test set up is shown in Fig. 5.1. The RFI test generator produces an S-band output signal whose bandwidth and center frequency agree with the values of the Shuttle S-band link under test. This signal is added to the return link signal between the spaceloss simulator and the [illegible] simulator.

The RFI test generator is shown in more detail in Fig. 5.2. It contains three channels, one to generate noise bursts and two to generate CW bursts. The gating and power level selection is done by a programmable attenuator under control of the burst timing and power control logic.

The frequency of the CW tone bursts is given by the instantaneous frequency of the sweep generators. To avoid generating chirp signals the sweep rate has to be slow enough to leave the frequency approximately constant over one burst. This means however, that consecutive CW pulses have very similar center frequencies. The effect of this unwanted correlation is minimized by using two sweep generators, one covering the data bandwidth, the other the rest of the channel bandwidth. Since the inband sweep generator is gated at a very low duty cycle it can change its frequency by an adequate amount between pulses to minimize the unwanted correlation.

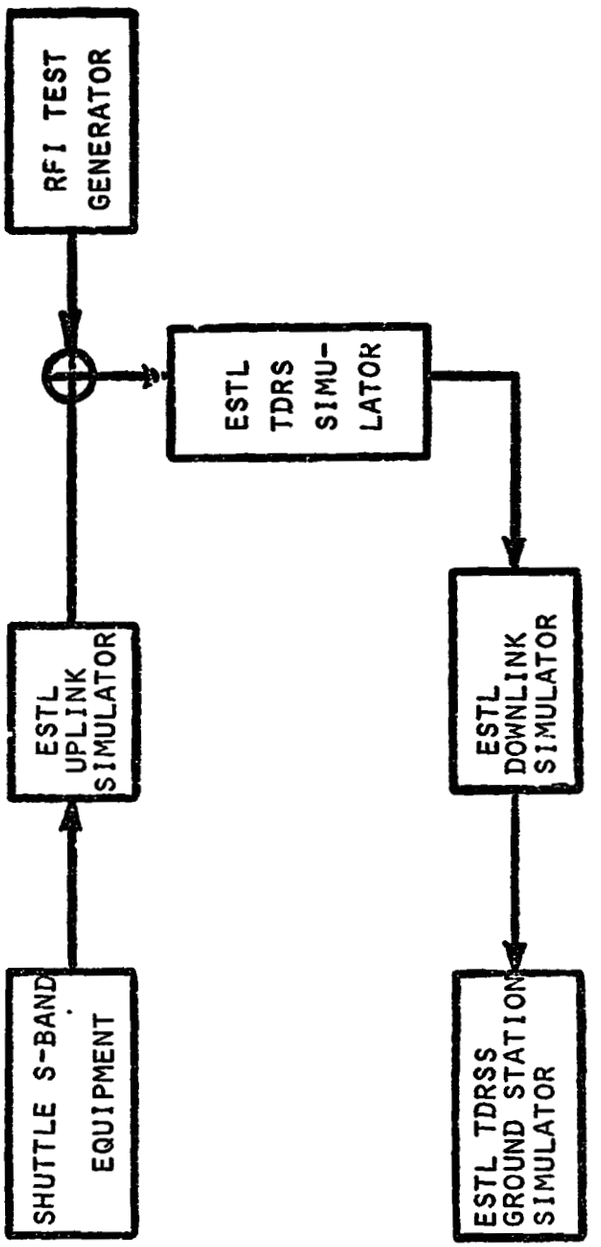

Figure 5.1. Proposed ESTL RFI Test Setup.

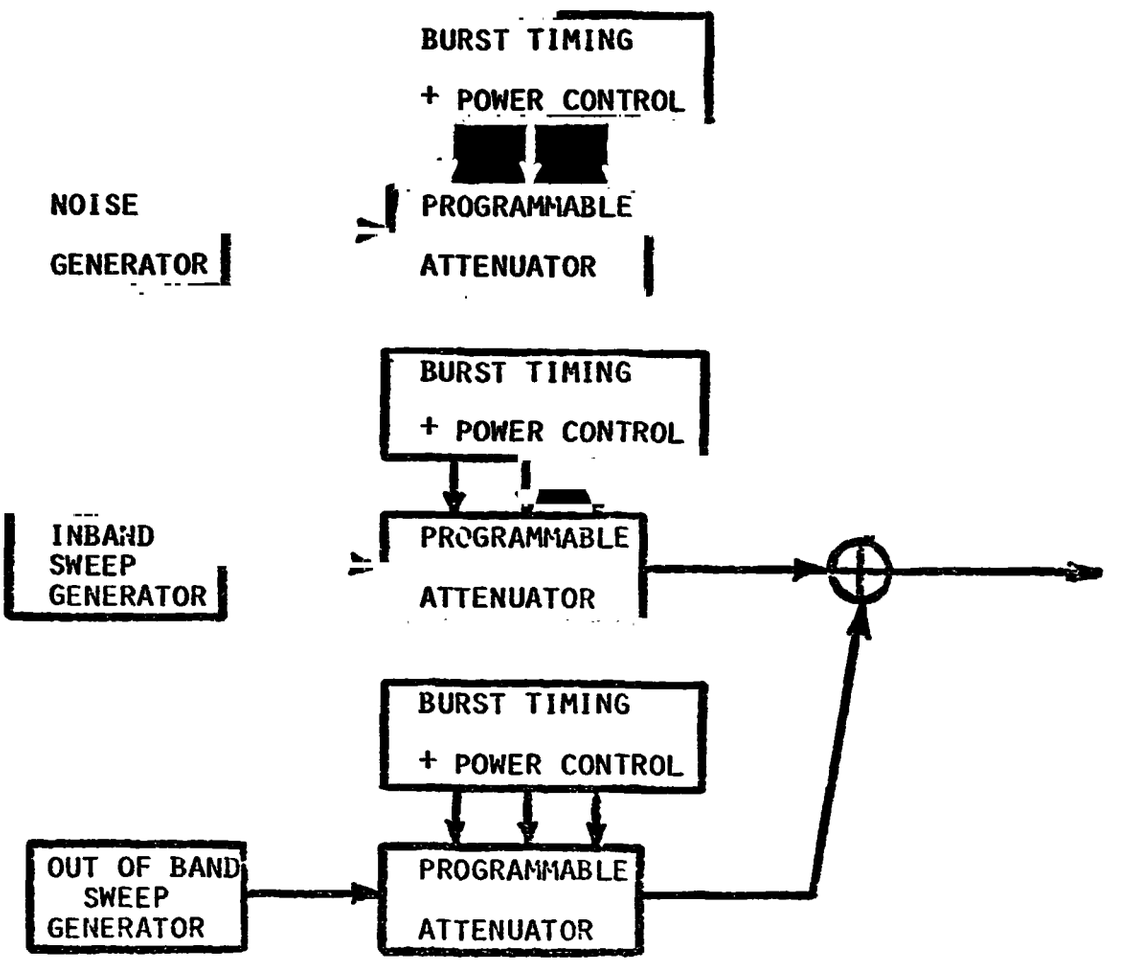

Figure 5.2. Proposed RFI Test Generator.

6. MISCELLANEOUS ANALYSES AND RECOMMENDATIONS

6.1 Introduction

This chapter documents several analyses performed under the current contract. These studies were short-term efforts in support of JSC but not directly related to the contract task statements. The findings and recommendations were communicated to JSC personnel in the form of short memos.

6.2 Waveguide Effects on PSK Signals

6.2.1 Introduction

In a typical satellite terminal there may be a long waveguide section from the low-noise amplifier near the antenna to the remaining signal processing equipment. Based on measurements taken at KSC it was predicted that the linear distortion in a 100 m section of WR62 copper waveguide could result in more than 10 dB performance degradation. LinCom predicted the degradation analytically using LinCsim and found it to be a fraction of a dB. A similar analysis was then made for the ESTL/SAIL test setup and an interpretation of the KSC measurements was found.

6.2.2 Linear Distortion of a Waveguide

The major linear distortion in a long waveguide section is the quadratic phase nonlinearity. Fig. 6.1 shows the phase characteristic of a 100 m section of waveguide WR62 for the center frequency 15.0034 GHz. The resulting performance degradation for a 50 Mb/sec BPSK NRZ bitstream is shown in Fig. 6.2.

The ESTL Shuttle/TDRSS link simulator uses a 275 ft section of the same waveguide and its effect was also analyzed using LinCsim. The results depend on the center frequency of the signal. For the

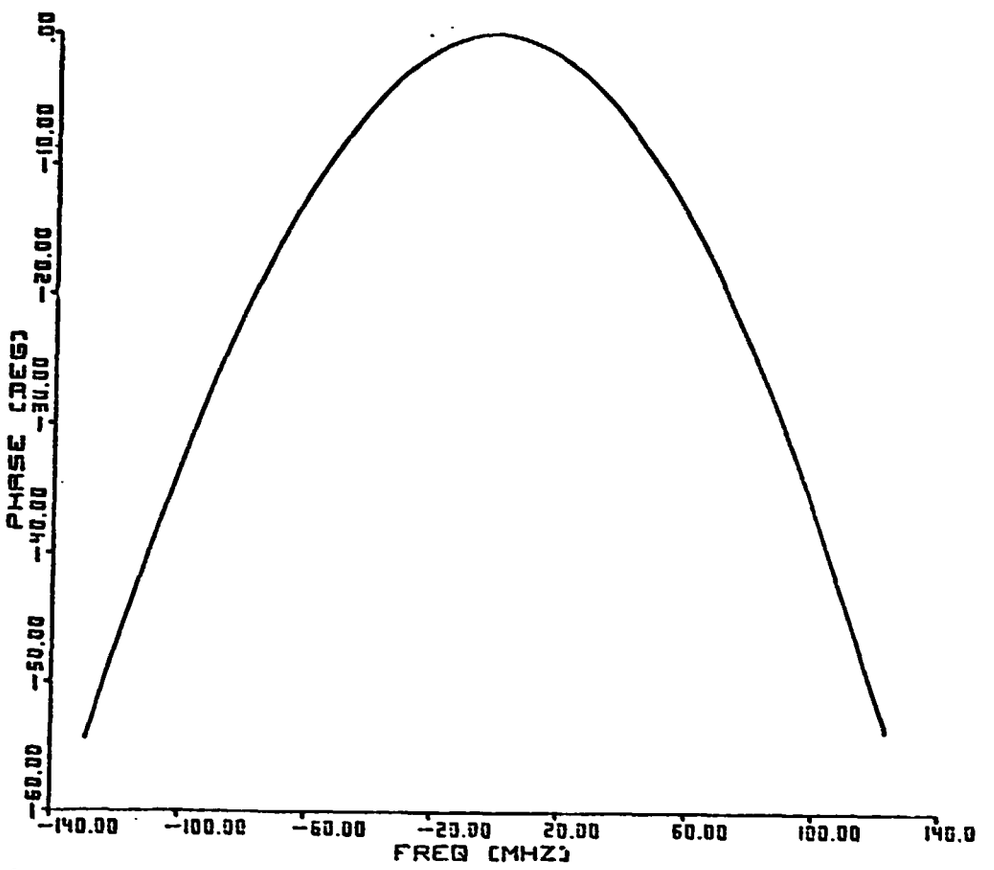

SO 0034

Figure 6.1. Phase Characteristic of 100m Waveguide Section.

Figure 6.2. Effect of Waveguide on Coded BER Performance
50 Mb/sec, rate 1/2 coded NRZ,BPSK.

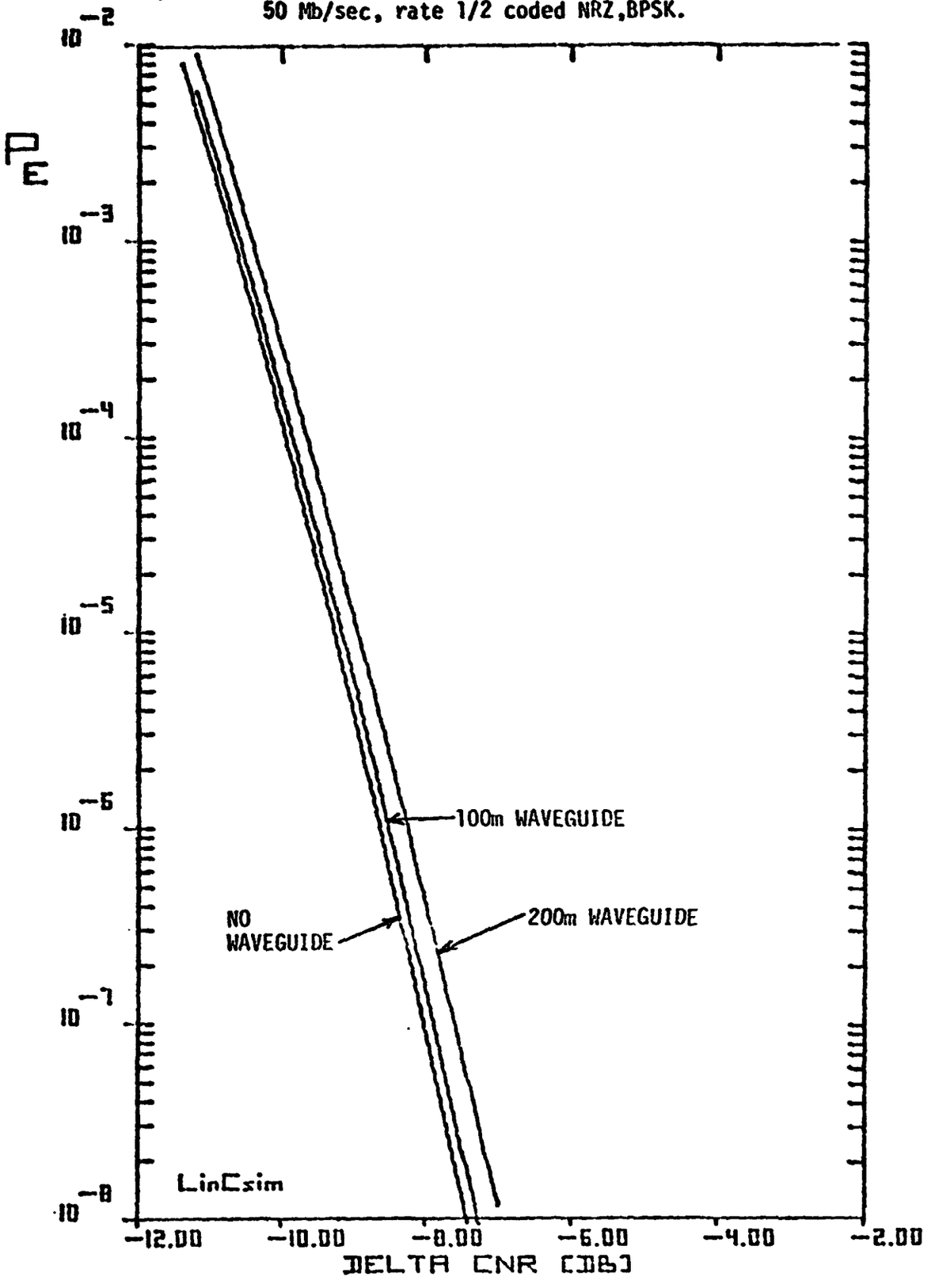

80 0635

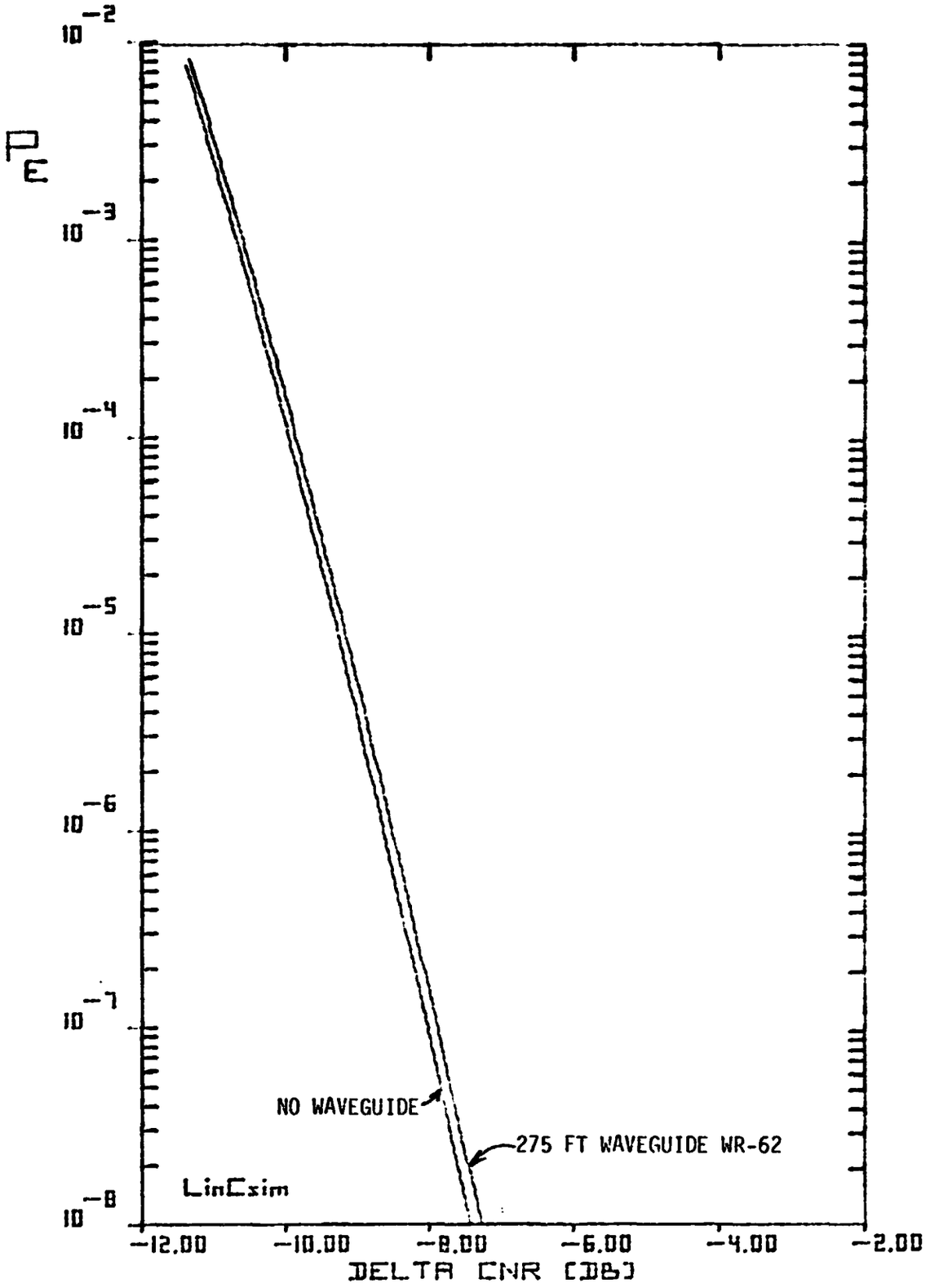

Figure 6.3. Effect of Waveguide on BER at 15 GHz.

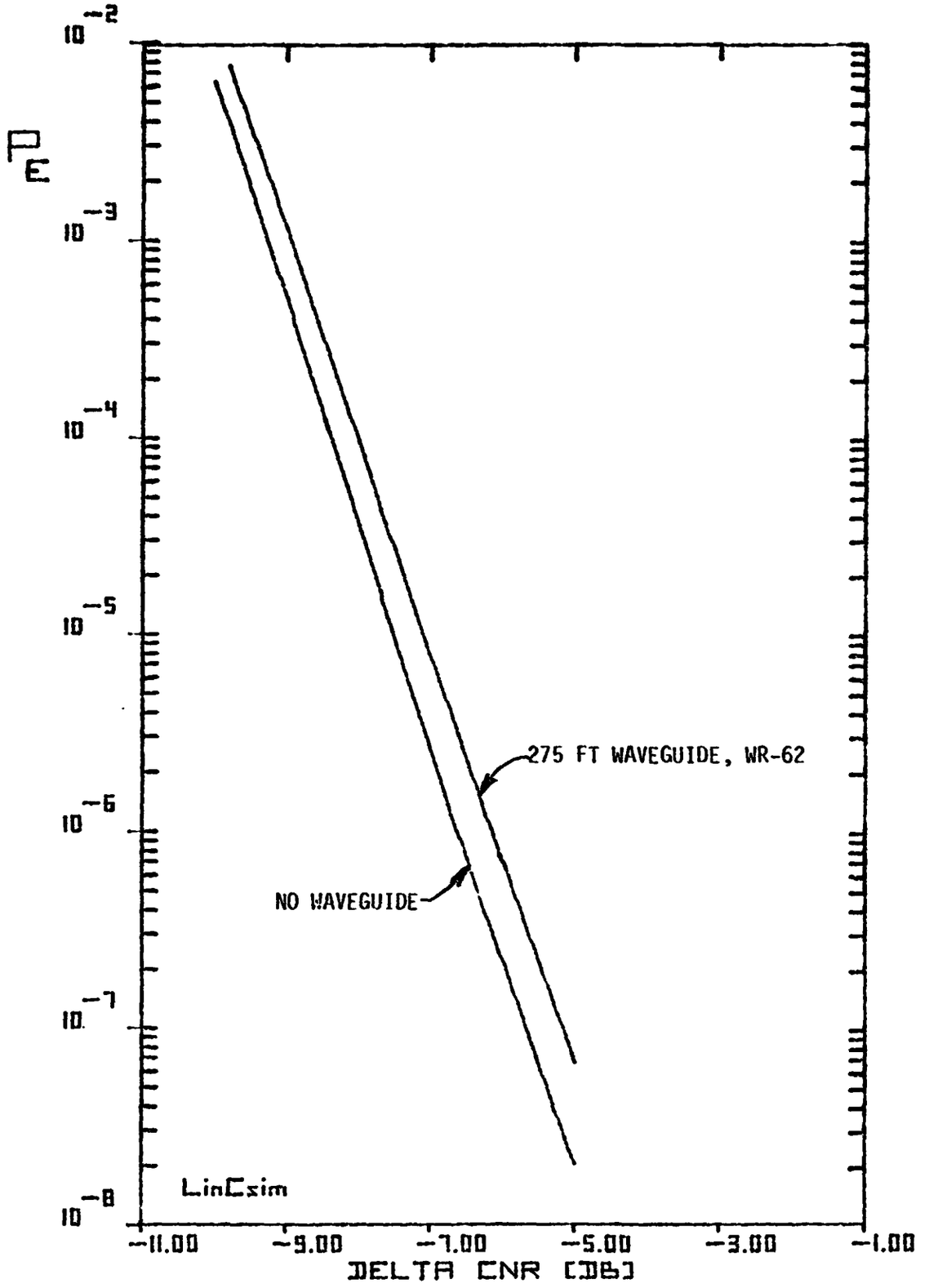

Figure 6.4. Effect of Waveguide on BER at 14 GHz.

SSO-to-TDRS link (f_c = 15.0085 GHz) the degradation is approximately .1 dB as shown in Fig. 6.3. For the TDRS-to-Ground link (f_c = 13.9375 GHz) the CNR ioss is close to .4 dB (Fig. 6.4). This is due to the increased linear distortion in closer proximity to the cutoff-frequency f_0 = 9.49 GHz.

6.2.3 Interpretation of KSC Measurements

The system assumed for the above computations is sketched in Fig. 6.5. There are two loss components which will be observed in the measurement setup, viz., signal attenuation and phase dispersion. Note that the signal-to-noise ratio is set by the LNA before the waveguide run. The signal distortion effect which the waveguide produced on E_b/N_0 is a linear phase dispersion which degrades link performance by .2 dB for 100 m waveguide in a coded system and may be .5 dB in an uncoded system. If the LNA at the antenna output is not present the signal-to-noise ratio is set after the waveguide and the waveguide attenuation shows up as an E_b/N_0 loss. This loss is tabulated in Table 6.1. From the magnitude of this loss it is obvious that no system should be implemented in this fashion. Also, the problem could not be solved by using a different type of waveguide.

The two sources of loss have different effects on the shape of the BER vs CNR curve and it is recommended that the measurement results of KSC be analyzed in order to find the source of the losses. If the BER curve looks like a shifted ideal BPSK curve of Fig. 6.6, the source of the loss is pure attenuation! If the curve levels off as illustrated in Fig. 6.7, the source of loss is phase dispersion.

6.3 S-Band Low Power Mode

6.3.1 Introduction

There is a requirement for the Shuttle S-band link to operate with

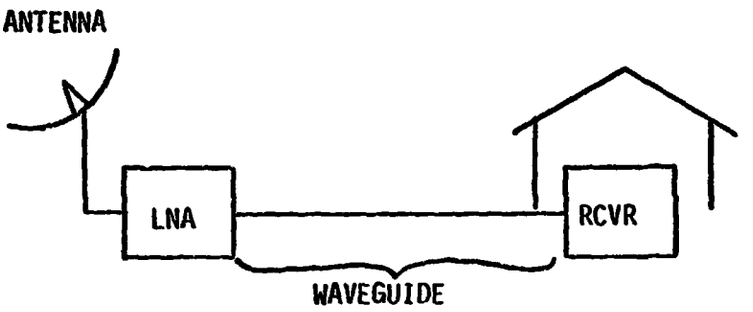

Figure 6.5. Receiver Configuration Assumed.

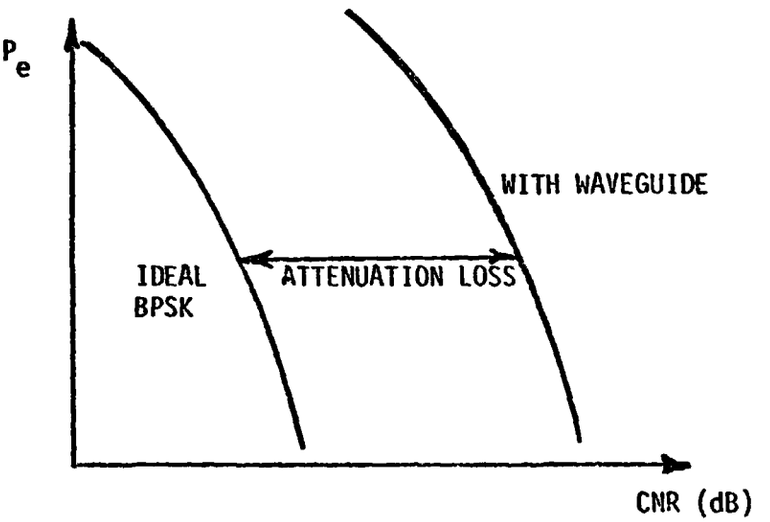

Figure 6.6. BER Curve for Attenuation Loss.

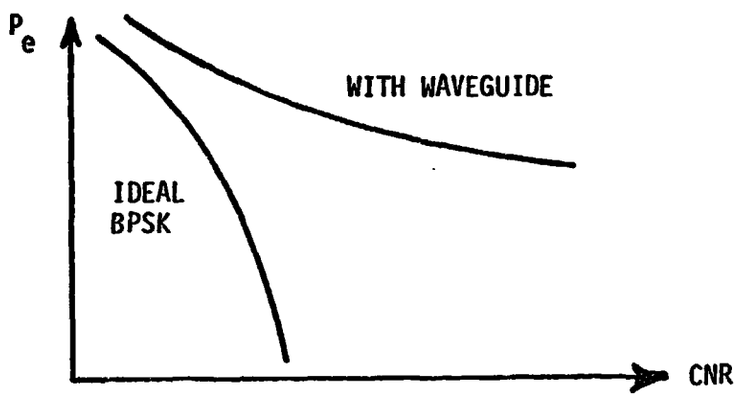

Figure 6.7.BER Curve for Dispersion Loss.

Length	Attenuation (dB)
280 ft	14.4 (KSC Experiment
100 m	16.8
200 m	33.7

Table 6.1.Waveguide Attenuation.

reduced prime power consumption during periods not requiring the transmission of high data rates. This section addresses the options available to reach this goal with minor modifications of the present hardware. First the options and the functional requirements of the relevant TDRSS services are discussed, then the available Shuttle equipment is reviewed and the necessary modifications are identified. Finally a solution is recommended.

6.3.2 TDRSS Services and Functional Requirements

For S-band return links the TDRSS offers the SSA and MA services. However, MA requires a greater user EIRP for a given data rate without providing any compensating advantages, hence its use is not recommended if the TDRSS SSA service is available. Tables 6.2 and 6.3 list the pertinent SSA return link characteristics for PN-spread and unspread signals, respectively. It must be noted that during acquisition the data modulation must be inhibited in both cases. Also, despite the fact that the acquisition EIRP is presently specified 10 dB higher for an unspread signal than for a PN-spread one, there is no reason to expect the hardware to show this difference in performance. Hence the unspread signal can be expected to be acquired with the same user EIRP as the PN-spread signal.

6.3.3 Shuttle Equipment Options

The Shuttle uses for its direct links to GSTDN, in addition to the regular SSO-TDRSS configuration, a low power mode of the above system and an FM link, both equipped with an omni antenna.

6.3.3.1 Low Power PM Mode

Making the low power PM mode (output power 2W, EIRP 1 dBW) available for SSO-TDRSS links would require PN spreading to meet the acquisition EIRP requirements. However, since there is no justification

Table 6.2. SSA Return Link Characteristics for PN-Spread Signals.

Minimum Data Rate	100 b/s
EIRP for Above Rate	-15 dBW
Min. Acquisition EIRP	-6 dBW

Table 6.3. SSA Return Link Characteristics for Unspread Signals

Minimum Data Rate	1 kb/s
EIRP for Above Rate	-6 dBW
Min. Acquisition EIRP	4 dBW

for the restrictive specification on the unspread signal it should be possible to have the required acquisition EIRP specification reduced to less than 1 dBW. Otherwise, the PN modulation would have to be included. Since the design 1-dB bandwidth is greater than 5 MHz, it should be sufficient for the spread signal.

Since the resulting signal satisfies regular SSA specifications, except for the FEC code used, the impact on the ground station is minimal: the soft-decision symbols from the low-rate demodulator have to be routed to the rate 1/3 Viterbi decoder.

6.3.3.2 FM Equipment

The FM link (output power 10W, EIRP 4.1 dBW) satisfies the present TDRSS EIRP specification for signals without PN spreading. However, a phase-modulator would have to be provided in order to obtain a signaling format compatible with the ground station equipment. Otherwise, the TDRSS IF service can be used with FM demodulation performed by NASA. This latter approach may suffer from the fact that the IF channel characteristics are presently not well defined due to the RFI hardware changes.

6.3.4 Recommendations

In the light of the above discussion we propose to use the low power PM mode for low rate data transmission. A discussion with Goddard personnel about the minimum acquisition EIRP for unspread links is recommended before the decision is made to add PN spreading to this link.

6.4 Effect of Spacelab Data Transition Density on Clock Recovery and BER

6.4.1 Introduction

The Spacelab data do not meet the specifications imposed on the

transition density and on the maximum length of transition-free runs. The effect of these two factors on the quality of the recovered clock and on the bit error probability was estimated using a worst-case analysis. The results show that for a reasonable loop bandwidth (.1% of symbol rate) the tracking loop can track well through the transition free runs and that the recovered clock and the bit error rate are only slightly degraded by the low transition density. The error rate degradation is expected to be less than .1 dB. The following sections summarize the known facts about the data transition statistics and the analysis supporting the above results.

6.4.2 Characterization of Spacelab Data Transition Density

Maximum all-zero or all-one runs into encoder are 128 bits long.

Maximum runs occur frequently; up to one every 256 bits.

Average density is 300 transitions in 1536 bits.

After the convolutional encoder the maximum all-zero runs will be approximately 256 symbols, spaced 256 symbols apart. The average transition density will be more than (300/1536), most likely in the range 30% to 40%.

6.4.3 Analysis

The above transition statistics can affect the clock recovery loop performance through three mechanisms: 1) the recovered clock frequency may drift off during transition-free periods due to loop stress, 2) the noise-induced phase jitter may increase during such periods since the restoring force is missing, 3) the loop signal-to-noise ratio is lowered if the transition density is less than 50%.

If a second-order tracking system is used the first effect may be neglected since the drift time-constant is the time-constant of

the (imperfect) integrator which is typically many times higher than the inverse of the bandwidth.

The second effect may be upper-bounded by assuming a first-order tracking loop. Then the phase error is described by a first order Gauss-Markov process during the transition-free period and the variance increases by a factor of 4 over 512 symbol-times (neglecting the reduction of the variance which takes place between two 256-symbol all-zero strings).

The effect of the low transition density is to reduce the effective loop SNR by approximately 2 dB. Since the r.m.s. tracking error for a transition density of 50% is epxected to be 1.4% the resulting tracking error is 1.7%, yielding in an incremental CNR loss of .02 dB [2]. Adding the effect of long all zero strings results in 3.5% r.m.s. tracking error or approximately .1 dB CNR loss for the bit error rate.

6.5 Spacelab Risetime and Jitter Specifications

6.5.1 Introduction

The predicted Spacelab symbol rise-time was increased from 3.5 ns to 4.5 ns and the combined bit jitter and data asymmetry from 1 ns to 2 ns. In this section the effect of these changes on the overall link performance is computed.

6.5.2 Analysis

The basic pulse shape for the highest data rate is sketched in Fig. 6.8. Due to data asymmetry and bit jitter the actual transitions are within ± 1 ns from their expected time (Fig. 6.9). Since the scrubber implementation assures that the sampling point is at least 5 ns from the worst case transition [1] it occurs always beyond the 90%-point of the transition and the signal-to-noise ratio is very

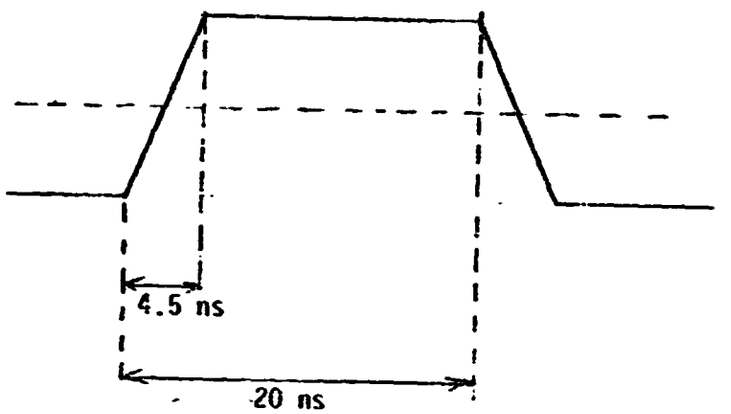

Figure 6.8. Basic Pulse Shape.

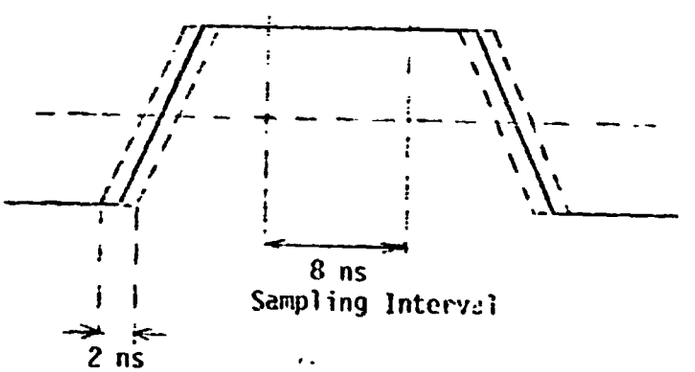

Figure6.9. Effect of Bit Jitter/Asymmetry.

little degraded. The remaining 8 ns interval allows approximately 6% r.m.s. jitter on the recovered clock while the predicted value is less than 2% [2]. This value increases only slightly for increased bit jitter since it is dominated by thermal effects [2,p.126]. We may therefore conclude that the overall link performance is not measurably degraded.

REFERENCES

[1] Cager, R. H., LaFlame, D. T., and Parode, L. C., "Orbiter Ku-Band Integrated Radar and Communications Subsystems," IEEE Trans. on Communications, Vol. COM-26, no. 11, November, 1978.

[2] "Shuttle/TDRSS Modelling and Link Simulation Study," LinCom Report No. TR-79-4-0476a, April, 1979.